NASA Contractor Report 187228

NASA-CR-187228
19920010307

Linear and Nonlinear Dynamic Analysis by Boundary Element Method

Shahid Ahmad
State University of New York at Buffalo
Buffalo, New York

October 1991

Prepared for
Lewis Research Center
Under Contract NAS3–23697

National Aeronautics and
Space Administration

ACKNOWLEDGEMENT

The author wishes to express his sincere gratitude to his advisor, Professor P.K. Banerjee, for his guidance, support and constant encouragement during the course of this research. Professor Banerjee's contribution in the area of the Boundary Element Method and his encouragement and advice led the author to undertake this topic of research. The author also wants to thank Dr. G.D. Manolis for his encouragement and many valuable discussions and Prof. Rowland Richards, Jr. for his valuable suggestions for improving the manuscript.

The author is indebted to Dr. Chris Chamis, the NASA program manager, and Dr. Edward Todd, the Pratt and Whitney program manager, for their financial support without which this work would have been impossible. He is also indebted to Dr. R.B. Wilson, Miss Nancy Miller and Mr. D.W. Snow of Pratt and Whitney for their helpful suggestions during the development of computer code for three-dimensional dynamic analysis.

Finally, the author wishes to thank Mrs. Ikuko Isihara for her exceptionally high-quality typing of this dissertation.

ABSTRACT

In this dissertation, an advanced implementation of the direct boundary element method applicable to free-vibration, periodic (steady-state) vibration and linear and nonlinear transient dynamic problems involving two and three-dimensional isotropic solids of arbitrary shape is presented. Interior, exterior and half-space problems can all be solved by the present formulation.

For the free-vibration analysis, a new real variable BEM formulation is presented which solves the free-vibration problem in the form of algebraic equations (formed from the static kernels) and needs only surface discretization.

In the area of time-domain transient analysis the BEM is well suited because it gives an implicit formulation. Although the integral formulations are elegant, because of the complexity of the formulation it has never been implemented in exact form. In the present work, linear and nonlinear time domain transient analysis for three-dimensional solids has been implemented in a general and complete manner. The formulation and implementation of the nonlinear, transient, dynamic analysis presented here is the first ever in the field of boundary element analysis.

Almost all the existing formulation of BEM in dynamics use the constant variation of the variables in space and time which is very unrealistic for engineering problems and, in some cases, it leads to unacceptably inaccurate results. In the present work, linear and quadratic, isoparametric boundary elements are used for discretization of geometry and functional variations in space. In addition higher order variations in time are used.

These methods of analysis are applicable to piecewise-homogeneous materials, such that not only problems of the layered media and the soil-structure interaction can be analyzed but also a large problem can be solved by the usual sub-structuring technique.

The analyses have been incorporated in a versatile, general-purpose computer program. Some numerical problems are solved and, through comparisons with available analytical and numerical results, the stability and high accuracy of these dynamic analyses techniques are established.

LIST OF CONTENTS

LIST OF CONTENTS (continued)

LIST OF CONTENTS (continued)

LIST OF CONTENTS (continued)

NOTATIONS

A short list of notation is given below. All other symbols are defined when first introduced. A few symbols have different meanings in different contexts, but no confusion should arise.

E	Young's modulus
ν	Poisson's ratio
λ, μ	Lame's elastic constants
ρ	mass density
c_1	pressure wave velocity
c_2	shear wave velocity
T	time
s	Laplace transform parameter
ω	circular frequency
S	surface of the domain
V	volume of the domain
u_i, t_i	displacements and tractions
σ_{ij}	stresses
δ_{ij}	Kronecker's delta function
σ^o_{ij}	initial stress
$\underline{x}$	global coordinates of the receiver or field point
$\underline{\xi}$	global coordinates of the source point
G_{ij}, F_{ij}	displacement and traction fundamental singular solutions
$[A], [B]$	matrices of coefficients multiplying the known and unknown field quantitites, respectively
$\{x\}.\{y\}$	known and unknown boundary field quantities
$\{R_N\}$	vector containing past dynamic hisotry
N_α	spatial shape functions for boundary elements
M_β	spatial shape functions for volume cells

Δ	incremental quantity
,	spatial derivative
$\sum$	summation

Superscripts

.	time derivative
–	Laplace or Fourier transformed quantity
σ	quantity related to interior stress
u	quantity related to interior displacement
b	quantity related to a boundary point
s	quantity related to elasto-static

LIST OF TABLES

LIST OF FIGURES

LIST OF FIGURES (continued)

LIST OF FIGURES (continued)

LIST OF FIGURES (continued)

CHAPTER I

INTRODUCTION

I.1 THE NEED FOR THE PRESENT WORK

The dynamic analyses of engineering problems involving two and three-dimensional solids have been a subject of intense research for the last two decades. For these problems, closed-form analytic solutions are extremely difficult to obtain except for very simple geometries and boundary conditions which hardly exist in practice. Experiments, on the other hand, are expensive and difficult to perform. They also involve elaborate apparatus in order to reproduce the desired excitations and to scale the important parameters correctly. Therefore, resort has to be made to numerical methods of solution.

There are currently two major categories of numerical methods available for dynamic analysis of solids; namely, approximate continuum and discrete (lumped parameter) models. The most widely used approximate continuum method at present is the Finite Element Method (FEM). In principle it appears to be a very versatile technique because it can handle complex structure geometry, medium inhomogeneities and complicated material behavior in both two and three dimensions. The finite element formulation results in a system of equations that may be solved by modal analysis, Fourier transform techniques, or step-by-step integration schemes (Ref. Zienkiewicz, 1977). However, the major deficiency of the FEM is that an infinite or semi-infinite medium has to be modeled by a mesh of finite size. This results in undesirable wave reflections from the artificial boundaries. This situation is remedied by the use of transmitting boundaries (e.g. Kausel et al, 1975), hybrid techniques (e.g. Tzong et al, 1981), or infinite elements (e.g. Bettess, 1977). The use of infinite element is restricted to homogeneous far fields because it does not permit variation in material properties, and hence problems involving layered media cannot be solved by using infinite elements. Similarly, a

transmitting boundary encompassing all possible cases of waves impinging at the ends of a mesh has yet to be devised. Furthermore, the computational cost involved in analyzing three-dimensional problems by the FEM is so enormous that only a few researchers can afford it. Another continuum method is the Finite difference method (FDM). It has been used less frequently than the FEM, primarily because of the difficulties associated with it in handling complicated geometries and boundary conditions.

Discrete models are also in use for a certain class of problems (Ref. Hadjian et al, 1974). The basic idea behind the discrete model approach is the evaluation of the mass, stiffness and damping coefficients that essentially represents the medium. With the use of these frequency dependent coefficients known as impedance functions, the dynamic analysis of the structure is possible. However, exact expressions for impedance functions can be obtained for very few cases only and therefore the use of discrete models is rather restricted to some simple problems, e.g. some foundation problems (Ref. Arnold et al, 1955; Veletsos, 1971).

In contrast, it is convincingly demonstrated that accurate and efficient solutions to dynamic problems can be easily obtained by using the Boundary element method (Ref. Banerjee and Butterfield, 1981) because the radiation condition is automatically (and correctly) satisfied and for linear problems only the surface of the problem needs to be discretized. Even for problems with material nonlinearity (e.g. soil), in addition to the surface discretization, only a small part of the domain where nonlinear behavior is expected needs to be discretized. Thus, a tremendous reduction in the size of the problem can be achieved. A brief description of the Boundary element method (BEM) is provided in Section II.2 and a complete review of the existing work on dynamic analysis by BEM is presented in Chapter III. From this review, it can be seen that most of the existing

work on dynamic analysis by BEM suffers either from the lack of generality or from unacceptable level of accuracy. In addition, all of the existing work is based on the assumption of linear elastic behavior and most of them assume steady-state conditions. However, in the real world of engineering problems, steady-state conditions and linear behavior are at best a first order approximation. For truly transient processes it is thus mandatory to consider time response and nonlinear behavior.

Because of the reasons discussed above, there is a need for a complete and general analysis method for dynamic problems of two and three-dimensional solids, particularly for problems related to the semi-infinite mediums.

The work described in this thesis represents a comprehensive attempt towards the development of a general numerical methodology for solving two and three-dimensional dynamic problems by using BEM. The developed methodology is applicable to free-vibration, periodic vibration and linear as well as nonlinear transient dynamic analysis of solid bodies of arbitrary shape.

I.2 RELEVANT PROBLEMS OF ENGINEERING ANALYSIS AND THE SCOPE OF THE PRESENT WORK

The ability to predict the dynamic response of solid bodies subjected to time and space dependent loads and boundary conditions has gained considerable importance in all engineering fields such as machine foundation design, seismology, non-destructive testing of materials, soil-structure interaction analysis, structural dynamics, metal forming by explosives, auto-frettage, and aircraft structure design.

The methodology for dynamic analysis presented in this dissertation can be used for solving a number of problems described above. Brief descriptions of some of these problems are given below.

(i) Machine Foundation Design: The design of a machine foundation essentially consists in limiting its motion to amplitudes and frequencies which will neither endanger the satisfactory operation of the machine nor will they disturb the people working in the immediate vicinity. Therefore, for a successful machine foundation design, a careful engineering analysis of the foundation response to the dynamic loads from the anticipated operation of the machine is desirable. The existing methods for analyzing machine foundations can be categorized into two groups: namely, lumped parameter approaches and the finite element method. In the lumped parameter approach all the motions are assumed to be uncoupled and for complicated geometries it is impossible to find impedance functions. On the other hand, as discussed earlier the finite element method is unable to handle realistic three-dimensional foundation problems because of its finite boundaries and computational costs. Therefore, the methodology presented here provides a viable tool for analyzing machine foundations with complex geometries embedded in layered soils. The multi-region capability of the present code will allow the realistic modeling of the foundation as well as the soil. It should be noted that the assumption of a rigid or flexible foundation is not needed in the present case. Also, different combinations of dynamic loading and boundary conditions can be easily incorporated.

(ii) Seismology: In the field of seismology, one is concerned with the study of wave propagation in soils. For this purpose, linearized theory of elastodynamics are commonly used. Thus, the present work provides a general methodology for studying wave propagation in a homogeneous halfspace as well as in layered soils.

(iii) Auto-frettage Process: This process is used in gun-building and in the construction of pressure vessels. In this process, walled structures such as pipes and spherical and cylindrical shaped containers are deliberately subjected to high pressure during their construction. This causes plastic deformation and thereby raises the yield strength of the material and induces favorable stress distributions. As a result, the working loads (i.e. internal pressures) are now carried out by purely elastic deformations. In order to achieve an optimum design of a pressure vessel by auto-frettage, the auto-frettage process has to be analyzed numerically. For this purpose, nonlinear static analysis algorithms are generally used. However, a realistic simulation of this problem can only be achieved by using a nonlinear dynamic analysis algorithm. The nonlinear transient dynamic algorithm presented in this thesis can serve this purpose.

(iv) Structural Dynamics: The problems related to forced and free-vibration of structural components such as beams, columns, and shear walls can all be analyzed by the proposed methodology. The nonlinear behavior of a structure subjected to an arbitrary transient loading can also be obtained by using the present method including the cracking and yielding of joints.

(v) Soil-structure Interaction: The safety of structures such as nuclear power plants, dams, bridges, schools, hospitals, and utility pipelines during an earthquake is of great concern to the designers and the local authorities. Thus, to determine the response of these structures during an earthquake, a great deal of research has been done and several techniques have been developed. Nevertheless, the problem is so complicated that it is still a subject of intensive study.

The response of structure during an earthquake depends on the characteristics of the ground motion, the surrounding soil, and the structure itself. For structures founded on soft soils, the foundation motion differs from that in the free-field due to the coupling of the soil and structure during an earthquake. Thus, soil-structure interaction has to be taken into account in analyzing the response of structures founded on soft soils. The available soil-structure analysis techniques can be categorized in two groups: i.e., the direct method and the substructure approach. In the substructuring approach, one of the steps involved is the determination of the dynamic stiffness of the foundation as a function of the frequency. The steady-state dynamic algorithm of the present work can be used to determine the dynamic stiffnesses of two or three-dimensional foundations and embedment of the foundation and layering of the soil can both be taken into account. As discussed earlier this methodology is a better alternative to the finite element method for this type of problem.

The time-domain, nonlinear, transient algorithm presented in this thesis is a strong candidate for realistic analysis of soil-structure interaction problems because, in addition to embedment and layering, it can also take into account the nonlinear behavior of soils. Finally, for structures subjected to wind load, the present implementation provides an accurate and efficient analysis.

I.3 OUTLINE OF THE DISSERTATION

This dissertation presents a complete and general numerical implementation of the direct boundary element method applicable to free-vibration, periodic vibration and linear and nonlinear transient dynamic problems involving two and three-dimensional isotropic piecewise homogeneous solids of arbitrary shape.

The early history of elastodynamics is presented in Chapter II. Also presented is a brief introduction to the boundary element method, its historical background and recent developments.

A literature review of the existing work on dynamic analysis by boundary element method is presented in Chapter III. In this chapter, for completeness, work on scalar wave problems is also reviewed although it is not related to the present work because in elastodynamics waves are considered to be vectors not scalars.

In Chapter IV, an advanced implementation of the direct boundary element method for two-dimensional problems of periodic vibrations is introduced. The governing equations of elastodynamics are presented followed by the boundary integral formulation in transformed domain. Subsequently, numerical implementation is introduced which includes discussions on the use of isoparametric elements, advanced numerical integration techniques, and an efficient solution algorithm. Some numerical problems are solved and the results are compared with available analytical and numerical results.

A new real-variable BEM formulation for free-vibration analysis and its numerical implementation for two-dimensional problems are presented in Chapter V. This method solves the free-vibration problem in the form of algebraic equations and needs only surface discretization. First, the formulation of the problem is introduced and then some simple problems are solved and compared with available results to demonstrate the accuracy of this new method.

In Chapter VI, an advanced implementation of the BEM applicable to steady-state dynamic problems of three-dimensional solids is presented. The governing equations and boundary integral formulation are the same as those introduced in Chapter IV. The numerical implementation for three-

dimensional problems is discussed first. Additional features like built-in symmetry and sliding at interfaces are also introduced. Finally, a few numerical problems are solved and are compared with the available results.

The Laplace-transform-domain, transient, dynamic algorithm applicable to two and three-dimensional solids is introduced in Chapter VII. The basic formulation and the inverse transformation techniques are discussed first followed by a number of example problems which demonstrates the stability and accuracy of this algorithm.

In Chapter VIII, the boundary element formulation for time domain transient elastodynamics and its numerical implementation for three-dimensional solids is presented for the first time in a general and complete manner. Higher order shape functions are used for approximating the variation of field quantities in space as well as in time. The unconditional stability and accuracy of this algorithm is demonstrated by solving a number of problems and comparing the results against available analytical solutions.

Chapter IX presents for the first time in the history of boundary-element analysis a direct boundary-element formulation for nonlinear transient dynamic analysis of solids and its numerical implementation for three-dimensional problems. The formulation is discussed first followed by discussions on constitutive model, volume integration, time stepping and iterative solution algorithm. Subsequently, a few numerical problems are solved and results are presented.

Finally, conclusions and recommendation for future research are set forth in Chapter X.

CHAPTER II

HISTORICAL BACKGROUND

II.1 HISTORICAL ACCOUNT OF ELASTO-DYNAMICS

The study of wave propagation in elastic solids has a long and distinguished history. Until the middle of the nineteenth century light was thought to be the propagation of a disturbance in an elastic ether. This view was espoused by such great mathematicians as Cauchy and Poisson and to a large extent motivated them to develop what is now generally known as the theory of elasticity. The solution of the scalar wave equation as a potential was first achieved by Poisson (1829). In 1852, Lamé added the vector potential appropriate to the solenoidal displacement component to the Poisson's general solution. Thus, through the efforts of Poisson and Lamé it was shown that the general elastodynamic displacement field can be represented as the sum of the gradient of a scalar potential and the curl of a vector potential, each satisfying a wave equation (i.e. longitudinal and transverse wave equations). Clebsch (1863), Somigliana (1892), Tedone (1897), and Duhem (1898) provided the proof for the completeness of Lamés solution; and in 1885 Neumann gave the proof of the uniqueness for the solutions of the three fundamental boundary initial value problems for finite elastic medium (recently, the proof of the uniqueness is extended to infinite medium by Wheeler and Sternberg, 1968). Later, Poisson's solution was presented in a more general form by Kirchoff (1883). This problem of scalar wave was further studied as a problem with retarded potentials by Love (1904).

Investigation of elastic wave motion due to body forces was first carried out by Stokes (1849) and later by Love (1904). In 1887, Rayleigh made the very important discovery of his now well known surface wave. In 1904 Lamb was the first to study the propagation of a pulse in an elastic half-space. He derived his solutions through Fourier synthesis of the steady-state propagation solutions. The ingenious technique of Cagniard

for solving transient wave problems came along in 1939. He developed the technique of solving the problem in the Laplace transform domain and then obtained the solution by inverse Laplace transform. This technique is the basis for much of the modern work in transient elastodynamics.

The classical works on elastodynamics are collected and presented with the recent analytical developments in a number of books, such as Achenbach (1973), Eringen and Suhubi (1975), and Miklowitz (1980).

During the early 1960s, some pioneering work using an integral equation formulation was done for acoustic problems by Friedman and Shaw (1962), Banaugh and Goldsmith (1963a), Papadopoulis (1963) and others. Kupradze (1963) also has done a great deal of work in the extension of Fredholm theory to the formulation of problems ranging from linear, homogeneous, isotropic elasto-statics to the vibrations of piecewise homogeneous bodies. The general transient problem was attempted by Doyle (1966) who used the singular solution for the transformed equations to obtain representations for the displacement vector, dilatation, and rotation vector. However, he did not attack the general boundary value problem in terms of boundary data and did not attempt a solution and inversion to complete the problem. Nowacki (1964) also treated the transient problem but his solution method required finding a Green's function before attempting the Laplace inversion. During the past two decades, Banaugh and Goldsmith (1963a) were the first ones to use the boundary integral formulation to solve an elastodynamic problem. After that, a number of researchers have used the boundary element method for solving elastodynamic problems. A complete review of these works is presented in Chapter III.

II.2 HISTORICAL DEVELOPMENT OF THE BOUNDARY ELEMENT METHOD

The boundary element method (BEM) has now emerged as a powerful numerical technique for solving problems of continuum mechanics. In recent years, it has been successfully employed for the solution of a very wide range of physical problems such as those of potential flow, elastostatics, elastoplasticity, elastodynamics, acoustics etc. The BEM, has a number of distinct advantages over the Finite element (FEM) and Finite difference (FDM) methods such as; discretization of only the boundary of the domain of interest rather than the whole domain (i.e., the dimensionality of the problem is reduced by one), ability to solve problems with high stress concentrations, accuracy, and the ease of solution in an infinite and semi-infinite domain.

This method essentially consists of transformation of the partial differential equation describing the behavior of the field variables inside and on the boundary of the domain into an integral equation relating only boundary values and then finding out the numerical solution of this equation. If the values of field variables inside the domain are required, they are calculated afterwards from the known boundary values of the field variables. The above described transformation of the partial differential equation into an integral equation is achieved through the use of an appropriate reciprocal work theorem, the fundamental singular solution of the partial differential equation (Green's function) and the divergence theorem. The BEM yields a system matrix which is much smaller than that of a differential formulation (i.e. FEM or FDM) but, in BEM, the system matrix is fully populated for a homogeneous region and block banded when more than one region is involved.

Historically, the first use of integral equations dates back to 1903 when Fredholm (1903) formulated the boundary value problems of potential

theory in the form of integral equations and demonstrated the existence of solutions to such equations. Since then they have been studied intensively particularly in connection with field theory (e.g. Kellog, 1953; Kupradze, 1963; Muskhelishvili, 1953; Smirnov, 1964). During the 1950s, a major contribution to the formal understanding of integral equations was provided by Mikhlin (1957, 1965a, 1965b) who studied the singularities and discontinuities of the integrands. Due to the difficulty of finding closed-form analytical solutions, all of the classical work has, to a great extent, been limited to the investigations of existence and uniqueness of solutions of problems of mathematical physics, except for the simplest of problems (Ref. Morse and Feshbach, 1953). However, the emergence of high-speed computers in late 1960s spurred the development of numerical algorithms based on adaptations of these integral formulations to the solution of general boundary value problems and the resulting technique came to be known as the Boundary Element Method.

The pioneering works in the field of BEM was done by Shaw and Friedman (1963a,b) for scalar wave problems; Banaugh and Goldsmith (1963a,b) for elastic wave scattering problems; Hess (1962a,b), Jaswon (1963), and Symm (1963) for potential problems; Jaswon and Ponter (1963), and Rizzo (1967) for elastostatic problems; Cruse (1967) for transient elastodynamic problems; Swedlow and Cruse (1971) for elastoplastic problems; and Banerjee and Butterfield (1977) for problems of geomechanics.

In recent years, advances such as the use of higher-order elements, accurate and efficient numerical integration techniques, careful analytical treatment of singular integrals and efficient solution algorithms have had a major impact on the competitiveness of the BEM in routine linear and nonlinear two and three-dimensional static analyses. The contributions of Lachat and Watson (1976), Rizzo and Shippy, (1977), Curse and Wilson

(1977), Banerjee et al (1979, 1985), Banerjee and Davies (1984), Raveendra (1984), Telles (1983, 1981), and Mukherjee (1982) should be mentioned. A number of textbooks, such as Banerjee and Butterfield (1981), Brebbia and Walker (1980), Liggett and Liu (1983), Mukherjee (1982), Brebbia, Telles and Wrobel (1984), and advanced level monographs, such as Banerjee and Butterfield (1979), Banerjee and Shaw (1982), Banerjee and Mukherjee (1984), and Banerjee and Watson (1986), provide a full description of the recent developments in the Boundary element method.

CHAPTER III

REVIEW OF THE EXISTING WORK ON DYNAMIC ANALYSIS BY BEM

III.1 SCALAR WAVE PROBLEMS

The phenomenon of scalar wave propagation is frequently encountered in a variety of engineering fields such as acoustics, electromagnetic field theory and fluid mechanics. The existence of integral equations for scalar wave problems in terms of unknown potential functions dates back to Kirchoff (1883). However, the use of boundary integral equations to solve the scalar wave problems started in early 1960s with Friedman and Shaw (1962) solving the transient acoustic wave scattering problem followed by Banaugh and Goldsmith (1963b) solving the steady-state (time harmonic) wave scattering problem. Since then a number of researchers have contributed in this field. Both transient and steady-state behavior have been analyzed for wave scattering as well as radiation problems. A radiation problem is one where a given displacement or velocity field is specified on a part of the surface. A problem wherein an obstacle with a prescribed boundary conditions (usually homogeneous) interacts with some incident wave field generated by sources elsewhere is called a scattering problem. It should be mentioned that both of the above problems are related to infinite or semi-infinite space where boundary element method has no competitor.

Some comparisons of the BEM against the FDM and the FEM are provided by Schenck (1967) for time-harmonic, acoustic scattering and radiation, Shaw (1970) for transient and time-harmonic, acoustic scattering and radiation, Chertock (1971) and Kleinman and Roach (1974) for acoustic problems, and Mittra (1973) for the electromagnetic case. For water wave problems, the boundary-integral-equation approach has been used by Garrison and Seetharama (1971) and Garrison and Chow (1972), with success. Recent works on scalar wave problems include that of Shaw (1975a,b), Shippy (1975), Meyer et al (1977), Morita (1978), Davis (1976), Groenenboom (1983), Mansur and Brebbia (1982), and Misljenovic (1982).

It should be noted that the scalar wave problem is much simpler than the elastodynamic problem because of the reduced dimensionality of the parameters involved in scalar problems and because the analytic complexities of the fundamental solutions are also not so severe.

III.2 TWO-DIMENSIONAL STRESS ANALYSIS

(A) Transient Dynamics

The existing work on two-dimensional linear transient elastodynamic or visco-elastodynamic problems can be categorized into the following four groups.

(i) Fourier domain solution: In this approach, the time domain response is reconstructed by Fourier synthesis of the steady-state solutions obtained by a frequency domain BEM formulation. This approach has been used by Banaugh and Goldsmith (1963b), Niwa et al (1975, 1976), and Kobayashi et al (1975, 1982). Banaugh and Goldsmith solved a problem of elastic wave scattering, Niwa et al and Kobayashi et al solved the problem of wave scattering by cavities of arbitrary shape due to the passage of travelling waves. Kobayashi and Nishimura (1982) also introduced a technique for the problems of fictitious eigenfrequency in certain exterior problems.

(ii) Laplace domain solution: This approach involves solution of the problem in the Laplace-transform domain by the BEM followed by a numerical inverse transformation to obtain the response in the time domain. Doyle (1966) was the first to develop a Laplace domain formulation by BEM, but he did not solve any problem while Cruse (1967) presented numerical results for the two-dimensional problem of the elastic halfspace under transient load in plane strain. Numerical results using this approach have been also presented by Cruse and Rizzo (1968) and Manolis and Beskos

(1981).

(iii) Time domain solution: In this approach, the problem is formulated in the time domain by the BEM and solved through a step-by-step time integration scheme. The fundamental solution used in this approach is a function of time and has time retarding properties. This approach has been used by Cole et al (1978) for the anti-plane strain case (i.e. one-dimensional problem), by Niwa et al (1980) for the two-dimensional wave scattering problem, by Rice and Sadd (1984) for anti-plane strain wave scattering problem, and by Spyrakos (1984) for strip-footing problems.

(iv) Domain integral transform approach: In this approach the domain integral related to the inertia term is transformed into a boundary integral by approximating the displacements inside the domain. This results in a finite element type matrix differential equation formulation which can be solved by using a direct time integration procedure such as the Wilson theta method, Houbolt method etc. This approach has been used by Brebbia and Nardini (1983) to solve a two-dimensional simple frame. This method uses a static Green's function instead of time embedded Green's functions and therefore it cannot satisfy the radiation condition nor can it reproduce the actual transient response at early times. Because of the radiation condition, it cannot be used for semi-infinite problems where the BEM has a definite edge over all other numerical methods.

A comparison of the first three approaches on the basis of their accuracy and efficiency was done by Manolis (1983). It should be noted that, in the above, some simple two-dimensional or anti-plane strain elastodynamic problems were solved such as: (a) the case of an unlined or lined circular cylindrical cavity under the passage of longitudinal or transverse waves; (b) the cases of square or horseshoe shaped cylindrical cavities under longitudinal waves; (c) the case of wave propagation in

half-planes, etc.

Most of the above mentioned work suffers from one or more of the following: lack of generality, crude assumption of constant variation of the field variables in space and time, inadequate treatment of singular integrals, and unacceptable level of accuracy. For example, Cole et al found the transient dynamic formulation to be unstable, leading to a building up of errors as the time stepping progresses; Rice and Sadd found that dominant errors in the method arises from integrating the Green's function over the singularity and the time domain formulation when applied to time harmonic problems reveals solution error propagation; Spyrakos finds his flexible strip results to be affected due to the absence of corner and edges in his modeling (this is a consequence which arises due to the use of constant elements); and Niwa et al (1976) suggest that use of higher approximating techniques for time and space variation of field variables may improve the accuracy and stability of their method. All these fears has been put to rest in the present work by using a higher order interpolation function in time and space, taking care of singular integral in an accurate and elegant manner (Ref. Sec. IV.4), using superior and sophisticated integration techniques and implementing the BEM formulation in a complete and general manner. The time-domain transient algorithm developed in this work is unconditionally stable and capable of producing accurate results for general three-dimensional problems.

(B) STEADY-STATE (PERIODIC) DYNAMICS

Two dimensional steady-state dynamic problems have been solved by using the BEM by a number of researchers, such as, Banaugh and Goldsmith (1963b) and Niwa et al (1975) obtained the steady-state solution of their respective problems before reconstructing the transient response by Fourier

synthesis. Recently, Dravinsky (1982a,b) used a indirect BEM formulation to study two-dimensional problems of plane wave diffraction by subsurface topography, Alarcon and Dominguez (1981) applied the direct BEM to determine the dynamic stiffnesses of 2D rigid strip footings, and Kobayashi and Nishimura (1983) used the direct BEM to obtain steady-state responses of a tunnel and a column in the halfspace subjected to plane waves of oblique incidence. Askar et al (1984) presented an interesting, approximate, iterative boundary-element formulation for steady-state wave scattering problems which does not require any matrix inversion. He presented the results for the problem of wave scattering by a tunnel in half-space. Another interesting study has been done by Nakai et al (1984), they introduced viscous dashpots in a two-dimensional analysis to simulate energy dissipation in the third direction due to radiation. Lately, Estorff and Schmid (1984) has applied the BEM to study the effects of depth of the soil layer, embedment of the foundation, and percentage of hysteretic soil damping on the dynamic stiffness of a rigid strip in a viscoelastic soil. Another work related to rigid strip footing was recently presented by Abascal and Dominguez (1984, 1985), where they studied the influence of a non-rigid soil base on the compliances (flexibility) of a rigid surface footing and response of the rigid surface strip footing to incident waves.

In all the works discussed above, the singularity which arises in the traction kernels (fundamental solution) is not taken into account properly (Ref. Sec. IV.4), and in all of them except that of Kobayashi and Nishimura (1983) it is assumed that the field variables remains constant within an element. As pointed out by Kobayashi and Nishimura, it is crucial to use higher-order boundary elements for boundary modelling of a steady-state dynamic problem so that it is fine enough to be compatible with the wavy

nature of the solution. In addition, it should be noted that none of the above mentioned algorithm, is capable of solving general two-dimensional steady-state elastodynamic or visco-elastodynamic problems because they cannot take care of corner and edges which are always present in a real engineering problem. To remedy all the above discussed problems, this thesis presents a versatile steady-state dynamic algorithm by BEM which is capable of solving two-dimensional problems involving complicated geometries and boundary conditions.

III.3 THREE-DIMENSIONAL STRESS ANALYSIS

Three-dimensional problems of elastodynamics were not attempted until recently principally because of enormous computing requirements and formidable task of numerical implementation. In order to reduce the computation and complications involved, simplifications of the BEM formulation dictated by the nature of the problem to be solved have been developed by a number of workers.

Dominguez (1978a) simplified the steady-state dynamic kernel functions for the special case of periodic surface loading on rectangular foundations. He also used another simplified formulation (1976b) to study the response of embedded rectangular foundations subjected to travelling waves. Karabalis and Beskos (1984) have done similar simplifications to the time domain transient boundary integral formulation. Yoshida et al (1984) used a simplified BEM formulation for determining the response of a square foundation on an elastic halfspace, subjected to periodic loading and harmonic waves. Tanaka and Maeda (1984) have developed a Green's function for two-layered visco-elastic medium, and using this Green function in a simplified BEM formulation they numerically calculated the compliances for a hemispherical foundation. More complex problems

involving the periodic response of piles and pile groups have been attempted by Sen et al (1984, 1985a, 1985b), and Kaynia and Kausel (1982). They simplified the boundary integral formulation so that only displacement kernels are involved in the formulation. Some authors (Ref. Apsel, 1979; Dravinski, 1983) have introduced a potentially unstable method involving an 'auxiliary boundary' so that singular integration can be avoided. In all of the above works, the displacements and tractions are assumed to be constant within each element.

Recently, Rizzo et al (1985) and Kitahara and Nakagawa (1985) have implemented the BEM formulation for steady-state elastodynamic problems in a general form. Rizzo also implemented a mixed-transform inversion to obtain the response in the time domain and a technique for the problem of fictitious eigenfrequency in certain exterior problems with homogeneous boundary conditions. Kitahara and Nakagawa have introduced a series expansion of the periodic kernels for low frequency range, to obtain a stable solution at low frequencies.

In the present work, the direct boundary element formulations for periodic dynamic analysis, transformed domain transient analysis and time-domain transient analysis have been implemented for problems involving isotropic, piecewise-homogeneous, three-dimensional solids. These implementations are general and complete in all respects. In addition, for nonlinear transient dynamic analysis of three-dimensional solids, the direct boundary element formulation and its numerical implementation are presented for the first time. To the best of the author's knowledge, a comparable system for steady-state and time dependent analyses by the BEM has not yet appeared in the published literature.

III.4. FREE-VIBRATION ANALYSIS

The existing methods for free-vibration analysis by Boundary element method can be classified into the following two categories:

(A) Determinant search method, and

(B) Domain integral transform method.

(A) Determinant search method:

Most of the existing work on the application of BEM to eigenvalue problems falls into this category. This includes the work of Tai and Shaw (1974), Vivoli and Filippi (1974), DeMey (1976, 1977), Hutchinson (1978, 1985), Hutchinson and Wong (1979), and Shaw (1979) for membrane (Helmholtz equation) and plate vibrations. Niwa et al (1982) also used this method for free-vibration problems of Elasto-dynamics. A review of the existing work by this approach can also be found in Shaw (1979), and Hutchinson (1984).

In this method, after the usual discretization and the integration process, the boundary integral equation for the eigenvalue problem leads to a homogeneous set of simultaneous equations, i.e.

$$[A(\omega)]\{X\} = \{0\} \tag{3.1}$$

where the elements of vector {X} are the unknown boundary conditions at each node and the coefficients of matrix [A] are the transcendental function of the frequency. These coefficients are complex when calculated by using the fundamental solution for the corresponding forced vibration problem (e.g. Tai and Shaw, 1974; Niwa et al, 1982), or real when calculated by using an arbitrary singular solution (e.g. Hutchinson (1978), DeMey (1977)).

The necessary and sufficient condition for equation (3.1) to have a non-trivial solution is

$$D = |A(\omega)| = 0 \qquad (3.2)$$

The eigenvalues are characteristic roots of this determinant. However, in the numerical calculation, the eigenvalue can only be determined as parameters which attain local minima of the absolute value of the determinant, D, as a function of the frequency, ω. This requires the formation of equation (3.1) for a large number of trial frequencies, which makes this method extremely uneconomical for practical applications. Moreover, when the eigenvalues are closely spaced, this method may fail to give correct eigenvalues.

As pointed out by Shaw (1979), this approach also leads to fictitious roots when an arbitrary singular solution is used rather than a fundamental solution. However, Hutchinson (1985) justifies the use of an arbitrary singular solution by stating that one can easily sort out the fictitious roots by a brief look at the mode shapes.

(B) Domain Integral Transform Method:

In this approach, the displacements within the domain are approximated by some suitable functions. Due to this approximation, the domain integral (related to the displacements within the domain) of the integral equation is transformed into boundary integrals by using the divergence theorem. Since all the integrals of the integral equation are now related to the boundary, after some manipulation, the integral equation is reduced to a simple algebraic eigenvalue equation. This method was first proposed by Nardini and Brebbia (1982). A similar way of achieving volume to surface integral conversion has also been outlined recently by Kamiya and Sawaki (1985).

The main advantage of this method is that the boundary integrals need to be computed only once as they are frequency independent rather than

frequency dependent (as in the case of determinant search method). Moreover, since all of the calculations are in terms of real arithmetic, it appears to be economical when compared to the determinant search method. The method proposed in this thesis has some superficial similarities with this method and, therefore, it is briefly reviewed below.

The governing differential equation for free-vibration of an isotropic homogeneous elastic body can be written as:

$$\sigma_{ik,k} + \rho\omega^2 u_i = 0 \tag{3.3}$$

where u_i = components of displacement amplitudes

σ_{ik} = stress tensor components

ω = natural circular frequency

ρ = mass density.

By using the static Kelvin's point force solution the above differential equation can be transformed into an integral representation:

$$c_{ij}u_i(\underline{\xi}) = \int_S G_{ij}(\underline{x},\underline{\xi})t_i(\underline{x})ds - \int_S F_{ij}(\underline{x},\underline{\xi})u_i(\underline{x})ds + \rho\omega^2 \int_V u_i(\underline{z})G_{ij}(\underline{z},\underline{\xi})dv \tag{3.4}$$

where $\underline{x}$ = field point

$\underline{\xi}$ = source point

t_i = traction components = $\sigma_{ik}n_k$

n_k = components of outward normal on the boundary

F_{ij} = traction kernel corresponding to the displacement kernel G_{ij}

$c_{ij} = \delta_{ij} - \beta_{ij}$, where β_{ij} is the jump term.

Equation (3.4) not only contains the unknown displacement $u_i(\underline{x})$ and

the traction $t_i(\underline{x})$ on the boundary, but also the unknown displacements $u_i(\underline{z})$ within the domain appearing in the inertial term. In order to formulate the problem in terms of the boundary unknowns only, the displacements within the domain $u_i(\underline{z})$ are approximated by using a set of unknown coefficients α_{im} and a class of functions $f^m(\underline{z})$ (superscript m denoting the member of the class), such that

$$u_i(\underline{z}) = \alpha_{im} f^m(\underline{z}) \tag{3.5}$$

where

$$f^m(\underline{z}) = c - r(\underline{z},\underline{\xi}_m) \tag{3.6}$$

where c = a suitably chosen constant

$r(\underline{z},\underline{\xi}_m)$ = distance from the point $\underline{\xi}_m$ where the function is applied to a point $\underline{z}$.

With this approximation, the domain integral of equation (3.5) becomes,

$$\int_V u_i(\underline{z}) G_{ij}(\underline{z},\underline{\xi}) dv = \alpha_{im} \int_V f^m(\underline{z}) G_{ij}(\underline{x},\underline{\xi}) dv \tag{3.7}$$

Now if one can find a displacement field ψ^m_{li} with the corresponding stress tensor τ^m_{lik} such that

$$\tau^m_{lik,k} = \delta_{li} f^m \tag{3.8}$$

the volume integral in (3.7) can be transformed into a boundary integral via the divergence theorem. Thus equation (3.4) can be expressed as (Ref. Nardini, 1982).

$$c_{ij} u_i(\underline{\xi}) - \int_S G_{ij}(\underline{x},\underline{\xi}) t_i(\underline{x}) ds + \int_S F_{ij}(\underline{x},\underline{\xi}) u_i(\underline{x}) ds$$

$$= \rho\omega^2 \{-c_{ij}\ \psi_i^m(\xi) + \int_S G_{ij}(\underline{x},\xi)p_{li}^m(\underline{x})ds - \int_S F_{ij}(\underline{x},\xi)\ \psi_{li}^m(\underline{x})ds\}\alpha_{lm} \tag{3.9}$$

where $p_{li}^m = \tau_{lik}^m n_k$ = traction vector corresponding to the displacement field ψ_{li}^m, where

$$\psi_{li}^m = \left[\frac{1-2\nu}{5-4\nu}\, c + \frac{r}{30(1-\nu)}\right] y_l y_i - \frac{9-10\nu}{90(1-\nu)}\,\delta_{li} r^3 \tag{3.10}$$

After the usual discretization and integration process, equation (3.10) can be written in a matrix form as

$$[F]\{u\} - [G]\{t\} = \rho\omega^2([G]\{p\} - [F]\{\psi\})\{\alpha\} \tag{3.11}$$

The relationship between $\{u\}$ and $\{\alpha\}$ can be established using equation (3.5), i.e.

$$\{u\} = [Q]\{\alpha\} \tag{3.12}$$

where elements of matrix $[Q]$ are simply the values of the functions $f^m(\underline{z})$ at the nodal points.

Since matrix $[F]$ is square and possess an inverse, therefore

$$\{\alpha\} = [Q]^{-1}\{u\} \tag{3.13}$$

It is important to note that $[Q]$ is a fully populated matrix and therefore its inversion is costly for a realistic problem.

Substituting (3.13) into (3.11), we obtain

$$[F]\{u\} - [G]\{t\} = \omega^2[M]\{u\} \tag{3.14}$$

where

$$[M] = \rho([G]\{p\} - [F]\{\psi\})[Q]^{-1} \tag{3.15}$$

Equation (3.14) is now written in a submatrix form as follows:

$$\begin{bmatrix} F_{11} & F_{12} \\ F_{21} & F_{22} \end{bmatrix} \begin{Bmatrix} u_1 \\ u_2 \end{Bmatrix} - \begin{bmatrix} G_{11} & G_{12} \\ G_{21} & G_{22} \end{bmatrix} \begin{Bmatrix} t_1 \\ t_2 \end{Bmatrix} = \omega^2 \begin{bmatrix} M_{11} & M_{12} \\ M_{21} & M_{22} \end{bmatrix} \begin{Bmatrix} u_1 \\ u_2 \end{Bmatrix} \tag{3.16}$$

where u_1 and u_2 are the displacement vectors related to boundaries s_1 and s_2 respectively, and t_1 and t_2 are the traction vectors related to boundaries s_1 and s_2 respectively.

The homogeneous boundary conditions state that on any part of the boundary either u or t is zero. Therefore, assuming $u_1 = 0$ and $t_2 = 0$:

$$[F_{12}]\{u_2\} - [G_{11}]\{t_1\} = \omega^2[M_{12}]\{u_2\} \tag{3.17}$$

$$[F_{22}]\{u_2\} - [G_{21}]\{t_1\} = \omega^2[M_{22}]\{u_2\} \tag{3.18}$$

From these two sets of equations, $\{t_1\}$ can be eliminated resulting in:

$$[\bar{F}]\{u_2\} = \omega^2[\bar{M}]\{u_2\} \tag{3.19}$$

Equation (3.19) represents the generalized eigenvalue problem.

Although the method outlined above (first proposed by Nardini and Brebbia) eliminates much of the difficulties of the determinant search techniques, it still has a number of deficiencies as a practical problem solving tool:

(1) the form of proposed approximation for the internal displacements via equation (3.5) seems to be based on a rather ad hoc basis,

(2) it is rather difficult to find the displacement tensor ψ_{li} and the corresponding stress tensor τ_{lik} to satisfy equation (3.8) for more complex problems such as axi-symmetric and three-dimensional ones or those involving inhomogeneity and anisotropy,

(3) the matrix algebra involved in the construction of the final system equations via (3.13), (3.16-18) restricts the method essentially to small test problems. In particular, equation (3.19) cannot be formed for a multi-region problem where the interface traction and displacements must remain in the system equations for the algebraic eigenvalue problem.

In addition to the two above discussed methods, Benzine (1980) presented a mixed boundary-integral finite-element approach for plate vibration problems which also reduces the problem to a standard algebraic eigenvalue problem. However, his approach is computationally more expensive than the Nardini and Brebbia's (1982) method.

CHAPTER IV

ADVANCED TWO-DIMENSIONAL STEADY-STATE DYNAMIC ANALYSIS

IV.1 INTRODUCTION

In this chapter an advanced numerical implementation of the boundary element formulation for the periodic dynamic analysis of two-dimensional problems is described. In this implementation, isoparametric curvilinear boundary elements are used. The present analysis is capable of treating very large, multizone problems by substructuring and satisfying the equilibrium and compatibility conditions at the interfaces. With the help of this substructuring capability, problems related to layered media and soil-structure interaction can be analyzed.

In the next few sections, the governing equations of elastodynamics are presented followed by a discussion on the boundary element formulation of elasto-dynamic problems in the transformed domain. Subsequently, materials pertaining to the numerical implementation and the solution algorithm are introduced. A number of numerical examples are finally presented to demonstrate the accuracy of the present implementation.

IV.2 GOVERNING EQUATIONS

The governing differential equation of linear elastodynamics for homogeneous, isotropic, linear elastic bodies is called Navier-Cauchy equation, which is expressed as

$$(c_1^2 - c_2^2)u_{i,ij} + c_2^2 u_{j,ii} + b_j = \ddot{u}_j \qquad (4.1)$$

where $u_i(\underline{x},T)$ is the displacement vector and b_j is the body force vector. Indices i and j corresponds to cartesian coordinates; these ranges from 1 to 2 for two-dimensional problem and 1 to 3 for three-dimensional problems. Commas indicate differentiation with respect to space, dots indicate differentiation with respect to time T, and repeated

indices imply the summation convention.

The constants c_1 and c_2 are the propagation velocities of the dilatation (P-wave) and distorsional (S-wave) waves, respectively, and are given as

$$c_1^2 = (\lambda + 2\mu)/\rho \qquad c_2^2 = \mu/\rho \tag{4.2}$$

where λ and μ are Lamé constants and ρ is the mass density.

In equation (4.1) the displacement u_i is assumed to be twice differentiable with respect to space and time, except at possible surfaces of discontinuity due to shock wave propagations. The kinematical and dynamical conditions related to the propagating surfaces of discontinuity are discussed in Appendix B.

Finally, the constitutive equations for the homogeneous, isotropic, linear elastic material are of the form

$$\sigma_{ij} = \rho[(c_1^2 - 2c_2^2)u_{m,m}\delta_{ij} + c_2^2(u_{i,j} + u_{j,i})] \tag{4.3}$$

where σ_{ij} is the stress tensor and

δ_{ij} is the Kronecker delta.

IV.3 THE BOUNDARY-INITIAL VALUE PROBLEMS OF ELASTODYNAMICS

For a well posed problem, the governing differential equations (4.1) and constitutive equations (4.3) have to be accompanied by the appropriate boundary and initial conditions. Thus, the displacements $u_i(\underline{x},T)$ and tractions $t_i(\underline{x},T)$ must satisfy the boundary conditions

$$u_i(\underline{x},T) = q_i(\underline{x},T) \qquad \underline{x} \in S_u$$

$$t_i(\underline{x},T) = \sigma_{ij}(\underline{x},T)n_j(\underline{x}) = p_i(\underline{x},T) \quad \underline{x} \in S_t \quad \text{for } T > 0 \tag{4.4}$$

where n_j is the outward unit normal at the surface,

S_u is the part of the surface where displacements are specified,

S_t is the part of the surface where tractions are specified and the bonding surface of the body is $S = S_u + S_t$,

and the displacements and velocities satisfy the initial conditions:

$$u_i(\underline{x},T=0) = U_{io}(\underline{x}) \qquad \underline{x} \in V+S$$

$$\dot{u}_i(\underline{x},T=0) = U_{io}(\underline{x}) \qquad \underline{x} \in V+S \tag{4.5}$$

In addition, the displacements and velocities have to satisfy the Sommerfeld radiation condition at infinity.

The proof of the existence and uniqueness of the boundary-initial value problems of elastodynamics was first provided by Neumann (1995) for a bounded region. Later, it is extended to the infinite domain by Wheeler and Sternberg (1968). These proofs are discussed in detail in Miklowitz (1980, Secs. 1.11 and 1.12), Eringen and Suhubi (1974, Chapter V), Achenbach (1973, Sec. 3.2) and Hudson (1980, Sec. 5.3).

IV.4 BOUNDARY INTEGRAL FORMULATION

In many practical applications, it is desirable to predict the dynamic response of structures under harmonic excitation. If we assume that enough time has elapsed after the initial excitation, the transient part of the response will vanish and we will be dealing only with the steady-state motion. This problem of steady-state motion can be formulated by taking the Fourier or Laplace transform of the equations of motion.

In steady-state, the excitation and response both are harmonic, therefore, the displacement and traction will have the form

$$u_i(\underline{x},T) = \bar{u}_i(\underline{x},\omega)e^{-i\omega T}$$

$$t_i(\underline{x},T) = \bar{t}_i(\underline{x},\omega)e^{-i\omega T}$$

where ω is the circular frequency,

$\bar{u}_i$ is the amplitude of the displacement,

$\bar{t}_i$ is the amplitude of the traction, and

$i = \sqrt{-1}$

Substitution of (4.6) into the governing differential equation (4.1) and cancellation of the common factor $e^{-i\omega T}$ yields the Helmholtz equation

$$(c_1^2 - c_2^2)\bar{u}_{i,ij} + c_2^2\bar{u}_{j,ii} + \rho\omega^2\bar{u}_j = 0 \qquad (4.7)$$

The time variable is thereby eliminated from the governing differential equation and the initial-value-boundary-value problem reduces to a boundary value problem only. In equation (4.7) the body force is assumed to be zero.

Similarly, substitution of (4.6) in the constitutive equation (4.3) and cancellation of the common factor $e^{-i\omega T}$ yields:

$$\bar{\sigma}_{ij} = \rho\,[(c_1^2 - 2c_2^2)\bar{u}_{m,m}\delta_{ij} + c_2^2(\bar{u}_{i,j} + \bar{u}_{j,i})] \qquad (4.8)$$

where $\bar{\sigma}_{ij}$ is the stress amplitude, and is given by

$$\bar{\sigma}_{ij} = \bar{t}_i\, n_j \qquad (4.9)$$

Similarly, application of Laplace transform to the governing equation (4.1) under zero initial conditions and zero body force, and to the constitutive equation (4.3) yields

$$(c_1^2 - c_2^2)\bar{u}_{i,ij} + c_2^2\bar{u}_{j,ii} - s^2\bar{u}_j = 0 \tag{4.10}$$

$$\bar{\sigma}_{ij} = \rho[(c_1^2 - 2c_2^2)\bar{u}_{m,m}\delta_{ij} + c_2^2(\bar{u}_{i,j} + \bar{u}_{j,i}) \tag{4.11}$$

$$\bar{\sigma}_{ij}n_j = \bar{t}_i \tag{4.12}$$

where the Laplace transform $\bar{f}(\underline{x},s)$ of a function $f(\underline{x},T)$ with respect to T is defined as

$$L\{f(\underline{x},T)\} = \bar{f}(\underline{x},s) = \int_0^\infty f(\underline{x},T)e^{-sT}dt \tag{4.13}$$

where s is the Laplace transform parameter.

A comparison of equation (4.7)-(4.9) with (4.10)-(4.12) indicates that the steady-state, elastodynamic problem can be solved in the Laplace domain if the complex Laplace transform parameter s is replaced by $-i\omega$, ω being the circular frequency. It should also be noted that the transformed Navier-Cauchy equations are now elliptic, and thus more amenable to numerical solutions.

The boundary integral equation in the Laplace transformed domain can be derived by combining the fundamental, point-force solution of equation (4.10) with the Graffi's dynamic reciprocal theorem (Graffi, 1947), as

$$c_{ij}(\underline{\xi})\bar{u}_i(\underline{\xi},s) = \int_S [\bar{G}_{ij}(\underline{x},\underline{\xi},s)\bar{t}_i(\underline{x},s) - \bar{F}_{ij}(\underline{x},\underline{\xi},s)u_i(\underline{x},s)]dS(\underline{x}) \tag{4.14}$$

In the above equation, $\underline{\xi}$ and $\underline{x}$ are the field points and source points, respectively, and the body force and initial conditions are assumed to be zero. The fundamental solutions $\bar{G}_{ij}$ and $\bar{F}_{ij}$ (Ref. Cruse and Rizzo, 1968) are the displacements and tractions at $\underline{x}$, resulting from a unit harmonic force of the form $e^{-i\omega T}$ (or e^{sT}) at $\underline{\xi}$ and are listed in

Appendix A1. It can be seen that these fundamental solutions have modified Bessel functions embedded in them. The asymptotic series expansions of these functions for small and large values of argument (i.e. frequencies) are also discussed in the Appendix A1.

The tensor c_{ij} of equation (4.14) can be expressed as:

$$c_{ij} = \delta_{ij} - \beta_{ij} \tag{4.15}$$

where β_{ij} is the discontinuity (or jump) term and it has the following characteristics: (i) for a point $\underline{\xi}$ inside the body $\beta_{ij} = 0$, (ii) for a point $\underline{\xi}$ exterior to the body $\beta = \delta_{ij}$, and (iii) for a point $\underline{\xi}$ on the surface it is a real function of the geometry of the surface in the vicinity of $\underline{\xi}$. For Liapunov smooth surfaces, $\beta_{ij} = 0.5\ \delta_{ij}$.

Once the boundary solution is obtained, equation (4.14) can also be used to find the interior displacements; and the interior stresses can be obtained from

$$\bar{\sigma}_{jk}(\underline{\xi},s) = \int_S [\bar{G}^{\sigma}_{ijk}(\underline{x},\underline{\xi},s)\bar{t}_i(\underline{x},s) - \bar{F}^{\sigma}_{ijk}(\underline{x},\underline{\xi},s)\bar{u}_i(\underline{x},s)]dS(\underline{x}) \tag{4.16}$$

The functions $\bar{G}^{\sigma}_{ijk}$ and $\bar{F}^{\sigma}_{ijk}$ of the above equation are listed in Appendix A3.

The stresses at the surface can be calculated by combining the constitutive equations, the directional derivatives of the displacement vector and the values of field variables in an accurate matrix formulation (Ref. Sec. IV.5.H). Also, the loads and moments on the elements can be obtained by numerically integrating the known tractions on the elements.

The boundary integral formulation can also take account of internal viscous dissipation of energy (damping); this can be accomplished by

replacing the elastic parameters λ and μ (Lame constants) by their complex counterparts λ^* and μ^* .

$$\lambda^* = \lambda(1 + 2i\beta)$$
$$\mu^* = \mu(1 + 2i\beta) \qquad (4.17)$$

leaving Poisson's ratio unaltered. By analogy with single degree-of-freedom systems, the damping ratio β is equal to $\omega\eta/2\mu$, where η is the coefficient of viscosity for a Kelvin-Voigt model.

IV.5 NUMERICAL IMPLEMENTATION

The boundary integral equation (4.14) cannot be solved analytically and therefore resort must be made to the numerical methods of solution. The basic steps involved in a numerical solution process for the boundary element formulation are:

(i) Discretization of the boundary into a series of elements over which the geometry and the variation of displacements and tractions are approximated by using a suitable set of shape functions.

(ii) Application of the equation (4.14) in discretized form to each nodal point of the boundary and thereby evaluation of the integrals by a numerical quadrature scheme.

(iii) Assembly of a set of linear algebraic equations by imposing the boundary conditions specified for the problem.

(iv) Finally, the system of equation are solved by standard methods to obtain the unknown boundary tractions and displacements.

In the present work, the numerical implementation of the transformed boundary element formulation for two-dimensional problems of elastodynamics has the following aspects and features:

(A) Representation of Geometry and Functions

For the discretization of equation (4.14) the boundary S is approximated by using a series of elements whose geometry is defined using the quadratic shape functions of intrinsic coordinates proposed by Ergatoudis (1968). The boundary elements for two-dimensional problems are shown in figure 4.1. On each element the variation of the cartesian coordinates $x_i(\eta)$ are approximated as:

$$x_i(\eta) = N_\alpha(\eta) X_{i\alpha} \tag{4.18}$$

where $X_{i\alpha}$ are the nodal coordinates of the element, and N_α are the interpolation functions (Ref. Appendix C1). For a quadratic variation α ranges from 1 to 3, and for a linear variation it ranges from 1 to 2.

Isoparametric shape functions are used to approximate the variation of displacements and tractions over each element. In some cases, the full quadratic variation of the field quantities is not required so the option of using the linear, the quadratic or a mixture of linear and quadratic interpolation functions for displacement and traction variation is provided. However, the boundary is always modeled using the quadratic shape functions. Using the interpolation functions, the displacement and traction at an arbitrary point of a boundary element are expressed in terms of nodal values of displacements and tractions by:

$$\bar{u}_i(\eta) = N_\alpha(\eta)\bar{u}_{i\alpha}$$

$$\bar{t}_i(\eta) = N_\alpha(\eta)\bar{t}_{i\alpha} \tag{4.19}$$

where η is the intrinsic coordinate which ranges from 0 to 1, and

$u_{i\alpha}$ and $t_{i\alpha}$ are the values of the displacement and traction vectors at node α.

(B) Substructuring Capability

In the present implementation, the substructuring capability is provided. This is a very useful tool for solving problems related to piecewise homogeneous material, layered media and soil-structure interaction. This technique actually allows a problem geometry to be modelled as an assembly of several generic modeling regions (GMR). The GMRs are joined by enforcing appropriate compatibility conditions across common boundary elements.

(C) Numerical Integration

Taking into account the boundary discretization and function representation, the transformed, boundary-integral equation (4.14) can be written as:

$$c_{ij}(\underline{\xi})\bar{u}_i(\underline{\xi},s) = \sum_{q=1}^{Q} \left[\int_{S_q} [\bar{G}_{ij}(\underline{x}(\eta),\underline{\xi},s)N_\alpha(\eta)\bar{t}_{i\alpha}dS(\underline{x}(\eta)) \right.$$

$$\left. - \int_{S_q} \bar{F}_{ij}(\underline{x}(\eta),\underline{\xi},s)N_\alpha(\eta)\bar{u}_{i\alpha}(\underline{x}(\eta)) \right] \qquad (4.20)$$

In the above equation, S_q is the length of the qth element and Q is the total number of elements. In order to express $dS(\underline{x})$ in intrinsic coordinates, we have

$$dS(\underline{x}) = |J|\, d\eta \qquad (4.21)$$

where $|J|$ is the Jacobian which performs the transformation from the cartesian coordinate system (x,y) to the elements intrinsic coordinate system η, and is given by

$$|J(\eta)| = \left[\frac{dN_\alpha(\eta)}{d\eta} X_{1\alpha}\right]^2 + \left[\frac{dN_\alpha(\eta)}{d\eta} X_{2\alpha}\right]^2 \qquad (4.22)$$

Therefore, in view of the above, the equation (4.20) can be written as

$$c_{ij}(\underline{\xi})\bar{u}_i(\underline{\xi},s) = \sum_{q=1}^{Q}\left[\sum_{\alpha=1}^{A}\bar{t}_{i\alpha}\int_0^1 \bar{G}_{ij}(\underline{x}(\eta),\underline{\xi},s)N_\alpha(\eta)|J|d\eta\right.$$

$$\left. - \sum_{\alpha=1}^{A}\bar{u}_{i\alpha}\int_0^1 \bar{F}_{ij}(\underline{x}(\eta),\underline{\xi},s)N_\alpha(\eta)|J|d\eta\right] \qquad (4.23)$$

where A is the number of nodes in an element.

The global system of boundary element equations is obtained by the usual nodal collocation scheme, i.e., by allowing field point $\underline{\xi}$ in equation (4.23) to coincide sequentially with all the nodal points of the boundary. All the boundary integrals involved are calculated numerically. Essentially two types of integrals, singular and nonsingular, are involved. The integrals are singular if the field point for which the equations being constructed lies on the element being integrated. Otherwise, the integrals are nonsingular although numerical evaluation is still difficult if the field point and the element being integrated are close to each other.

In both singular and nonsingular cases a Gaussian quadrature scheme is used. The basic technique was first developed by Lachat (1975) and is discussed in detail by Watson (1979) and Banerjee and Butterfield (1981). For the nonsingular case, an approximate error estimate for the integrals was developed by Lachat based on the work of Stroud and Secrest (1966). This allows the determination of element subdivisions and orders of Gaussian integration which will assure roughly uniform precision of integrations throughout the integration process. In the present work, this automatic choice of integration order and element subdivision has been

implemented: where the order of integration points varies from 2 to 12 and the number of element subdivisions varies from 1 to 4. When the field point is very close to the element being integrated, use of a uniform subdivision of the element leads to excessive computing time. Therefore, in order to improve efficiency while still retaining accuracy, a graded element subdivision is employed. This subelement division grows geometrically away from the point closest to the field point on the element being integrated.

In the case of singular integration, which arises when the field point is on the element being integrated, the elementsis divided into subelements. The nature of this division depends on the node of singularity of the element. This division produces nonsingular behavior in all except one of the required integrals. Normal Gaussian rules are used, with orders 4 to 8. The integral of the traction kernel times the shape function which is 1.0 at the source point is still singular and cannot be numerically evaluated with reasonable efficiency and accuracy. Hence, this integral is evaluated indirectly by a scheme discussed in the next section.

The integration of the surface integrals required for the calculation of displacement and stress at interior points are carried out in the same manner as that for boundary values (described above) except, in this case, all the integrals are nonsingular.

(D) Evaluation of the Diagonal Blocks of $\bar{F}$ Matrix

The diagonal 2x2 block (or 3x3 block for three-dimensional problems) of the assembled $\bar{F}$ matrix contains the tensor c_{ij} as well as the Cauchy principal value of the traction kernel integral, i.e.

$$\bar{D}_{ij} = c_{ij} + \int_{S_1} \bar{F}_{ij} N_1 \, dS \tag{4.24}$$

where:

c_{ij} is the term which depends only on the geometry at the singular node,

$\bar{D}_{ij}$ is the diagonal 2x2 (or 3x3 for 3D) blocks of the assembled $\bar{F}$ matrix for the dynamic problem,

$\bar{F}_{ij}$ is the singular traction kernel for the dynamic problem,

N_1 is the shape function for the singular node, and

S_1 is the length of the singular element.

Similarly for a static problem:

$$D^S_{ij} = c_{ij} + \int_{S_1} F^S_{ij} N_1 \, dS \tag{4.25}$$

where the variables are the static counterpart of those of equation (4.24).

From (4.24) and (4.25) we can obtain

$$\bar{D}_{ij} = D^S_{ij} + \int_{S_1} (\bar{F}_{ij} - F^S_{ij}) N_1 \, dS \tag{4.26}$$

In the above equation, the diagonal blocks D^S_{ij} of coefficients of the traction matrix, for a static problem of the same geometry can be obtained by using the rigid body motion, i.e.

$$D^S_{ij} = c_{ij} + \int_{S_1} F^S_{ij} N_1 dS$$

$$= - \Big[\sum_{\alpha=2}^{A} \int_{S_1} F^S_{ij} N_\alpha dS + \sum_{q=2}^{Q} \sum_{\alpha=1}^{A} \int_{S_q} F^S_{ij} N_\alpha dS \Big] \tag{4.27}$$

In addition, the integral involving the difference $(\bar{F}_{ij} - F^S_{ij})$ is nonsingular, therefore, equation (4.26) can be used to obtain $\bar{D}_{ij}$.

Recently, a somewhat similar approach is used by Rizzo et al (1985) for three-dimensional problems.

In almost all of the past works, the nonsingular integral of equation (4.26) has been neglected. This results in inaccuracy, particularly at high frequencies. However, for problems related to ground surface the above technique is not applicable. Thus, for halfspace problems a new scheme is developed to calculate the diagonal blocks of $\bar{F}$ matrix. This scheme is discussed in the following section.

(E) Diagonal Blocks of $\bar{F}$ Matrix for Problems of Halfspace Having Corners and Edges

The conventional approach of assuming $0.5\delta_{ij}$ as the block diagonal terms of the $\bar{F}$ matrix does not hold true for cases where the geometry of the problem has corners and edges except for the case where the field variables are assumed to be constant within each element. Thus, for higher order variation of the field variables, one needs to have a general method for calculating the diagonal blocks of $\bar{F}$ matrix for halfspace problems. In the present work, a new technique to handle the above discussed problem in an approximate manner has been developed. To this purpose, this new technique uses special types of elements called 'enclosing elements' (Ref. figure 4.2). The basic assumption in this technique is that the displacements and tractions at the enclosing elements has negligible effect on the displacements and tractions at any point on the modeled boundary.

Using this scheme, the diagonal blocks D^s_{ij} of F matrix are obtained by the summation of nonsingular integrations of the static traction kernel over all the boundary elements as well as all the enclosing elements, i.e.

$$D^S_{ij} = -\Big[\sum_{\alpha=2}^{A}\int_{S_1} F^S_{ij}N_\alpha dS + \sum_{q=2}^{Q}\sum_{\alpha=1}^{A}\int_{S_q} F^S_{ij}N_\alpha dS$$

$$+ \sum_{e=1}^{L}\sum_{\alpha=1}^{A}\int_{S_e} F^S_{ij}N_\alpha dS\Big] \qquad (4.28)$$

where the third summation of the integrals corresponds to the enclosing element (L being the total number of enclosing elements). Once D^S_{ij} is evaluated, the diagonal blocks $\bar{D}_{ij}$ related to the dynamic problem can be easily found by using equation (4.26).

In order to show the validity of the above technique, the dynamic response of a rigid strip on an elastic halfspace under vertical loading is analyzed by using this approach and other two approaches. The real and imaginary part of the vertical stiffness for two different frequencies were tabulated in table 4.1 obtained by using all the three approaches for calculating the block diagonals of $\bar{F}$ matrix. It can be seen that results obtained by using the enclosing element technique compares well with the correct results (method 1). However, method 2 which is invariably used by the past researchers gives erroneous result at high frequencies (e.g. compare the real part of the stiffness at non-dimensional frequency $a_o = \omega b/c_2 = 7.0$)

(F) Assembly of System Equations

Once the boundary collocation and integrations are completed, we have a set of coefficients which function as multipliers of field quantities, i.e. (Ref. Banerjee and Butterfield, 1981):

$$[\bar{G}]\{\bar{t}\} - [\bar{F}]\{\bar{u}\} = \{0\} \qquad (4.29)$$

where:

$[\bar{G}]$ is an unassembled matrix whose coefficients are the values obtained by the numerical integration of the product of the tensor $\bar{G}_{ij}$, the shape functions and the Jacobian. The size of matrix $[\bar{G}]$ is dn x dm ;

$[\bar{F}]$ is an assembled (for nodes) matrix whose coefficients are obtained by the numerical integration of the product of the tensor $\bar{F}_{ij}$, the shape functions and the Jacobian. The size of matrix $[\bar{F}]$ is dn x dn ;

$\{\bar{t}\}$ and $\{\bar{u}\}$ are the transformed traction and displacement vectors at the boundary of the problem, with size dm and dn, respectively;

n is the total number of nodes;

$m = \sum_{q=1}^{Q} A_q$, where Q is the total number of elements and A_q is the number of nodes in the qth element; and

d is the dimensionality of the problem (i.e. for two-dimensional problems d = 2).

Since some of the field quantities are known from the specified boundary conditions, during the assembly of the system equations the coefficients related to the known and unknown variables are separated. For the case when the boundary conditions are specified in local coordinate system, the corresponding coefficients of the matrices $[\bar{G}]$ and $[\bar{F}]$ are multiplied by the appropriate local transformation matrix. Finally, boundary conditions are imposed including any required modification to the coefficient matrices for bonded or sliding contact between different regions (GMRs). The results of all the above operations is a linear system of matrix equations of the form:

$$[A]\{x\} = [B]\{y\} = \{b\} \tag{4.30}$$

$$\{u^{in}\} = [A^{u}]\{x\} + [B^{u}]\{y\} \tag{4.31}$$

$$\{\sigma\} = [A^{\sigma}]\{x\} + [B^{\sigma}]\{y\} \tag{4.32}$$

where

$\{y\}$ and $\{x\}$ are the vectors of known and unknown field quantitites, respectively;

$\{u^{in}\}$ and $\{\sigma\}$ are the vectors of displacements and stresses at interior points, respectively.

In any substructured (multi-zone) problem, the matrix [A] in (4.30) contains large blocks of zeros because separate GMRs communicate only through common surface elements. In order to save both storage space and computer time, the matrix [A] is stored in a block basis with zero blocks being ignored. Since interior results in any GMR involves only the boundary values related to that GMR, the matrices in (4.31) and (4.32) are also block diagonal. In addition, for added accuracy the system equations are scaled so that all the coefficients of matrix [A] (and [B]) are of the same magnitudes (for detail, Ref. Banerjee and Butterfield, 1981).

(G) Solution of Equations

Since the system equations (4.30) are complex it requires a complex solver. In the present work, an out-of-core complex solver is developed using softwares from LINPACK (Dongarra et al, 1979). In this solver in order to minimize the time requirements the solution process is carried out using block form of the matrix. Thus, this block banded solver operates at the submatrix level using software from LINPACK to carry out all operations on submatrices. The system matrix is also stored by submatrices on a direct access file. The first operation in the solution process is the

decomposition of the system matrix using the block form of it. This decomposition process is a Gaussian reduction to upper triangular (submatrix) form. The row operations required during the decomposition are stored in the space originally occupied by the lower triangle of the system matrix. Finally, the calculation of the solution vector is carried out by using the decomposed form of the system matrix from the direct access file.

(H) Calculation of Stresses on the Boundary for 2D Problems

Once the boundary solution is obtained, the stress and strain at any point on the boundary can be calculated without any integration by using the procedure outlined as follows.

Let us assume that we are interested in finding stress and strain at a point P, which lies on a boundary element and has intrinsic coordinate η^b. Recalling equations (4.19), we can write:

$$u_i(\eta^b) = \sum_{\alpha=1}^{A} N_\alpha(\eta^b) u_{i\alpha}$$

$$t_i(\eta^b) = \sum_{\alpha=1}^{A} N_\alpha(\eta^b) t_{i\alpha} \qquad (4.33)$$

where:

A is the number of nodes in the element,

N_α is the shape functions, and

$u_{i\alpha}$ and $t_{i\alpha}$ are the nodal values of u_i and t_i.

In addition, we also have the following relationships:

$$t_i = \sigma_{ij} n_j \qquad (4.34)$$

$$\sigma_{ij} = c_{ijkl}\left(\frac{u_{k,l}+u_{l,k}}{2}\right) \tag{4.35}$$

$$u_{i,\eta} = u_{i,j}X_{j,\eta} \tag{4.36}$$

$$u_{i,\eta} = \sum_{\alpha=1}^{A} \frac{\partial N_\alpha}{\partial \eta} u_{i\alpha} \tag{4.37}$$

where:

c_{ijkl} is a tensor containing elastic constants, and

$X_{j,\eta}$ are the directional derivatives.

Equations (4.34), (4.35) and (4.36) can be combined to form a matrix equation:

$$\begin{bmatrix} n_1 & 0 & n_2 & 0 & 0 & 0 & 0 \\ 0 & n_2 & n_1 & 0 & 0 & 0 & 0 \\ 1 & 0 & 0 & -\lambda-2\mu & 0 & 0 & -\lambda \\ 0 & 1 & 0 & -\lambda & 0 & 0 & -\lambda-2\mu \\ 0 & 0 & 1 & 0 & -\mu & -\mu & 0 \\ 0 & 0 & 0 & -n_2 & 0 & n_1 & 0 \\ 0 & 0 & 0 & 0 & -n_2 & 0 & n_1 \end{bmatrix} \begin{Bmatrix} \sigma_{11} \\ \sigma_{22} \\ \sigma_{12} \\ u_{1,1} \\ u_{2,1} \\ u_{1,1} \\ u_{2,2} \end{Bmatrix} = \begin{Bmatrix} t_1 \\ t_2 \\ 0 \\ 0 \\ 0 \\ u_{1,\eta} \\ u_{2,\eta} \end{Bmatrix} \tag{4.38}$$

where n_1 and n_2 are the unit normal on the boundary at point P ; i.e.

$$n_1 = X_{2,\eta} \quad \text{and} \quad n_2 = -X_{1,\eta}$$

Now, the stress and strain at point P can be obtained by inverting the matrix of equation (4.38) and then multiplying the inverted matrix by the right-hand-side vector. For this purpose, the right hand side vector is obtained by using equations (4.33) and (4.37). The procedure described above is valid for both plane stress and plane strain problems. However,

for plane strain problems the Poisson's ratio ν has to be replaced by $\bar{\nu} = \frac{\nu}{1+\nu}$.

IV.6 EXAMPLES OF APPLICATIONS

In order to demonstrate the accuracy and applicability of the present implementation, the detailed solution of three numerical examples are presented. In the first example, the forced oscillations of a massless rigid strip foundation on an elastic halfspace (plane strain) subjected to external dynamic forces is analyzed. The purpose of this example is to compare the response predicted by the present implementation to that available in the literature. The second example is that of a machine foundation embedded in an elastic halfspace (plane strain) and subjected to external dynamic forces, and the third example is a wall in an elastic half-space subjected to a time-harmonic lateral pressure distribution. These last two examples are intended to show the applicability of the present implementation to real engineering problems. In both examples, English units are used with foot (ft.) for length, pound (lbf.) for force, and second (s) for time.

(a) Dynamic Response of a Rigid Strip on an Elastic Halfspace

A large number of numerical results have been published for the rigid strip with vertical, horizontal and rocking vibrations (Karasudhi et al, 1968; Luco et al, 1974; Luco and Westmann, 1972; Wickham, 1977; Hryniewicz, 1981; etc.). However, most of them are limited to a small range of frequency parameter and are based on the assumption that one of the contact stress components is zero. For the purpose of comparison, a rigid strip footing on an elastic halfspace under relaxed boundary conditions is analyzed for vertical, horizontal and rocking vibrations. The rigid strip

footing and the boundary element mesh used are shown in figure 4.3 (this mesh was selected after a convergence study at a high frequency). In all cases, a homogeneous soil material with a Poisson's ratio $\nu = 1/4$ is considered. The dynamic stiffnesses obtained by the present method are compared with that reported by Hryniewicz (1981). He defines the vertical, horizontal and rocking stiffness coefficients by the following expressions respectively:

$$K_{11} + iC_{11} = \frac{P}{\pi\mu w_o} \tag{4.39}$$

$$K_{22} + iC_{22} = \frac{H}{\pi\mu u_o} \tag{4.40}$$

$$K_{33} + iC_{33} = \frac{M}{\pi\mu b^2 \phi_o} \tag{4.41}$$

where:

P, H and M are the amplitudes of vertical force, horizontal force and moment, respectively;

w_o, u_o and ϕ_o are amplitudes of vertical displacement, horizontal displacement and rotation, respectively;

K_{11}, K_{22} and K_{33} are the real parts of the stiffness coefficients;

C_{11}, C_{22} and C_{33} are the imaginary parts of the stiffness coefficients;

2b is the width of the footing;

μ is the shear modulus of the soil; and

$i = \sqrt{-1}$

The real part of the stiffness coefficients are plotted against non-dimensional frequency ($a_o = \omega b/c_2$, where ω is the excitation frequency)

in figure 4.4. It can be seen that the present results are in good agreement with the results of Hryniewicz (1981) for low to medium frequencies. However, for higher frequencies the the agreement is not good, particularly for rocking stiffness. This difference is due to the fact that in the present work quadratic shape functions are used for representation of the variation in the boundary variables over each element whereas Hryniewicz assumes that the unknown contact stresses are constant within each element. This results in stress discontinuities at the interface of two elements. Therefore at high frequencies, Hryniewicz's method will produce correct results only when the foundation-soil interface is divided into a very large number of elements. Figure 4.5 shows the plot of imaginary part of the stiffness coefficients against the nondimensional frequency a_o. A good agreement between the present results and the results due to Hryniewicz can be seen. Real and imaginary parts of vertical stiffness for a bonded rigid strip are also plotted in figures 4.4 and 4.5, respectively. The imaginary part is identical to that of a frictionless rigid strip.

Dynamic contact-stress distributions at the interface between the rigid strip and the halfspace are also presented. For the purpose of plotting, the contact stresses are defined as follows:

For vertical vibration:

$$\sigma_{zz} = -\frac{\pi\mu w_o}{b}\,(\bar{\sigma}^R_{zz} + i\,\bar{\sigma}^I_{zz})e^{i\omega T}$$

$$\sigma_{xz} = -\frac{\pi\mu w_o}{b}\,(\bar{\sigma}^R_{xz} + i\,\bar{\sigma}^I_{xz})e^{i\omega T} \qquad (4.42)$$

For horizontal vibration:

$$\sigma_{zz} = -\frac{\pi\mu u_o}{b}(\bar{\sigma}^R_{zz} + i\,\bar{\sigma}^I_{zz})e^{i\omega T}$$

$$\sigma_{xz} = -\frac{\pi\mu u_o}{b}(\bar{\sigma}^R_{xz} + i\,\bar{\sigma}^I_{xz})e^{i\omega T} \qquad (4.43)$$

For rocking:

$$\sigma_{zz} = -\pi\mu\phi_o(\bar{\sigma}^R_{zz} + i\,\bar{\sigma}^I_{zz})e^{i\omega T}$$

$$\sigma_{xz} = -\pi\mu\phi_o(\bar{\sigma}^R_{xz} + i\,\bar{\sigma}^I_{xz})e^{i\omega T} \qquad (4.44)$$

where superscripts R and I represent real and imaginary parts, respectively.

The real and imaginary parts of the contact stress distribution for vertical vibration are plotted in figures 4.6 and 4.7, respectively. Because of the singularity at the edge, the contact stresses on the element close to the edge are obtained in an average sense (by taking the average of nodal values) and are indicated by dashed lines. From the figures, it can be seen that the contact stresses are quite sensitive to variations in the frequency parameter a_o. As frequency increases, the imaginary part of the contact stress distribution increases and the singularities at the edge gets sharper for real and imaginary parts. Figures 4.8, 4.9, 4.10 and 4.11 shows the dynamic contact stress distributions for horizontal vibration and rocking. In all cases, the preceding comment about the singularities at the edge holds true.

(b) Dynamic Response of a Machine Foundation Embedded in the Elastic Halfspace

In order to show the applicability of the present implementation for solving real engineering problems, the dynamic stiffnesses of a machine foundation (made of concrete) embedded in the halfspace are computed. Dynamic contact stress distributions at the interface between the foundation and the soil are also presented. The machine foundation and the boundary element discretization for this problem are shown in figure 4.12. The discretization of the soil free-surface are the same as in figure 4.3. The substructuring technique is used in solving this problem, i.e., the concrete foundation is modeled as one GMR (or region) and the halfspace as another GMR. The contact between the foundations and the soil is assumed to be welded (or glued), and the weight of the foundation is considered automatically by the analysis. This problem has corners and edges, and therefore, enclosing elements are used to obtain the diagonal blocks of the $\bar{F}$ matrix. The conventional approach of using $0.5\delta_{ij}$ as the diagonal blocks cannot be used for this type of problem which has corners and edges.

The material properties are as follows:

Soil:	Elastic modulus,	$E_s = 8.64 \times 10^5$
	Poisson's ratio,	$\nu_s = 0.3$
	Mass Density,	$\rho_s = 3.57$
Foundation:	Elastic modulus,	$E_c = 4.527 \times 10^8$
	Poisson's ratio,	$\nu_c = 0.17$
	Mass density,	$\rho_c = 4.5$

In order to compute the foundation stiffnesses, unit displacements and unit rotation are prescribed on the top face of the foundation with zero traction conditions being imposed along the soil free-surface. Upon the solution of boundary equations, the tractions over the element at the soil-

foundation interface are obtained. The resultant of these tractions for different rigid body motions gives the foundation stiffness coefficients. The real and imaginary parts of the stiffnesses (minus the inertial contribution of the foundation block) are plotted against the frequency parameter a_o in figures 4.13 and 4.14, respectively. It can be seen that, in general, the stiffnesses in this case are greater than that of a rigid strip. This is understandable, because the embedment reduces the maximum frequency response (Ref. Estorff and Schmid, 1984) and therefore increases the stiffness. Figures 4.15 and 4.16 show the real and imaginary parts of the contact stresses between the foundation and the soil for vertical vibration whereas figures 4.17 and 4.18 show the same for rocking of the foundation. It is obvious from the results, that at higher frequency the stresses at the edge are more severe.

(c) Dynamic Response of a Wall on an Elastic half-space Subjected to a Time Harmonic Lateral Pressure Distribution

A wall with its base embedded in an elastic half-space is subjected to a time-harmonic lateral pressure distribution as depicted in figure 4.19. The dimensions of the wall and its base are shown in figure 4.19. The material properties of the wall, its base and half-space are the same as those of the machine foundation of example (b).

The boundary element discretization of the wall consists of 20 quadratic line elements, and its base is modelled by 17 quadratic line elements. The discretization of the soil free-surface is the same as in figure 4.3. Plane strain conditions are assumed for the present problem.

The distribution of the applied lateral pressure is shown in figure 4.19. It can be seen that it is a triangular pressure distribution with maximum pressure $P(t) = 600$ psf at the free end of the wall. This problem is analyzed by using two different approaches to model the half-

space, namely, (i) continuum model , and (ii) spring-dashpot model. For the spring-dashpot model, the values of stiffness coefficients are calculated by assuming the base of the wall to be rigid, and using the present dynamic algorithm by following a procedure similar to that described in example (a). The lateral displacements along the loaded face of the wall are plotted in figure 4.20. From this figure, it can be seen that the results obtained by using spring-dashpot model are almost similar to those obtained by using continuum model for the half-space. This example shows the usefulness of the present algorithm for obtaining the response of a structure partially embedded in a half-space in one single step or in two-steps, i.e. by using spring-dashpot approach.

In all of the examples presented in this section, the material damping is neglected because for halfspace problems the radiation damping is dominant and the material damping is negligible. However, the present implementation has the capability for the inclusion of material damping (Ref. Sec. IV.4).

IV.7 CONCLUDING REMARKS

An advanced implementation of the direct boundary element method for dynamic analysis of two-dimensional problems in the frequency domain is presented. By comparing the results with those obtained by other methods, the accuracy and the stability of the present method is established. Since only the boundary of the region of interest has to be discretized instead of the whole domain, the proposed methodology is a better alternative to the conventional finite element method, particularly for the solution of soil-structure interaction problems. For soil-structure interaction problems the finite element method presents two restraints: (i) the model must be bounded at the bottom by rigid bedrock, and (ii) the soil away from

the vicinity of the foundation is represented by parallel layers unbounded on the horizontal direction. These two conditions are not always close to reality. On the other hand, in Boundary element method, the fundamental solution satisfies the radiation condition at infinity and therefore no bounding surfaces are needed and only a small number of elements is necessary to model the problem. Furthermore, the numerical implementation employed here is one of the most general currently available and can be used in conjunction with substructuring technique to solve not only the problems of layered media and soil-structure interactions, but also any problem of two-dimensional solids of complicated geometry and connectivity.

Table 4.1. Vertical compliance of a rigid strip footing on half-space, by using three different methods to obtain the diagonal blocks of $[\bar{F}]$ matrix

	Real part of the stiffness at $a_o = 2.0$	Imaginary part of the stiffness at $a_o = 2.0$	Real part of the stiffness at $a_o = 7.0$	Imaginary part of the stiffness at $a_o = 7.0$
Method 1	0.330	2.24	0.408	7.85
Method 2	0.335	2.27	0.456	7.81
Method 3	0.334	2.27	0.410	7.81

Method 1: using $0.5\,\delta_{ij} + \int_{\Delta S} (\bar{F}_{ij} - F^{S}_{ij})ds$ as the diagonal blocks.

Method 2: using $0.5\,\delta_{ij}$ as the diagonal block.

Method 3: using enclosing elements.

CHAPTER V

FREE VIBRATION ANALYSIS OF TWO-DIMENSIONAL PROBLEMS

V.1 INTRODUCTION

In this chapter a new method for free-vibration analysis by BEM is presented. It utilizes a fictitious vector function to approximate the inertia forces and then uses the well known concept of complementary functions and particular integrals to solve the resulting governing differential equations. This method not only reduces the problem of free-vibration to an algebraic eigenvalue problem but also saves the computation time by having fewer matrix manipulations as compared to that of the domain integral transformed method (outlined earlier in III.4). Because of the generalized form proposed here it can be used for multi-region problems and extensions to axi-symmetric problems as well as those involving inhomogeneity and anisotropy are possible. Some example problems, such as a triangular cantilever plate, a square cantilever plate, a cantilever beam, a shear wall and a fixed elliptic arch are presented to establish the accuracy, efficiency and convergence of this new method.

V.2 GOVERNING EQUATION:

The governing differential equation for free-vibration of an elastic, homogeneous and isotropic body can be written as:

$$(\lambda + \mu) \frac{\partial^2 u_j}{\partial x_i \partial x_j} + \mu \frac{\partial^2 u_i}{\partial x_j \partial x_j} + \rho\omega^2 u_i = 0 \qquad (5.1)$$

where:

λ and μ are Lame's constants,

u_i = displacement amplitudes

ρ = mass density

ω = natural circular frequency.

V.3 PARTICULAR INTEGRAL:

The governing differential equation (5.1) can also be written in differential operator notation as

$$L(u_i) + \rho\omega^2 u_i = 0 \tag{5.2}$$

The solution of the above equation can be represented as the sum of a complementary function u_i^c satisfying

$$L(u_i^c) = 0 \tag{5.3}$$

and a particular integral u_i^p satisfying

$$L(u_i^p) + \rho\omega^2 u_i = 0 \tag{5.4}$$

However, equation (5.4) still contains the unknown displacement field u_i within the domain, which can be eliminated by using an unknown fictitious density function ϕ and a known function C , exactly as in an indirect boundary element analysis (Ref. Banerjee and Butterfield, 1981). More specifically:

$$u_i(\underline{x}) = \sum_{m=1}^{\infty} C_{ik}(\underline{x}, \underline{\xi}^m)\phi_k(\underline{\xi}^m) \tag{5.5}$$

where ϕ_k is a fictitious density and

C_{ik} is a known function which can be selected as any linear function of spatial coordinates.

The above approximation in the inertia term is a valid practice in other numerical methods such as the use of lumped mass matrix in finite element method. This is possible because the inertia term does not contain any derivative and, hence, it can be approximated by using simpler functions.

A simple function which is selected for C_{ik} in the present analysis has the form:

$$C_{ik}(\underline{x},\underline{\xi}^m) = \delta_{ik}(R - r) \tag{5.6}$$

where:

R = largest distance between two points of the body

r = distance between $\underline{x}$ (field point) and $\underline{\xi}^m$ (source point).

On the basis of above assumption (5.5), equation (5.4) can be written as

$$L(u_i^p) + \rho\omega^2 \sum_{m=1}^{\infty} C_{ik}(\underline{x},\underline{\xi}^m)\phi_k(\underline{\xi}^m) = 0 \tag{5.7}$$

Now, the particular integral u_i^p can be chosen as any function which satisfies the differential equation (5.7). Accordingly it can be represented as:

$$u_i^p(\underline{x}) = \sum_{m=1}^{\infty} D_{ik}(\underline{x},\underline{\xi}^m)\phi_k(\underline{\xi}^m) \tag{5.8}$$

The displacement field satisfying equation (5.7) is found to be

$$D_{ik}(\underline{x},\underline{\xi}^m) = \frac{\rho\omega^2}{\mu}\left[(c_1 r - c_2 R)\delta_{ik} r^2 - c_3 y_i y_k r\right]$$

where: $y_i = x_i - \xi_i^m$

$$c_1 = \frac{2(d+3)(1-\nu)-1}{18(3d-1)(1-\nu)}$$

$$c_2 = \frac{1-2\nu}{2[(1+d)-2\nu d]}$$

$$c_3 = \frac{1}{6(3d-1)(1-\nu)}$$

ν = Poisson's ratio, and

d = dimensionality of the problem (e.g. for 2D problems, $d = 2$).

For 2-D analysis;

$$D_{ik} = \frac{\rho\omega^2}{\mu}\left[\left\{\frac{(9-10\nu)}{90(1-\nu)}\, r - \frac{1-2\nu}{6-8\nu}\, R\right\}\delta_{ik} r^2 - \frac{1}{30(1-\nu)}\, y_i y_k r\right] \qquad (5.9)$$

By comparing the functions C_{ik} and D_{ik} (for 2D) with the corresponding functions f^m (eq. 3.6) and ψ^m_{li} (eq. 3.10) of Nardini's method, it can be seen that even though the functions C_{ik} and f^m are similar, their displacement functions D_{ik} and ψ^m_{li} are different from each other. One of the reasons for this difference is that the function D_{ik} satisfies the governing differential equation (5.7) but the function ψ^m_{li} does not. Instead, the function ψ^m_{li} satisfies the differential equation (3.8) which has the form:

$$L(\psi^m_{li}) = \delta_{li} f^m \qquad (5.10)$$

The surface traction t^p_i related to the displacement u^p_i can be determined using the strain-displacement relationship and constitutive equation and is given by:

$$t^p_i(\underline{x}) = \sum_{m=1}^{\infty} T_{ik}(\underline{x}, \underline{\xi}^m)\phi_k(\underline{\xi}^m) \qquad (5.11)$$

where:

$$T_{ik}(\underline{x},\underline{\xi}^m) = \rho\omega^2 \left[(c_4 r - c_5 R)y_k n_i + (c_6 r - 2C_2 R)y_i n_k + \{(c_6 r - 2c_2 R)\delta_{ik} - 2c_3 y_i y_k / r\} y_j n_j\right] \tag{5.12}$$

and:

$$c_4 = \frac{(d+3)\,\nu - 1}{3(3d-1)(1-\nu)}$$

$$c_5 = \frac{2\,\nu}{(1+d)-2\nu d}$$

$$c_6 = \frac{(d+2)-(d+3)\nu}{3(3d-1)(1-\nu)}$$

V.4 BOUNDARY ELEMENT FORMULATION:

The boundary values of real displacements and tractions u_i and t_i can be related to the complementary and particular integral via:

$$u_i = u_i^c + u_i^p \tag{5.13}$$

$$t_i = t_i^c + t_i^p \tag{5.14}$$

The boundary integral equation related to the displacement function u_i^c can be written as

$$c_{ij}(\underline{\xi})u_i^c(\underline{\xi}) = \int_S \left[G_{ij}(\underline{x},\underline{\xi})t_i^c(\xi) - F_{ij}(\underline{x},\underline{\xi})u_i^c(x)\right] ds(\underline{x}) \tag{5.15}$$

where $G_{ij}(\underline{x},\underline{\xi})$ and $F_{ij}(\underline{x},\underline{\xi})$ are the fundamental solution of equation

(5.3) (Ref. Banerjee and Butterfield, 1981), i.e., $G_{ij}(\underline{x},\underline{\xi})$ is the resulting displacement at any point $\underline{x}$ in direction i of an infinite medium due to a static unit force acting at a point $\underline{\xi}$ in direction j, and $F_{ij}(\underline{x},\underline{\xi})$ is the resulting traction.

By usual discretization of boundary S, we can express equation (5.15) in matrix form as

$$[G]\{t^c\} - [F]\{u^c\} = \{0\} \tag{5.16}$$

Equation (5.16) can be solved once the displacements u_i^c and the tractions t_i^c are expressed using equation (5.13) and (5.14) in terms of real displacement u_i and traction t_i, i.e.

$$[G]\{t\} - [F]\{u\} = [G]\{t^p\} - [F]\{u^p\} \tag{5.17}$$

where vectors $\{t^p\}$ and $\{u^p\}$ can be obtained at boundary nodes from equations (5.8) and (5.11) as

$$\{u^p\} = \rho\omega^2 [D]\{\phi\} \tag{5.18}$$

$$\{t^p\} = \rho\omega^2 [T]\{\phi\} \tag{5.19}$$

Substituting these equations into equation (5.17), we obtain

$$[G]\{t\} - [F]\{u\} = \rho\omega^2([G][T] - [F][D])\{\phi\} \tag{5.20}$$

Recalling that

$$u_i(\underline{x}^n) = \sum_{m=1}^{\infty} \delta_{ij}(R - r^{nm})\phi_j(\underline{\xi}^m)$$

where r^{nm} is the distance between the points $\underline{x}^n$ and $\underline{\xi}^m$, we can express this relationship between the displacements and the fictitious

density at all boundary nodes as:

$$u_i^n = \delta_{ij} P^{nm} \phi_j^m$$

$$\phi_j^m = \delta_{ij} K^{nm} u_i^l \qquad (5.21)$$

where $K^{nm} = (P^{nm})^{-1}$

It should be mentioned here that we only have to invert a NxN matrix [P] instead of [Q] (as in the case of Nardini's method, eq. 3.12), a dNxdN matrix, where d = 2 and 3, respectively for two and three-dimensional problems and N is the total number of boundary nodes of the problem.

We can now write (5.21) as

$$\{\phi\} = [K]\{u\} \qquad (5.22)$$

Substituting $\{\phi\}$ from equation (5.22) into equation (5.20), we get

$$[G]\{t\} - [F]\{u\} = \rho\omega^2([G][T] - [F][D])[K]\{u\} \qquad (5.23)$$

or $$[G]\{t\} - [F]\{u\} = \rho\omega^2[M]\{u\} \qquad (5.24)$$

Equation (5.24) can also be written in terms of known and unknown variables as

$$[A]\{x\} - [B]\{y\} = \rho\omega^2([\bar{M}]\{x\} - [M^*]\{y\}) \qquad (5.25)$$

Since all the known variables are zero, (i.e. specified boundary conditions are either $u_i = 0$ or $t_i = 0$) equation (5.25) reduced to

$$[A]\{x\} = \rho\omega^2[\bar{M}]\{x\} \qquad (5.26)$$

.

The modified mass matrix $[\bar{M}]$ contains zero in its sub-columns related to specified displacements (i.e. fixed boundaries).

V.5 EIGENVALUE EXTRACTION:

Equation (5.26) is an algebraic expression for the eigenvalue problem which can be solved by using a eigenvalue extraction subroutine. It should be noted that both the matrices $[A]$ and $[\bar{M}]$ are fully populated and nonsymmetric. There is no satisfactory eigenvalue extraction routine available for efficient determination of eigenvalues of such a system. In the present work the algorithm developed by Moller and Stewart (1973) was utilized. The necessary set of subroutines were developed by Garbow (1980) of Argonne National Laboratory. In general a nonsymmetric fully populated system such as (5.26) cannot be guaranteed to provide real eigenvalues. However, it will be seen from the examples presented in this chapter that the eigenvalues of (5.26) are in fact real.

V.6 ADVANTAGES OF THE PROPOSED METHOD:

In comparing this new method with that of Nardini's (1982), the following three important points need to be mentioned:

(i) The final algebraic expression of Nardini's method is in terms of unknown displacements whereas that of this new method is in terms of unknown variables (both displacements and tractions). In a multi-region (piecewise homogeneous) problem both the displacements and tractions are unknown at the interface. Therefore, Nardini's assumption that at any node either the displacement or the traction is zero is not always valid.

(ii) Nardini's approach involves too many matrix manipulations which are costly and somewhat impractical for a realistic practical problem.

(iii) Because of the use of a well-established method of solving any nonhomogeneous differential equation by using complementary functions and particular integrals, we can now utilize a large number of particular integrals already in use in BEM for dealing with centrifugal forces. Many of these have already been developed for axi-symmetric and three-dimensional problems involving anisotropic materials and, with minor modifications, can be made to satisfy the governing differential equation (5.7).

V.7 EXAMPLES OF APPLICATIONS:

(a) Comparison with Nardini and Brebbia (1982)

In order to provide a meaningful comparison between the present method and that described by Nardini and Brebbia, both methods were implemented. Tables 5.1 and 5.2 show the convergence studies of the first four modes of triangular and square cantilever plates of unit thickness under in plane vibration. The triangular plate had a 10-inch depth at the support and an 8-inch span. The square plate was 6 inch deep and had a span of 6 inches. The material parameters were $E/\rho = 10^4$ and $\nu = 0.2$. Three-noded, isoparametric-conforming boundary elements were used to describe both geometry and functions.

Both these problems were also solved by Nardini and Brebbia (1982). The results of the present implementation agree exactly with their quoted results indicating that their analysis has been correctly interpreted. They do not, however, agree well with those given by the new method proposed in this paper for some modes. Specifically, for the triangular cantilever, there is a marked difference in the third mode and small differences exist in all other modes. For the rectangular cantilever once again third-mode response differs significantly but the second mode agrees

quite well.

(b) Comparisons with Finite Element and Beam Theory

The finite element system MHOST (MARC-HOST) was used to analyze a cantilever beam. The beam has a length of 6.5 units and a square (1 x 1) cross section. The finite element mesh (using 8-noded isoparametric elements) was matched with the boundary element mesh to provide the same number of boundary nodes. The first four bending modes from BEM were (0.368, 2.214, 5.591 and 9.986 Hz) and those of the FEM were (0.378, 2.188, 5.583 and 9.908 Hz), indicating good agreement between the two analyses.

Further the mode shapes calculated using the two techniques are indistinguishable. The first and the fourth bending modes are shown in Figure 5.1. It should be noted that the fourth mode displays a nonzero slope near the fixed end. This real feature of the two-dimensional solution is absent in the beam theory with the imposed fixed end boundary conditions normally used in the beam theory. The material parameters for the beam are assumed to be $E/\rho = 10^4$ and $\nu = 0$.

In order to study the convergence of the results with an increase in number of boundary elements, a similar cantilever having a span of 6.0 inches was analyzed. Figure 5.2 shows the convergence of the first six modes plotted against the boundary mesh numbers. Total number of boundary elements is equal to 2x(Mesh number + 2) (Ref. Fig. 5.3). The convergence is excellent for the first six modes. Since this analysis is fully two-dimensional rather than based on beam or column theory, it provides both the axial and flexural modes. In addition, some of the higher modes (not shown here) have mixed responses. As expected, a finer discretization is required for higher modes of vibration. Even the most slowly convergent case, the fifth (the fourth flexural) mode required only 8 boundary elements. This indicates that the present analysis could be further

developed to provide a powerful analytical tool for free vibration analysis.

Figure 5.2 also shows the beam theory results for modes 1, 2 and 4 (the first three flexural modes). The increasing departure of the results from the beam theory is due almost entirely to the neglect in beam theory of shear distortion. Approximate modifications of the beam theory results for a simply supported beam (Ref. Clough and Penzien, 1975) to account for this effect indicate frequency reductions of approximately the magnitude observed.

(c) An Example of a Shear Wall

In order to compare the results obtained from the proposed method with those from the Finite element method and Nardini's BEM, a shear wall with four square openings was analyzed for in-plane vibration. The boundary element and the finite element meshes (Ref. Nardini and Brebbia, 1982) are shown in Figure 5.4. The material parameters were $E/\rho = 10^4$ and $\nu = 0.2$.

Table 5.3 shows free-vibration periods for the first eight modes. The first mode is identically same as that obtained by FEM. The present results for 2nd, 3rd and 5th modes are also close to the FEM results. The results from the present analysis agree well with those reported by Nardini for 4th, 6th, 7th and 8th modes. However, they do not agree well for the rest of the modes.

(d) An Example of an Arch with Square Openings

An arch in plane stress and fully fixed at the supports was analyzed (Figure 5.5) for in-plane vibration. Four different cases involving the full arch with or without openings and symmetric halves with or without openings were considered. The material parameters were $E/\rho = 10^7$ and

$\nu = 0.2$.

Table 5.4 shows the natural frequencies of the full arch with and without openings. In general the natural frequencies are reduced due to the presence of openings which affects some modes more than others. Similar results for the symmetrical half of the arch are shown in Table 5.5. In this latter case, of course, some of the nonsymmetric modes of the full arch are absent. Modes 1 and 6 of the full arch are identical to the first two modes of the symmetric half.

V.8 CONCLUDING REMARKS:

A new method based on the well known technique of solving a nonhomogeneous differential equation by complementary function and particular integrals for the analysis of free vibration problems by boundary element is presented. The method has been compared with that of Nardini and Brebbia (1982) and found to yield different results for some of the higher modes of vibration. It has also been compared with MARC-HOST finite element analysis and was found to yield essentially similar results for a cantilever beam problem. When the beam theory is corrected for the shear deformation, the analytical results tend to agree well with those of the present analysis.

The present analysis can be easily extended to axi-symmetric and three-dimensional problems involving inhomogeneity and anisotropy by utilizing a number of particular integrals already in use in boundary element analysis.

TABLE 5.1: Time Periods of Free Vibration of a Triangular Cantilever Plate

Number of Elements	Mode 1		Mode 2		Mode 3		Mode 4	
	Nardini's method	New method	Nardini's method	New method	Nardini's method	New method	Nardini's method	New method
3	0.415	0.432	0.216	0.207	0.174	0.138	0.089	0.081
6	0.415	0.430	0.223	0.212	0.200	0.180	0.097	0.095
9	0.416	0.430	0.225	0.212	0.206	0.189	0.108	0.104
12	0.416	0.430	0.226	0.212	0.210	0.191	0.113	0.109
15	0.416	0.430	0.226	0.212	0.212	0.192	0.119	0.111
18	--	0.430	--	0.212	--	0.192	--	0.112

TABLE 5.2: Time Periods of Free Vibration of a Square Cantilever Plate

Number of Elements	Mode 1		Mode 2		Mode 3		Mode 4	
	Nardini's method	New method	Nardini's method	New method	Nardini's method	New method	Nardini's method	New method
4	0.536	0.561	0.232	0.235	0.195	0.172	0.109	0.107
6	0.545	0.568	0.234	0.237	0.214	0.179	0.118	0.116
8	0.559	0.581	0.236	0.238	0.210	0.185	0.127	0.122
10	0.562	0.581	0.236	0.238	0.209	0.187	0.129	0.123
12	0.563	0.584	0.237	0.238	0.209	0.187	0.131	0.125
16	--	0.585	--	0.238	--	0.187	--	0.125

TABLE 5.3: Time Periods of Free Vibration of a Shear Wall

Modes	1	2	3	4	5	6	7	8
FEM (SAPIV)	3.029	0.885	0.824	0.526	0.409	0.342	0.316	0.283
Nardini's BEM	3.022	0.875	0.822	0.531	0.394	0.337	0.310	0.276
New Method	3.029	0.878	0.823	0.533	0.400	0.337	0.311	0.276

TABLE 5.4: Free vibration modes of full arch without and with openings (Hz)

Modes	Without openings	With openings
1	87.8	78.9
2	124.1	113.5
3	177.4	146.8
4	230.9	212.4
5	275.7	235.0
6	380.7	265.5
7	428.1	401.1
8	506.1	537.1
9	622.0	590.9
10	648.0	595.2

TABLE 5.5: Free vibration modes of the symmetric half of the arch without and with openings (Hz)

Modes	Without openings	With openings
1	123.9	113.4
2	378.9	264.4
3	429.3	395.7
4	649.4	590.5
5	820.1	670.6

CHAPTER VI

ADVANCED THREE-DIMENSIONAL STEADY-STATE DYNAMIC ANALYSIS

VI.1 INTRODUCTION

In this chapter, an advanced implementation of the direct boundary element method applicable to the steady-state dynamic analysis of problems involving three-dimensional solids of arbitrary shape and connectivity is presented. Isoparametric curvilinear surface elements are used for mapping geometry and for approximating variation of the field variables. In the present implementation, substructuring capability is incorporated for solving problems involving piecewise-homogeneous materials such as problems of layered media and soil-structure interaction. Also provided is a feature called built-in-symmetry; this allows one to solve the problems having geometric and loading symmetry by modelling only a part of the actual geometry. In this chapter, the discussion starts with the boundary element formulation for steady-state dynamics followed by techniques related to the numerical implementation. The assembly and solution algorithms for general three-dimensional problems are the same as those for two-dimensional problems (Ref. Secs. IV.4.G and IV.4.H), and therefore they are not repeated in this chapter. Finally, a number of numerical examples are presented to demonstrate the accuracy and applicability of the present implementation. This dynamic analysis technique seems to provide an accurate and efficient tool for solving truly three-dimensional problems and particularly those relevant for problems of soil-structure interaction, where it has clear advantages over existing finite element solutions.

VI.2 BOUNDARY INTEGRAL FORMULATION

The boundary integral equation for three-dimensional problems of steady-state elastodynamics is the same as that of two-dimensional problems (eq. 4.13) and it can be expressed as:

$$C_{ij}(\underline{\xi})\bar{u}_i(\underline{\xi},\omega) = \int_S [\bar{G}_{ij}(\underline{x},\underline{\xi},\omega)\bar{t}_i(\underline{x},\omega) - \bar{F}_{ij}(\underline{x},\underline{\xi},\omega)\bar{u}_i(\underline{x},\omega)]dS(\underline{x}) \tag{6.1}$$

The above equation is identical to equation (4.13), except that here the field variables and the fundamental solution are functions of circular frequency ω rather than that of the Laplace parameter s. This is possible because s and ω are interchangeable ($s = -i\omega$). The fundamental solution $\bar{G}_{ij}$ and $\bar{F}_{ij}$ are listed in Appendix A2. It should be noted here that although the functions $\bar{G}_{ij}$ and $\bar{F}_{ij}$ becomes identical to their static counterpart as s tends to zero, it is important to evaluate this limit carefully because of the presence of s in the denominator.

Once the boundary solution is obtained, the stresses at the boundary nodes can be calculated by combining the constitutive equations, the directional derivatives of the displacement vector and the values of the field variables at the boundary nodes in an accurate matrix formulation (Ref. Sec. VI.3.G). Also the loads and moments can be obtained by numerically integrating the known tractions on each element.

For displacements at interior points, equation (6.1) can be used with appropriate C_{ij} tensor (Ref. Sec. IV.3); and the interior stresses can be obtained from

$$\bar{\sigma}_{jk}(\underline{\xi},\omega) = \int [\bar{G}^{\sigma}_{ijk}(\underline{x},\underline{\xi},\omega)\bar{t}_i(\underline{x},\omega) - \bar{F}^{\sigma}_{ijk}(\underline{x},\underline{\xi},\omega)\bar{u}_i(\underline{x},\omega)]dS(\underline{x}) \tag{6.2}$$

The functions $\bar{G}^{\sigma}_{ijk}$ and $\bar{F}^{\sigma}_{ijk}$ in the above equation are listed in Appendix A3.

The constitutive equations and boundary conditions are the same as described in Chapter IV (Ref. Secs. IV.1-IV.3). This boundary integral formulation presented above can also take account of viscous damping (Ref. IV.3).

IV.3 NUMERICAL IMPLEMENTATION:

Since the basic governing equations for dynamic analysis in the transformed space (either in ω or s space) are similar to the corresponding equations for the static analysis, the numerical implementation developed for the static case can be used to extract solution for the dynamic problem for one value of the Laplace transform parameter s or frequency parameter ω. The current numerical implementation of the boundary integral equation for three-dimensional problems of steady-state dynamics has the following aspects and features.

(A) Representation of Geometry and Field Variables

The boundary integral equation (6.1) represents an exact formulation involving integrations over the surface of the domain. Therefore, if one does not make grossly simplified assumptions in the spatial variations of the boundary quantities, accurate solutions can be obtained. To this purpose, each surface is discretized in a number of elements with each element defined in terms of several geometric nodes. All surface-element types employed represent surface geometry using quadratic shape functions. Three sided elements, defined using six rather than eight geometric nodes, are used for mesh transition purposes. The terms quadrilateral and triangle are normally used to refer to the eight and six noded elements although the real geometry represented is, in general, a nonplanar surface patch in three dimensions (Ref. Fig. 6.1). Over each element the variation of field variables can be defined using either the linear or quadratic shape functions. Linear and quadratic elements can share a common side which is then constrained to have linear displacement and traction variation.

In addition to the element types mentioned above, elements which extend to infinity are provided. These elements are designed to allow

modeling of structures connected to the ground and automatically incorporate appropriate decay conditions. The characteristics of the various element types are summarized below (Ref. Appendix C2).

Element type	Geometry Nodes	Field variable Nodes
Linear Quadrilateral	8	4
Linear Triangle	6	3
Quadratic Quadrilateral	8	8
Quadratic Triangle	6	6
Quadratic Infinite	8	3

The cartesian coordinates x_i of an arbitrary point P on a surface element are given in terms of the nodal coordinates $X_{i\alpha}$ as:

$$x_i(p) = N_\alpha(\underline{\eta})X_{i\alpha} \tag{6.3}$$

where $i = 1,2,3$ and $\alpha = 1,2,\ldots,A$, with A the number of nodal points necessary to describe the element. Furthermore, N_α are the shape functions defined in the local or intrinsic coordinate system (η_1,η_2). The Jacobian matrix relating the transformation from the cartesian coordinate system (x,y,z) to the element's intrinsic coordinate system (η_1,η_2) is

$$J_{ij} = (\partial N_\alpha/\partial \eta_j)X_{i\alpha} \tag{6.4}$$

where $j = 1,2$ and the summation convention is again implied for repeated indices such as α.

The field variables are also represented by the same shape functions, i.e.

$$\bar{u}_i(\underline{x}) = N_\alpha(\underline{\eta})\bar{U}_{i\alpha} \quad \text{and}$$

$$\bar{t}_i(\underline{x}) = N_\alpha(\underline{\eta})\bar{T}_{i\alpha} \tag{6.5}$$

where $\bar{U}_{i\alpha}$ and $\bar{T}_{i\alpha}$ are nodal values of the displacements and tractions, respectively, in the transformed domain.

Infinite elements, which are essential if problems involving the half-space are to be solved, can be constructed by modifying the eight-node quadrilateral as shown in Fig. 6.3. The intrinsic coordinate along the dimension of the quadrilateral that we want extended to infinity (say η_1) is modified as

$$\eta_1' = (3\eta_1 + 1)/(1 - \eta_1) \tag{6.6}$$

This way the original interval (-1,1) is mapped into $(-1,+\infty)$. It should be noted that only the three nodes on the side of the infinite element that is adjacent to a surface element belonging to the 'core' region contribute to the system equations. The original shape functions N_α for these three nodes are then modified by the ratio $d = [(x_i-z_i)(x_i-z_i)/(y_i-z_i)(y_i-z_i)]^{1/2}$ for the displacement kernel and d^2 for the traction kernel where x_i are the cartesian coordinates of the integration points, y_i their projection on the common side with the core, and z_i an arbitrary reference point. This type of stretching of a quadrilateral results in a Jacobian determinant equal to $4/(1-\eta_1)^2$ that must be included in the kernel integrations. The infinite element thus obtained reproduces the correct spatial decay of the fundamental singular solutions as $r \to \infty$.

(B) Built-in Symmetry and Sub-structuring Capabilities

In obtaining the numerical solutions, the built-in symmetry capability allows one to solve the problems having geometric and loading symmetry by modeling only a part of the actual geometry. The major steps in this procedure are briefly explained as follows. If the geometry and the boundary condition are symmetric with respect to a plane (or a number of planes), then only that portion of the boundary which lies on the one side

of the plane (or planes) is modeled. The symmetry can be with respect to y-z plane (half-symmetry), y-z and x-z planes (quadrantal symmetry), or y-z, x-z and x-y planes (octan symmetry). The effect of the unmodeled part of the boundary is included according to the following scheme: For all the field points, the contribution of the unmodeled portion to the matrices of coefficients F_{ij} and G_{ij} are accounted for by reflecting the modeled surface elements with respect to the plane (or planes) of symmetry and then integrating over the reflected elements (with proper normals). For the source nodes on the plane (or planes) of symmetry the contributions are added up directly whereas for all other source nodes the correct signs of the contributions are determined by the directions associated with the field variables with respect to the plane (or planes) of symmetry. By avoiding the calculation of identical quantities, this procedure shortens the time required to evaluate the matrices. In addition, it reduces the time required to solve the set of linear equations, because the system matrix will have fewer rows and columns.

The substructuring capability allows a structure to be modeled as an assembly of several generic modeling regions (GMR). The GMRs, each of which must be a complete portion of the structure, are joined by enforcing appropriate compatibility conditions across common surface patches (elements). This feature can also be used to solve piecewise inhomogeneous problems because the GMRs can have different material properties.

(C) Numerical Integration

In view of the surface elements introduced in the previous section, Eq. (6.1), when integrated over the surface of the problem in question, assumes the following form:

$$c_{ij}(\xi)\bar{u}_i(\xi) = \sum_{q=1}^{Q} \{ \int_{S_q} \bar{G}_{ij}(\underline{x}(\eta),\xi,s)N_\alpha(\eta)dS(\underline{x}(\eta)\bar{T}_{i\alpha}$$

$$- \int_{S_q} \bar{F}_{ij}(\underline{x}(\eta),\xi,s)N_\alpha(\eta)dS(\underline{x}(\eta))\bar{U}_{i\alpha}\} \qquad (6.7)$$

In the above equation, S_q is the surface of the qth element and Q is the total number of elements. The global system of boundary element equations at a given value of s is obtained by the usual nodal collocation scheme, i.e., by allowing point ξ to coincide sequentially with all the nodal points of the boundary.

With the exception of strongly singular traction integrals, all surface integrals in the numerical implementation have been calculated numerically. Since this is the most time consuming portion of the analysis, it is essential to optimize this effort. Essentially two types of integrals, singular and nonsingular, are involved. The integrals are singular if the field point for the equations being constructed lies on the element being integrated. Otherwise, the integrals are nonsingular although numerical evaluation is still difficult if the field point and the element being integrated are close together.

In both the singular and nonsingular cases, Gaussian integration is used. The basic technique is developed in Banerjee and Butterfield (1981) and was first applied in the three-dimensional boundary element method by Lachat and Watson (1976). In the nonsingular case an approximate error estimate for the integrals was developed based on the work of Stroud and Secrest (1966). This allows the determination of element subdivisions and orders of Gaussian integration which will retain a consistent level of error throughout the structure. Numerical tests have shown that the use of

3x3 , 4x4, and 5x5 Gaussian rules provide the best combination of accuracy and efficiency. In the present implementation the 4x4 rule is used for nonsingular integration and error is controlled through element subdivision. Typical element subdivisions into three-node triangles and four node quadrilaterals are shown in Fig. 6.4. The distance R that controls the subdivision process is measured from the field point to the point closest to the field point on the element being integrated. In general, higher values of s require lower integration tolerance leading to more element subdivision. If the field point is very close to the element being integrated, use of a uniform subdivision of the element can lead to excessive computing time. In order to improve efficiency while still retaining accuracy, a graded element subdivision is employed. Based on one-dimensional tests, it was found that the subelement divisions could be allowed to grow geometrically away from the origin of the element subdivision. Numerical tests on a complex three-dimensional problem have shown that a mesh expansion factor as high as 4.0 can be employed without significant degradation of accuracy.

In the case of singular integration, which arises when the field point is on the element being integrated, the element is first divided into triangular sub-elements. The integration over each sub-element is carried out in a polar coordinate system with the origin at the field point. This coordinate transformation produces nonsingular behavior in all except one of the required integrals. Normal Gaussian rules can then be employed. The integral of the traction kernel times the isoparametric shape function which is 1.0 at the source point is still singular and cannot be numerically evaluated with reasonable efficiency and accuracy. Its calculation is carried out indirectly as discussed in Chapter IV, Section 4.D. It has been found that subdivision in the circumferential (angular)

direction is required to preserve accuracy in the singular integration. A maximum included angle of 15 degrees is used. Subdivision in the radial direction has not been found necessary. This process is illustrated in Fig. 6.5 for a quadrilateral element.

The surface integrals required for calculation of displacement and stress at interior points are of the same type as those involved in the boundary problem with the exception that only nonsingular integrals are involved. In general, the integrals appearing in the surface integrals are continuously differentiable and solution accuracy can, therefore, be improved by use of increased integration order.

(D) Calculation of Stresses on the Boundary for 3D Problems

Once the boundary solution is obtained, the stress and strain at any point on the boundary can be calculated without any integration, by using the procedure outlined as follows.

Let us assume that we are interested in finding stress and strain at a point P, which lies in a boundary element and has intrinsic coordinates (η_1^b, η_2^b). Recalling equations (6.5), we can write

$$u_i(\eta_1^b, \eta_2^b) = \sum_{\alpha=1}^{A} N_\alpha(\eta_1^b, \eta_2^b) u_{i\alpha}$$

$$t_i(\eta_1^b, \eta_2^b) = \sum_{\alpha=1}^{A} N_\alpha(\eta_1^b, \eta_2^b) t_{i\alpha} \qquad (6.8)$$

where:

A is the number of nodes in the element,

N_α is the shape functions, and

$u_{i\alpha}$ and $t_{i\alpha}$ are the nodal values of u_i and t_i.

In addition, we also have the following relationships:

$$t_i = \sigma_{ij} n_j \tag{6.9}$$

$$\sigma_{ij} = c_{ijkl}\left(\frac{u_{k,l}+u_{l,k}}{2}\right) \tag{6.10}$$

$$u_{i,\eta} = u_{i,j} X_{j,\eta} \tag{6.11}$$

$$u_{i,\eta} = \sum_{\alpha=1}^{A} \frac{\partial N_\alpha}{\partial \eta} u_{i\alpha} \tag{6.12}$$

where

c_{ijkl} is a tensor containing elastic constants, and

$X_{j,\eta}$ are the directional derivatives.

Equations (6.9), (6.10) and (6.11) can be combined to form a matrix equation:

$$[S]\{p\} = \{q\} \tag{6.13}$$

where [S] is a 15x15 matrix which contains unit normals, a 3x3 unit matrix and material constants; {p} is the unknown vector of σ_{ij} and $\partial u_i / \partial \xi_j$; and {q} is a vector containing the tractions t_i and local derivatives of the displacements at point P .

Finally,the stress and strain at point P can be obtained by inverting the matrix of equation (6.13) and then multiplying the inverted matrix by the right-hand-side vector. For this purpose, the right hand side vector is obtained by using equations (6.8) and (6.12).

VI.4 EXAMPLES OF APPLICATIONS

A number of representative problems were solved in order to test the steady-state solution. In all cases, English units are used with foot (ft) for length, pound (lbf) for mass, and second (s) for time.

(a) Cantilever Subjected to End Shear

A uniform beam with a rectangular cross-section is completely fixed at one end and a uniformly distributed traction $t_y = 1000\, e^{i\Omega T}$, with $\Omega = 314$ r/s, is applied at the other end. Traction-free conditions hold along the sides. The dimensions of the beam are $L = 10$, $w = 1$, and $d = 3$. The material properties are as follows: modulus of elasticity $E = 1.16 \times 10^7$ and mass density $\rho = 2.0$. In order to reproduce the one-dimensional characteristics the Poisson's ratio is assumed to be equal to zero. This cantilevered beam is modelled by 18 quadrilateral surface elements resulting in 56 nodes. In reference to Fig. 6.6, it is observed that the surface elements are arranged closer to the loaded end. This is so because the displacement function varies more sharply at the loaded end than at the fixed end. The same figure plots the absolute value of the vertical displacement $\bar{u}_y$ along the length of the beam at a frequency ω equal to the forcing frequency Ω. The results are in very good agreement with the analytical solution for a flexural beam which was developed from Clough and Penzien (1975).

(b) Cantilever Subjected to Harmonic Transverse Load

The same model discussed in (a) was subjected to a time harmonic patch load as shown in Fig. 6.7. The agreement between the three-dimensional calculation and beam theory (Clough and Penzien, 1975) was, once again, excellent.

(c) Vertical Compliance of a Rigid Square Footing

A rigid square foundation of side length $2b = 2$ is resting on the surface of a homogeneous halfspace under relaxed boundary conditions (i.e., there is no friction between soil and foundation). The halfspace has a shear modulus $\mu = 1.0$, $\nu = 1/3$, and $\rho = 1.0$. The foundation is

subjected to a uniform harmonic vertical displacement u_z of amplitude equal to unity. The surface of the halfspace is traction free. The traction distribution under the foundation obtained by the BEM is integrated to give the total vertical load P_z . The foundation's normalized compliance in the vertical direction is obtained as $C_{vv} = \mu b u_z / P_z$. The two meshes shown in Fig. 6.8 are used for modelling the foundation as well as surface of the halfspace. Since the transformed domain BEM computer program can take advantage of symmetry, only 1/4 of the problem needs to be discretized. The coarse mesh uses 4 and 12 elements to model the foundation and the halfspace, respectively. Note that the outermost 4 elements are infinite elements. This discretization results in 44 nodes. The finer mesh uses 6 and 12 elements for the same purpose. There are 2 infinite elements here and 65 nodes.

This problem was originally solved by Wong and Luco (1976). They numerically integrated the vertical displacement at the surface of a homogeneous halfspace due to a unit point load over the foundation, which was discretized into small squares. This problem was recently revisited by Rizzo et al (1985) using a BEM approach. In their work (Rizzo et al), both frictionless and welded cases are considered and two approaches are used: The exact one employs the halfspace kernels (Lamb's solution) and the approximate one uses the fullspace kernels (Stoke's solution). In both cases, only the rigid foundation is discretized and these two approaches are practically indistinguishable except at the very low frequency range. All three solutions mentioned are plotted in Fig. 6.9, along with the vertical compliance obtained by the present method using the fine mesh. The good agreement between the present results and that of Rizzo et al (1985) should be noticed. However, the major difference between Wong and Luco's results and the boundary element results is due to the fact that

quadratic shape functions are used for representation of the variation in the field variables over each element in the present work as well as that of Rizzo et al whereas Wong and Luco assumed that the unknown contact stresses are uniform within each element which is a crude approximation. Finally, the difference in results obtained by both coarse and fine meshes is contrasted in Table 6.1.

VI.5 CONCLUDING REMARKS

An advanced algorithm based on the direct boundary element method for the steady-state dynamic analysis of structures behaving elastically or viscoelastically has been presented. The numerical implementation employed is one of the most general presently available and can be used in conjunction with substructuring to treat three-dimensional solids of complicated geometry and connectivity. The algorithm is stable and capable of producing very accurate results except perhaps at high frequencies in which case finer meshes are required for better accuracy. Nevertheless, the present method is a viable alternative to algorithms based on finite element methodology. Specifically for halfspace problems, the present method does not require discretization of the domain of the halfspace and the use of energy absorbing elements as is required by the finite element method.

The present method can very easily be extended to solve time-harmonic wave scattering problems by simply adding the displacements due to the incident field on the right hand side of the final system equation.

Table 6.1: Comparison of vertical compliances obtained by using two different meshes

$a_o = \frac{\omega b}{c_2}$	$Re\{C_{VV}(a_o)\}$		$Im\{C_{VV}(a_o)\}$	
	Coarse Mesh	Fine Mesh	Coarse Mesh	Fine Mesh
0.5	0.118	0.117	-0.057	-0.058
1.0	0.064	0.069	-0.083	-0.081
1.5	0.032	0.034	-0.076	-0.070
2.0	0.021	0.018	-0.059	-0.052
2.5	0.015	0.015	-0.052	-0.048
3.0	0.010	0.012	-0.036	-0.037
3.5	0.005	0.006	-0.035	-0.032
4.0	0.004	0.004	-0.027	-0.027

CHAPTER VII

TRANSIENT DYNAMIC ANALYSIS BY LAPLACE TRANSFORM

VII.1 INTRODUCTION

In this chapter, an advanced implementation of the transformed domain boundary element formulation applicable to transient dynamic problems involving two and three-dimensional solids of arbitrary shape and connectivity is presented. Using the correspondence principle (Lee, 1955), the transient dynamic problem is first solved in the Laplace transform space and then time domain solutions are obtained by numerical transform inversion. The transformed governing equations and the transformed boundary element formulation are presented in Chapter IV (Sec. 4). The materials pertaining to the fundamental singular solutions and the numerical implementation of the boundary integral equation for one value of Laplace transform parameter are discussed in Chapter IV (Secs. 4-5) and Chapter VI (Secs. 2-4) for two and three-dimensional problems, respectively. This chapter starts with a discussion on the Laplace transformed equations of elastodynamics followed by numerical inversion of Laplace transform. Numerical examples are finally presented and, through comparisons with available analytical and numerical results, the stability and high accuracy of this dynamic analysis technique are established.

VII.2 LAPLACE TRANSFORMED EQUATIONS OF ELASTODYNAMICS

The governing differential equation of linear elastodynamics in Laplace transform domain can be written as:

$$(c_1^2 - c_2^2)\bar{u}_{i,ij} + c_2^2\bar{u}_{j,ii} + \bar{b}_j - s^2\bar{u}_j + \dot{U}_{jo} + sU_{jo} = 0 \qquad (7.1)$$

With the assumption of zero initial condition and absence of body force, the above equation reduces to:

$$(c_1^2 - c_2^2)\bar{u}_{i,ij} + c_2^2\bar{u}_{j,ii} - s^2\bar{u}_j = 0 \qquad (7.2)$$

Since the boundary condition and the constitutive equations do not involve time derivatives, their Laplace transforms are simply:

$$\bar{u}_i = \bar{q}_i(\underline{x},s)$$

$$\bar{t}_i = \bar{\sigma}_{ij}n_j = \bar{p}_i(\underline{x},s)$$

$$\bar{\sigma}_{ij} = \rho\,[(c_1^2 - 2c_2^2)\bar{u}_{m,m}\delta_{ij} + c_2^2(\bar{u}_{i,j} + \bar{u}_{j,i})] \qquad (7.3)$$

Finally, the boundary integral equation in Laplace transform domain has the form

$$c_{ij}(\underline{\xi})\bar{u}_i(\underline{\xi},s) = \int_S [\bar{G}_{ij}(\underline{x},\underline{\xi},s)\bar{t}_i(\underline{x},s) - \bar{F}_{ij}(\underline{x},\underline{\xi},s)\bar{u}_i(\underline{x},s)]\, dS(\underline{x}) \qquad (7.4)$$

The main advantage of casting the equations in the Laplace transform domain is that the equations of motion become elliptic partial differential equations, and as such are more amenable to numerical solutions than their hyperbolic counterparts in the time domain. The numerical solution of the transient elastodynamic problem in the Laplace-transform domain essentially consists of a series of solutions to a static-like problem for a number of discrete values of the transformed parameter s. The final solution is, of course, then obtained by a numerical inversion of the transformed domain solutions to the time domain.

VII.3 DIRECT LAPLACE TRANSFORM OF BOUNDARY CONDITIONS

In order to solve equation (7.4), the boundary conditions have to be transformed to the Laplace domain. As the input boundary conditions are

piecewise linear in time, a numerical scheme is used to transform the boundary conditions from time domain to Laplace domain. The formula used for this purpose is exact for the forcing functions (i.e. boundary conditions in our case) which are piecewise linear in time, and is given by

$$\bar{f}(\underline{x},s) = \sum_{n=1}^{N-1} \frac{1}{s^2 \Delta T} \{\Delta F(e^{-sT_n} - e^{-sT_{n+1}}) + s\Delta T(F_n e^{-sT_n} - F_{n+1} e^{-sT_{n+1}})\} \tag{7.5}$$

where:

$F_n = f(\underline{x},T_n)$ = value of f at time T_n , and

$\Delta F = F_{n+1} - F_n$

The above formula is tested for a number of trial functions (such as $\cos\omega t$, e^{-T}, $\log T$, etc.) for $N = 20$ and $N = 50$. The average error for $N = 50$ is 0.5 percent and that for $N = 20$ is 1.2 percent. Therefore, (7.5) can also be used for taking Laplace transform of any arbitrary loading function.

VII.4 NUMERICAL INVERSION OF TRANSFORM DOMAIN SOLUTION

After numerically integrating equation (7.4) over the surface and imposing known boundary conditions, the final system equations can be assembled to the form

$$[\bar{A}]\{\bar{X}\} = [\bar{B}]\{\bar{Y}\} \tag{7.6}$$

All expressions in the above equation are dependent on the transform parameter s . Therefore, for a transient dynamic problem, the above equation is formed and solved for $\{X\}$ for a spectrum of values of the transform parameter.

Finally, all that remains to be done is to invert the solutions back to the real time domain. In general, transformation from the Laplace transform domain back to the time domain by analytical methods is impossible except for simple functions. Therefore, numerical evaluation of the inverse Laplace transform is imperative. The inverse Laplace transform can be defined as

$$f(\underline{x},T) = \frac{1}{2\pi i}\int_{\gamma-i\infty}^{\gamma+i\infty} \bar{f}(\underline{x},s)e^{sT}ds \quad , \quad i = \sqrt{-1} \tag{7.7}$$

where γ (> 0) is arbitrary but greater than the real part of all the singularities of $\bar{f}(\underline{x},s)$ and s is a complex number with $Re(s) \geq \gamma > 0$.

The various methods available for numerical inverse Laplace transformation may be grouped (Ref. Narayanan, 1982) as follows: (a) Interpolation-collocation methods, (b) methods based on expansion of orthogonal functions, and (c) methods based on numerical Fourier transforms.

In this work, Durbin's (1974) method is used because of its high accuracy (Ref. Manolis et al, 1981; and Ahmad et al, 1985). Durbin's method is classified under group (c) and combines both the Fourier sine and the cosine transforms to arrive at the inversion formula:

$$f(\underline{x},T_j) = 2\left(\frac{e^{j\gamma\Delta T}}{T_N}\right)\left[-0.5\ Re\{\bar{f}(\underline{x},\gamma)\} + Re\left\{\sum_{n=o}^{N-1}(A(n) + iB(n))W^{jn}\right\}\right] \tag{7.8}$$

where

T_N = total time interval of interest,

$$S_n = \gamma + i\frac{2\pi n}{T_N} \quad , \quad W = e^{i2\pi/N} \quad ,$$

$$A(n) = \sum_{l=o}^{L} \mathrm{Re}\{\bar{f}(\underline{x},\gamma + i(n + lN)\frac{2\pi}{T_N})\} \quad , \quad \text{and}$$

$$B(n) = \sum_{l=o}^{L} \mathrm{Im}\{\bar{f}(\underline{x},\gamma + i(n + lN)\frac{2\pi}{T_N})\} \tag{7.9}$$

Thus, the numerical values of $f(\underline{x},T)$ are computed at N equally spaced time points $T_j = j\Delta T$, $j = 0,1,2,\ldots,N-1$. For best results, it is suggested that the product LxN must range from 50 to 5000 and γT_N from 5 to 10 . The computations involved in equation (7.8) are performed by employing the Fast Fourier algorithm of Cooley and Tukey (1965). In case of the Fourier transform ($s = -i\omega$), the above algorithm is equivalent to a Fourier synthesis.

The above algorithm was tested for a number of trial functions (Ref. Ahmad, 1983). For $L = 1$, $N = 200$, and $\gamma T_N = 6$ the numerical inversion results were highly accurate. Using $N = 20$ and neglecting the results for very early time steps (up to $t = 0.05T$) and for late time (after $t = 0.75T$) introduces a maximum error of only 2-3 percent and an average error of 0.6 percent. Since use of $N = 20$ results in very substantial savings in computation time, this option is employed for three-dimensional problems and the results are plotted up to 15 time steps (i.e. $T = 0.75T_N$). However, for two-dimensional problems both $N = 20$ and $N = 50$ are used.

VII.5 EXAMPLES OF APPLICATIONS

In order to demonstrate the range and accuracy of the transformed domain solution with the numerical inverse transformation, a series of examples are presented ranging from a simply supported beam to a cavity in infinite space. The accuracy of the technique developed is compared to the available analytical and numerical results. In all cases, English units

are used with foot (ft) for length, pound (lbf.) for force, and second (s) for time, except otherwise specified.

(A) Two-dimensional Applications

(a) Simply-supported beam subjected to step loading:

A simply supported beam with a rectangular cross-section is subjected to a uniformly distributed step pressure as shown in figure 7.1. The dimensions of the beam are, length L = 30, depth d = 2, and width w = 1. The material properties are, modulus of elasticity $E = 3 \times 10^7$, Poisson's ratio $\nu = 0.3$, and mass density $\rho = 0.733 \times 10^{-3}$. The purpose of this analysis is to compare the solution predicted by the present method with that reported by Bathe et al (1974) by using NONSAP. The Boundary element mesh as well as the finite element mesh are also shown in figure 7.1.

Figure 7.2 shows the response (i.e. deflection at midspan) calculated using BEM and that from NONSAP. The time step used in the finite element solution to obtain the same results from the Wilson θ and the Newmark integration schemes was $\Delta T = 0.5 \times 10^{-4}$ sec; whereas, the time step used in the present analysis is $\Delta T = 0.5 \times 10^{-3}$ sec. In spite of the larger time step, the present analysis produces results identical to that reported in NONSAP. This help confirm the high accuracy and stability of the method presented in this chapter.

(b) Half-space under prescribed time-dependent stress distribution:

In this application, the results obtained by the present transformed domain, transient, dynamic formulation are compared against the solutions from finite difference by Tseng et al (1975) and those from time-domain Boundary elements by Mansur and Brebbia (1985).

The problem to be analyzed is depicted in figure 7.3(a). The half-space was initially at rest and then a part of its surface is disturbed by

a vertical pressure which is continuous in both time and space. Tseng used a transmitting boundary along with a generalized lumped parameter model to analyze this problem. His finite difference grid is shown in figure 7.4(a). The boundary element discretization is shown in figure 7.4(b).

The material properties of the half-space are, modulus of elasticity $E = 200$ ksi, Poisson's ratio $\nu = 0.15$, and mass density $\rho = 1.9534 \times 10^{-4}$ lb-sec^2/in^4. For this problem, the time increments used by Tseng and Mansur and Brebbia was $\Delta T = 1$ msec and $\Delta T = 3.65$ msec, respectively whereas, in the present analysis, a much larger time increment, $\Delta T = 6$ msec, is used.

The time history of the vertical displacements plotted in figures 7.3(b), 7.5, 7.6 and 7.7 are in reasonably good agreement with the previous results, even though a larger time-increment is used in the present analysis. The major difference in the results are in the displacements of point G(150,-10). In Tseng's work, this point is located on the transmitting boundary hence the finite-difference displacements at this point are not accurate. Similarly, in the case of boundary element analysis by Mansur, this point is located just below a boundary node which is a very difficult point to calculate interior displacements In the present analysis, none of the above mentioned problem is present and thus the displacements obtained in the present work is more accurate. The difference between the displacements, at point F(80,-60) obtained by Mansur and Brebbia and present analysis is probably caused by the error due to numerical integrations. The present analysis uses a more sophisticated integration scheme than that used by Mansur and Brebbia and hence the results obtained by the present analysis should be more accurate.

The time history of stresses at points A(45,-75), B(75,-75) and C(5,75) are plotted in figures 7.8, 7.9 and 7.10, respectively. It can be

seen that the results from the present analysis are in very good agreement with the results reported by Tseng during earler times, and are in good agreement with those reported by Mansur and Brebbia during later times. The difference at short times is due to an approximation used by Mansur and Brebbia in the calculation of interior stresses, i.e., the stress at a interior point is obtained by calculating the stresses on a triangular cell with the specified point as its centroid, whereas, the difference at later times is caused by errors generated at the transmitting boundaries used by Tseng. Finally, it should be noted that the results from the present analysis are in reasonably good agreement with the finite difference and the time-domain, boundary element solutions.

(c) Semi-infinite beam subjected to a suddenly-applied bending moment:

A semi-infinite beam simply supported along its edge is subjected to a suddenly applied bending moment $M = M_o H(T-O)$, as shown in figure 7.11. The beam is considered to be under a plane-stress condition and the Poisson ratio is taken as $\nu = 1/3$.

A finite element analysis of this problem was carried out by Fu (1970), and a boundary element analysis was carried out by Mansur and Brebbia (1985). Boley and Chao (1958) obtained the results for the same problem using beam theory. Transverse displacements along the axes of the beam obtained by the above researchers and the present method are shown in figure 7.12. This displacements plotted in figure 7.12 refer to $T = 5r/c_o$ where r is the radius of gyration of the beam cross section and c_o is the one-dimensional wave propagation speed.

In the present analysis two types of boundary conditions are used. In the first case, the beam is fixed from transverse movement by incorporating zero transverse displacement at the midpoint of the finite end of the beam,

and in the second case, zero transverse displacements are incorporated for all the nodes along the finite end of the beam. The displacements obtained by incorporating the first boundary-condition case are in good agreement with finite element results whereas the displacements obtained by using the second boundary-condition case are in good agreement with the beam theory and Mansur's solutions . Therefore, the difference in the results of Mansur and Fu are essentially due to end boundary conditions.

(B) Three-dimensional Applications

(a) Cantilever Beam subjected to time-harmonic axial tension:

A uniform beam with a rectangular cross-section has a modulus of elasticity $E = 1.16 \times 10^7$, a Poisson's ratio $\nu = 0.0$, and a mass density $\rho = 2.0$. It is fixed at one end and a uniformly distributed axial tension $p = 1000 \sin\Omega T$, $\Omega = 0.628$ r/s , is applied at the free end. Traction-free conditions hold along the sides. The dimensions of the beam are length $L = 4$, depth $d = 2$, and width $w = 1$. The beam is modelled by six quadrilateral elements resulting in 20 nodes, as shown in Fig. 7.13. The same figure plots the axial displacement at the free end as a function of time along with the analytic solution developed from Clough and Penzien (1975). Agreement is very good considering that only 20 points were used in the Laplace transform domain and that the sinusoidal load was represented by straight line segments for the purpose of the direct Laplace transformation, Eq. (7.5).

(b) Spherical cavity in infinite space:

A spherical cavity is embedded in an infinitely extending medium with $E = 8.993 \times 10^6$, $\nu = 0.25$, and $\rho = 2.5 \times 10^{-4}$. The radius of the cavity is $a = 212$ and its surface is discretized into 3 triangular elements per octant for a total of 50 nodes, as shown in figure (7.14). The characteristic times required for the pressure and shear waves to travel a

cavity radius are 0.00102s and 0.00177s , respectively. Two cases are considered:

(i) Spherical cavity under sudden radial pressure: A radial pressure p = 1000 is suddenly applied and maintained at the cavity surface. Figure 7.15 shows the radial displacement history obtained by using the inverse Laplace transform algorithm with only 20 data points. The response is obtained for two different time steps, ΔT equal to 0.0005s and 0.00035s . Concurrently plotted is the exact solution (Ref. Timoshenko, 1970). In general, the numerical results are in good agreement with the analytical solution. These is some oscillation in the Laplace transform solution towards the end of the total time so that about 85% of the time spectrum obtained is actually plotted.

(ii) Spherical cavity engulfed by a pressure wave: A propagating plane pressure wave whose front is perpendicular to the Z-axis first impinges on the pole with coordinates (0,0,212). The resulting non-zero incident stresses are $\sigma_{zz}^{(i)} = -1000\ H(T-T_o)$, and $\sigma_{xx}^{(i)} = \sigma_{yy}^{(i)} = (\nu/(1-\nu))\sigma_{zz}^{(i)}$, where H is the Heaviside function and T_o the time required for the wave to reach the station in question. This wave propagation type of problem is solved by superposition (Ref. Eringen, 1975). A three-quadrilaterals-per-octant mesh resulting in 74 nodes (Ref. figure 7.14) is used here in conjunction with the numerical inverse transformation utilizing 20 data points. Figure 7.16 shows the hoop stresses $\sigma_{\phi\phi}^{*}$ and $\sigma_{\theta\theta}^{*}$ normalized by the magnitude of the incident stress $\sigma_{zz}^{(i)}$ versus the non-dimensional time $\tau^* = aT/c_1$. The plots are for three locations on the surface of the cavity: the two poles ($\phi = 0,\pi$) and the equator ($\phi = \pi/2$) . Concurrently plotted are the analytic results (Ref. Pao and Mow, 1973). Good agreement is observed between the two solutions.

VII.6 CONCLUDING REMARKS

An advanced algorithm based on the transformed domain boundary element formulation for transient dynamic analysis has been presented. The numerical implementation employed is one of the most general currently available and can be used in conjunction with substructuring to treat two and three-dimensional solids of complicated geometry and connectivity. Interior, exterior and halfspace problems can all be solved by the present algorithm. The current implementation is also capable of handling sliding interfaces in the soil-structure interaction problems. Thus, the algorithm presented is a viable alternative to that based on finite element methodology.

CHAPTER VIII

TIME DOMAIN TRANSIENT DYNAMIC ANALYSIS

VIII.1 INTRODUCTION

The work described in this chapter is based on the numerical implementation of the direct boundary element method for time-domain, transient analysis of three-dimensional solids in a most general and complete manner. The present formulation employs the space and time dependent fundamental solution (Stoke's solution) and the Graffi's dynamic reciprocal theorem to formulate the boundary integral equations in the time domain. A time-stepping scheme is then used to solve the boundary-initial value problem by marching forward in time. Interpolation functions in space and time are used to approximate the field quantities, and a combination of analytical (time-integration) and numerical integration is then carried out to form a system of linear equations. At the end of each time step, these equations are solved to obtain the unknown field quantities at that time.

In the following sections, a description of the proposed methodology is presented in detail. The materials related to the representation of geometry, spatial variation of field quantities, numerical integration and solution of equations at each time step are similar to those already described in Chapter VI for one value of transform parameter s except for the fact that, in the present case, all the quantities are real. The matrix equation solver used for the present case is a real-variable version of the out of core complex solver described in Chapter IV, Sec. 4.G. The built-in symmetry and substructuring capabilities described in Sec. VI.3.B are also included in this implementation. A number of numerical examples are finally presented to demonstrate the stability and accuracy of this dynamic analysis technique.

VIII.2 TRANSIENT BOUNDARY INTEGRAL FORMULATION

The direct boundary integral formulation for a general, transient, elastodynamic problem can be constructed by combining the fundamental point-force solution of the governing equations (4.1) (Stoke's solution) with Graffi's dynamic reciprocal theorem. Details of this construction can be found in Banerjee and Butterfield (1981). For zero initial conditions and zero body forces, the boundary integral formulation for transient elastodynamics reduces to:

$$c_{ij}(\underline{\xi})u_i(\underline{\xi},T) = \int_S [G_{ij}(\underline{x},\underline{\xi},T)*t_i(\underline{x},T) - F_{ij}(\underline{x},\underline{\xi},T)*u_i(\underline{x},T)]dS(\underline{x}) \qquad (8.1)$$

where:

$$G_{ij}*t_i = \int_0^T G_{ij}(\underline{x},T;\underline{\xi},\tau)t_i(\underline{x},\tau)d\tau$$

$$F_{ij}*u_i = \int_0^T F_{ij}(\underline{x},T;\underline{\xi},\tau)u_i(\underline{x},\tau)d\tau \qquad (8.2)$$

are Riemann convolution integrals and $\underline{\xi}$ and $\underline{x}$ are the space positions of the receiver (field point) and the source (source point). The fundamental solutions G_{ij} and F_{ij} are the displacements and tractions at a point $\underline{x}$ and at a time T due to a unit force vector acting at a point $\underline{\xi}$ at a time τ. These functions are listed in a compact form in Appendix A4.

Equation (8.1) represents an exact formulation involving integration over the surface as well as the time history. It should also be noted that this is an implicit time-domain formulation because the response at time T is calculated by taking into account the history of surface tractions and displacements up to and including the time T. Furthermore, equation (8.1) is valid for both regular and unbounded domains.

Once the boundary solution is obtained, the stresses at the boundary nodes can be calculated without any integration by using the scheme described in Sec. VI.3.D. For calculating displacements at interior points equation (8.1) can be used with $c_{ij} = \delta_{ij}$ and the interior stresses can be obtained from

$$\sigma_{jk}(\underline{\xi},T) = \int_S [G^{\sigma}_{ijk}(\underline{x},\underline{\xi},T) * t_i(\underline{x},T) - F^{\sigma}_{ijk}(\underline{x},\underline{\xi},T) * u_i(\underline{x},T)]dS(\underline{x}) \tag{8.3}$$

The functions G^{σ}_{ijk} and F^{σ}_{ijk} of the above equation are listed in Appendix A5.

The constitutive equation and the boundary and initial conditions are described in Chapter IV (Ref. Secs. IV.1 and IV.2).

VIII.3 TIME STEPPING SCHEME

In order to obtain the transient response at a time T_N, the time axis is discretized into N equal time intervals, i.e.

$$T_N = \sum_{n=1}^{N} n\Delta T \tag{8.4}$$

where ΔT is the time step.

Utilizing equations (8.4) and (8.2), equation (8.1) can be written as:

$$c_{ij}u_i(\underline{\xi},T_N) - \int_{T_{N-1}}^{T_N} \int_S [G_{ij}t_i - F_{ij}u_i]dSd\tau$$

$$= \int_{\tau=0}^{T_{N-1}} \int_S [G_{ij}t_i - F_{ij}u_i]dSd\tau \tag{8.5}$$

where the integral on the right hand side is the contribution due to past dynamic history.

It is of interest that equation (8.5) like equation (8.1) still remains an exact formulation of the problem since no approximation has yet been introduced. However, in order to solve equation (8.5), one has to approximate the time variation of the field quantities in addition to the usual approximation of spatial variation. For this purpose two types of interpolation functions are used which are described with the resulting time-stepping algorithms as follows.

(A) Constant Time Interpolation

In this case, both displacements and tractions are assumed to remain constant during a time step, i.e.,

$$u_i(\underline{x},\tau) = \sum_{n=1}^{N} u_i^n(\underline{x})\phi_n(\tau) \qquad \text{and}$$

$$t_i(\underline{x},\tau) = \sum_{n=1}^{N} t_i^n(\underline{x})\phi_n(\tau) \tag{8.6}$$

where

$\phi_n(\tau) = 1$ for $(n-1)\Delta T \leq \tau \leq n\Delta T$, and

$= 0$ otherwise; and

$u_i^n(\underline{x})$ and $t_i^n(\underline{x})$ represents the spatial variation of u_i and t_i , respectively, at time T_n .

For illustrative purposes, first consider the form of equation (8.5) for the first time step; i.e.

$$c_{ij}u_i(\xi,T_1) - \int_{T_o}^{T_1} \int_S [G_{ij}t_i - F_{ij}u_i]dSd\tau = 0 \tag{8.7}$$

The time integration in (8.7) is done analytically (Ref. Appendix D1) and the surface integration is performed in the usual manner (i.e. numerically). After the integrations and the usual assembly process, the resulting system of algebraic equations is of the form:

$$[A^1]\{X^1\} = [B^1]\{Y^1\} \tag{8.8}$$

where A and B are coefficient matrices, Y and X are the known and unknown components of the boundary tractions and displacements respectively, and the superscript pertains to the time step.

Now consider the boundary integral equation for the second time step, i.e.;

$$c_{ij}u_i(\xi,T_2) - \int_{T_1}^{T_2} \int_S [G_{ij}t_i - F_{ij}u_i]\, dSd\tau$$

$$= \int_{T_o}^{T_1} \int_S [G_{ij}t_i - F_{ij}u_i]dSd\tau \tag{8.9}$$

If the time interval (T_2-T_1) is same as (T_1-T_o) the resulting coefficient matrices of the left hand sides of equations (8.7) and (8.9) become identical. This is so because the time translation properties of the fundamental solutions G_{ij} and F_{ij} (Ref. figure 8.1), contain time functions with arguments $(T-\tau)$ and therefore the convoluted integral corresponding to the interval $T_1 \leq \tau \leq T_2$ with $T = T_2$ is identical to that of the interval $T_o \leq \tau \leq T_1$ with $T = T_1$.

The right hand side of equation (8.9) is evaluated at time $T = T_2$ with the time integration over the interval T_o to T_1 and thus provides the effects of the dynamic history of the first time interval on the

current time node (i.e. T_2). Now, the resulting system equation for this time node (T_2) is of the form:

$$[A^1]\{X^2\} = [B^1]\{Y^2\} - [A^2]\{X^1\} + [B^2]\{Y^1\} \tag{8.10}$$

where superscripts on X and Y pertains to the time nodes and superscripts on A and B denote the time step in which they are calculated.

Using equations (8.8) and (8.10), equation (8.5) can be written in an assembled form as:

$$[A^1]\{X^N\} = [B^1]\{Y^N\} - \sum_{n=2}^{N} \left[[A^n]\{X^{N-n+1}\} - [B^n]\{Y^{N-n+1}\} \right] \tag{8.11a}$$

or

$$[A^1]\{X^N\} = [B^1]\{Y^N\} + \{R^N\} \tag{8.11b}$$

where R^N is the effect of the past dynamic history on the current time node.

The above equation can be solved to find the unknown X^N at time T_N. It may appear at first glance that a prodigious coefficient calculations are involved. However, a closer examination will reveal that:

(i) If the time step size is constant, the A^1 and B^1 matrices do not change from time step to time step.

(ii) For each time step, a new R^N needs to be formed. This involves the evaluation of a new set of coefficients A^n and B^n involving the effects of the dynamic history of the first time interval on the current time node. Eventually, however, this contribution to R^N reduces to zero and from that point onwards no new coefficients need to be evaluated.

In the present implementation, the representative values of the displacements and tractions during a time stepping interval is obtained by averaging the values of these quantities at two time nodes of that interval.

(B) Linear Time Interpolation

In this case, both displacements and tractions are assumed to vary linearly during a time step, i.e.

$$u_i(\underline{x},\tau) = \sum_{n=1}^{N} [\bar{M}_1 u_i^{n-1}(\underline{x}) + \bar{M}_2 u_i^n(\underline{x})]$$

$$t_i(\underline{x},\tau) = \sum_{n=1}^{N} [\bar{M}_1 t_i^{n-1}(\underline{x}) + \bar{M}_2 t_i^n(\underline{x})] \qquad (8.12)$$

where $\bar{M}_1$ and $\bar{M}_2$ are the time functions, and are of the form:

$$\bar{M}_1 = \frac{T_n - \tau}{\Delta T} \phi_n(\tau)$$

$$\bar{M}_2 = \frac{\tau - T_{n-1}}{\Delta T} \phi_n(\tau) \qquad (8.13)$$

Again for illustration proposes, consider the boundary integral equation for the first time step, i.e.

$$c_{ij}u_i(\xi,T_1) - \int_{T_o}^{T_1} \int_S [G_{ij}t_i - F_{ij}u_i]dSd\tau = 0 \qquad (8.14)$$

The time integration in equation (8.14) by utilizing (8.12) is done analytically (Ref. Appendix D2). After the usual numerical integration and

assembly process, the resulting system equation is of the form:

$$[A_2^1]\{X^1\} - [B_2^1]\{Y^1\} + [A_1^1]\{X^0\} - [B_1^1]\{Y^0\} = \{0\} \qquad (8.15a)$$

where:

A and B are the matrices related to the unknown and known field quantities, respectively;

X and Y are the vectors of unknown and known field quantities, respectively;

for X and Y superscript denotes the time;

for A and B supercript denotes the time step at which they are calculated, and the subscript denotes the local time nodes (1 or 2) during that time-stepping interval.

Since all the unknowns at time $T = 0$ are assumed to be zero, equation (8.15a) reduces to

$$[A_2^1]\{X^1\} = [B_2^1]\{Y^1\} + [B_1^1]\{Y^0\} \qquad (8.15b)$$

For second time step, the assembled system equation has the form

$$[A_2^1]\{X^2\} - [B_2^1]\{Y^2\} + [A_1^1]\{X^1\} - [B_1^1]\{Y^1\} =$$

$$- \{[A_2^2]\{X^1\} - [B_2^2]\{Y^1\} + [A_1^2]\{X^0\} - [B_1^2]\{Y^0\}\} \qquad (8.16a)$$

Similar to the constant time variation scheme, only the matrices on the right hand side of equation (8.16a) need to be evaluated. However, one needs to integrate and assemble four matrices at each time step as compared to two in the case of constant time variation. This can be done with only a small increase in computational time by integrating all the kernels together and then assembling all the matrices together. Equation (8.16a) can be rearranged such that:

$$[A_2^1]\{X^2\} = [B_2^1]\{Y^2\} - [A_1^1+A_2^2]\{X^1\} - [B_1^1+B_2^2]\{Y^1\} + [B_1^2]\{Y^0\} \tag{8.16b}$$

In the above equation, all the quantities on the right hand side are known. Therefore the unknown vector X^2 at time T_2 can be obtained by solving the above equation.

Thus, for the present case, the boundary integral equation (8.5) can be written in a discretized form as:

$$[A_2^1]\{X^N\} - [B_2^1]\{Y^N\} = -\sum_{n=2}^{N} \Big[[A_2^n+A_1^{n-1}]\{X^{N-n+1}\} - [B_2^n+B_1^{n-1}]\{Y^{N-n+1}\} \Big] + [B_1^n]\{Y^0\} \tag{8.17}$$

or

$$[A_2^1]\{X^N\} = [B_2^1]\{Y^N\} + \{R^N\} \tag{8.18}$$

The discussion in the previous section regarding the causal properties of the fundamental solution holds true for the present case also.

It is of interest to note that, if time interpolation functions $\bar{M}_1$ and $\bar{M}_2$ are replaced by $\bar{M}_1 = \bar{M}_2 = 0.5\ \phi_n(\tau)$, the time stepping scheme for linear variation can be used for the case of constant variation with averaging between the local time nodes.

VIII.4 SOME ASPECTS OF NUMERICAL IMPLEMENTATION

The numerical implementation of the boundary integral equation for time-domain, transient elastodynamics is essentially similar to that described in Chapter VI for steady-state elastodynamics, except for the following:

(i) All the quantities involved in the time domain analysis are real, instead of complex as in the case of steady-state dynamics.

(ii) There is a fundamental difference between static or steady-state dynamic analysis and time-domain transient analysis when it comes to the numerical integration schemes outlined in Chapter VI. In the static or the steady-state case, the integrands in all of the nonsingular surface integrals are infinitely differentiable and solution accuracy can, therefore, always be improved by the use of increased integration order. In the transient case, however, the point load solutions are only continuous. Physically this corresponds to the fact that the disturbance at some later time due to an impulse applied to a spatial location at a given time (past) is only present in a finite portion of the space (Ref. figure 8.19). This means that the kernel function may be nonzero over only part of a given surface element. While the integrand is infinitely differentiable within both the zero and nonzero regions considered separately, its overall continuity over the entire element is only C_o. The use of higher order quadrature rules is, therefore, of little use in improving accuracy. Based on these observations, a revised integration strategy was adopted for the transient case. All surface elements are subdivided into a relatively large number of subelements and relatively low-order (usually 2nd or 3rd) quadrature rules together with the usual distortion in mapping (so that the kernel shape functions and Jacobian products remain well behaved) are used over each subelement. This has led to much improved accuracy in the transient analysis.

(iii) In the case of singular integration, the subelements are subdivided in the radial direction also. This subdivision has been found to increase both the accuracy and the stability in the time domain approach.

(iv) In time domain analysis, the fundamental solution as well as the field variables are functions of real time T and therefore the system

equation at each step corresponds to a time T rather than to a transformed parameter s as in the case of Laplace domain analysis (Ref. Chapter VII).

(v) All the matrices related to the past convolution are stored on sequential tapes, and at each time increment they are used along with the boundary excitation history (of tractions and displacements) to calculate the effect of the past dynamic history on the current time node.

(vi) The matrix B^1 (Ref. eq. 8.11) is stored on a sequential tape and at each time increment it is used to calculate the contribution to the right hand side due to the known field quantities at the current time.

(vii) During the solution process at the first time increment, the decomposed form of the system matrix A^1 (Ref. eq. 8.11) is stored on a direct-access file for later use. After that, at each time step, all of the known tractions and displacements are multiplied by appropriate coefficient matrices to form a new right-hand-side vector. The decomposed form of the system matrix is then used with the new right hand side vector to calculate the unknown displacements and tractions at the current time. This process of repeated solution by using the decomposed form of the system matrix is highly efficient and thus results in considerable saving in solution time.

VIII.5 NUMERICAL ACCURACY, STABILITY AND CONVERGENCE OF SOLUTION

In order to investigate the accuracy, stability and convergence of the proposed numerical technique, the problem of the radial expansion of a spherical cavity in an infinitely extending medium, subjected to suddenly applied and maintained internal pressure [p(T) = 1000] was studied. The material properties were as follows: $E = 8.993 \times 10^6$ psf, $\nu = 0.25$, and $\rho = 2.5 \times 10^{-9}$ lb-sec^2/ft^4. The radius of the cavity was taken as R = 212 ft

and three different meshes shown in figure 7.11 were used to discretize the cavity surface. Using built-in symmetry capabilities, this problem was modeled by one octant only. The first mesh has one six-noded triangular element, the second has three triangular elements (total of 10 nodes), and the third has three eight-noded quadrilateral elements (total of 16 nodes).

In figures 8.2-8.4 the radial displacement $u_r(r = R,T)$ normalized by the static value is plotted against time for a total of nine different time steps. Concurrently plotted is the exact solution (Ref. Timoshenko, 1970). These results conclusively demonstrated the unconditional stability of the BEM formulation. The accuracy is highest when the time step is between 1/3 to 3/4 of the characteristic time R/c_1. In all cases the results approach the static response without exhibiting any supurious oscillations.

The effect of the surface discretization is demonstrated in figure 8.5, where the time variation of $u_r(R,T)$ is plotted for all three meshes for the same time step $\Delta T = 0.00035$ s. It is observed that the errors in the dynamic response are consistent with the average error committed in the static response which is 12% for the first mesh, 3% for the second mesh and 1.5% for the third mesh. Thus, the numerical technique presented here converges to the actual results with finer discretization of the surface of the boundary.

VIII.6 EXAMPLES OF APPLICATIONS

A number of representative problems are chosen to test the accuracy and the stability of the time-stepping solution. In all cases, English units are used with foot (ft) for length, pound (lbf) for force, and second (s) for time.

(a) Bar Subjected to a Transient End Load.

(i) Square cross-section: A bar with square cross-section is held along its sides by lubricated rollers and is fixed at one end. The free end is subjected to a suddenly applied and maintained uniform compression $t_z = 1000$. The dimensions of the bar are $L = 8.0$ and $b = 2.0$. In view of the material properties, the characteristic time required for the compressive wave to reach the fixed end is 0.03578 sec. Figure 8.6 shows the discretization and the numerical results for the normal stress σ_{zz}. in which the results from the time domain algorithm for two different time steps ΔT are compared with the exact analytical solution for one-dimensional stress wave propagation (Ref. Timoshenko, 1970). Although the numerical results are in good agreement with the analytical solution, it is clearly very difficult to reproduce the sharp jump in the stress as the disturbance reaches the point initially and when the reflected stress wave returns to the same location. This difficulty has been observed elsewhere as well (Ref. Belytschko et al, 1976).

The axial displacement history at the free end is shown in figure 8.7. The displacements are normalized by static displacements and the time is normalized w.r.t the characteristic time required for the compressive wave to reach the fixed end. It can be seen that the numerical results are in good agreement with the analytical solution. The differences are mainly due to the three-dimensional nature of the simulated problem.

(ii) Circular-cross-section: In order to investigate the effects of the cross-section on the numerical results, a bar with circular cross-section having the same material properties and boundary conditions as described in the last example was analyzed. The boundary element mesh for this problem is shown in figure 8.8. The bar has a length $L = 5$ and diamater $d = 1$. Thus, the characteristic time required for the

compressive wave to reach the fixed end is 0.02236 sec. The time step used in this example is $\Delta T = 0.004475$ sec.

Figure 8.9 shows the numerical results for the normal stress σ_{zz} at the midspan of the bar against a one-dimensional analytical solution. As mentioned in the last example, the sharp jumps in stress are diffused in the numerical results. However, by using more elements and smaller time steps, the numerical results in the vicinity of the jumps will agree more closely with the analytical solution.

The time history of the normalized axial displacements at the free-end is plotted in figure 8.10 against the one-dimensional analytical solution. The results are in good agreement, except for the peak displacements. The numerical peak values are less than that of the analytical solution and this results in an increase in the difference between the two solutions at later times. The difference, once again, is mainly due to the three-dimensional nature of the problem under consideration.

(b) Spherical Cavity.

A spherical cavity is embedded in an infinitely extending medium with $E = 8.993 \times 10^{6}$, $\nu = 0.25$, and $\rho = 2.5 \times 10^{-4}$. The radius of the cavity $R = 212$ and three different meshes for its surface discretization are shown in figure 7.11. Using the built in symmetry capabilities, this problem is modeled by one octant only. The characteristic times required for the pressure and shear waves to travel a cavity radius are 0.00102s and 0.00177s, respectively. Four cases are considered:

(i) Spherical cavity under sudden radial expansion: A radial pressure $p = 1000$ is suddenly applied and maintained at the cavity surface. Figure 8.11 shows the time variation of deviatoric stress at the cavity surface obtained by the time domain algorithm. Concurrently plotted is the result reported by Hopkins (1960) based on the work of Hunter

(1954). In general, the numerical results are in good agreement with the analytical solution. The transient, time-domain solution remains stable and reaches the expected static solution at larger times. It can be ssen that the maximum deviatoric stress for the transient case is 1.77 times the applied pressure whereas for static case it is 1.54 times the applied pressure.

(ii) Spherical cavity subjected to a rectangualr pulse of radial pressure: A triangular pulse of radial pressure, as shown in figure 8.12 is applied at the cavity surface. This example is solved by using linear time interpolation functions and two different time steps. The radial displacements at the cavity surface are plotted in figure 8.12. The numerical results from both the time steps are almost identical. Thus, this example once again demonstrates the stability of the present algorithm.

(iii) Spherical cavity subjected to a rectangular pulse of radial pressure: A rectangular pulse of radial pressure as shown in figure 8.13 is applied at the cavity surface. This example is also solved by using linear-time interpolation functions and two different time-increments. Figure 8.13 shows the time history of the radial displacement of the cavity. By comparing this results with those due to a triangular pulse (i.e. fig. 8.12), it can be seen that, in general, displacements at any time interval due to the rectangular pulse are twice that due to the triangular pulse. This is because the response depends upon the total impulse and the total impulse due to the rectangular pulse is double that due to the triangular one. Hence, the displacement amplitude response due to the rectangular pulse is also approximately double that of the triangular pulse. In addition, since the energy input is the same in both problems, the response curves for both cases have the same shape.

(iv) Spherical cavity engulfed by a pressure wave: A propagating plane pressure wave whose front is perpendicular to the Z-axis first impinges on the pole with coordinates (0,0,212). The resulting non-zero incident stresses are $\sigma_{zz}^{(i)} = -1000$, $\sigma_{xx}^{(i)} = \sigma_{yy}^{(i)} = (\nu/(1-\nu))\sigma_{zz}^{(i)}$. This wave propagation type of problem has been solved by superposition (Miklowitz, 1978). The three quadrilaterals per octant mesh is used here in conjunction with the time-domain approach. Figure 8.14 plots the hoop stresses $\sigma_{\phi\phi}^{*}$ and $\sigma_{\theta\theta}^{*}$ normalized by the magnitude of the incident stress $\sigma_{zz}^{(i)}$ versus the non-dimensional time $\tau^* = RT/c_1$. The plots are for three locations on the surface of the cavity: the two poles ($\phi = 0,\pi$) and the equator ($\phi = \pi/2$) . Concurrently plotted are the analytic results (Pao and Mow, 1973; Norwood and Miklowitz, 1967), obtained by analytical inversion of the Fourier transformed solution. Good agreement is observed between the two solutions. Finally, figure 8.15 plots the radial displacement time history at the same three locations as before.

(c) Transient point load on halfspace.

This example is Lamb's problem for an impulsive vertical point force on the surface of a semi-infinite solid (Pekeris, 1955). The modelling difficulty encountered here is that the point load must be represented by a finite (yet small) area, and hence the complicated mesh shown in figure 8.16. There are 7 co-centric rings, with four elements per ring, resulting in a total of 85 nodes. However, by using the symmetry only one quarter of the mesh is modeled as a input geometry data. Uniform vertical tractions $t_z = 1000$ are prescribed on the triangular elements of the inner ring which has an outer radius of 0.05. The outer ring has an inner radius of 3.0 and is modelled by infinite elements. Obviously the small circular load solution behaves differently from the analytical, point-force solution (labelled solution A). The static solution showed that the results agree

well at a radial distance of 0.2 where there is a 4.5% and a 1.0% difference in the horizontal and vertical displacements, respectively. Therefore, the results from the time domain algorithm shown in figure 8.17 are for the normalized horizontal displacements at $r = 0.2$. When the exact solution (Pekeris, 1955) is used to calculate the superimposed effects of multiple point forces to reproduce a finite area loading (labelled as analytic solution B), good agreement with the BEM results is obtained.

(d) Square flexible footing on half-space.

In this example, a square flexible footing on half-space is subjected to a time dependent vertical tractions. The mesh for this problem is shown in figure 6.8(a) and is the same as that used for calculating vertical compliance for rigid square footing. The side of the footing is $B = 2b = 2$, and the material properties of the half-space are: elastic modulus $E = 2.6$, Poisson's ratio $\nu = 0.3$ and mass density $\rho = 1.0$. The time step used for this analysis is $\Delta T = 0.2$. The time history of the applied pressure and the vertical displacements at the center and corner of the loaded area are plotted in figure 8.18. It can be seen that the vertical displacement at the center of the footing converges to the static value after 2.4 seconds. Whereas the vertical displacement at the corner of the footing seems to be converging to its static value at a later time. The mesh used for this problem gives a maximum error of 2% for static analysis, hence the results obtained for the present problem are supposed to be reasonably accurate. Finally, this example shows the usefulness of the present algorithm for transient dynamic analysis of half-space problems.

VIII.7 CONCLUDING REMARKS

An advanced algorithm based on the direct boundary element formulation for time-dependent elastodynamic analysis of three-dimensional solids has been presented. The algorithm is an unconditionally-stable, implicit, time-marching scheme and is capable of producing very accurate results. However, for better accuracy, it is recommended that the time step should remain smaller than L/c_1 , L being the smallest distance measured along the surface between two corner nodes of an element. This algorithm is a viable alternative to that based on the finite element methodology, particularly for soil-structure interaction problems.

CHAPTER IX

NONLINEAR TRANSIENT DYNAMIC ANALYSIS

IX.1 INTRODUCTION

In this chapter, a direct boundary element formulation and its numerical implementation for nonlinear transient dynamic analysis of three-dimensional deformable solids of arbitrary shape and connectivity is presented. The formulation is based on an initial stress approach, and is the first its type in the field of Boundary Element technique. The nonlinearity considered in this analysis is that due to the nonlinear constitutive relations, i.e. material nonlinearity. The boundary integral equations are cast in an incremental form, and thus, elasto-plastic relations of the incremental type are used for material description. These equations are solved by using a time-stepping algorithm in conjunction with a iterative solution scheme to satisfy the constitutive relations. The resulting algorithm is an unconditionally stable implicit scheme. However, the size of the time step that can be used is restricted by the size of the elements used for modelling the surface of the problem under consideration.

In the present analysis, the geometry and the field variables are represented by higher-order isoparametric shape functions to model complex geometries and rapid functional variations accurately. In this chapter, the discussion first focuses on the formulation of the method, followed by the numerical technique for discretization and spatial integration of volume integrals. For discretization and spatial integration of surface integrals, the numerical integration techniques developed in earlier chapters (Ref. Secs. VI.3 and VIII.4) are used. The material pertaining to the time-stepping scheme along with the iterative solution algorithm are presented next. Numerical examples are finally presented to demonstrate the accuracy and applicability of the present method.

IX.2 BOUNDARY INTEGRAL FORMULATION FOR DYNAMIC PLASTICITY

The direct boundary integral formulation for a nonlinear transient dynamic problem, based on an initial stress approach, can be constructed by following a procedure similar to the one that has been used for a nonlinear static problem (Ref. Sec. 12.4(b), Banerjee and Butterfield, 1981). Under zero initial conditions and zero body forces, the boundary integral equation for nonlinear transient dynamics is of the form

$$c_{ij}(\underline{\xi})u_i(\underline{\xi},T) = \int_S [G_{ij}(\underline{x},\underline{\xi},T)*t_i(\underline{x},T) - F_{ij}(\underline{x},\underline{\xi},T)*u_i(\underline{x},T)]dS(\underline{x}) + \int_V B_{ilj}(\underline{x},\underline{\xi},T)*\sigma^o_{il}(\underline{x},T)dV(\underline{x}) \qquad (9.1)$$

where $*$ denotes convolution (Ref. Sec. VIII.2);

$\underline{\xi}$ and $\underline{x}$ are the space positions of the receiver (field point) and the source (source point), respectively;

σ^o_{il} is the initial stress tensor;

V denotes the volume of the body; and

the fundamental solutions G_{ij}, F_{ij} and B_{ilj} are listed in Appendices A4 and A6.

Assuming all the field quantities to have a zero value at time $T = 0$, the boundary integral equation (9.1) can be written in an incremental form as follows:

$$c_{ij}(\underline{\xi})\Delta u_i(\underline{\xi},T) = \int_S [G_{ij}(\underline{x},\underline{\xi},T)*\Delta t_i(\underline{x},T) - F_{ij}(\underline{x},\underline{\xi},T)*\Delta u_i(\underline{x},T)]dS(\underline{x}) + \int_V B_{ilj}(\underline{x},\underline{\xi},T)*\Delta\sigma^o_{il}(\underline{x},T)dV(\underline{x}) \qquad (9.2)$$

where Δ denotes the incremental quantity.

The stress increment at an interior point $\underline{\xi}$ can be obtained by

taking derivatives of equation (9.2) and using the constitutive relationships ($\Delta\sigma_{ij} = D_{ijkl}\Delta\varepsilon_{kl} - \Delta\sigma^{o}_{ij}$) as:

$$\Delta\sigma_{jk}(\underline{\xi},T) = \int_S [G^{\sigma}_{ijk}(\underline{x},\underline{\xi},T)*\Delta t_i(\underline{x},T) - F^{\sigma}_{ijk}(\underline{x},\underline{\xi},T)*\Delta u_i(\underline{x},T)]dS + \int_V B^{\sigma}_{iljk}(\underline{x},\underline{\xi},T)*\Delta\sigma^{o}_{il}(\underline{x},T) + J_{iljk}\Delta\sigma^{o}_{il}(\underline{\xi},T) \quad (9.3)$$

The functions G^{σ}_{ijk}, F^{σ}_{ijk}, B^{σ}_{iljk} and J_{iljk} are defined in Appendices A5 and A6.

In equation (9.3), the volume integral must be evaluated in the sense of $(V - V_\varepsilon)$ with limit $V_\varepsilon \to 0$ and the tensor J_{iljk} is the jump term arriving from the analytical treatment of the integral over V_ε. This jump term is the same as that of static plasticity and is independent of the size of the exclusion V_ε provided the initial stress distribution is locally homogeneous (Ref. Banerjee and Davies, 1984; Raveendra, 1984; Banerjee and Raveendra, 1985).

The equations for incremental stresses cannot be constructed at the boundary points by taking the field point ($\underline{\xi}$) in equation (9.3) to the surface due to the strongly singular nature of the integrals involved. However, the equations for incremental stresses at boundary points can be constructed by using a scheme similar to that described in Sec. VI.3.D. Using this scheme, the incremental stresses and the global derivatives of the incremental displacements at a boundary point $\underline{\xi}^b$ can be obtained by coupling the following set of equations:

$$\Delta\sigma_{ij}(\underline{\xi}^b,T) = \left[\lambda\delta_{ij}\Delta u_{m,m}(\underline{\xi}^b,T) + \mu\{\Delta u_{i,j}(\underline{\xi}^b,T) + \Delta u_{j,i}(\underline{\xi}^b,T)\}\right] - \Delta\sigma^{o}_{ij}(\underline{\xi}^b,T)$$

$$\Delta t_i(\underline{\xi}^b,T) = \Delta\sigma_{ij}(\underline{\xi}^b,T)n_j(\underline{\xi}^b) \quad , \quad \text{and}$$

$$\frac{\partial \Delta u_i}{\partial \eta_\alpha} = \frac{\partial \Delta u_i}{\partial \xi_j^b} \frac{\partial \xi_j^b}{\partial \eta_\alpha} \tag{9.4}$$

where η_α is a set of local axes at the field point (ξ^b) .

The above equations can be combined together and written in a matrix form as

$$[S]\{p\} = \{q\} \tag{9.5}$$

where [S] is a 15x15 matrix which contains unit normals, a 3x3 unit matrix and material constants; p is the unknown vector of $\Delta\sigma_{ij}$ and $\partial \Delta u_i / \partial \xi_j$; and q is a vector containing the tractions Δt_i and local derivatives of the displacements Δu_i .

By making use of equation (6.5), the right hand side of equation (9.5) can be written as

$$\{q\} = [E]\{g\} \tag{9.6}$$

where [E] is a 15x48 matrix of shape functions and derivatives of shape functions; and g is a vector of incremental nodal tractions and displacements over all of the local element nodes.

Inverting matrix [S] and utilizing equation (9.6), the set of equations (9.5) can be rearranged to form

$$\Delta\sigma_{jk}(\xi^b,T) = \bar{G}^{\sigma}_{ijk}\Delta t_i(\xi^b,T) - \bar{F}^{\sigma}_{ijk}\Delta u_i(\xi^b,T) + \bar{B}^{\sigma}_{iljk}\Delta\sigma^{o}_{il}(\xi^b,T) \tag{9.7}$$

It should be noted that the above equation is free of any integration and time convolution.

IX.3 CONSTITUTIVE MODEL

In dynamic plasticity, the choice of an appropriate constitutive model depends largely on the material properties and the loading conditions of the problem in hand. For this reason various constitutive models have been used for dynamic plasticity. However, for simplicity in the present analysis, the Von Mises model with isotropic variable hardening is used.

In this model, the behavior in the elastic and plastic region is governed by the stress-strain relations:

$$\Delta\sigma_{ij} = 2\mu \left[\Delta\varepsilon_{ij} + \frac{\nu}{1-\nu}\,\delta_{ij}\Delta\varepsilon_{kk} - \frac{3S_{ij}S_{kl}}{2\sigma_o^2(1+H/3\mu)}\,\Delta\varepsilon_{kl}\right] \tag{9.8}$$

where $\Delta\sigma_{ij} = D^{ep}_{ijkl}\Delta\varepsilon_{kl}$ = incremental stress tensor,

D^{ep}_{ijkl} = incremental elastoplastic material modulus,

μ = elastic shear modulus,

σ_o = uniaxial yield stress = $\sqrt{3S_{ij}S_{ij}/2}$,

S_{ij} = deviatoric stress = $\sigma_{ij} - \delta_{ij}\sigma_{kk}/3$, and

H = plastic-hardening modulus, the current slope of the uniaxial plastic stress-strain curve.

The present implementation is such that any other constitutive model can be included without any difficulty.

IX.4 DISCRETIZATION AND SPATIAL INTEGRATION OF THE VOLUME INTEGRALS

(A) Discretization

Equations (9.2) and (9.3) provide the formal basis for developing the dynamic plasticity algorithm. However, the initial stresses $\Delta\sigma^o_{ij}$ defined in equations (9.2) and (9.3) are not known a priori and have to be

determined by satisfying the constitutive relations discussed in Section IX.3. Thus, equations (9.2) and (9.3) and (9.8) can be regarded as a coupled system of nonlinear equations. In the present implementation, equation (9.3) and (9.7) are used to calculate the stresses at interior and boundary points and the nonlinear material model is then used to evaluate the inelastic stresses. Since the volume integrals of inelastic stress vanish except in regions of nonlinear material response, approximations of geometry and field quantities are required only where nonlinearity is expected. In the present work, isoparametric (quadratic) volume cells are used for approximating the geometry and the variation of initial stresses such that:

$$x_i = M_\beta(\underline{n})\bar{X}_{i\beta}$$

$$\sigma^o_{ij} = M_\beta(\underline{n})\bar{\sigma}^o_{ij\beta} \tag{9.9}$$

where x_i are carterian coordinates,

$\bar{X}_{i\beta}$ are nodal coordinates of the volume cell,

M_β is a quadratic shape function for the volume cell,

β represents the nodal points of the nodal points of the volume cell, and

$-$ denotes nodal quantities.

A typical volume cell is shown in figure 9.1.

The volume integral of equation (9.2) can be then represented as

$$\int_o^T \int_V B_{ilk}(\underline{x},T;\underline{\xi}^b,\tau)\Delta\sigma^o_{il}(\underline{x},\tau)dVd\tau$$

$$= \sum_{m=1}^{L} \int_o^T \int_{V_m} B_{ilj}[\underline{x}^m(\underline{n}),T;\underline{\xi}^b,\tau)]M_\beta(\underline{n})dV_m\ \Delta\bar{\sigma}^{o\ m}_{il\beta}\ d\tau \tag{9.10}$$

where:

ξ^b is the field point on the boundary (boundary node),

$\underline{x}^m(\underline{\eta})$ is the point in cell m,

$\Delta\bar{\sigma}^{o\ m}_{il\beta}$ are the nodal values of incremental initial stress of the m^{th} cell,

V_m is the m^{th} volume cell, and

L is the total number of cell in a single region.

Similarly, the volume integral of interior stress equation (9.3) can be expressed as

$$\int_o^T \int_V B^{\sigma}_{iljk}(\underline{x},T;\underline{\xi},\tau)\Delta\sigma^o_{il}(\underline{x},\tau)dVd\tau$$

$$= \sum_{m=1}^{L} \int_o^T \int_{V_m} B^{\sigma}_{iljk}[\underline{x}^m(\underline{\eta}),T;\underline{\xi},\tau)]M_\beta(\underline{\eta})dV_m\ \Delta\bar{\sigma}^{o\ m}_{il\beta}\ d\tau \qquad (9.11)$$

in which the time integral is treated analytically as before.

(B) Spatial Integration

The nonsingular, spatial integration of volume integrals of equations (9.2) and (9.3) are evaluated numerically by applying the Gaussian quadrature technique of the transformed integral as

$$\int_{V_m} B[\underline{x}(\underline{\eta}),\underline{\xi}]\ M_\beta(\underline{\eta})dV_m = \int_{-1}^{1}\int_{-1}^{1}\int_{-1}^{1} B[\underline{x}(\underline{\eta}),\underline{\xi}]M_\beta(\underline{\eta})J(\underline{\eta})d\eta_1 d\eta_2 d\eta_3$$

$$= \sum_{a=1}^{A}\sum_{b=1}^{B}\sum_{c=1}^{C} w^a w^b w^c B[x,(\eta^{abc}),\underline{\xi}]\ M_\beta(\eta^{abc})J(\eta^{abc}) \qquad (9.12)$$

where the Jacobian is defined by

$$dV_m = J(\eta_1,\eta_2,\eta_3)d\eta_1 d\eta_2 d\eta_3$$

and is given explicitly as

$$J(\eta_1,\eta_2,\eta_3) = \left| \frac{\partial x_i}{\partial \eta_j} \right| \qquad i,j = 1,2,3$$

For singular volume integrals, the volume cell can be transformed to a unit cube and the cube is subdivided into tetrahedra through the field point, as shown in figure 9.2. Using a local spherical polar coordinate system (r,θ,ϕ) with its origin at the field point, the integral of the sub-cell can be transformed by the Jacobian as

$$dV_1 = Jdrd\phi d\theta = r^2 \sin\alpha \; drd\phi d\theta$$

The integrand involving the B_{ilj} kernel is singular of the order $1/r^2$ and therefore the integral is bounded in the transformed domain. However, the volume integral B^{σ}_{iljk} is singular of the order $1/r^3$ and in the transformed domain the behavior is approximately of the order $1/r$. The integral, however, is made bounded by excluding a sphere and mapping the remainder of the tetrahedra to a unit cube as shown in figure 9.3. The integration is computed by applying the Gaussian quadrature to the transformed domain. A series of numerical trials with different sizes of the spherical exclusion led to the surprising conclusion that it could be set to zero for the most accurate three-dimensional analysis.

The above described volume integration scheme is based on the work of Mustoe (1984), Bajernee and Davies (1984), Raveendra (1984) and Banerjee and Reveendra (1985).

IX.5 TIME-STEPPING AND ITERATIVE SOLUTION ALGORITHM

(A) Time-stepping

In order to obtain the nonlinear transient response at a time T_N, the time axis is discretized into N equal time intervals, i.e.

$$T_N = \sum_{n=1}^{N} n\Delta T \tag{9.13}$$

where ΔT is the time step.

Using equation (9.13), the integral equation (9.2) can be written as

$$c_{ij}\Delta u_i(\xi,T_N) - \int_{T_{N-1}}^{T_N}\int_S [G_{ij}\Delta t_i - F_{ij}\Delta u_i]dSd\tau - \int_{T_{N-1}}^{T_N}\int_V B_{ilj}\Delta\sigma^o_{il}dVd\tau$$

$$= \int_{\tau=o}^{T_{N-1}}\int_S [G_{ij}\Delta t_i - F_{ij}\Delta u_i]dSd\tau + \int_{T_{N-1}}^{T_N}\int_V B_{ilj}\Delta\sigma^o_{il}dVd\tau \tag{9.14}$$

For the present case, the linear time interpolation scheme described in Sec. VIII.3.B is used to approximate the time variation of the field quantities during a time step because the same scheme can also be used for constant time interpolation with averaging.

Thus, after the usual discretization and integrations (time and spatial both), the integral equations (9.14) are transformed into an assembled system equation of the form

$$[A_2^1]\{\Delta X^N\} - [B_2^1]\{\Delta Y^N\} - [C_2^1]\{\Delta\sigma^{oN}\}$$

$$= -\sum_{n=2}^{N}\left[[A_2^n+A_1^{n-1}]\{\Delta X^{N-n+1}\} - [B_2^n+B_1^{n-1}]\{\Delta Y^{N-n+1}\}\right.$$

$$+ [C_2^n + C_1^{n-1}]\{\Delta\overset{o}{\sigma}^{N-n+1}\}\Big] \qquad (9.15)$$

or $$[A_2^1]\{\Delta X^N\} = [B_2^1]\{\Delta Y^N\} + [C_2^1]\{\Delta\overset{o}{\sigma}^N\} + \{R^N\} \qquad (9.16a)$$

or $$\underline{A}^b \Delta\underline{X}^N = \Delta\underline{b}^{bN} + \Delta\underline{b}^{obN} \qquad (9.16b)$$

where A and B are the matrices related to the unknown and known incremental displacements and tractions;

C is the matrix related to the initial stresses;

ΔX and ΔY are the vectors of unknown and known incremental displacements and tranctions;

for ΔX, ΔY and $\Delta\overset{o}{\sigma}$, superscript denotes time, i.e. $\Delta X^n = X^n - X^{n-1}$;

for A, B and C matrices, superscript denotes the time step when they are calculated, and the subscript denotes the local time node (1 or 2);

R^N is the effect of past dynamic history

$\Delta\underline{b}^{bN} = [B_2^1]\{\Delta Y^N\} + \{R^N\}$;

$\underline{A}^b = [A_2^1]$, and

$\Delta\underline{b}^{obN} = [C_2^1]\{\Delta\overset{o}{\sigma}^N\}$.

Similarly, the integral equation for stresses can be written in a discretized form as

$$\{\Delta\sigma^N\} = [\bar{A}_2^1]\{\Delta X^N\} + [\bar{B}_2^1]\{\Delta Y^N\} + [\bar{C}_2^1]\{\Delta\overset{o}{\sigma}^N\} + \{R^{\sigma N}\} \qquad (9.17a)$$

or $$\Delta\underline{\sigma}^N = \underline{A}^\sigma \Delta\underline{X}^N + \Delta\underline{b}^{\sigma N} + \Delta\underline{b}^{o\sigma N} \qquad (9.17b)$$

where '-' indicates that the matrices are related to the stress equation:

$$\underline{A}^{\sigma} = [\bar{A}_2^{-1}] \; ; \; \Delta\underline{\sigma}^N = [\bar{B}_2^{-1}]\{\Delta Y^N\} + \{R^{\sigma N}\} \; ; \text{ and}$$

$$\Delta\underline{b}^{o\sigma N} = [\bar{C}_2^{-1}]\{\Delta\overset{o}{\sigma}{}^N\}$$

(B) Iterative Solution Algorithm for Dynamic Plasticity

The algorithm described here provides the solution of system equations given by equations (9.16) and (9.17). The solution of these system equations requires complete knowledge of the initial stress distribution $\Delta\overset{o}{\underline{\sigma}}{}^N$ within the yielded region that is induced by the imposition of the current increment of boundary loading. This, unfortunately, is not known a priori for a particular load increment and therefore an iterative process must be employed within each time step.

This incremental algorithm can be described as follows:

(i) Obtain the transient elastic solution for an arbitrary increment of boundary loading $\Delta\underline{Y}^N$ during the time interval T_{n-1} to T_N, as

$$\underline{A}^b\Delta\underline{X}^N = \Delta\underline{b}^{bN}$$

and

$$\Delta\underline{\sigma}^N = \underline{A}^{\sigma}\Delta\underline{X}^N + \Delta\underline{b}^{\sigma N}$$

where N is the time step number.

If the material has not yielded yet, accumulate X-vectors, i.e. $\underline{X}^N = \underline{X}^{N-1} + \Delta\underline{X}^N$.

(ii) If the material was yielded before go to step (vi).

(iii) Check whether any node has yielded during the current time step. If the material has not yielded yet, accumulate stress and strain, and go back to step (i).

(iv) Calculate the value of σ_o, equivalent stress by using $\underline{\sigma}^T = \underline{\sigma}^{N-1} + \Delta\underline{\sigma}^N$ as the stress chnages and compile a list of yielded nodes. For elastic nodes accumulate the stress and strain, i.e., $\underline{\sigma}^N = \underline{\sigma}^T$ and $\underline{\varepsilon}^N = \underline{\varepsilon}^{N-1} + [D^e]^{-1}\Delta\underline{\sigma}^N$. Calculate the correct stress at the elastoplastic nodes by using the elastoplastic stress-strain relations $\Delta\underline{\sigma}^{ep} = \underline{D}^{ep}\Delta\underline{\varepsilon}$ and using the elastic strain increments as a first approximation. Modify the stress history for yielded cells $\underline{\sigma}^N = \underline{\sigma}^{N-1} + \Delta\underline{\sigma}^{ep}$. Calculate initial stress $\Delta\underline{\sigma}^o = \underline{\sigma}^T - \underline{\sigma}^N$.

(v) Assume $\Delta\underline{b}^{bN} = 0$ and $\Delta\underline{b}^{\sigma N} = 0$ and using the generated initial stress $\Delta\underline{\sigma}^o$ calculate a new $\Delta\bar{\underline{X}}^N$ by using equation (9.16b) and $\Delta\underline{\sigma}^N$ by using equation (9.17b). Calculate the equivalent stresses by using the history $\underline{\sigma}^T = \underline{\sigma}^N + \Delta\underline{\sigma}^N$ and compile a list of yielded nodes. For elastic nodes, accumulate the stress $\underline{\sigma}^N = \underline{\sigma}^T$ and strain. For the elastoplastic nodes calculate the currect stress $\Delta\underline{\sigma}^{ep} = \underline{D}^{ep}\Delta\underline{\varepsilon}$. The initial stresses generated are $\Delta\underline{\sigma}^o = \Delta\underline{\sigma}^N - \Delta\underline{\sigma}^{ep}$. Modify the stress history for the yielded nodes $\underline{\sigma}^N = \underline{\sigma}^N + \Delta\underline{\sigma}^{ep}$. Accumulate $\Delta\underline{X}^N$ and $\overset{o}{\underline{\sigma}}{}^N$ (i.e. $\Delta\underline{X}^N = \Delta\underline{X}^N + \Delta\bar{\underline{X}}^N$ and $\overset{o}{\underline{\sigma}}{}^N = \overset{o}{\underline{\sigma}}{}^N + \Delta\underline{\sigma}^o$), so that they can be used in the next time step for past convolution.

(vi) Check if the initial stresses $\Delta\underline{\sigma}^o$ are less than the acceptable norm and if so go to step (i) and if not go back to step (v). If the number of iteration exceeds, say, 50 then it is reasonable to assume that collapse has occurred.

IX.6. EXAMPLE OF APPLICATION

In order to demonstrate the accuracy and applicability of the proposed nonlinear transient dynamic analysis algorithm, a presentative problem is analyzed. English units are used with foot (ft) for length, pound (lbf) for force, and seconds (s) for time.

(a) Bar subjected to a step end load.

A bar with circular cross-section is held along its sides by lubricated rollers and is fixed at one end. The free end is subjected to a suddenly applied and maintained uniform compression $t_z = -333$ which exceeds the yield stress of the bar (i.e. yield stress of the bar is $Y = 300$). In this example, the bar has dimensions and material properties identical to that of example VIII.6.b(iii). The discretization of the bar is similar to the one shown in figure 8.8 except, in the present example, the full cross-section of the bar is modeled instead of one-quarter of it. The volume of the bar is discretized by using five 20-noded, volume cells of equal dimensions. A bilinear stress-strain relation as shown in figure 9.4, is assumed to describe the rod's material property. The time step used for this example is $\Delta T = 0.004473$. In figure 9.4, the elasto-plastic response of the bar at time $T = 0.8\ T_e$ (where $T_e = c_1 T/L$, i.e. the time taken by the compression wave to reach the fixed end of the bar) is plotted against the one-dimesnional analytical solution (Ref. Garnet and Armen, 1975). In this, the normal stress σ_{zz} are normalized by the elastic modulus and the distance along the bar is normalized by the length of the bar. The numerical results are in reasonable agreement with the analytical solution except for the sharp jumps in the stress which are diffused by the numerical analysis. The major differences in the results between the two solutions can be attributed to the three-dimensional nature of the present example. As the bar is on lubricated rollers, in addition to longitudinal stress, lateral stresses also exist in the bar. Simple one-dimensional theory considers longitudinal stress only and thus, the difference between the two solutions.

IX.7 CONCLUDING REMARKS

A direct boundary element formulation and its numerical implementation for nonlinear transient dynamic analysis of three-dimensional isotropic homogeneous or piecewise homogeneous solid has been presented. Due to the lack of available solutions for three-dimensional nonlinear transient dynamic problems, it was found impossible to compare results for a real three-dimensional problem. However, the present algorithm is found to produce very accurate results for three-dimensional static nonlinear problems by using large time steps, (i.e. when the loading is done slowly). Similarly, when a large value of yield stress is selected, the incremental nonlinear transient algorithm is found to produce results identical to that produced by the linear transient algorithm. This new formulation provides a numerical tool for solving three-dimensional transient problems involving material nonlinearity which are now impossible to solve by any other method.

CHAPTER X

GENERAL CONCLUSIONS AND RECOMMENDATIONS FOR FUTURE WORK

X.1 GENERAL CONCLUSIONS

A complete and general numerical implementation of the direct boundary element method applicable to free-vibration, periodic vibration, and linear as well as nonlinear transient dynamic problems has been presented. The developed methodology is applicable to problems involving two or three-dimensional, isotropic, piecewise-homogeneous solids of arbitrary shape. Since all of the proposed analyses are based on the boundary element method (BEM), they have all the advantages of the BEM over the Finite Element and Finite Difference methods such as, discretization of only the boundary of the domain of interest rather than the whole domain, ability to solve problems with high stress concentrations, accuracy and the ease of solution in infinite and semi-infinite mediums.

The real-variable BEM formulation presented in this dissertation provides a numerical tool for free-vibration analysis of solids with complex geometries. This method has been compared with MARC-HOST Finite element analysis and was found to yield essentially similar results for a cantilever beam problem. Thus, the proposed method is a viable alternative to algorithms based on Finite element schemes. In addition, it needs only the boundary discretization of the problem rather than the whole domain.

The advanced implementation of the BEM for steady-state dynamic analysis of two and three-dimensional, visco-elastic solids, presented in chapters IV and VI, are one of the most general numerical implementation presently available. By comparing the results obtained by the present implementation with those by other methods, the accuracy and stability of the present method is established. For half-space problems, the proposed methodology is a better alternative to the conventional finite element method. For half-space problems Finite element presents two restraints: (i) the model must be bounded at the bottom by a rigid bedrock, and (ii)

the soil away from the vicinity of the foundation is represented by parallel layers unbounded on the horizontal direction. These two conditions are not always close to reality whereas, in BEM, the fundamental solution satisfies the radiation condition at infinity and therefore no bounding surfaces are needed and only a small number of elements are necessary to model the problem.

The transformed-domain boundary element formulation presented in chapter VII is capable of providing accurate solutions to transient elasto-dynamic problems. The accuracy and stability of the present implementation are established by comparing the results obtained against the available solutions from Finite element, Finite Difference and Time-domain Boundary element methods. However, the transformed domain formulation suffers from the following defects.

(i) The transform solution is essentially a superposition of a series of steady-state solutions and is therefore applicable only to linear elasto-dynamic problems. For nonlinear problems, the solution must be obtained in the real time domain.

(ii) Since the Laplace/Fourier transform casts the entire problem in the complex domain, the computer time and storage requirements are considerably increased.

The time-domain boundary element formulation for linear and nonlinear transient dynamics presented in chapters VIII and IX eliminate the above mentioned problems. The proposed time domain methodology, in conjunction with the direct step-by-step integration, provides the transient response directly and thus it has been extended for nonlinear problems by using an iterative algorithm. Using this method, the transient phenomena during early response times, preceding the harmonic steady-state motion, can be captured while frequency domain methods are incapable of detecting them at

all. In addition, approximations related to the value of Poisson's ratio and to the number of modal shapes required in frequency synthesis are eliminated.

The versatility of the proposed time-domain methodology is evident in view of the results presented in this dissertation for various three-dimensional transient problems. Due to its general character, it can be used for solving more sophisticated problems. This algorithm is an unconditionally stable implicit time marching scheme and is capable of producing accurate results. However, for better accuracy, it is recommended that the time step should remain smaller than L/c_1 ; where L being the smallest distance measured along the surface between two corner nodes of an element and c_1 being the propagation velocity of pressure wave.

By taking the material nonlinearity into account, the proposed methodology for time-domain nonlinear transient analysis has the potential to provide a numerical tool for solving soil-foundation problems in a more realistic manner which cannot be accomplished by using the available transform domain algorithms.

X.2 RECOMMENDATIONS

In order to facilitate future research based on the findings of the present work the following are recommended:

1. The stability of the time-domain transient dynamic algorithm has been established for simple problems by analyzing the problem of radial expansion of a cavity in an infinite space for different time steps and meshes. However, to insure the stability and convergence of this algorithm for more sophisticated problems, further investigation by using a complex problem is recommended.

2. As mentioned earlier, the transformed domain dynamic analysis yields erroneous results when the forcing frequency happens to be one of the natural frequencies (or fictitious eigenfrequencies in the case of exterior problems) of the structure under consideration. To eliminate this problem, a computationally feasible modification of the transformed domain algorithm is needed.

3. In the present work, for nonlinear dynamic analysis, the Von Mises constitutive relations are used to model the material behavior. However, for materials like soils, a more realistic material model needs to be included to model the nonlinear material behavior during dynamic loadings and unloadings. Moreover, only a simple test problem has been solved in the present work. However, for solving realistic engineering problems further work is needed.

4. · The problems of soil-structure interaction during an earthquake excitation is of considerable importance to civil engineers. This problem can be tackled in a deterministic way by modifying the present formulations. For this purpose, extension of the present algorithms to solve the general wave scattering problems by including the effects of incident waves in the formulation is recommended.

5. The proposed time-domain transient formulation involving convolutions provides accurate results, but it is computationally expensive. However, for certain class of problems such as those related to structural dynamics, an approximate and computationally inexpensive boundary element formulation can be developed. This can be achieved by extending the method proposed for free-vibration analysis to linear and nonlinear transient dynamic analysis of solids.

6. In practice, inhomogeneity and anisotropy are present in most engineering problems. Whilst the inhomogneity can be handled by substructuring, it is of extreme importance to develop appropriate fundamental solutions for dynamic analysis of problems involving anisotropy.

7. Some of the dynamic problems such as non-destructive testing of materials involve material nonlinearity as well as geometric nonlinearity. Therefore, extension of the present nonlinear transient dynamic formulation to include geometric nonlinearity is desirable.

REFERENCES

Abscal, R. and Dominguez, J. (1984), 'Dynamic behavior of strip footings on non-homogeneous viscoelastic soils,' Proceedings of the International Symposium on Dynamic Soil-Structure Interaction, Minneapolis, A.A. Balkema Publishers, Beskos, D.E., ed., pp. 25-35.

Abscal, R. and Dominguez, J. (1985), 'Dynamic response of embedded strip foundation subjected to obliquely incident waves,' Proceedings of the seventh International Conference on Boundary Element Methods, Lake Como, Italy, Springer-Verlag, pp. 6-63 to 6-69.

Achenbach, J.D. (1973), Wave Propagation in Elastic Solids, North-Holland Publishing Company, Amsterdam.

Ahmad, S, (1983), 'Viscoelastic Analysis of Piles and Pile Groups,' M.S. Project, Department of Civil Engineering, SUNY at Buffalo.

Ahmad, S., Davies, T.G. and Manolis, G.D. (1985), 'Viscoelastic Analysis of Piles and Pile Groups,' Int. J. For Numerical and Analytical Methods in Geomechanics, Vol. 9, pp. 237-252.

Alarcon, E. and Dominguez, J. (1981), 'Elastodynamics,' Chapter 7 in Progress in Boundary Element Methods, Halstead Press, New York, Brebbia, C.A., ed.

Apsel, F.J. (1979), 'Dynamic Green's Functions for Layered Media and Applications to Boundary-Value Problems,' Ph.D. Thesis, Univ. of California, San Diego.

Arnold, R.N., Bycroft, G.N. and Warburton, G.B. (1955), 'Forced Vibrations of a Body on an Infinite Elastic Solid,' J. Appl. Mech., ASME, Vol. 22, pp.391-400.

Askar, A., Zeng, X. and Altay, S. (1984), 'Explicit Integration of Boundary Integral Equations and Scattering of Seismic Waves by Underground Structures,' Proc. of 8th WCEE, California, pp. 657-664.

Banaugh, R.P. and Goldsmith, W. (1963a), 'Diffraction of Steady Elastic Waves by Surface of Arbitrary Shape,' J. of Appl. Mech., Vol. 30, pp. 589-597.

Banaugh, R.P. and Goldsmith, E. (1963b), 'Diffraction of steady acoustic waves by surface of arbitrary shape,' J. Acoust. Soc. Am., Vol. 35, pp. 1590-1601.

Banerjee, P.K. and Butterfield, R. (1977), 'Boundary element methods in Geomechanics,' Finite Element in Goemechanics, Gudehus, G., ed., John Wiley and Sons, pp. 529-570.

Banerjee, P.K. and Butterfield, R. (1979), Developments in Boundary Element Methods - I, Applied Sci. Publishers, Barking, Essex, U.K.

Banerjee, P.K. and Butterfield, R. (1981), Boundary Element Methods in Engineering Science, McGraw Hill, London and New York.

Banerjee, P.K., Cathie, D.N. and Davies, T.G. (1979), 'Two and three-dimensional problems of elasto-plasticity,' Chapter IV in Developments in Boundary Element Methods - I, Applied Science Publishers, London.

Banerjee, P.K. and Shaw, R.P. (1982), Developments in Boundary Element Methods - II, Applied Sci. Publishers, U.K.

Banerjee, P.K. and Davies, T.G. (1984), 'Advanced implementation of the boundary element methods for three-dimensional problems of elasto-plasticity and viscoplasticity,' Development in Boundary Element Methods - III, Applied Science Publishers, U.K.

Banerjee, P.K. and Mukherjee, S. (1984), Developments in Boundary Element Methods - III, Applied Sci. Publishers, U.K.

Banerjee, P.K. and Raveendra, S.T. (1985), 'Advanced boundary element analysis of two and three-dimensional problems of elasto-plasticity,' to appear in International Journal for Numerical Methods in Engineering.

Banerjee, P.K., Wilson, R.B. and Miller, N. (1985), 'Development of a large BEM system for three-dimensional inelastic analysis,' Proc. of ASME Conf. on Advanced Topics in Boundary Element Analysis, AMD-Vol. 72.

Banerjee, P.K. and Watson, J.O. (1986), Developments in Boundary Element Methods - IV, Applied Sci. Publishers, U.K.

Bathe, K.L. Ozdemir, H. and Wilson, E.L. (1974), 'Static and Dynamic Geometric and material nonlinear analysis,' Report No. UC SESM 74-4, Structural Engineering Laboratory, University of California, Berkeley.

Belytschko, T., Chiapetta, R.L. and Bartel, H.D. (1976), 'Efficient large scale nonlinear transient analysis by finite elements,' Int. J. Num. Meth. in Engg., Vol. 10, pp. 579-596.

Benzine, G. (1980), 'A Mixed Boundary Integral-Finite Element Approach to Plate Vibration Problems,' Mechanics Research Communications, Vol. 7, pp. 141-150.

Brebbia, C.A. and Nardini, D. (1983), 'Dynamic analysis in solid mechanics by an alternative boundary element procedure,' Soil Dyn. and Earthquake Engg., Vol. 2, pp. 228-233.

Brebbia, C.A., Telles, J.C. and Wrobel, L.C. (1984), Boundary Element Techniques - Theory and Application in Engineering, Springer-Verlag, Berlin and New york.

Brebbia, C.A. and Walker, S. (1980), The Boundary Element Techniques in Engineering, Newes-Butterworths, London.

Bettess, P. and Zienkiewicz, O.C. (1977), 'Diffraction and refraction of surface waves using finite and infinite elements,' Int. J. Num. Meth. Engg., Vol. 11, pp. 1271-1290.

Boley, B.A. and Chao, C.C. (1958), 'An Approximate Analysis of Timoshenko Beams under Dynamic Loads,' J. Appl. Mech., ASME, Vol. E25, pp. 31-36.

Cagniard, L. (1939), 'Reflection and Refraction of Progressive Seismic Waves,' Translated and Revised by Flinn, E.A. and Dix, C.H. (1962), McGraw-Hill, New York.

Chertock, G. (1971), 'Integral equation methods in sound radiation and scattering from arbitrary surfaces,' NSRDC Rep. 3538, Washington, D.C.

Clebsch, A. (1863), Journal fur Reine und Angewan dte Mathematik - 61, p. 195.

Clough, R. and Penzien, J. (1975), Dynamics of Structures, McGraw-Hill, New York.

Cole, D.M., Kosloff, D.D., and Minster, J.B. (1978), 'A Numerical Boundary Integral Equation Method for Elastodynamics I,' Bull. Seismological Soc. Amer., Vol. 68, pp. 1331-1357.

Cooley, J.W. and Tukey, J.W. (1965), 'An Algorithm for Machine Calculation of Complex Fourier Series,' Math. Comp., Vol. 19, pp. 297-310.

Cruse, T.A. (1967), Transient Problem in Classical Elastodynamics Solved by Integral Equations, Ph.D. Thesis, University of Washington.

Cruse, T.A. and Rizzo, F.J. (1968), 'A Direct Formulation and Numerical Solution of the General Transient Elastodynamic Problem I,' J. Math. Analy. and Appl., Vol. 22, pp. 244-259.

Cruse, T.A. and Wilson, R.B. (1977), 'Advanced application of boundary integral equation methods,' Nucl. Engg. and Design, Vol. 46, pp. 223-234.

Davies, A.M.J. and Hood, M.J. (1976), 'Surface waves normally incident on a submerged horizontal cylinder,' SIAM J. Appl. Math., Vol. 31, pp. 16-30.

DeMey, G. (1976), 'Calculation of eigenvalues of the Helmholtz equation by an integral equation,' Int. J. Num. Meth. in Engg., Vol. 10, pp. 56-66.

DeMey, G. (1977), 'A simplified integral equation method for the calculation of the eigenvalues of the Helmholtz equation,' Int. J. Num. Meth. in Engg., Vol. 11, pp. 1340-1342.

Dominguez, J. (1978), 'Dynamic Stiffness of Rectangular Foundations,' Research Report R78-20, Dept. of Civil Engg., M.I.T.

Dominguez, J. (1978), 'Response of Embedded Foundation to Travelling Waves,' Research Report R78-24, Dept. of Civil Engg., M.I.T.

Dongarra, J.J., et al (1979), Linepack Users' Guide, SIAM, Philadelphia, PA.

Doyle, J.M. (1966), 'Integration of the Laplace Transformed Equations of Classical Elastokinetics,' J. Math. Anal. and Appl., Vol. 13, pp. 118-131.

Dravinski, M. (1982a), 'Scattering of SH waves by subsurface topography,' Proc. ASCE, EM1, pp. 1-17.

Dravinski, M. (1982b), 'Scattering of elastic waves by an alluvial valley,' Proc. ASCE, EM1, pp. 19-31.

Dravinski, M. (1983), 'Amplification of P,SV and Rayleigh Waves by Two Alluvial Valleys,' Int. J. of Soil Dyn. and Earthquake Engineering, Vol. 2, No. 2, pp. 65-77.

Duhem, P. (1898), 'Mém. Soc. Sci. Bordeaux,' Ser. V, Vol. 3, p. 316.

Durbin, F. (1974), 'Numerical Inversion of Laplace Transforms: An Efficient Improvement to Dubner and Abates' Method,' Computer J., Vol. 17, pp. 371-376.

Ergatoudis, J.G. (1968), 'Isoparametric finite elements in two and three-dimensional stress analysis,' Ph.D. Thesis, University of Wales, University College, Swansea, U.K.

Eringen, A.C. and Suhubi, E.S. (1975), Elastodynamics, Vols. I and II, Academic Press, New York.

Estorff, O.V. and Schmid, G. (1984), 'Application of the boundary element method to the analysis of the vibration behavior of strip foundations on a soil layer,' Proc. Int. Symp. on Dynamic Soil-structure Interaction, Minneapolis, A.A. Balkema Publishers.

Fredhom, I. (1903), 'Sur une classe d'equations fonctionelles,' Acta Math., Vol. 27, pp. 365-390.

Friedman, M.E. and Shaw, R.P. (1962), 'Diffraction of a plane shock wave by an arbitrary rigid cylindrical obstacle,' J. Appl. Mech., Vol. 29, pp. 40-46.

Fu, C.C. (1970), 'A method for the numerical integration of the equations of motion arising from a Finite-element Analysis,' J. Appl. Mech., ASME, Vol. E37, pp. 599-605.

Garbow, B.S. (1980), 'EISPACK - For the real generalized eigenvalue problem,' Applied Mathematics Division, Argonne National Laboratory.

Graffi, D. (1947), Memorie della Accademia Scienze, Bologna, Series 10, Vol. 4, pp. 103-109.

Garrison, C.J. and Chow, P.Y. (1972), 'Wave forces on submerged bodies,' ASCE, 98(WW3), pp. 375-392.

Garrison, C.J. and Seetharama, R.V. (1971), 'Interaction of waves with submerged obstacles,' ASCE, 97(WW2), pp. 259-277.

Garnet, H. and Armen, H. (1975), 'One dimensional elasto-plastic wave interaction and boundary reflections,' Computers and Structures, Vol. 5, pp. 327-334.

Groenenboom, P.H.L. (1983), 'Wave Propagation Phenomena', Chapter 2 in Progress in Boundary Element Methods, Brebbia, C.A., ed., Springer-Verlag.

Hadjian, A.H. Luco, J.E. and Tsai, N.C. (1974), 'Soil-Structure Interaction: Continuum or Finite Element?,' Nuc. Engng. and Des., Vol. 31, pp. 151-167.

Hess, J. (1962a), 'Calculation of potential flow about arbitrary three-dimensional bodies,' Douglas Aircraft Co. Rep. ES40622.

Hess, J. (1962b), 'Calculation of potential flow about bodies of revolution having axes perpendicular to the free stream direction,' J. Aero. Sci., Vol. 29, pp. 726-742.

Hopkins, H.G. (1960), 'Dynamic expansion of spherical cavities in metals,' Chapter III in Progress in Solid Mechanics, Vol. 1, Sneddon, I.N. and Hill, R., eds., North-Holland Publ. Comp., Amsterdam, pp. 83-164.

Hryniewicz, Z. (1981), 'Dynamic response of a rigid strip on an elastic half-space,' Computer Meth. in Appl and Mechanical Engg., Vol. 25, pp. 355-364.

Hudson, J.A. (1980), The Excitation and Propagation of Elastic Waves, Cambridge University Press, Cambridge.

Hunter, S.C. (1954), Unpublished Report, Ministry of Supply, United Kingdom.

Hutchinson, J.R. (1978), 'Determination of membrane vibrational characteristics by the boundary integral equation methods,' Recent Advances in Boundary Element Methods, Brebbia, C.A., ed., Pentech Press, London, pp. 301-316.

Hutchinson, J.R. (1984), 'Boundary methods for time dependent problems,' Proc. of 5th Engg. Mech. Div. Conference, ASCE, University of Wyoming, pp. 136-139.

Hutchinson, J.R. (1985), 'An alternative BEM formulation applied to membrane vibration,' Proc. of the 7th Int. Conf. on BEM, Italy, Springer-Verlag, pp. 6-13 to 6-25.

Hutchinson, J.R. and Wong, G.K.K. (1979), 'The Boundary element method for plate vibrations,' Proc. of ASCE 7th Conf. on Electronic Comp., St. Louis, Missouri, pp. 297-311.

Jaswon, M.A. (1963), 'Integral equation methods in potential theory, I,' Proc. Roy. Soc., London, Vol. 275(A), pp. 23-32.

Jaswon, M.A. and Ponter, A.R. (1963), 'An integral equation solution of the torsion problem,' Proc. Roy. Soc., London, Vol. 275(A), pp. 237-246.

Kausel, E., Roesset, J.M., and Waas, G. (1975), 'Dynamic Analysis of Footings on Layered Media,' J. of ASCE, EM5, Vol. 101, pp. 679-693.

Kamiya, N. and Sawaki, Y. (1985), 'An efficient BEM for some inhomogeneous and nonlinear problems,' Proc. 7th Int. Conf. on BEM, Italy, pp. 13-59 to 13-68.

Karabalis, D.L. and Beskos, D.E. (1978), 'Dynamic Response of 3-D Rigid Surface Foundations by Time Domain Boundary Element Method,' Earthquake Engg. and Struc. Dyn., Vol. 12, pp. 73-93.

Karasudhi, P., Keer, L.M. and Lee, S.L. (1968), 'Vibratory motion of a body on an elastic half-plane,' J. Appl. Mech., ASME 35, E4, pp. 184-194.

Kaynia, A.M. and Kausel, E. (1982), 'Dynamic Behavior of Pile Groups,' Proc. 2nd Int. Conf. on Numerical Methods in Offshore Piling, Austin, Texas.

Kellog, O.D. (1929), Foundations of Potential Theory, Dover Publ., New York, 1953.

Kirchoff, G. (1883), Zur Theorie der Lichstrahlen, Ann. Physik, Vol. 18, pp. 663-695.

Kitahara, M. and Nakagawa, K. (1985), 'Boundary integral equation methods in three-dimensional elastodynamics,' Proc. of 7th Int. Conf. on BEM, Italy, pp. 6-27 to 6-36.

Kleinmann, R.E. and Roach, G.F. (1974), 'Boundary integral equations for the three dimensional Helmholtz equation,' SIAM Review, Vol. 16, pp. 214-236.

Kobayashi, Y., Fukui, T., and Azuma, N. (1975), 'An Analysis of Transient Stresses Produced Around a Tunnel by the Integral Equation Method,' Proc. Symp. Earthquake Engg., Japan, pp. 631-638.

Kobayashi, S. and Nishimura, N. (1982), 'Transient stress analysis of tunnels and cavities of arbitrary shape due to travelling waves,' Chapt. 7 in Developments in BEM - II, Banerjee, P.K. and Shaw, R.P., eds., Applied Science Publishers.

Kobayashi, S. and Nishimura, N. (1983), 'Analysis of dynamic soil-structure interaction by Boundary integral equation method,' Num. Meth. in Engg., Proc. 3rd Int. Symp., Paris, Vol. 1, Pluralis Publ., pp. 353-362.

Kupradze, V.D. (1963), 'Dynamical Problems of Elasticity,' Progress in Solid Mechanics, Vol. III, Sneddon, I.N. and Hill, R., eds., Interscience Publishers, New York.

Lachat, J.C. (1975), 'Further developments of the boundary integral technique for elasto-statics,' Ph.D. Thesis, Southampton University, U.K.

Lachat, J.C. and Watson, J.O. (1976), 'Effective numerical treatment of boundary integral equation: a formulation for three-dimensional elasto-statics,' Int. Jour. Num. Methods in Engineering, Vol. 10, pp. 991-1005.

Lamb, H. (1904), Philosophical Transactions of the Royal Society (London), Series A, Vol. 203, pp. 1-42.

Lamé, G. (1952), Lecons sur la Theorie Mathématique de l'Elasticité des Corps Solides, Bachelier, Paris.

Ligget, J. and Liu, P. (1983), Boundary integral equation for porous media flow, Allen and Unwin, London.

Lee, E.H. (1955), 'Stress analysis in viscoelastic bodies,' Quart. Appl. Math., Vol. 13, pp. 183-190.

Love, A.E.H. (1904), 'The propagation of wave-motion in an isotropic elastic solid medium,' Proc. of the London Math. Soc., Second series 1, pp. 291-344.

Luco, J.E. Hadjian, A.H. and Bos, H.D. (1974), 'The dynamic modelling of the half-plane by finite elements,' Nucl. Engg. and Design, Vol. 31, pp. 189-194.

Luco, J.E. and Westman, R.A. (1972), 'Dynamic response of a rigid footing bonded to an elastic half-space,' J. Appl. Mech., Vol. 39, pp. 527-534.

Manolis, G.D. (1983), 'A Comparative Study on Three Boundary Element Method Approaches to Problems in Elastodynamics,' Int. J. of Num. Meth. Engg., Vol. 19, pp. 71-93.

Manolis, G.D. and Beskos, D.E. (1981), 'Dynamic Stress Concentration Studies by Boundary Integrals and Laplace Transform,' Int. J. Num. Meth. Engg., Vol 17, pp. 573-599.

Mansur, W.J. and Brebbia, C.A. (1982), 'Numerical implementation of the boundary element method for two dimensional transient scalar wave propagation problems,' Appl. Math. Model., Vol. 6, pp. 299-306.

Mansur, W.J. and Brebbia, C.A. (1985), Transient Elastodynamics, Chapter 5 in Topics in Boundary Element Research, Vol. 2, Springer-Verlag.

Meyer, W.L., Bell, W.A. and Zinn, B.T. (1977), 'Integral solution of three dimensional acoustic radiation problems,' Proc. Int. Sym. Innovative Num. Ana. in Appl. Engg. Sci., CETIM, pp. 179-182.

Mikhlin, S.G. (1957), Integral Equation, Pergamon Press, Oxford.

Mikhlin, S.G. (1965a), Multi-dimensional singular integrals and integral equations, Pergamon Press, Oxford.

Mikhlin, S.G. (1965b), Approximate Solutions of Differential and Integral Equations, Pergamon Press, Oxford.

Miklowitz, J. (1980), The Theory of Elastic Waves and Waveguides, North-Holland Series in Appl. Math. and Mech., Vol. 22.

Misljenovic, D.M. (1982), 'The Boundary Element Method and Wave equation,' Appl. Math. Modelling, Vol. 6, pp. 205-208.

Mittra, R. (1973), Computer Techniques in Electromagnetics, Permagon Press, New York.

Morita, N. (1978), 'Surface Integral representations for electromagnetic scattering from dielectric cylinders,' IEEE Trans., AP-26(2), pp. 261-266.

Moller, M. and Stewart, S. (1973), 'An algorithm for solving the generalized matrix eigenvalue problems,' SIAM Jour. Num. Anal., Vol. 10, pp. 241-256.

Morse, P.M. and Feshbach, H. (1953), Method of Theoretical Physics, McGraw-Hill.

Mukherjee, S. (1982), Boundary elements in creep and fracture, Applied Science Publishers, London.

Muskhelishivili, N.I. (1953), Some Basic Problems of the Mathematical Theory of Elasticity, Noordoff, Groningen.

Mustoe, G.G. (1984), 'Advanced integration schemes over boundary elements and volume cells for two and three-dimensional nonlinear analysis,' Chapter IX of Developments in BEM - IV, Applied Science Publishers, U.K.

Nakai, S., Fukuwa, N. and Hasegawa, M. (1984), 'Approximate three-dimensional analyses of embedded structures,' Proc. of 8th W.C.E.E., pp. 689-696.

Narayanan, G.V. and Beskos, D.E. (1982), 'Numerical operational methods for time-dependent linear problems,' Int. J. Num. Meth. Engg., Vol. 18, pp. 1829-1854.

Nardini, D. and Brebbia, C.A. (1982), 'A new approach to free vibration analysis using boundary elements,' Proc. of the Fourth Int. Conf. in BEM, Springer-Verlag, pp. 313-326.

Neumann, F. (1885), Vorlesungen uber die Theorie der Elasticitat der festen Korper und des Lichtathers, B.G. Teubner, Leipzig.

Niwa, Y., Kobayashi, S. and Azuma, N. (1975), 'An analysis of transient stresses produced around cavities of an arbitrary shape during the passage of travelling wave,' Memo. Fac. Engg., Kyoto Univ., Vol. 37, pp. 28-46.

Niwa, Y., Kobayashi, S. and Fukui, T. (1976), 'Application of integral equation method to some geomechanical problems,' Proc. 2nd Int. Conf. Num. Meth. Geomech., ASCE, pp. 120-131.

Niwa, Y., Kobayashi, S. and Kitahara, M. (1982), 'Determination of eigenvalues by boundary element methods,' Chapter 6 of Developments in BEM-II, Applied Science Publishers, U.K., pp. 143-176.

Niwa, Y., Fukui, T., Kato, S., and Fujiki, K. (1983), 'An Application of the Integral Equation Method to Two-Dimensional Elastodynamics,' Theor. Appl. Mech., University of Tokyo Press, Vol. 28, pp. 281-290.

Norwood, F.R. and Miklowitz, J. (1967), 'Diffraction of transient-elastic waves by a spherical cavity,' J. Appl Mech., Vol. 34(3), pp. 735-741.

Nowacki, W. (1964), 'Mixed Boundary-value Problems in Elastodynamics,' Proc. of Vibration Problems, Warsaw, Vol. 35.

Pao, Y.H. and Mow, C.C. (1973), Diffraction of Elastic Waves and Dynamic Stress Concentration, Crane Russak, New York.

Papadopoulis, M. (1963), 'The use of singular integral in wave propagation problems; with applications to the point source in a semi-infinite medium,' Proc. of the Royal Soc. of London, Series A, Vol. 276, p. 1365.

Pekeris, C.L. (1955), 'The Seismic Surface Pulse,' Proc. Nat. Acad. of Sci., Vol. 41, pp. 469-480.

Poisson, S.D. (1829), Mémoires Académie Science, Paris, Vol. 8, pp. 356 and 623.

Raveendra, S.T. (1984), 'Advanced development of BEM for two and three-dimensional nonlinear analysis,' Ph.D. Thesis, State University of New York at Buffalo.

Rayleigh (1887), Proceedings of the London Mathematical Society, Vol. 20, pp. 225-234.

Rice, J.M. and Sadd, M.H. (1984), 'Propagation and scattering of SH waves in semi-infinite domains using a time-dependent boundary element method,' J. of Appl. Mech., Vol. 51, pp. 641-645.

Rizzo, F.J. (1967), 'An integral equation approach to boundary value problems of classical elastostatics,' Quart. Appl. Math., Vol. 25, pp. 83-85.

Rizzo, F.J. and Shippy, D.J. (1964), 'An advanced boundary integral equation method for three-dimensional thermoelasticity,' Int. J. Numer. Methods in Engg., Vol. 11, pp. 1753-1768.

Rizzo, F.J., Shippy, D.J., and Rezayat, M. (1985), 'Boundary Integral Equation Analysis for a Class of Earth-Structure Interaction Problems,' Final Report to NSF, Grant No. CEE80-13461, Dept. of Engng. Mech., University of Kentucky, Lexington.

Schenck, H.A. (1967), 'Formulation and solution of acoustic radiation problems as integral equations - selected references,' Naval Undersea Warfare Centre, San Diego, California.

Sen, R. (1984), 'Dynamic analysis of buried structures,' Ph.D. Thesis, State University of New York at Buffalo.

Sen, R., Davies, T.G., and Banerjee, P.K. (1985a), 'Dynamic Analysis of Piles and Pile Groups Embedded in Homogeneous Soils,' Earthquake Engg. and Struc. Dyn., Vol. 13, pp. 53-65.

Sen, R., Kausel, E., and Banerjee, P.K. (1985b), 'Dynamic Analysis of Piles and Pile Groups Embedded in Nonhomogeneous Soils,' Int. J. Num. Anal. Methods in Geomechanics, Vol. 9, (to appear).

Shaw, R.P. (1970), 'An integral equation approach to acoustic radiation and scattering,' Topics in Ocean Engineering II, Bretschneider, C., ed., Gulf, Publ. Co., Houston, pp. 143-163.

Shaw, R.P. (1975a), 'An outer boundary integral equation applied to transient waves scattering in an inhomogeneous medium,' J. Appl. Mech., Vol. 42, pp. 147-152.

Shaw, R.P. (1975b), 'Boundary integral equation methods applied to water waves,' Boundary Integral Equation Method, Cruse, T. and Rizzo, F., eds., AMD Vol. 11, ASME, New York, pp. 7-14.

Shaw, R.P. (1979), 'Boundary integral equation methods applied to wave problems,' Developments in Boundary Element Methods, Vol. 1, Eds. Banerjee, P.K. and Butterfield, R., Applied Science Publishers, London, pp. 121-153.

Shippy, D.J. (1975), 'Application of the boundary integral equation method to transient phenomena in solids,' Boundary Integral Equation Method: Computational Application in Applied Mechanics, AMD, Vol. 11, ASME, New York.

Smirnov, V.J. (1964), 'Integral equations and partial differential equations,' A course in Higher Mathematics, Vol. IV, Addison-Wesley, London.

Somigliana, C. (1892), Atti Reale Accad. Linc. Roma, Series 5, Vol. 1, p. 111.

Spyrakos, C.C. (1984), 'Dynamic Response of Strip-foundation by the time domain BEM-FEM method,' Ph.D. Thesis, University of Minnesota, Minneapolis.

Stokes, G.G. (1849), 'Dynamic theory of diffraction,' transactions of the Cambridge Philosophical Society, Vol. 9, pp. 1-62.

Stroud, A.H. and Secrest, D. (1966), Gaussian Quadrature Formulas, Prentice Hall, New York.

Swedlow, J.L. and Cruse, T.A. (1971), 'Formulation of boundary integral equations for three-dimensional elasto-plastic flow,' Int. Jour. Solids and Structures, Vol. 7, pp. 1673-1684.

Symm, G.T. (1963), 'Integral equation methods in potential theory, II', Proc. Roy. Soc., London, Series A, Vol. 275, pp. 3346.

Tai, G.R.C. and Shaw, R.P. (1974), 'Helmholtz equation eigenvalues and eigenmodes for arbitrary domains,' J.A.S.A., Vol. 56, pp. 796-804.

Tanaka, Y. and Maeda, T. (1984), 'Dynamic interaction of a rigid foundation embedded in two-layered visco-elastic medium,' Proc. of 8th W.C.E.E., California, pp. 865-872.

Tedone, O. (1897), Mem. Reale Accad, Scienze Torino, Series 2, Vol. 47, p. 181.

Telles, J.C.F. (1983), 'The boundary elements method applied to inelastic problems', Lecture Notes in Engineering, Springer Verlag.

Tseng, M.N. and Robinson, A.R. (1975), 'A transmitting boundary for finite difference analysis of wave propagation in solids,' Project No. NR. 064-183, University of Illinois, Urbana.

Timoshenko, S.P. and Gere, J.M. (1970), Theory of Elasticity, 3rd Edition, McGraw-Hill, New York.

Tzong, T.G., Gupta, S. and Penzien, J. (1981), 'Two dimensional hybrid modelling of soil-structure interaction,' EERC Report 81/11, Univ. of California, Berkeley.

Veletsos, A.S. and Wei, Y.T. (1971), 'Lateral and Rocking Vibration of Footings,' Proc. ASCE, SM9, Vol. 97, pp. 1227-1248.

Vivoli, J. and Filippi, P. (1974), 'Eigenfrequencies of thin plates and layer potentials,' J.A.S.A., Vol. 55(3), pp. 562-567.

Watson, J.O. (1979), 'Advanced implementation of the boundary element method for two and three-dimensional elastostatics,' Chapter 3 of Developments in Boundary Element Methods - I, Applied Science Publishers, London.

Wheeler, L.T. and Sternberg, E. (1968), 'Some Theorems in Classical Elastodynamics,' Archive for Rational Mechanics and Analysis, Vol. 31, pp. 51-90.

Wickham, G.M. (1977), 'The forced two dimensional oscillations of a rigid strip in smooth contact with a semi-infinite elastic solid,' Math. Proc. Cambridge Phil. Soc., Vol. 81(2), pp. 291-311.

Wong, H.L. and Luco, J.E. (1976), 'Dynamic Response of Rigid Foundations of Arbitrary Shape,' Earthquake Engineering and Struct. Dyn., Vol. 4, pp. 579-587.

Yoshida, K., Sato, T. and Kawase, H. (1984), 'Dynamic response of rigid foundations subjected to various types of seismic wave,' Proc. 8th W.C.E.E., California, pp. 745-752.

Zienkiewicz, O.C. (1977), The Finite Element Method, Third edition, McGraw Hill, London.

FIGURES

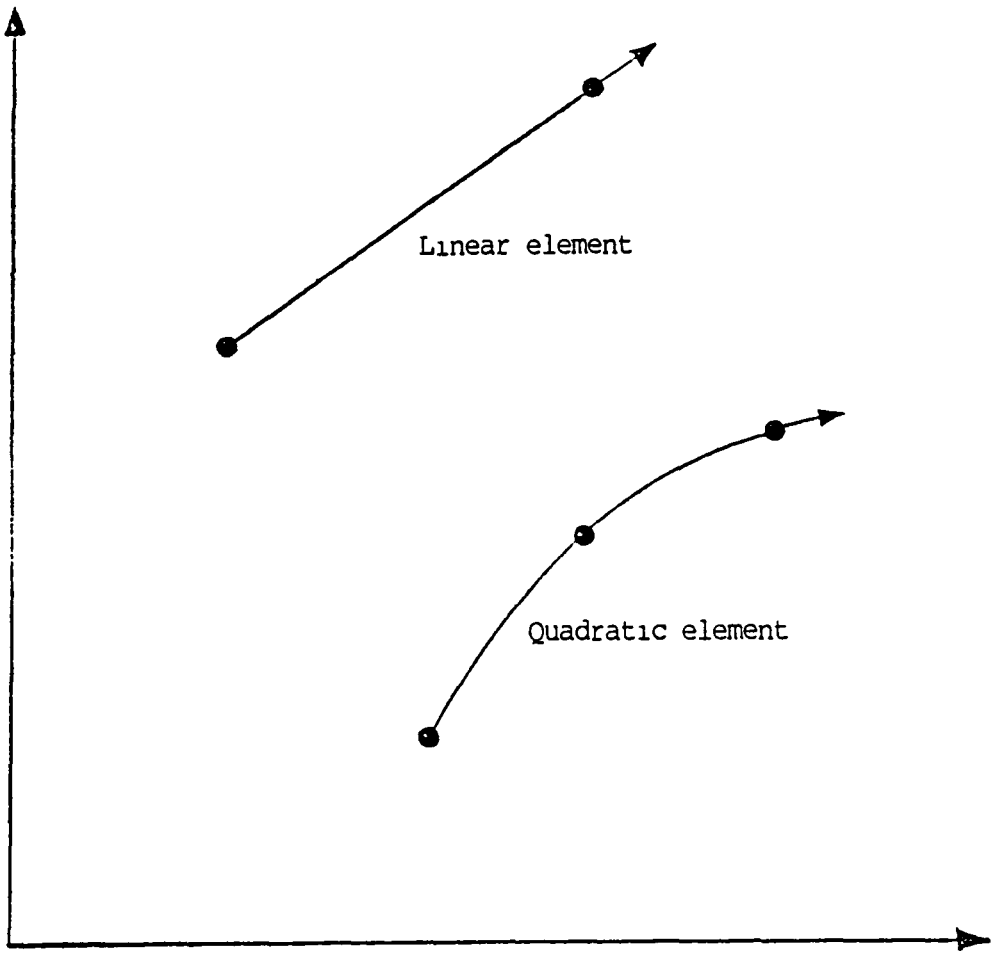

Two-dimensional boundary elements

Figure 4.1

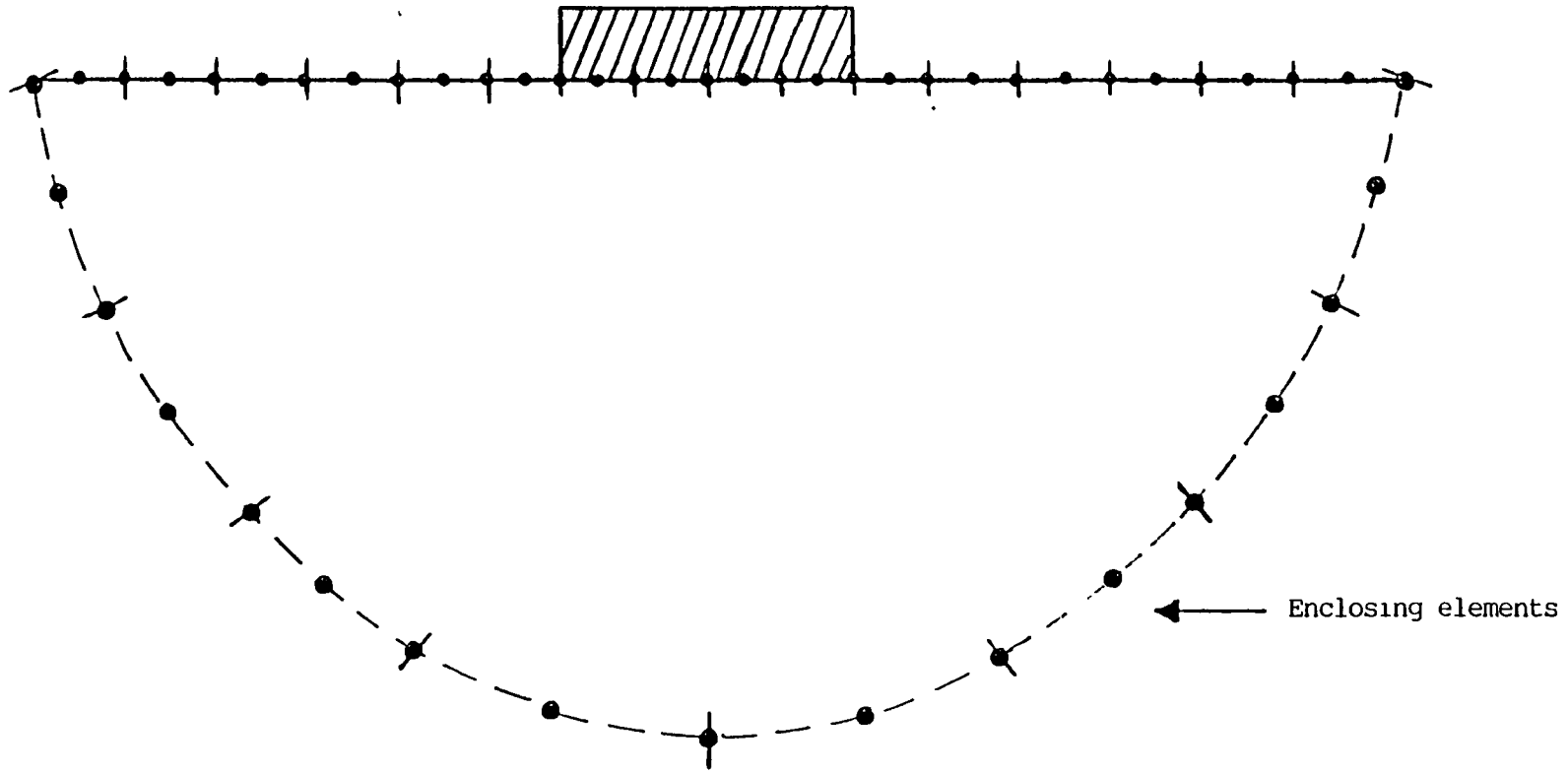

Boundary Element discretization of a half-space Problem

Figure 4.2

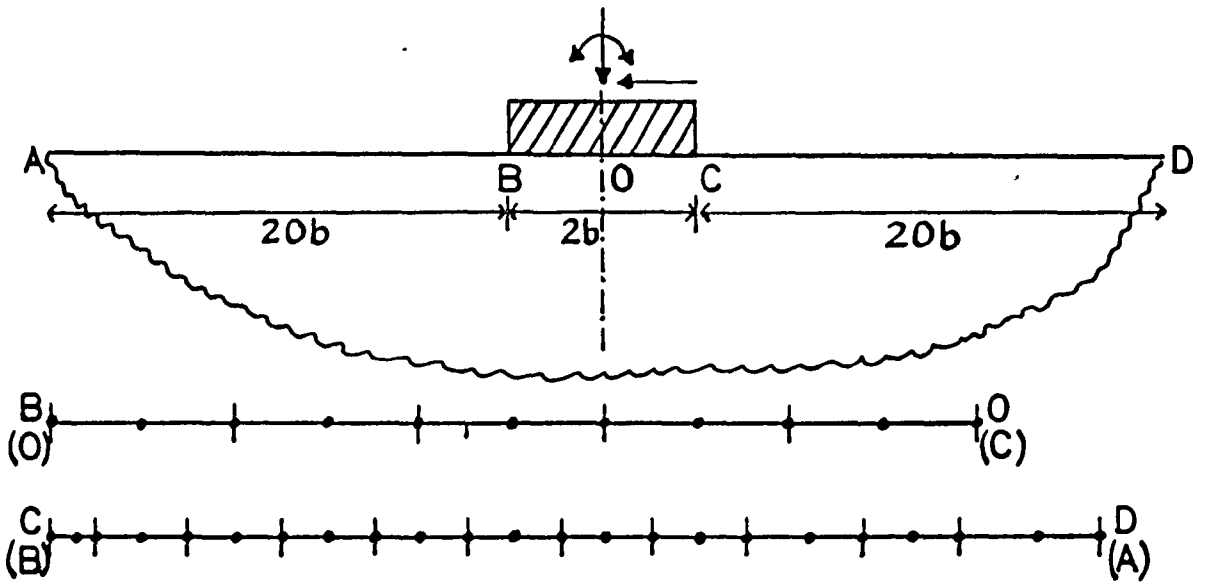

DISCRETIZATION OF A RIGID STRIP FOOTING ON AN ELASTIC HALF SPACE

Figure 4.3

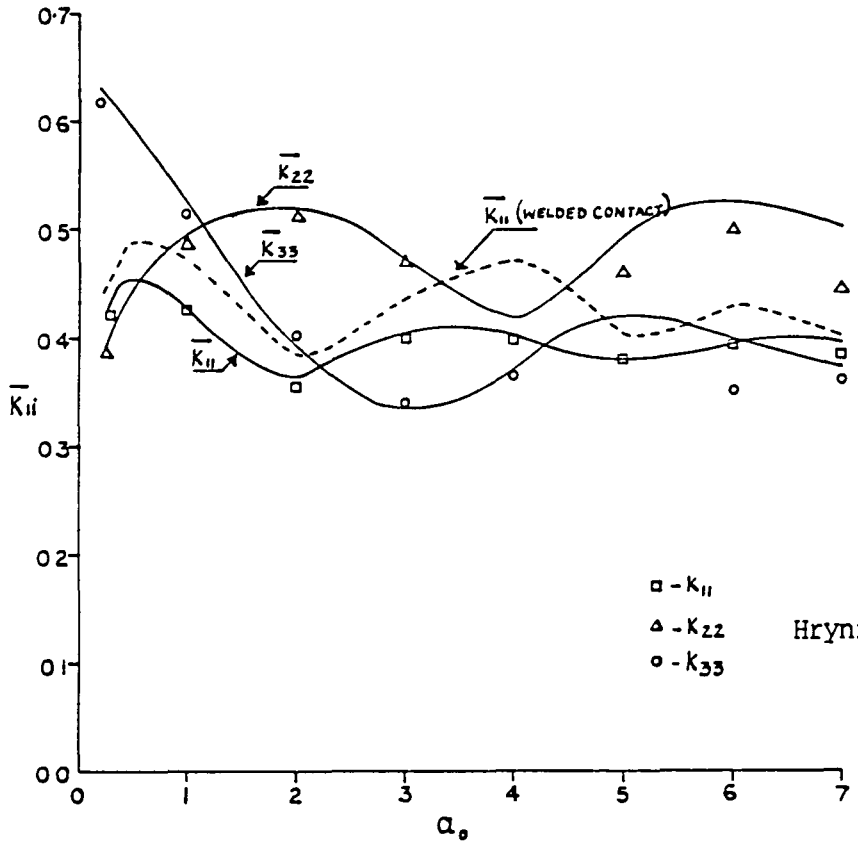

Hryniewicz (1981)

REAL PART OF STIFFNESS CO-EFFICIENTS FOR A RIGID STRIP FOOTING ($y = \frac{1}{4}$)

Figure 4.4

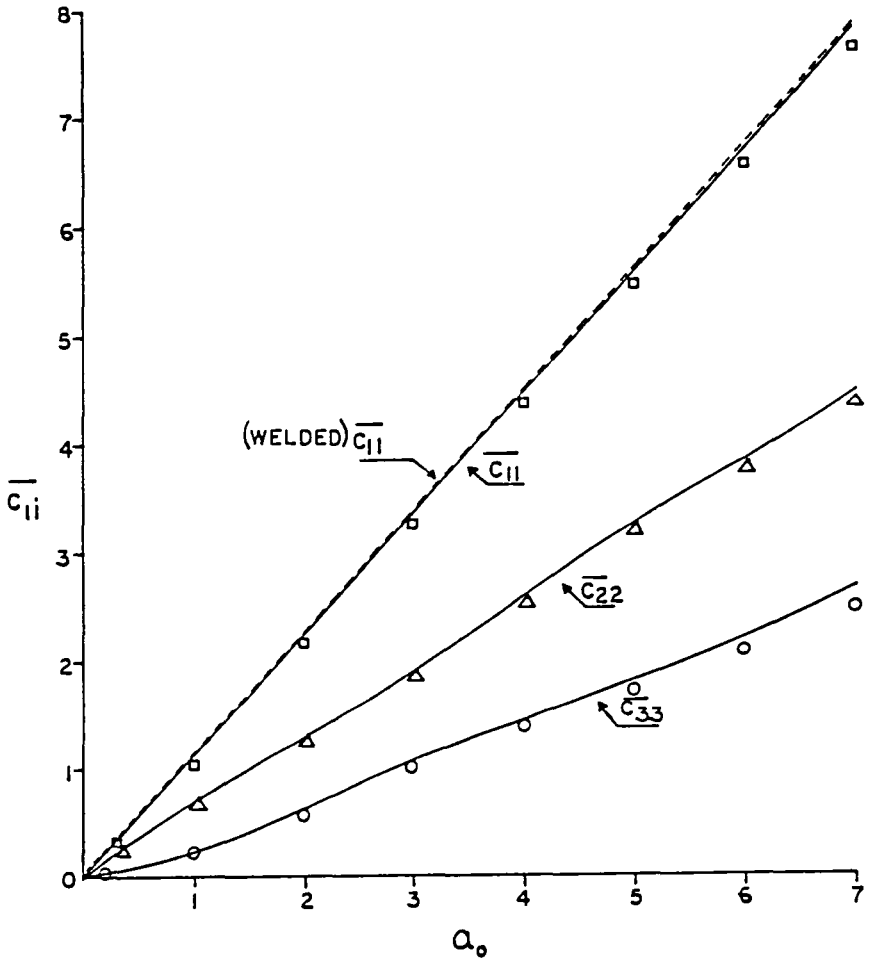

IMAGINARY PART OF STIFFNESS CO-EFFICIENTS FOR A RIGID STRIP FOOTING ($y = 1/4$)

Figure 4.5

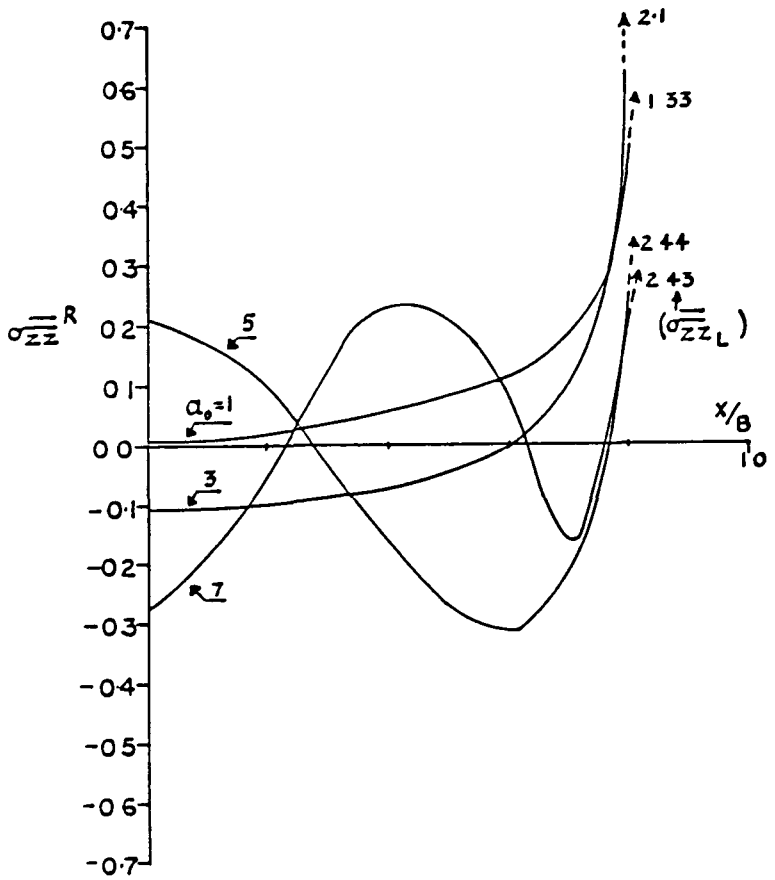

REAL PART OF CONTACT STRESS FOR VERTICAL VIBRATION OF A RIGID STRIP FOOTING

Figure 4.6

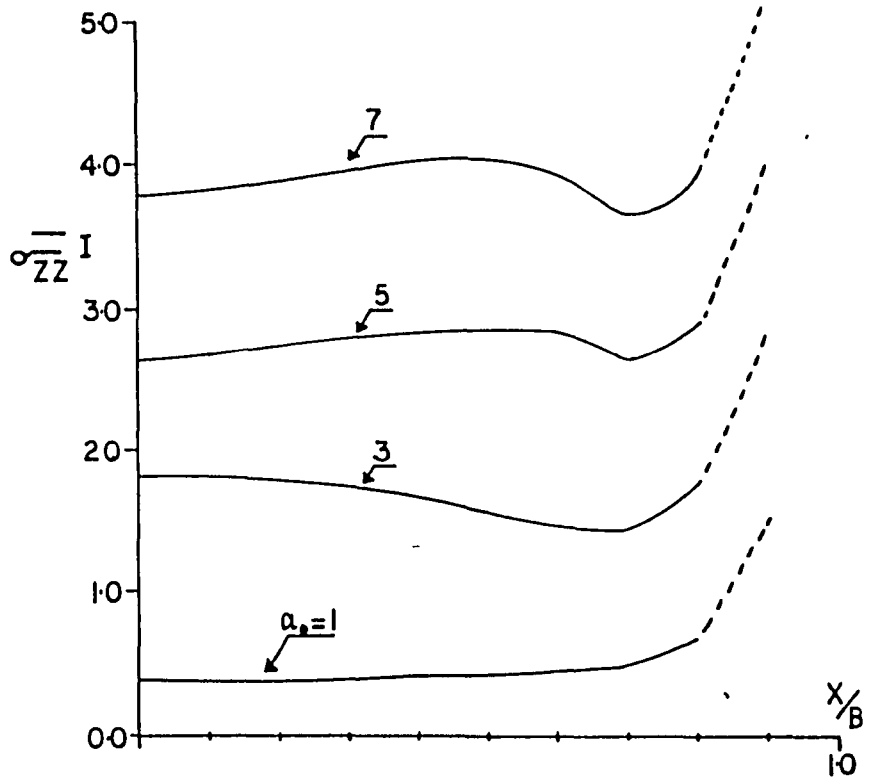

IMAGINARY PART OF CONTACT STRESS FOR VERTICAL VIBRATION OF A RIGID STRIP FOOTING

Figure 4.7

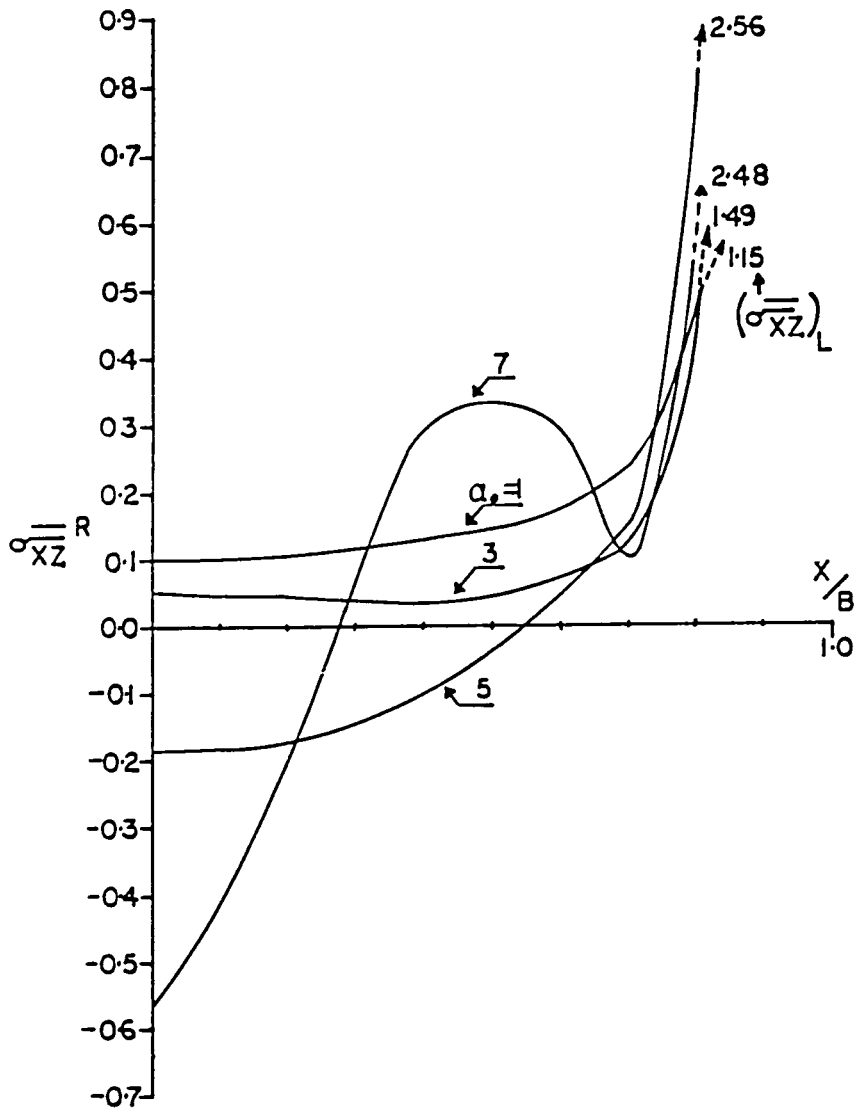

REAL PART OF CONTACT STRESS FOR
HORIZONTAL VIBRATION OF A RIGID STRIP

Figure 4.8

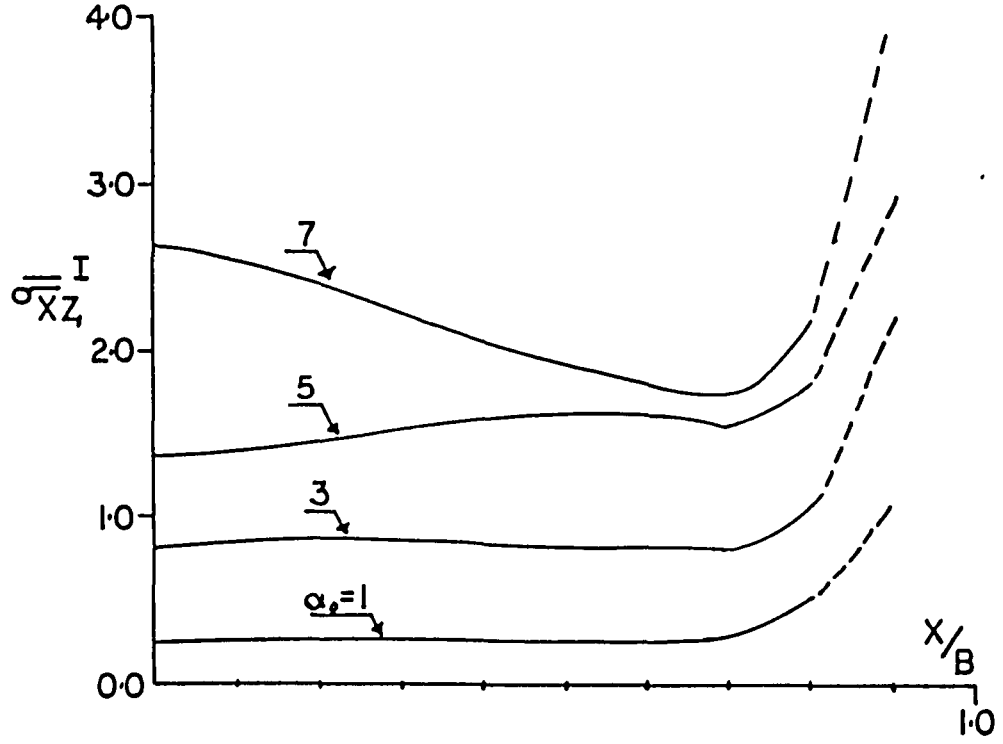

IMAGINARY PART OF CONTACT STRESS FOR HORIZONTAL VIBRATION OF A RIGID STRIP FOOTING

Figure 4.9

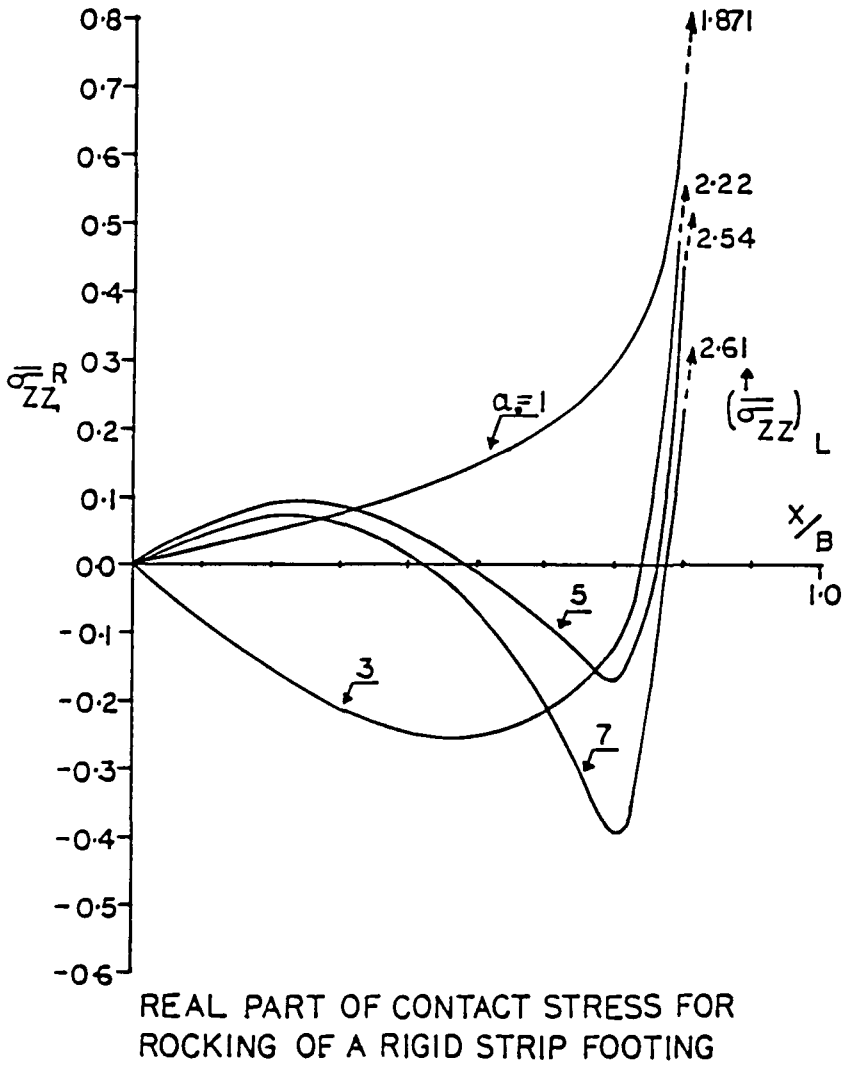

REAL PART OF CONTACT STRESS FOR ROCKING OF A RIGID STRIP FOOTING

Figure 4.10

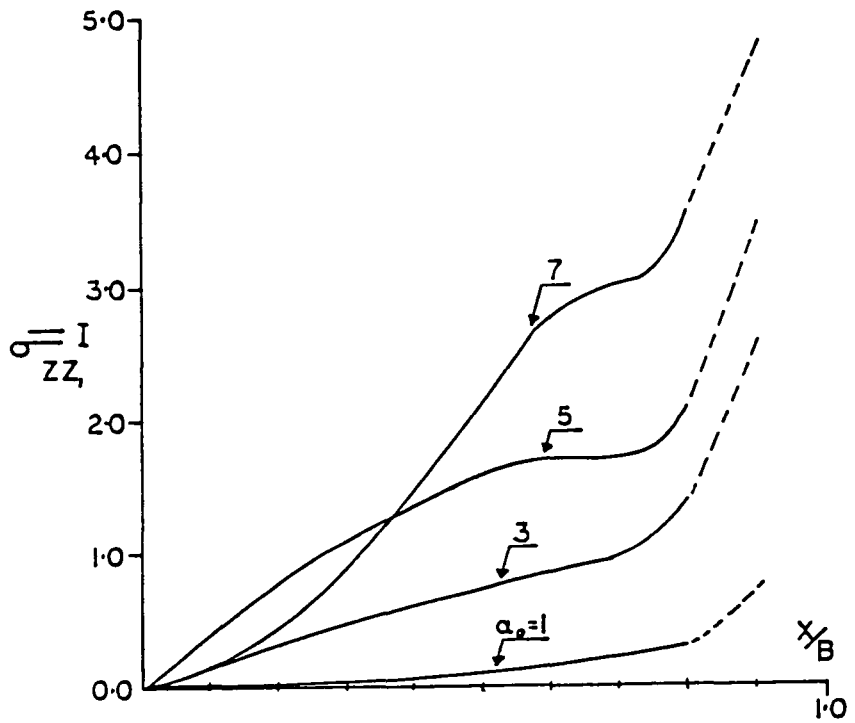

IMAGINARY PART OF CONTACT STRESS FOR ROCKING OF A RIGID STRIP FOOTING

Figure 4.11

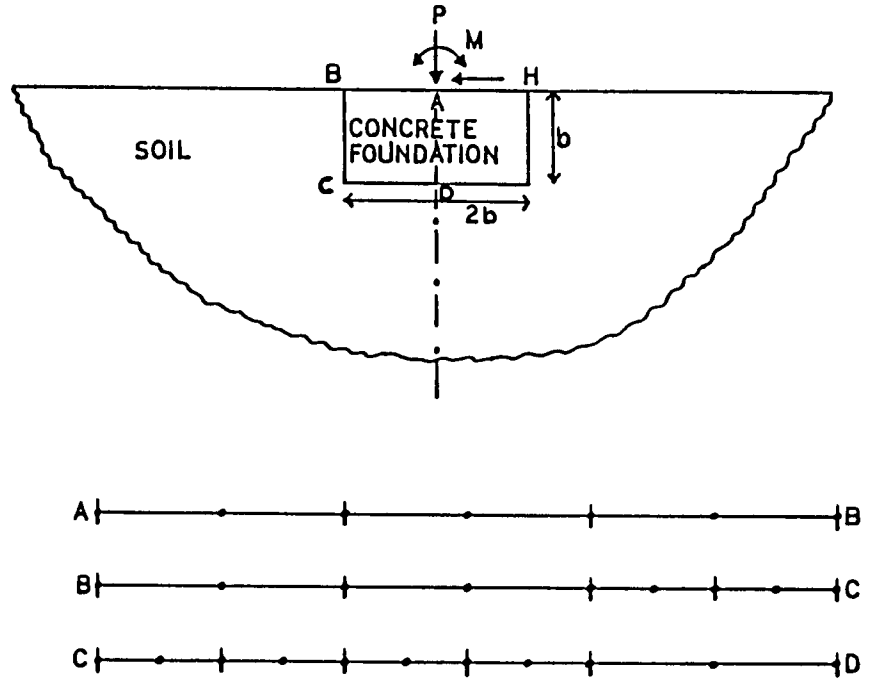

DISCRETIZATION OF A MACHINE FOUNDATION
ON AN ELASTIC HALF SPACE

Figure 4.12

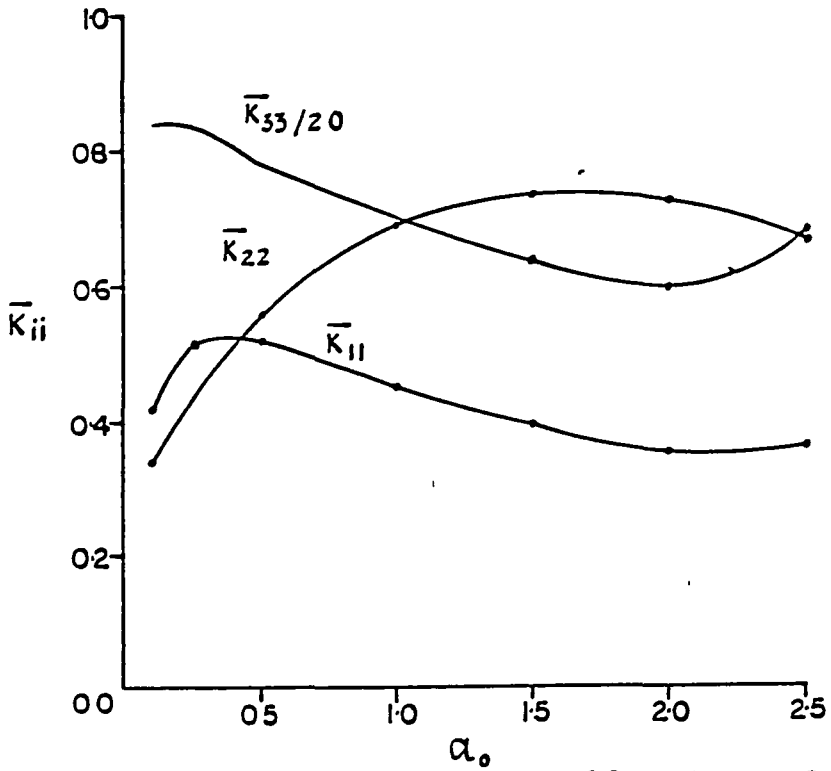

REAL PART OF STIFFNESS CO-EFFICIENTS FOR A MACHINE FOUNDATION

Figure 4.13

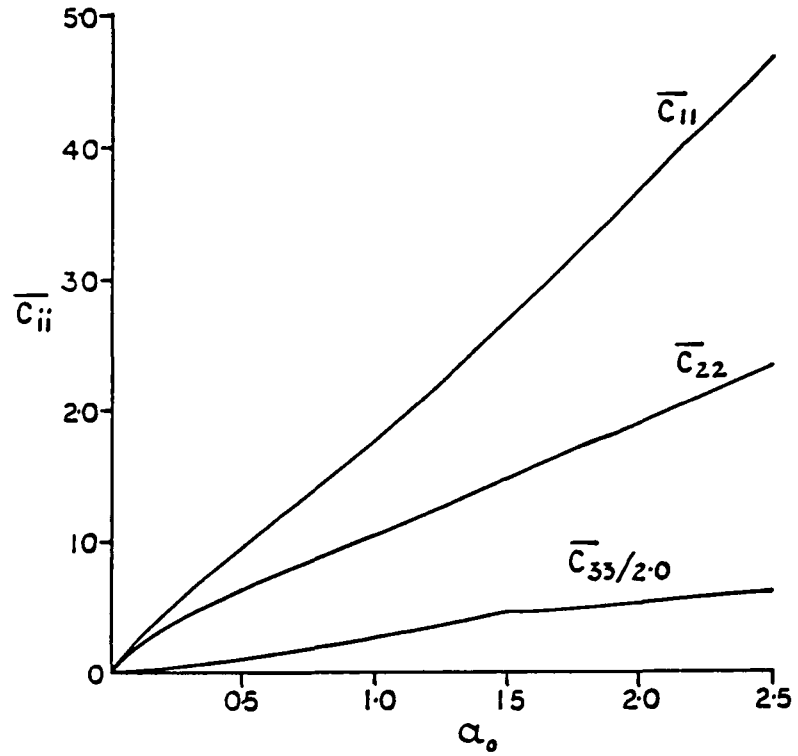

IMAGINARY PART OF STIFFNESS CO-EFFICIENTS FOR A MACHINE FOUNDATION

Figure 4.14

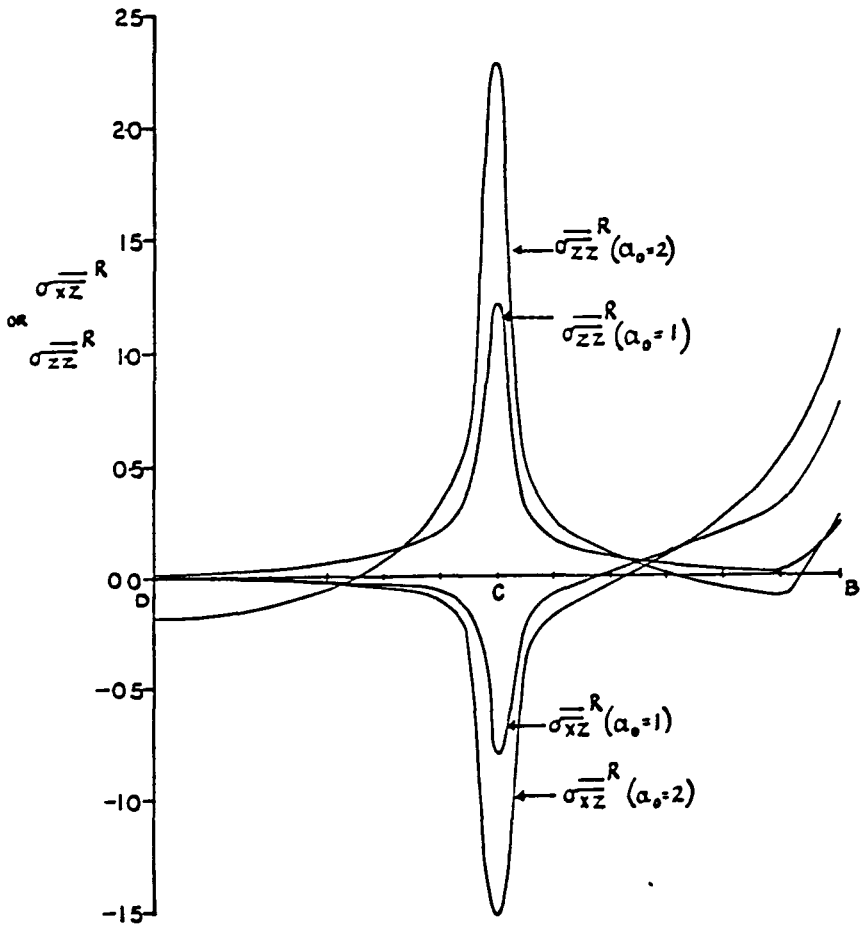

REAL PART OF STRESSES FOR VERTICAL VIBRATION OF A MACHINE FOUNDATION

Figure 4.15

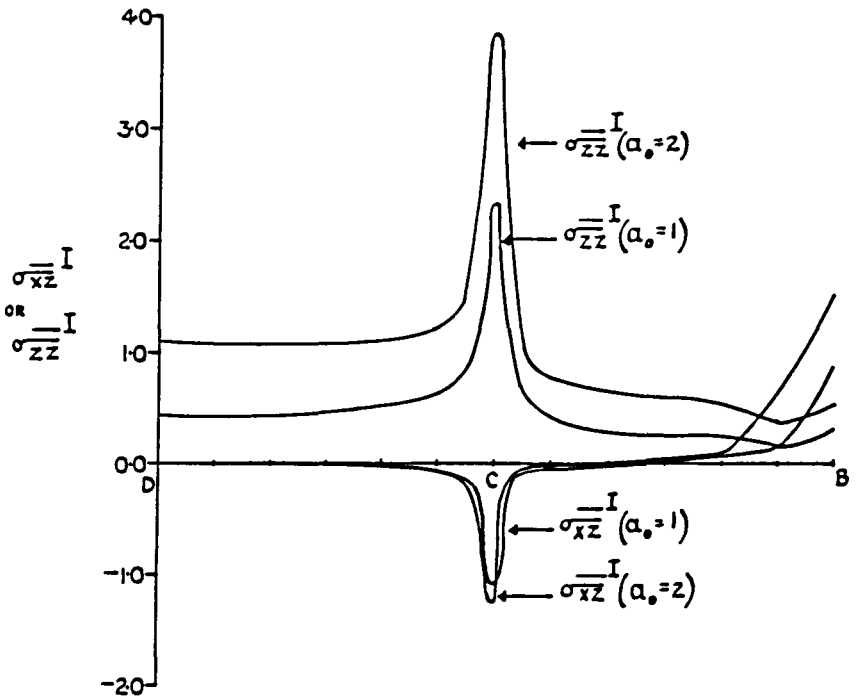

IMAGINARY PART OF STRESSES FOR VERTICAL VIBRATION OF A MACHINE FOUNDATION

Figure 4.16

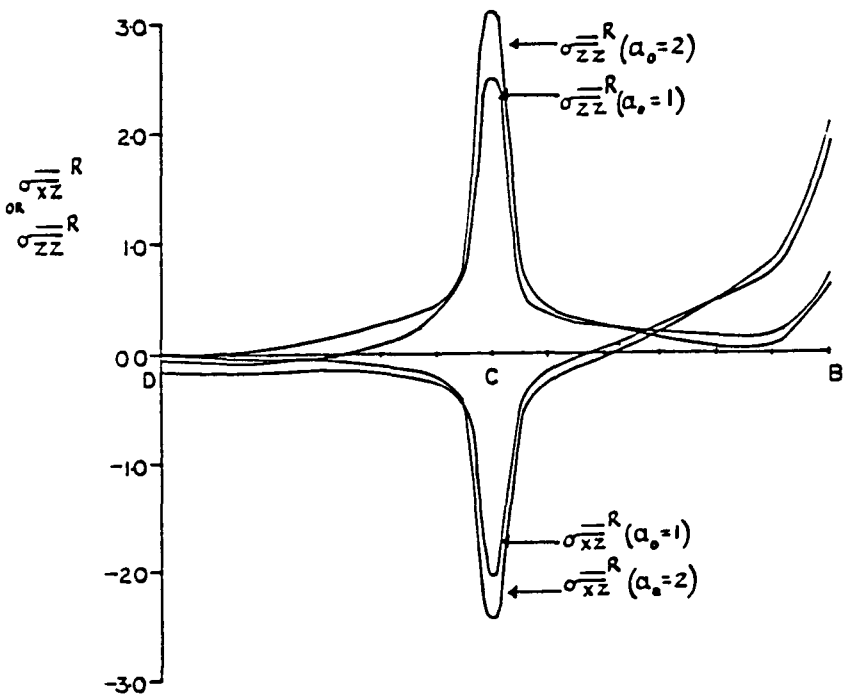

REAL PART OF STRESSES FOR ROCKING OF A MACHINE FOUNDATION

Figure 4.17

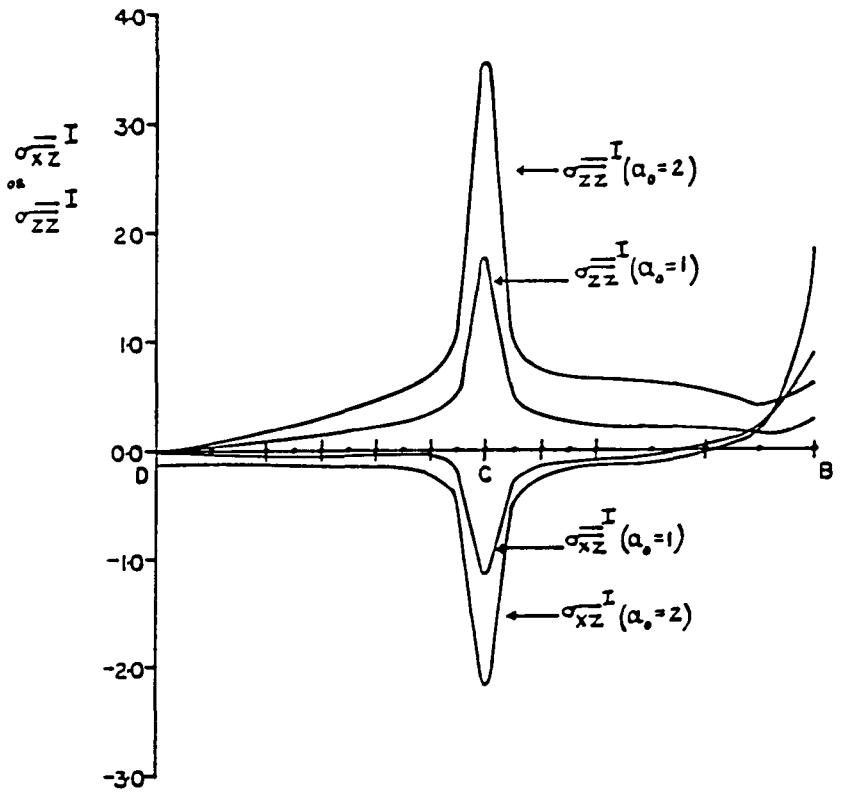

IMAGINARY PART OF STRESSES FOR ROCKING OF A MACHINE FOUNDATION

Figure 4.18

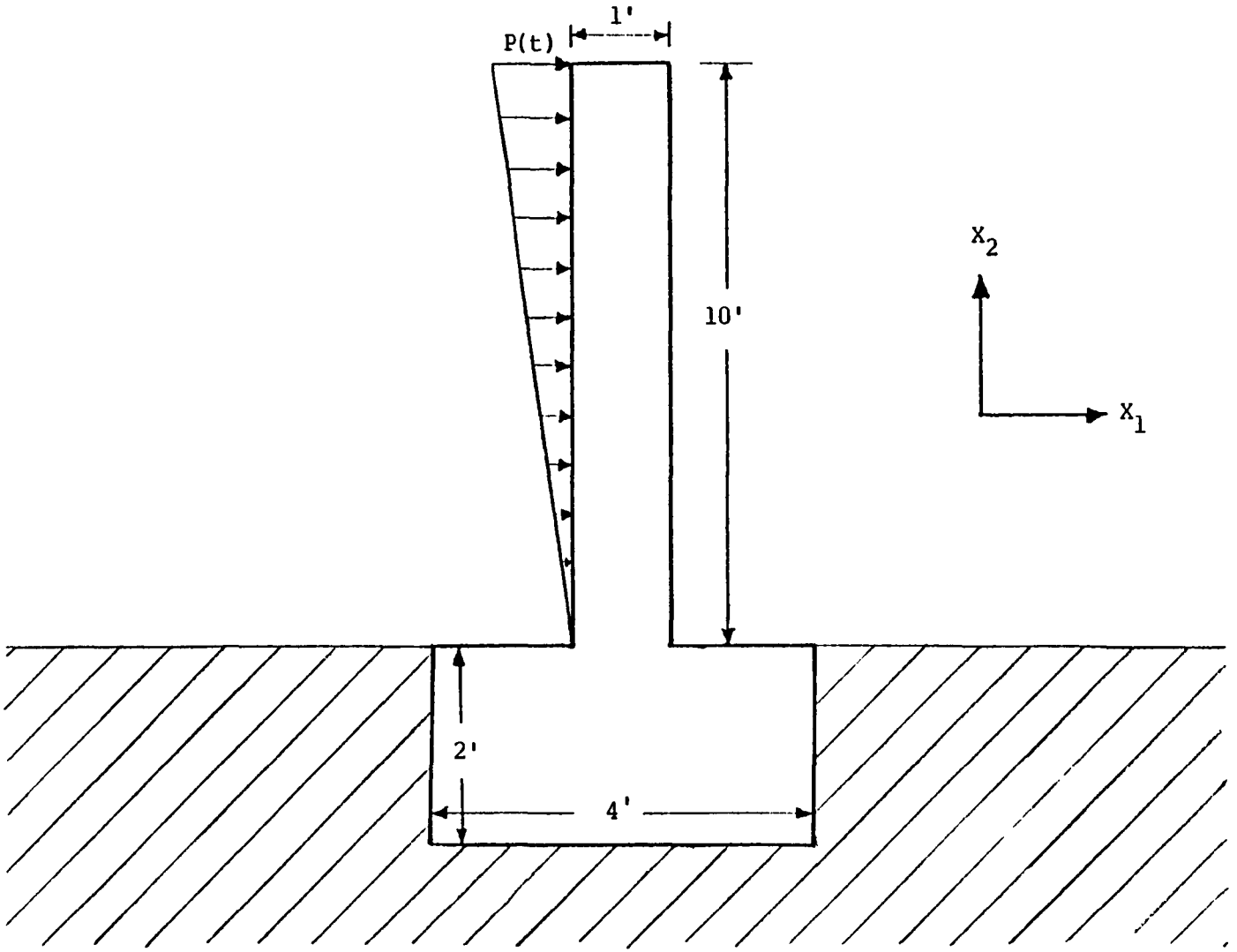

A wall in an elastic half-space subjected to a time harmonic lateral load

Figure 4.19

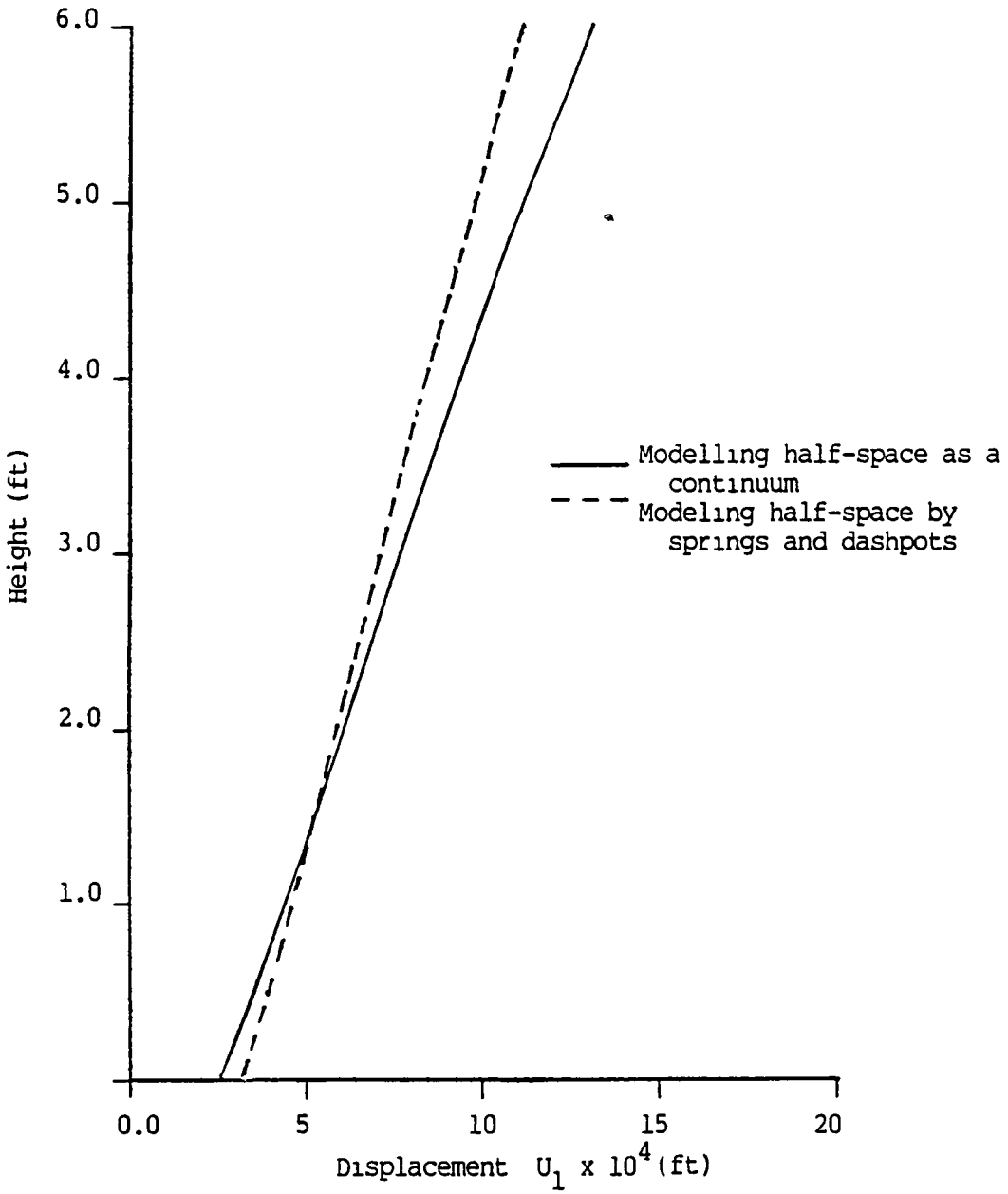

Lateral displacement of a wall in an elastic half-space

Figure 4.20

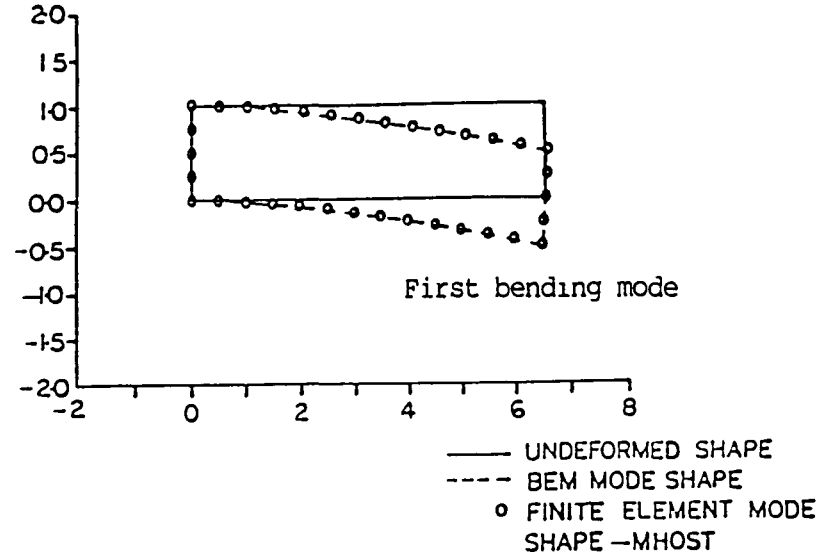

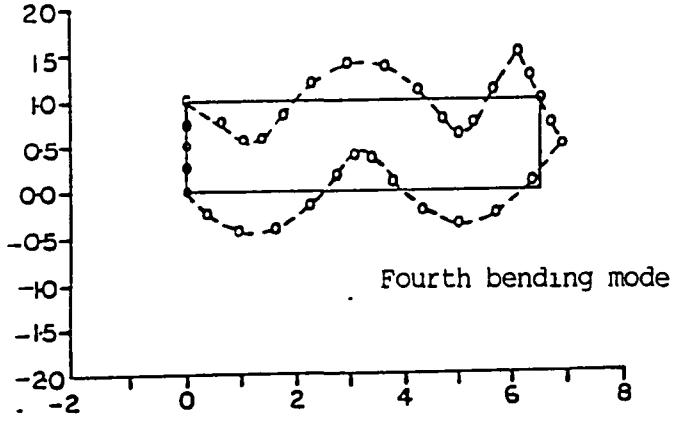

Comparison of Mode Shapes from BEM Solution and MARC Finite Element Solution

Figure 5.1

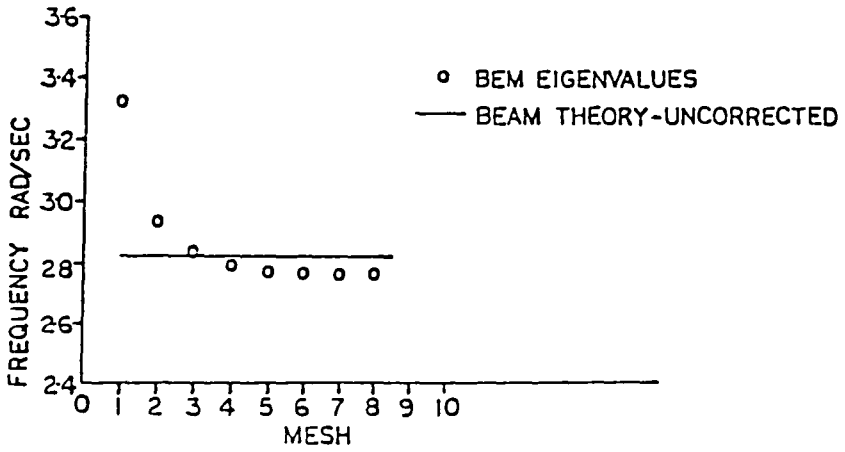

CONVERGENCE OF BEM EIGENVALUES—MODE 1 (1ST FLEXURAL)

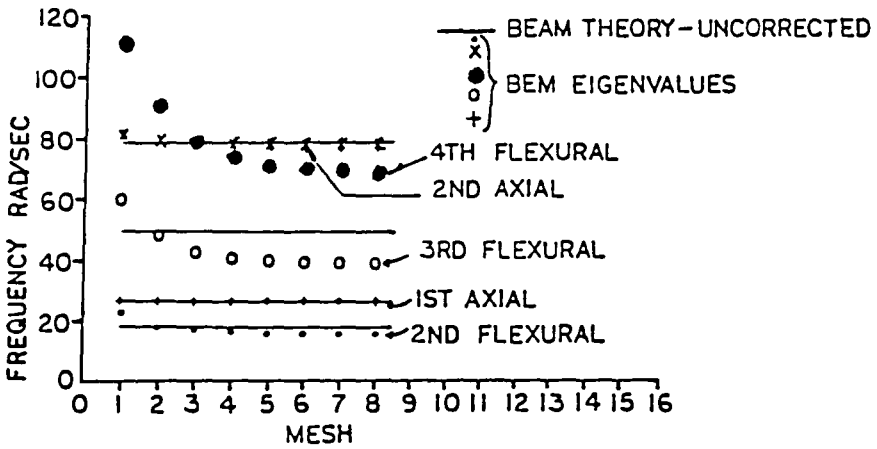

CONVERGENCE OF BEM EIGENVALUES—MODES 2-6

Comparison of BEM Eigenvalues with analytical beam-column Eigenvalues

Figure 5.2

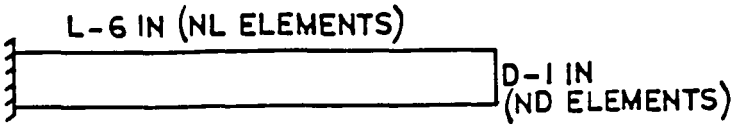

B(WIDTH)=1 IN
E=10000 PSI
M=1 LB/IN
NT=TOTAL ELEMENTS (2(NL+ND))

MESH	NL	ND	NT
1	2	1	6
2	3	1	8
3	4	1	10
4	5	1	12
5	6	1	14
6	7	1	16
7	8	2	20
8	10	2	24

Boundary element discretization of a cantilever beam

Figure 5.3

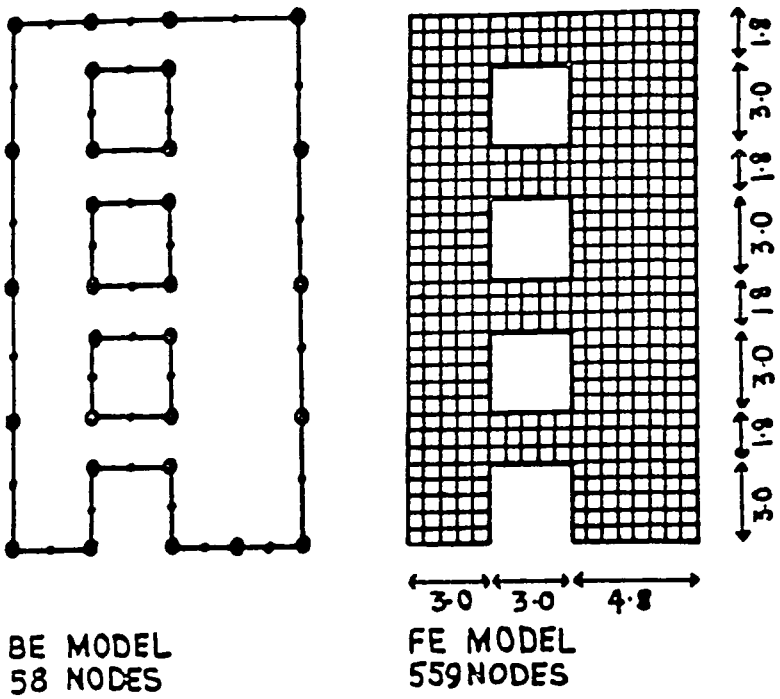

Discretizations of a shear wall

Figure 5.4

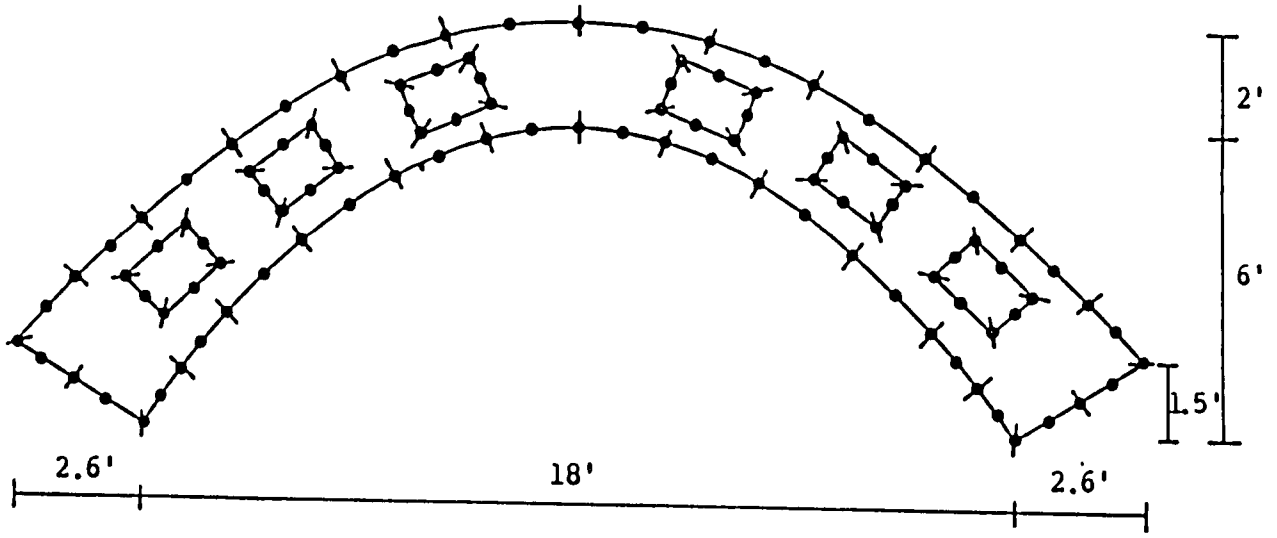

Boundary Element Discretization of a fixed end arch with openings

Figure 5.5

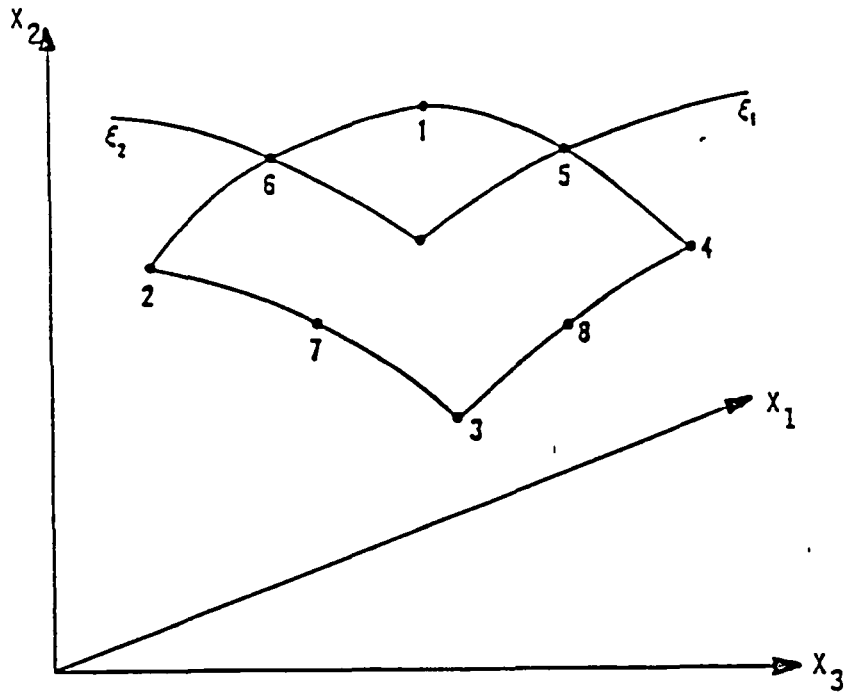

Three-dimensional nonplanar surface patch

Figure 6.1

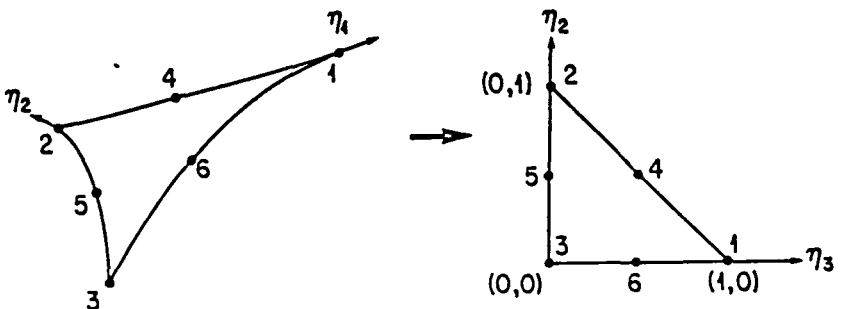

(a) Six-noded triangle

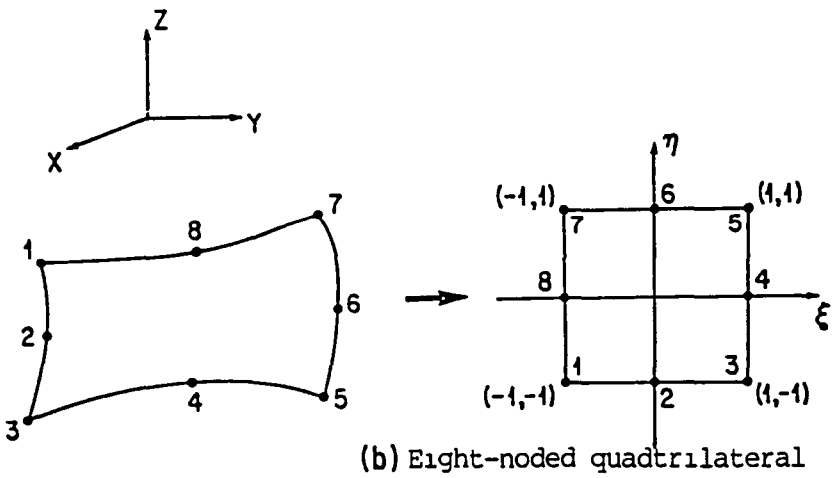

(b) Eight-noded quadrilateral

Three-dimensional surface elements

Figure 6.2

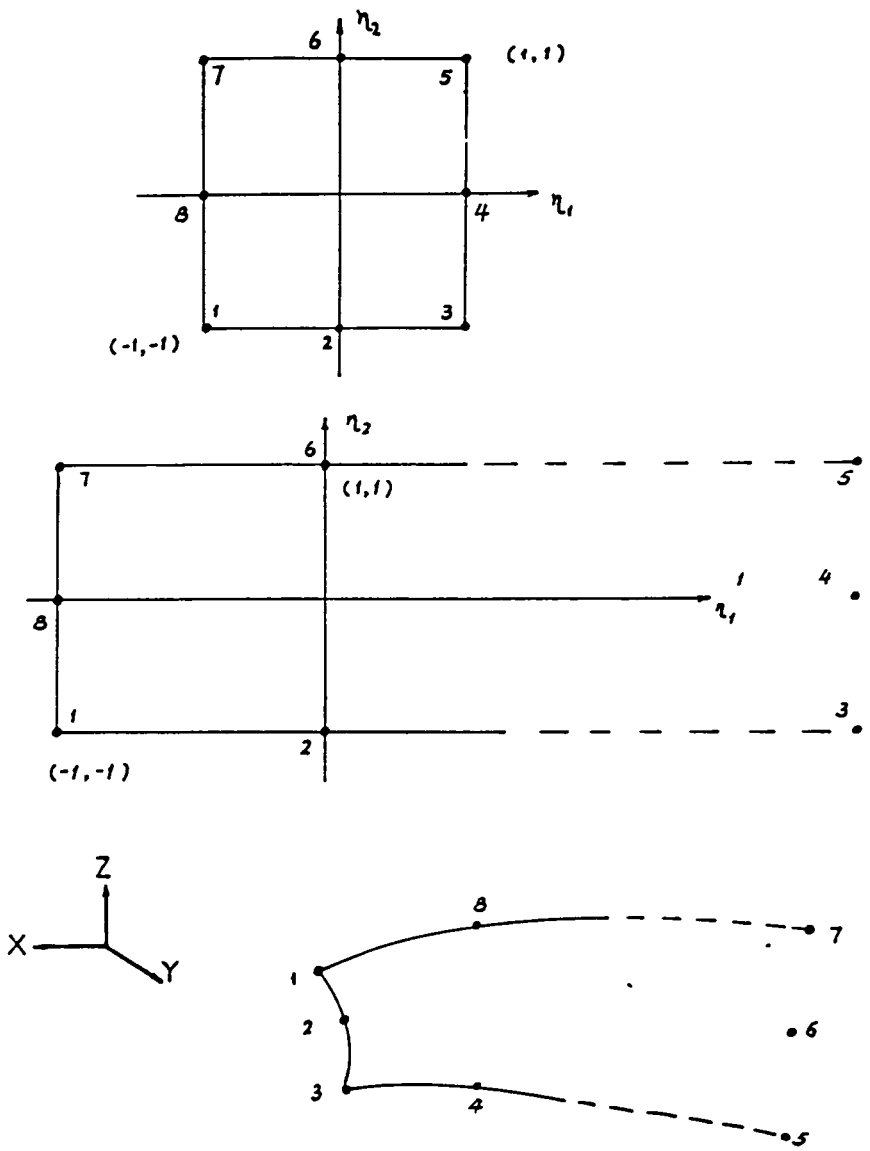

Infinite element

Figure 6.3

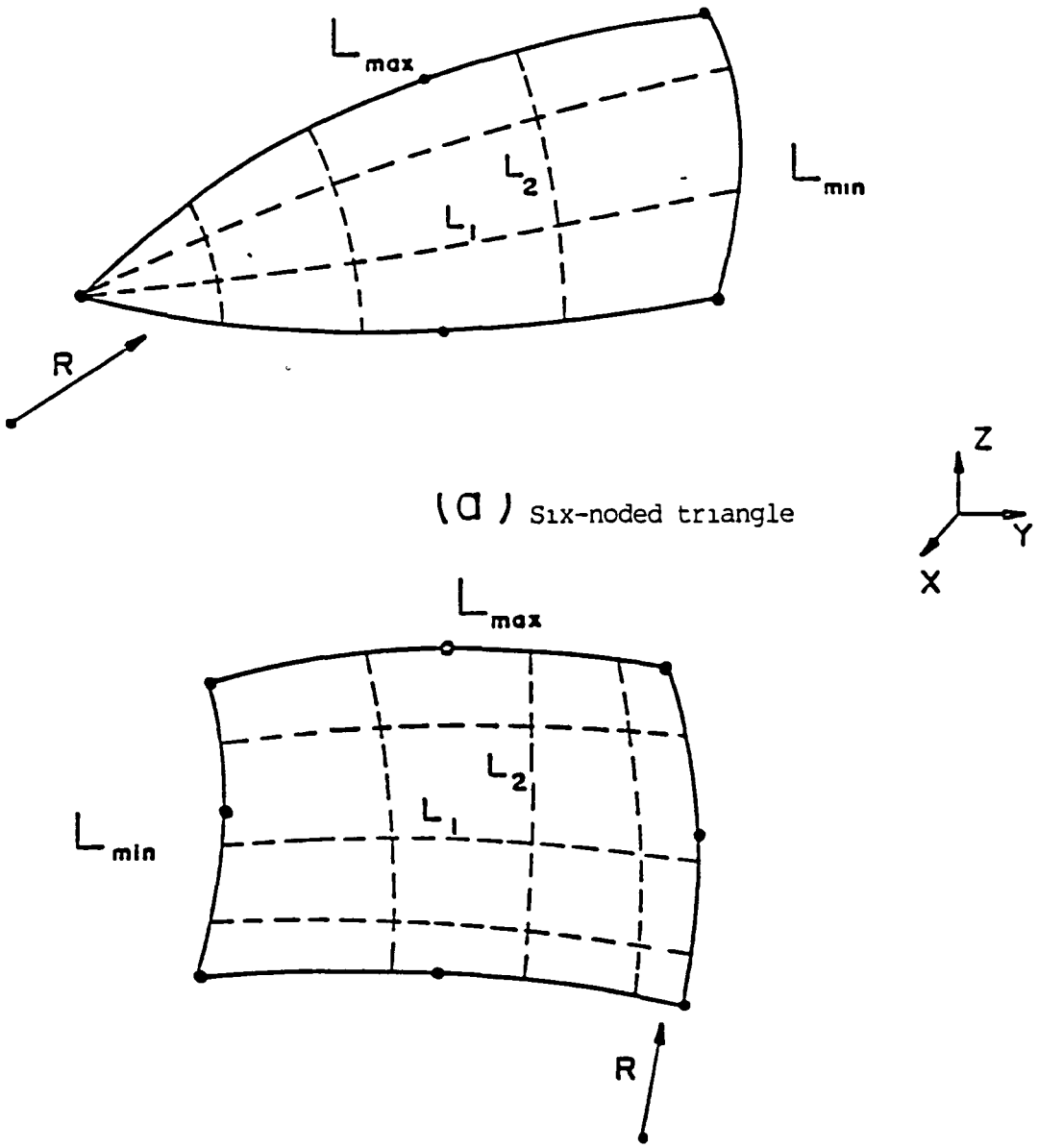

(a) Six-noded triangle

(b) Eight-noded quadrilateral

Typical subdivision patterns for surface elements

Figure 6.4

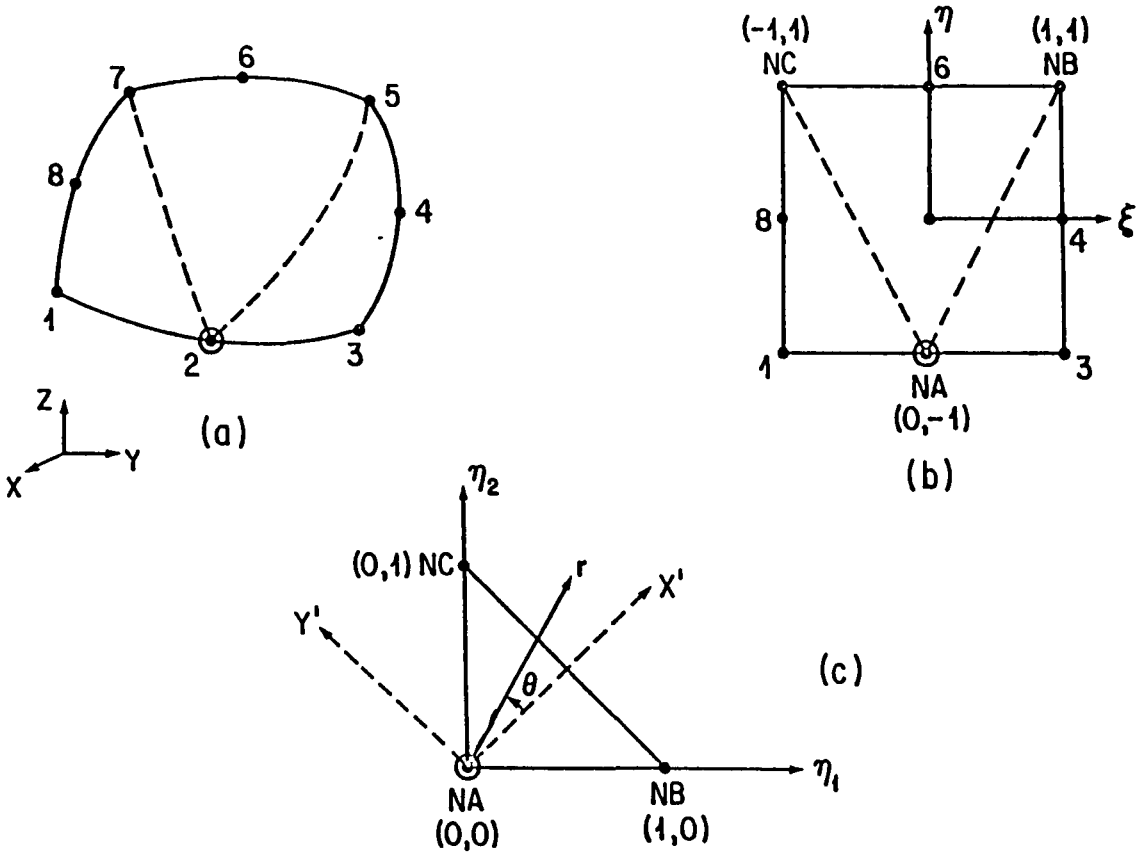

Singular integration process for a quadrilateral element

Figure 6.5

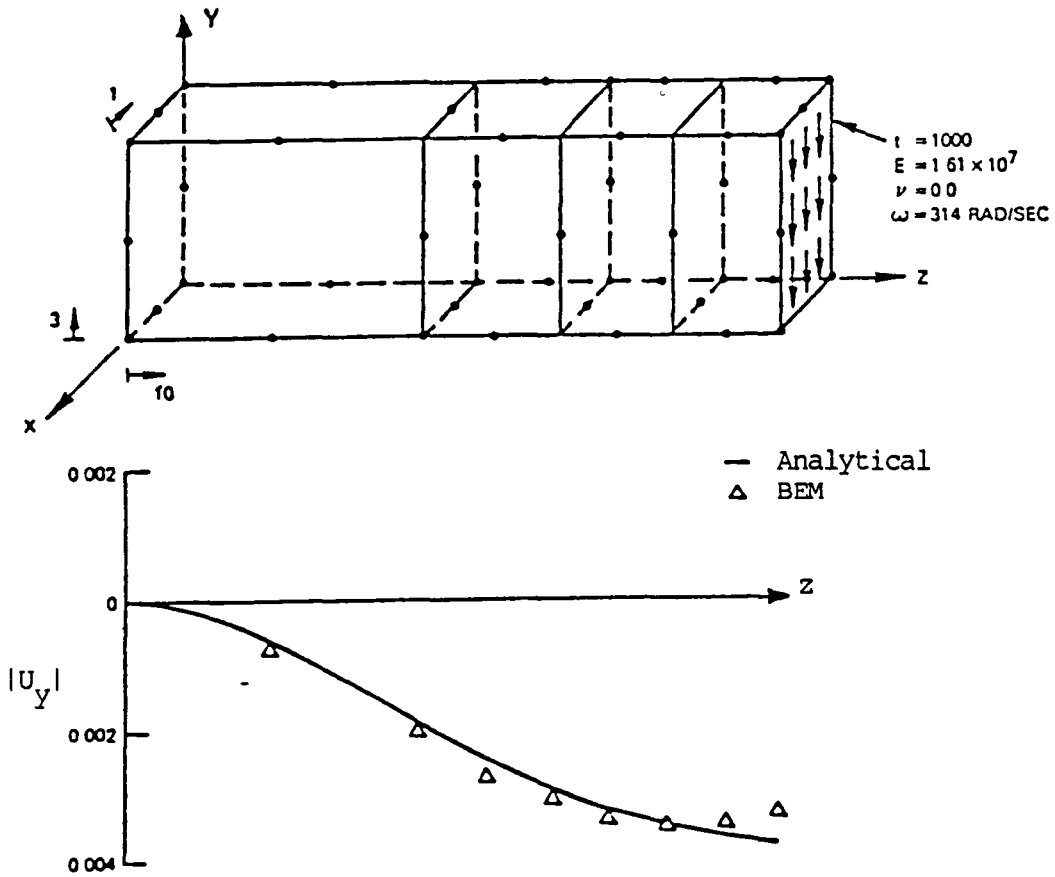

Cantilever subjected to harmonic end shear

Figure 6.6

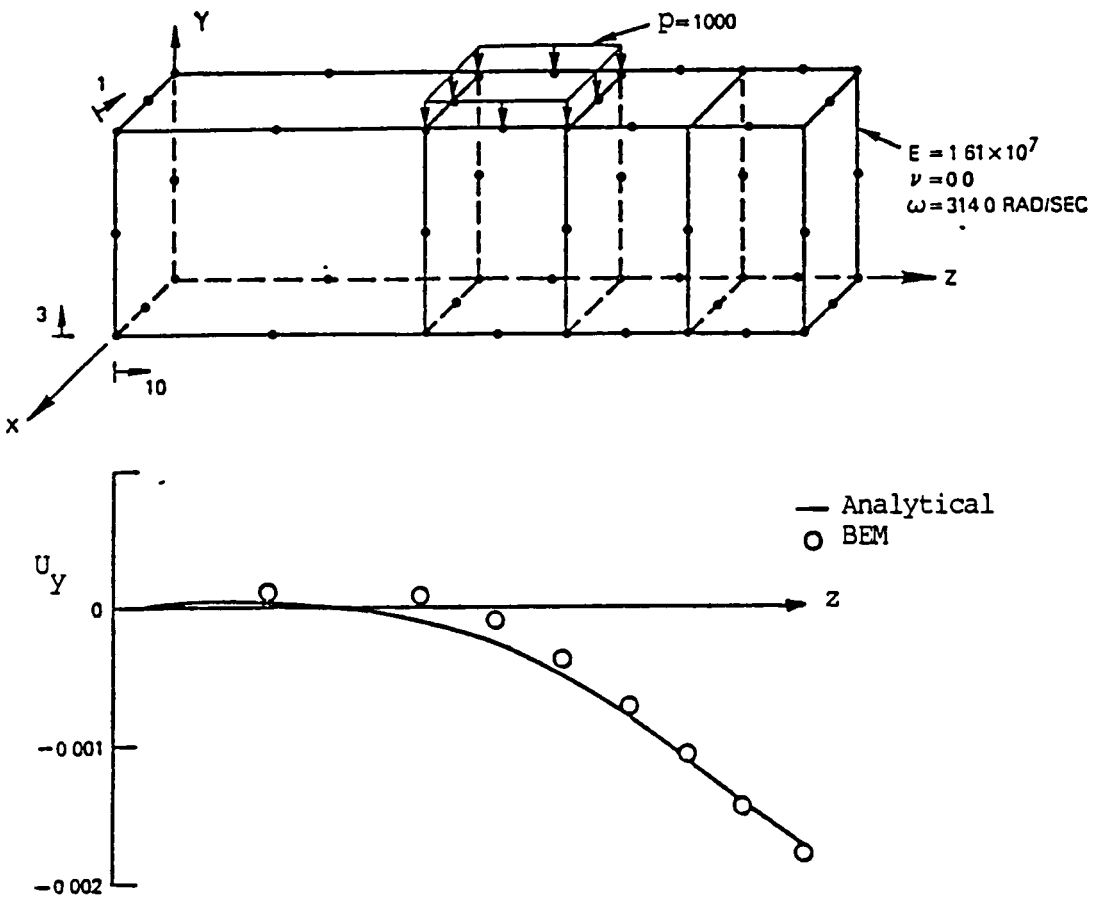

Cantilever subjected to harmonic patch load

Figure 6.7

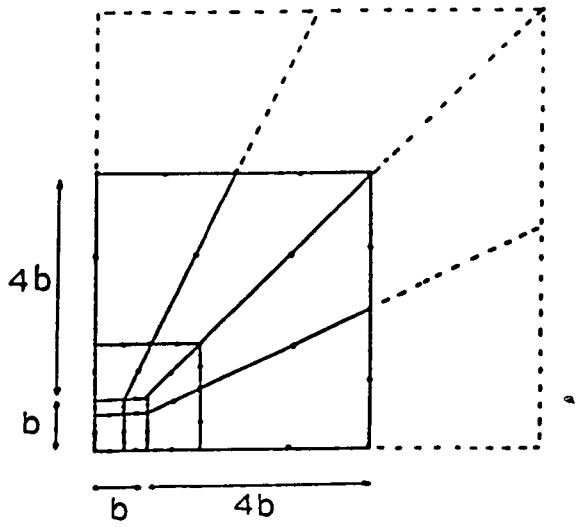

(a)

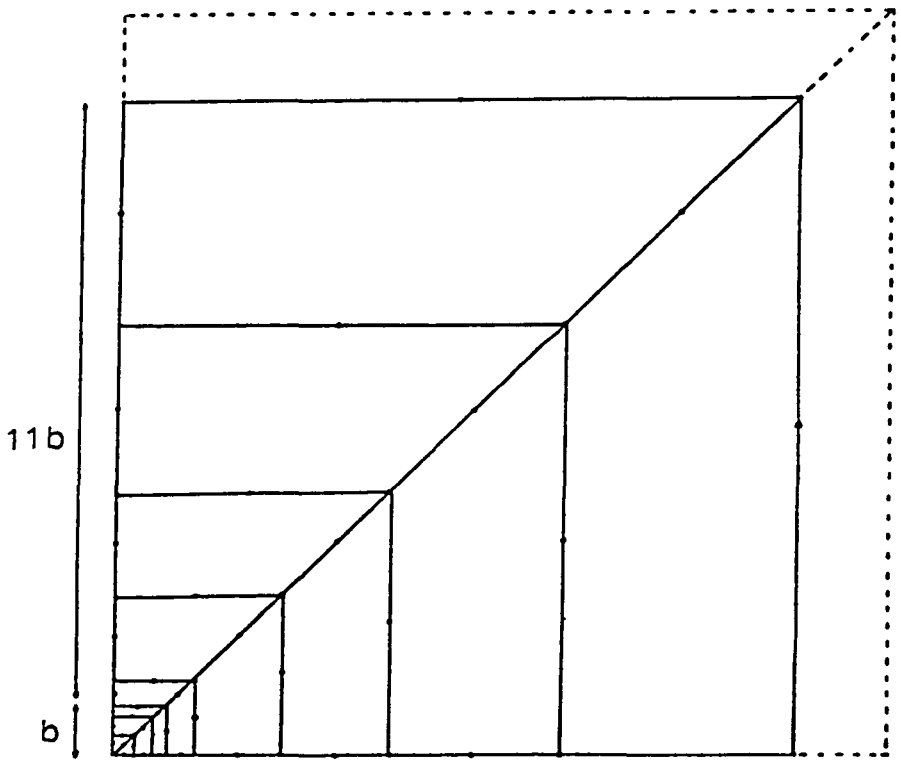

(b)

Boundary element discretization for a square footing on half-space

Figure 6.8

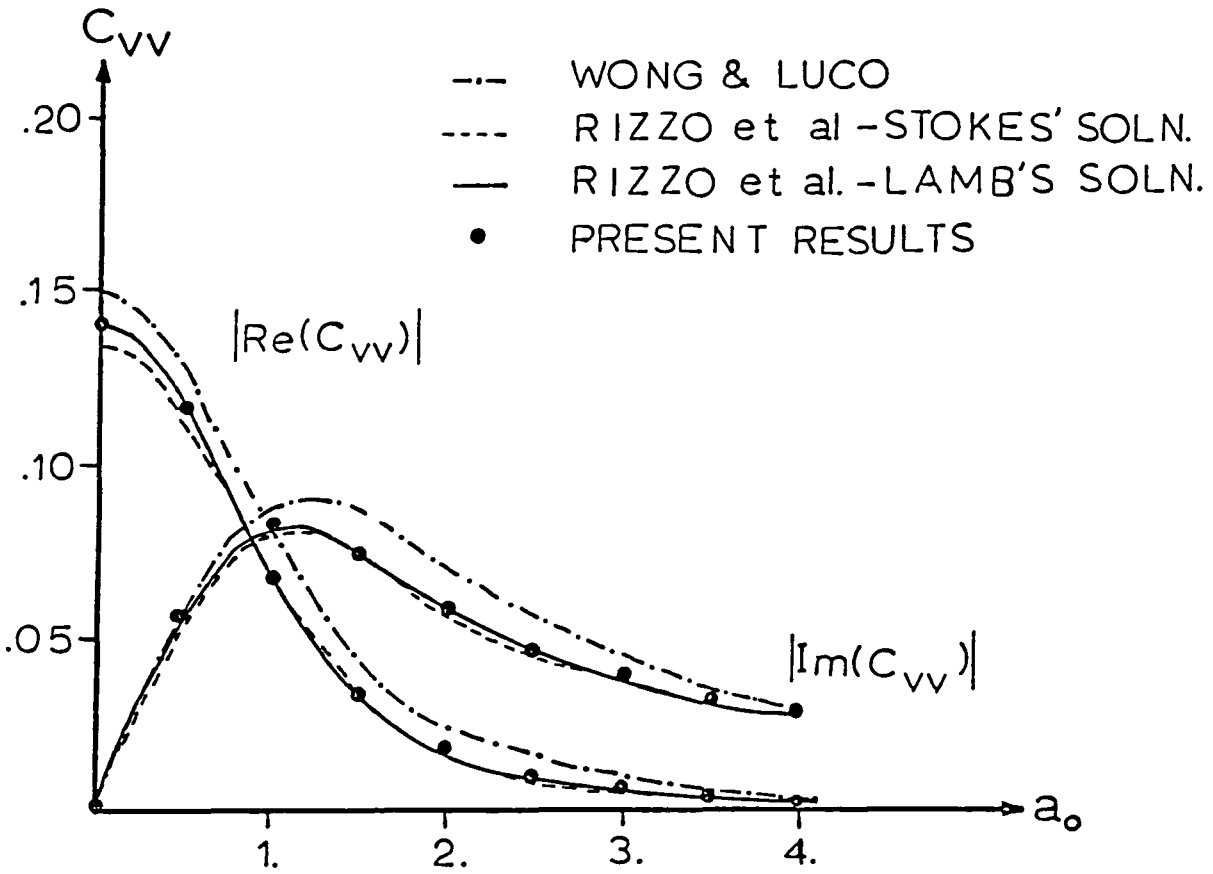

Vertical compliance for square footing

Figure 6.9

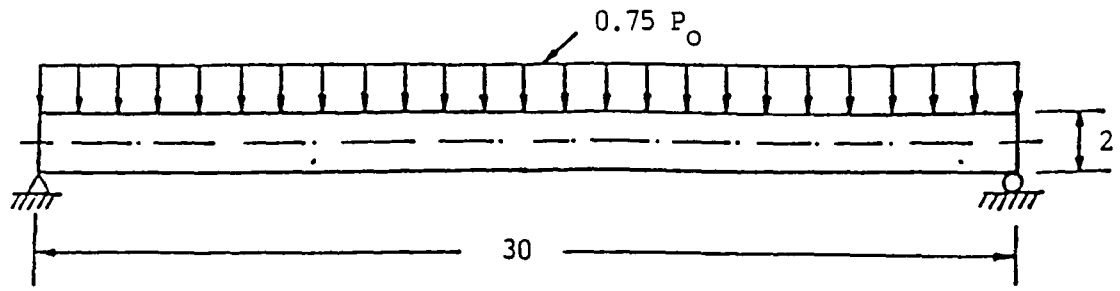

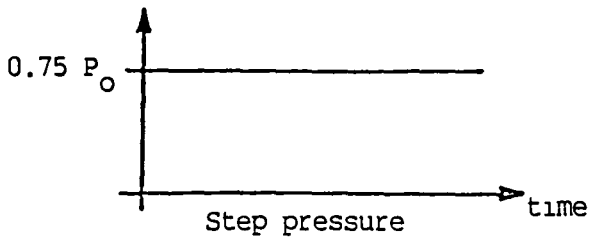

$E = 3 \times 10^7$

$\nu = 0.3$

$\rho = 0.733 \times 10^{-3}$

P_o = Static collapse load

Beam thickness = 1

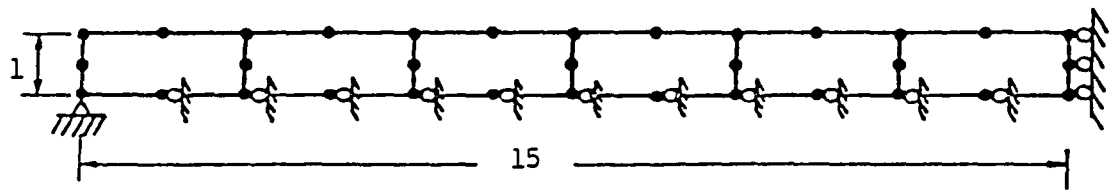

Finite element idealization

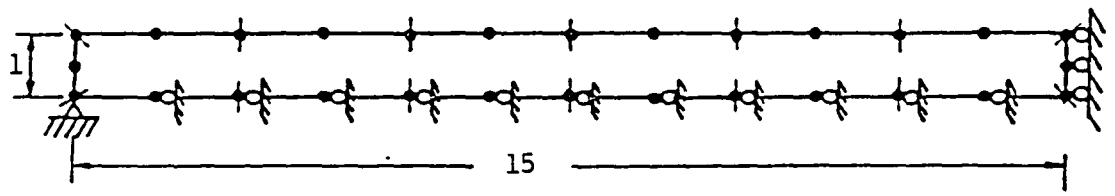

Boundary element idealization

Simple supported beam subjected to step loading

Figure 7.1

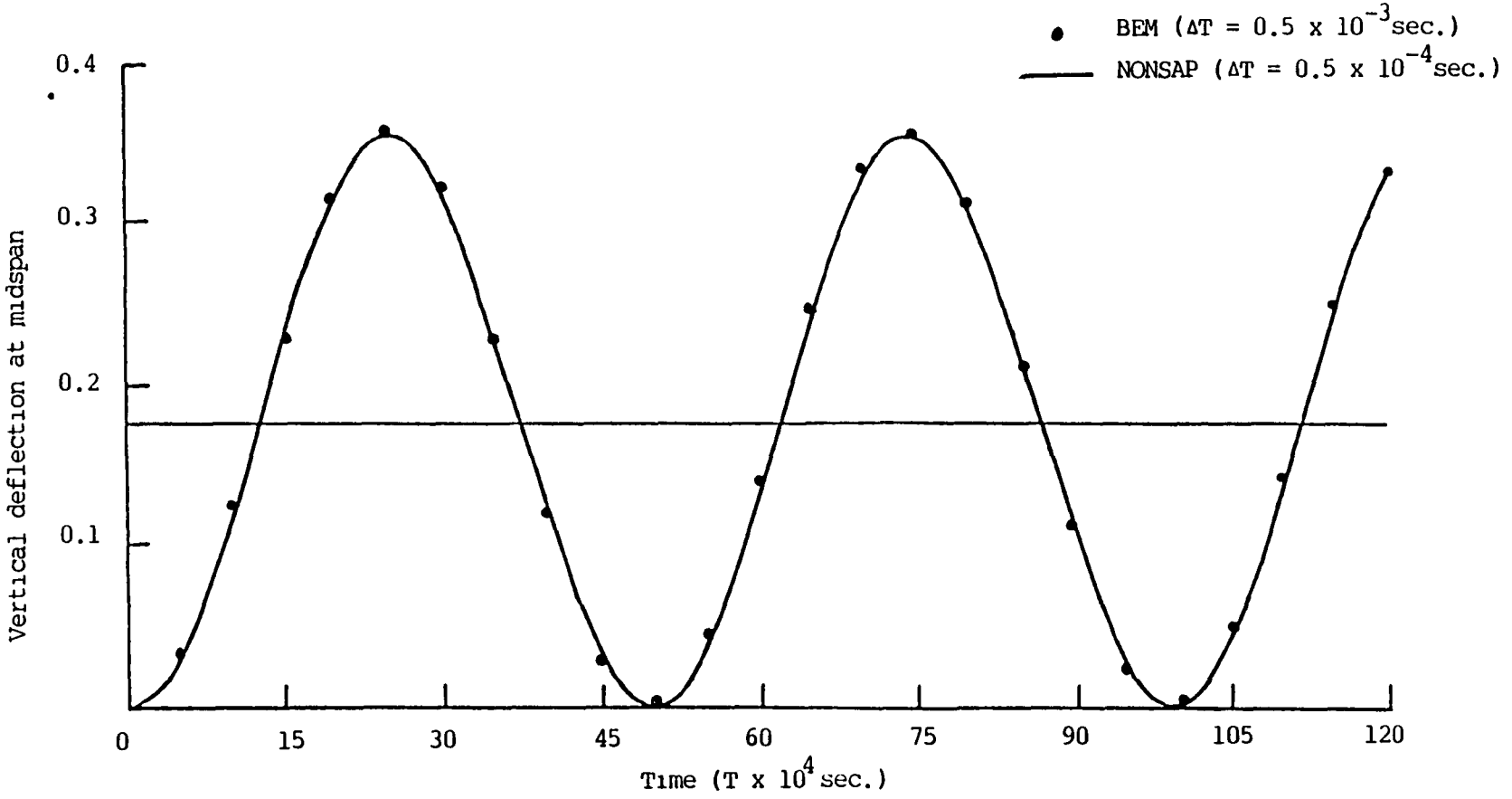

Dynamic response of simple supported beam

Figure 7.2

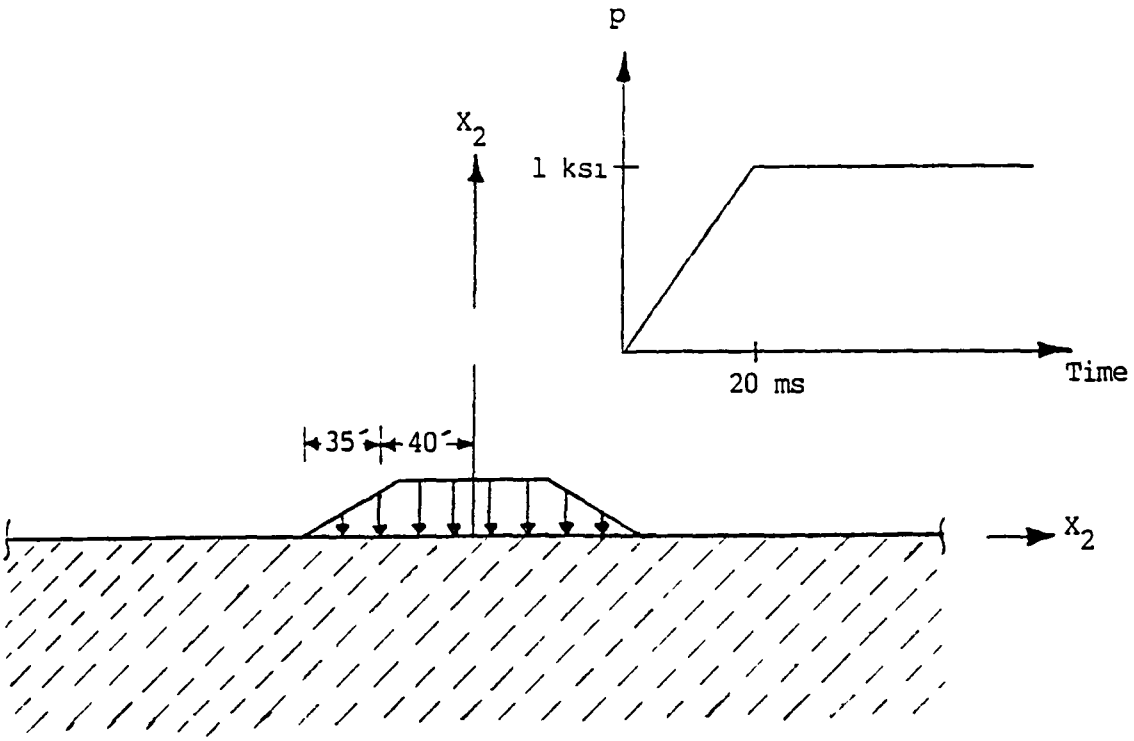

(a) Half-space under prescribed time-dependent stress distribtuion

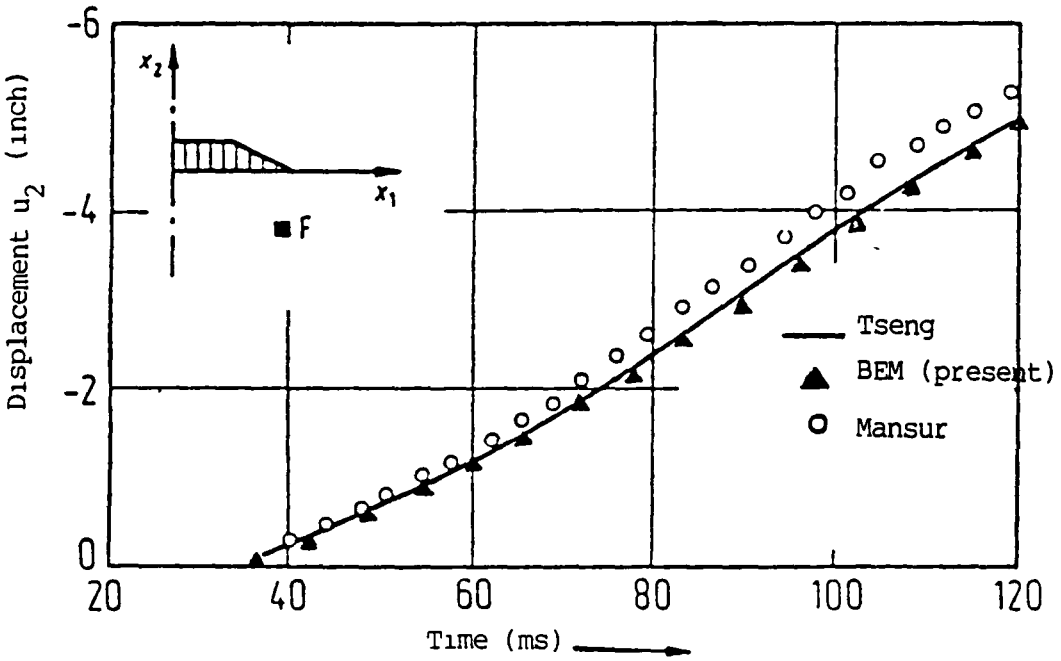

(b) Time history of displacement u_2 at the internal point F(80',-60').

Figure 7.3

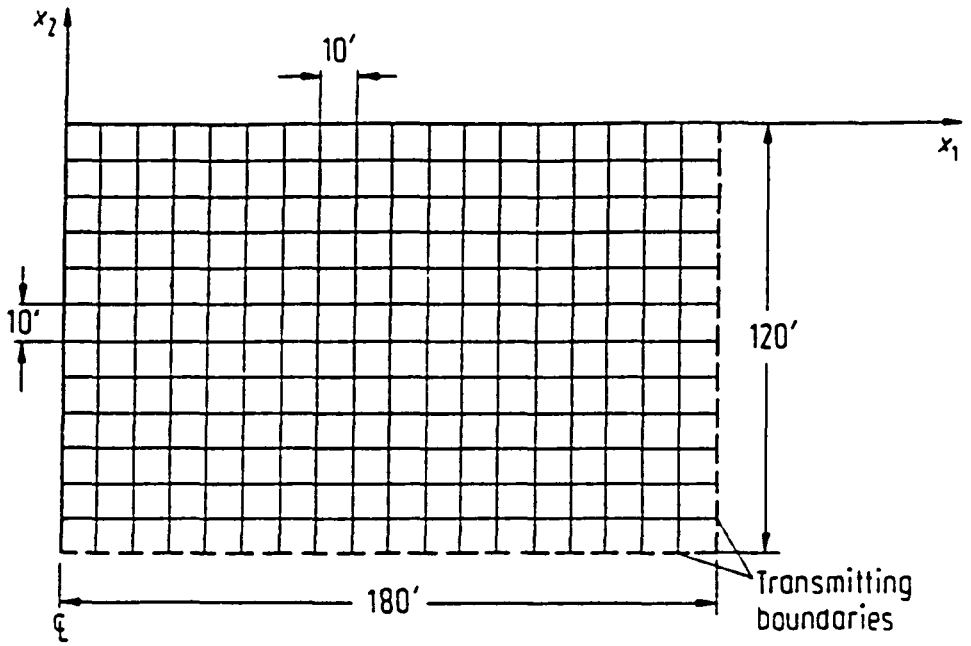

(a) Finite-difference discretization of the half-space

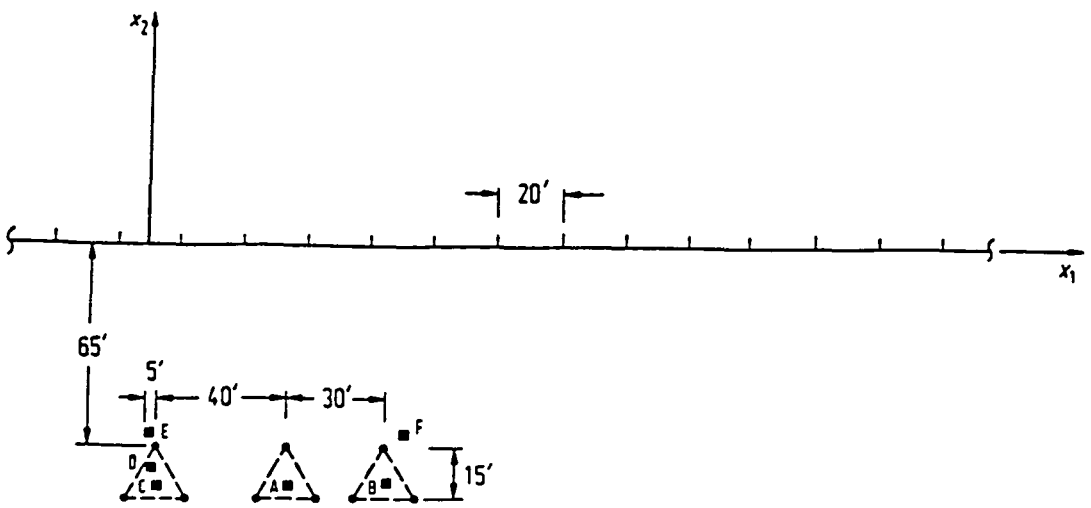

(b) Boundary element dicretization of the half-space

Figure 7.4

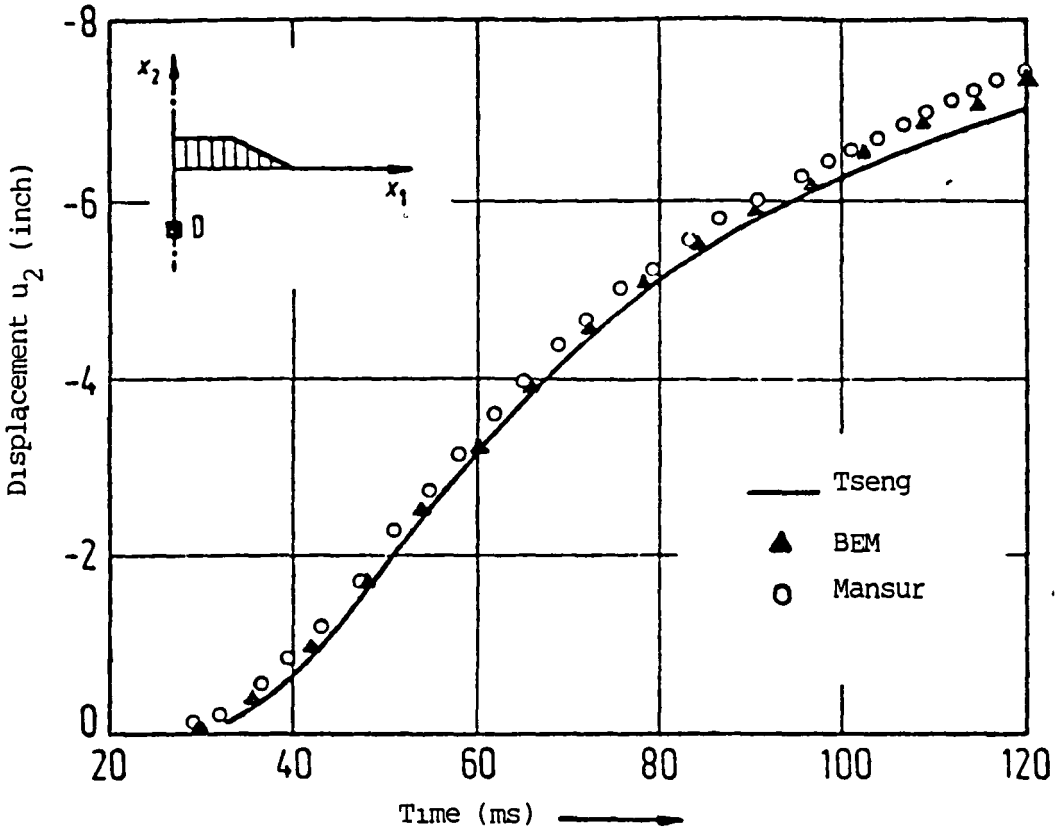

Time history of displacement u_2 at the internal point D(0,-70')

Figure 7.5

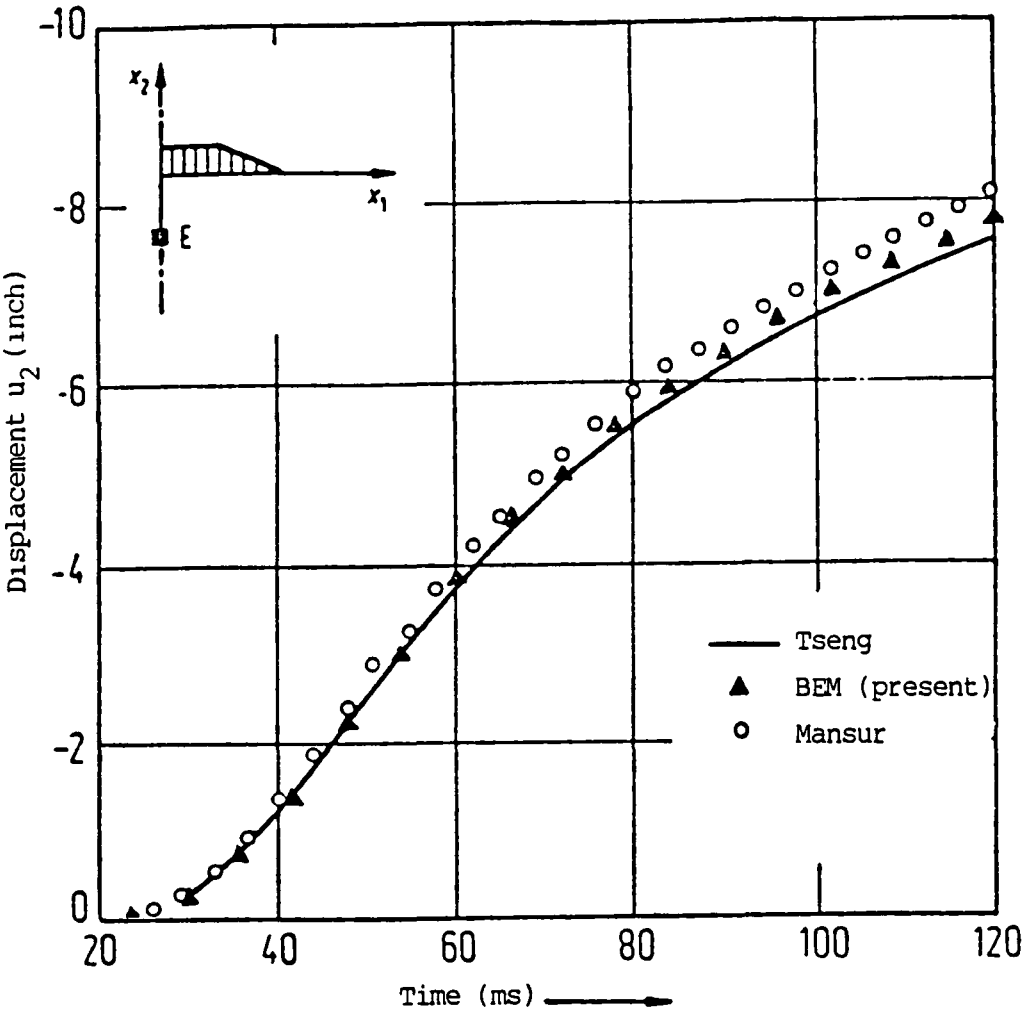

Time history of displacement u_2 at the internal point E(0,-60')

Figure 7.6

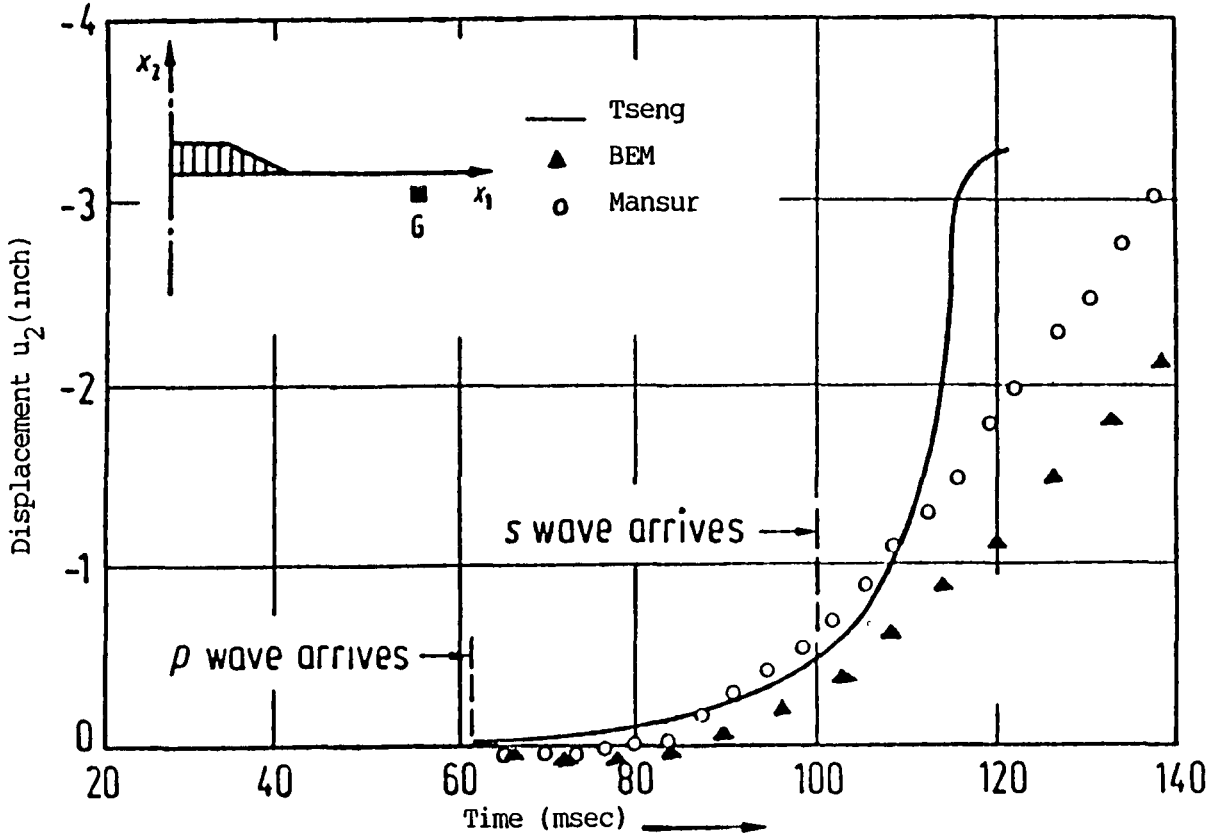

Time history of displacement u_2 at the internal point G(150',-10')

Figure 7.7

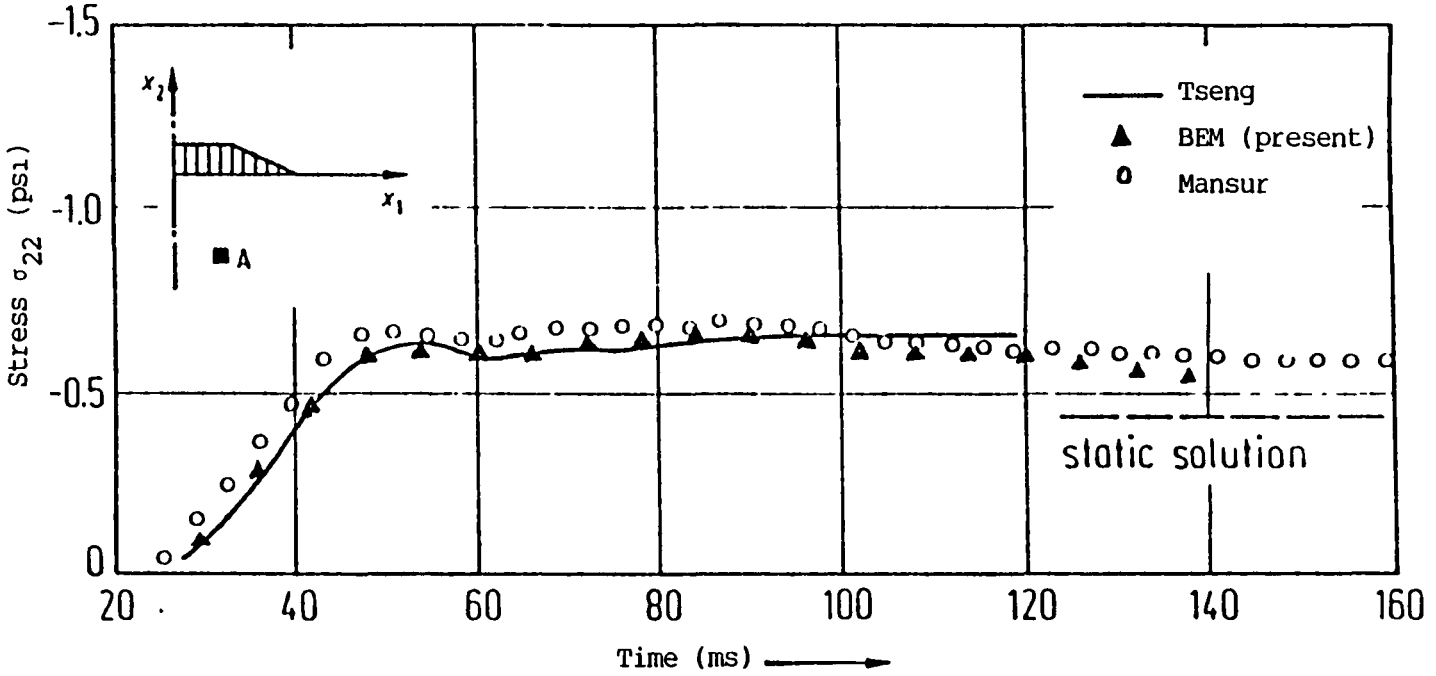

Stress σ_{22} at the internal point A(45',-75')

Figure 7.8

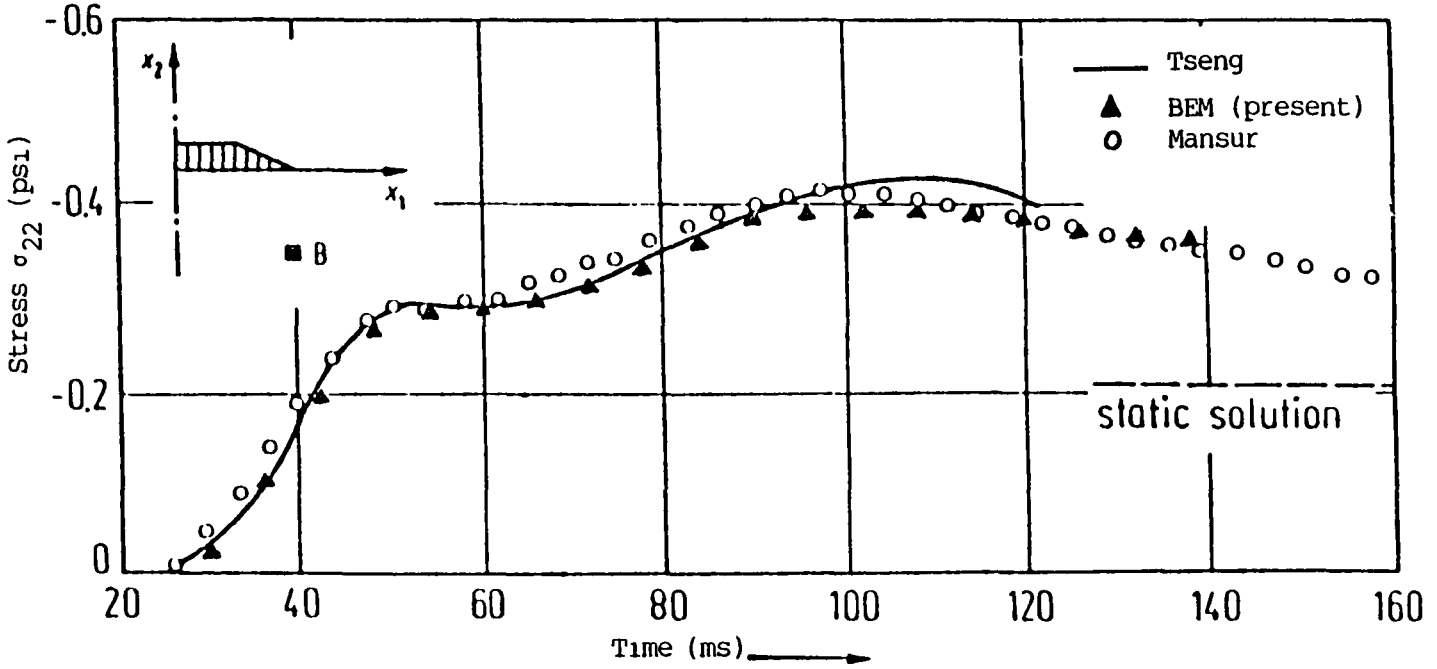

Stress σ_{22} at the internal point B(75',-75')

Figure 7.9

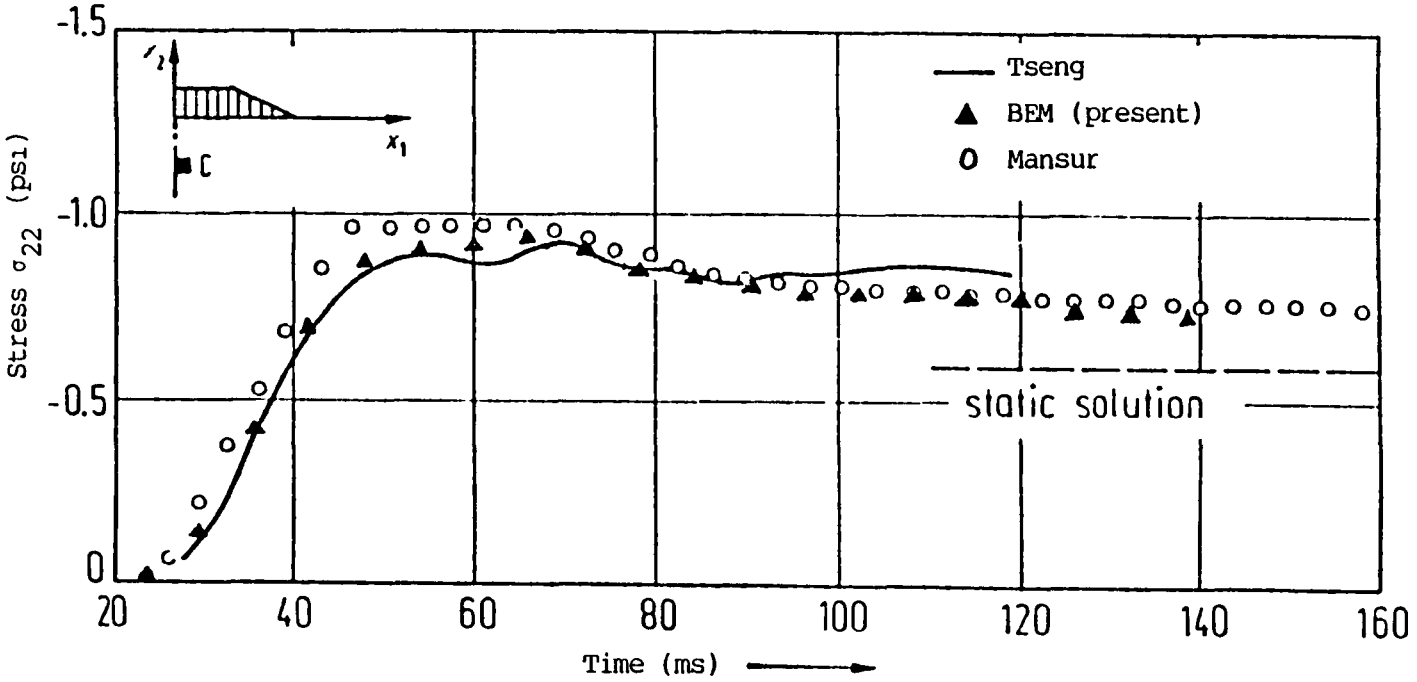

Stress σ_{22} at the internal point C(5',-75')

Figure 7.10

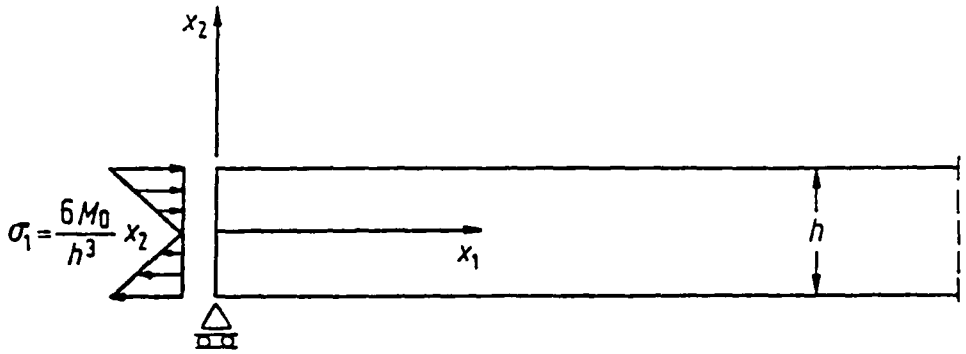

(a) Geometry and loading of the semi-infinite beam

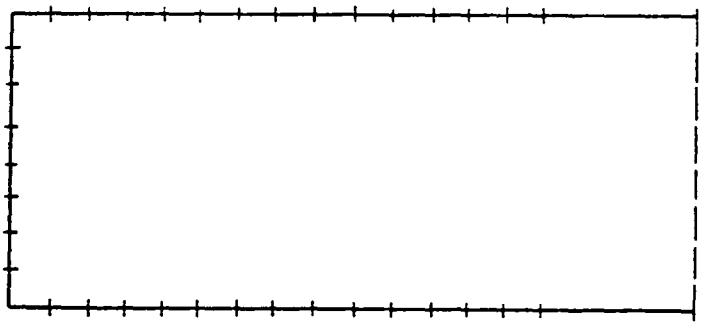

(b) Boundary element discretization of the semi-infinite beam

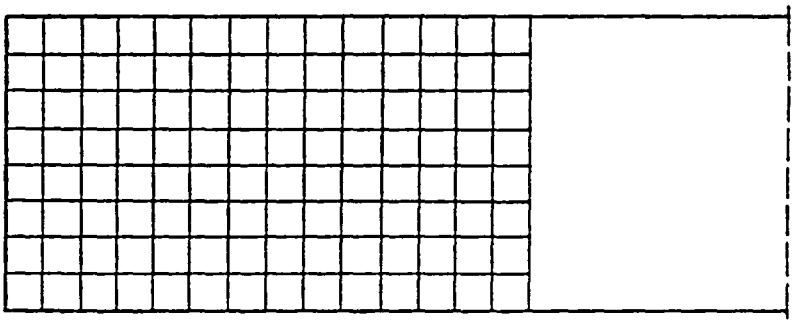

(c) Finite element discretization of the semi-infinite beam

Figure 7.11

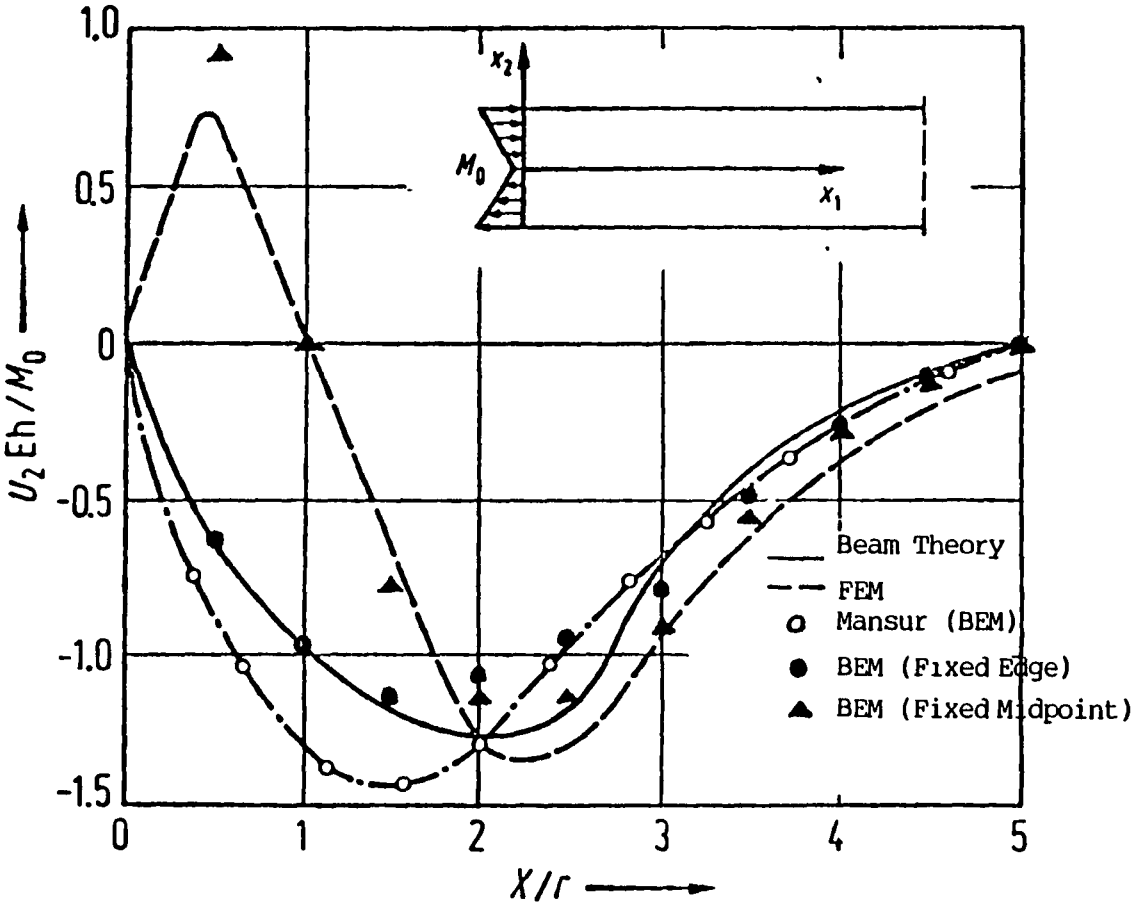

Transverse displacement along the semi-infinite beam at time $T = 5r/c_o$

Figure 7.12

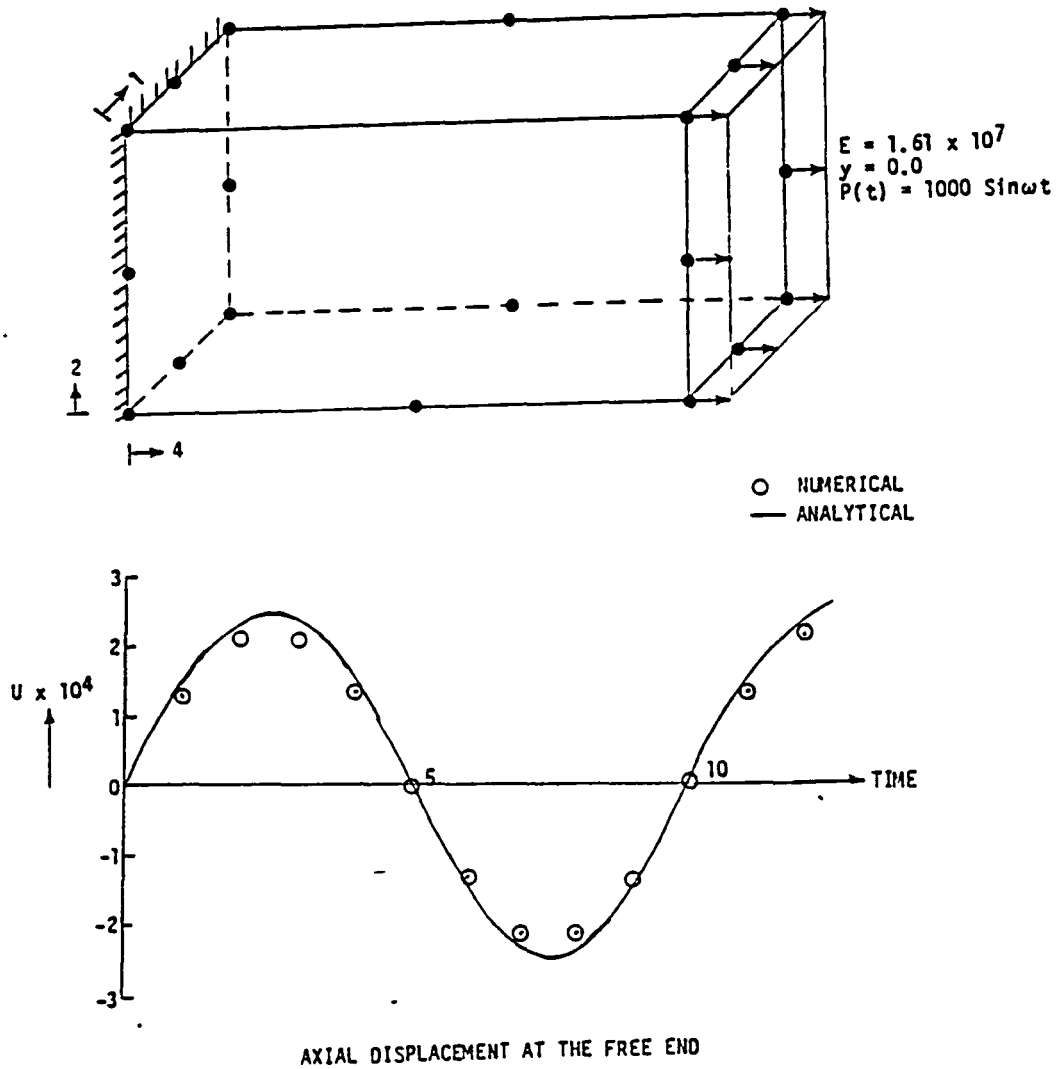

Transient Analysis of a Cantilever Subjected to a Harmonic Axial Loading

Figure 7.13

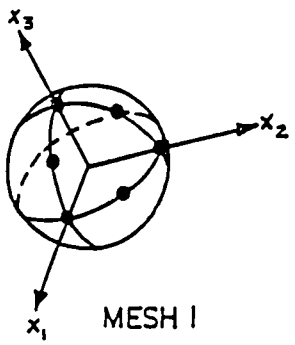

MESH 1

NODES & ELEMENT CONFIGURATION
WITH 8 TRIANGULAR ELEMENTS

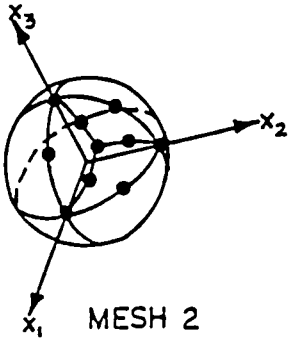

MESH 2

NODES & ELEMENT CONFIGURATION
WITH 24 TRIANGULAR ELEMENTS

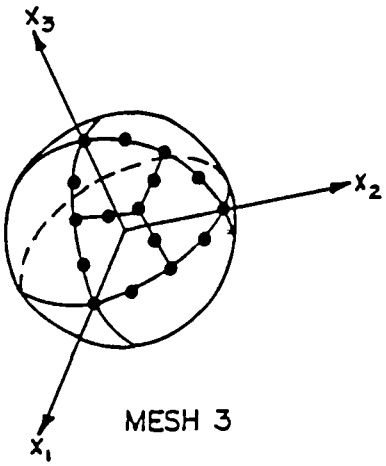

MESH 3

NODES & ELEMENT CONFIGURATION
WITH 24 RECTANGULAR ELEMENTS

BOUNDARY ELEMENT METHOD MESHES USED IN ANALYSIS
OF EXPLOSION IN A SPHERICAL CAVITY

Figure 7.14

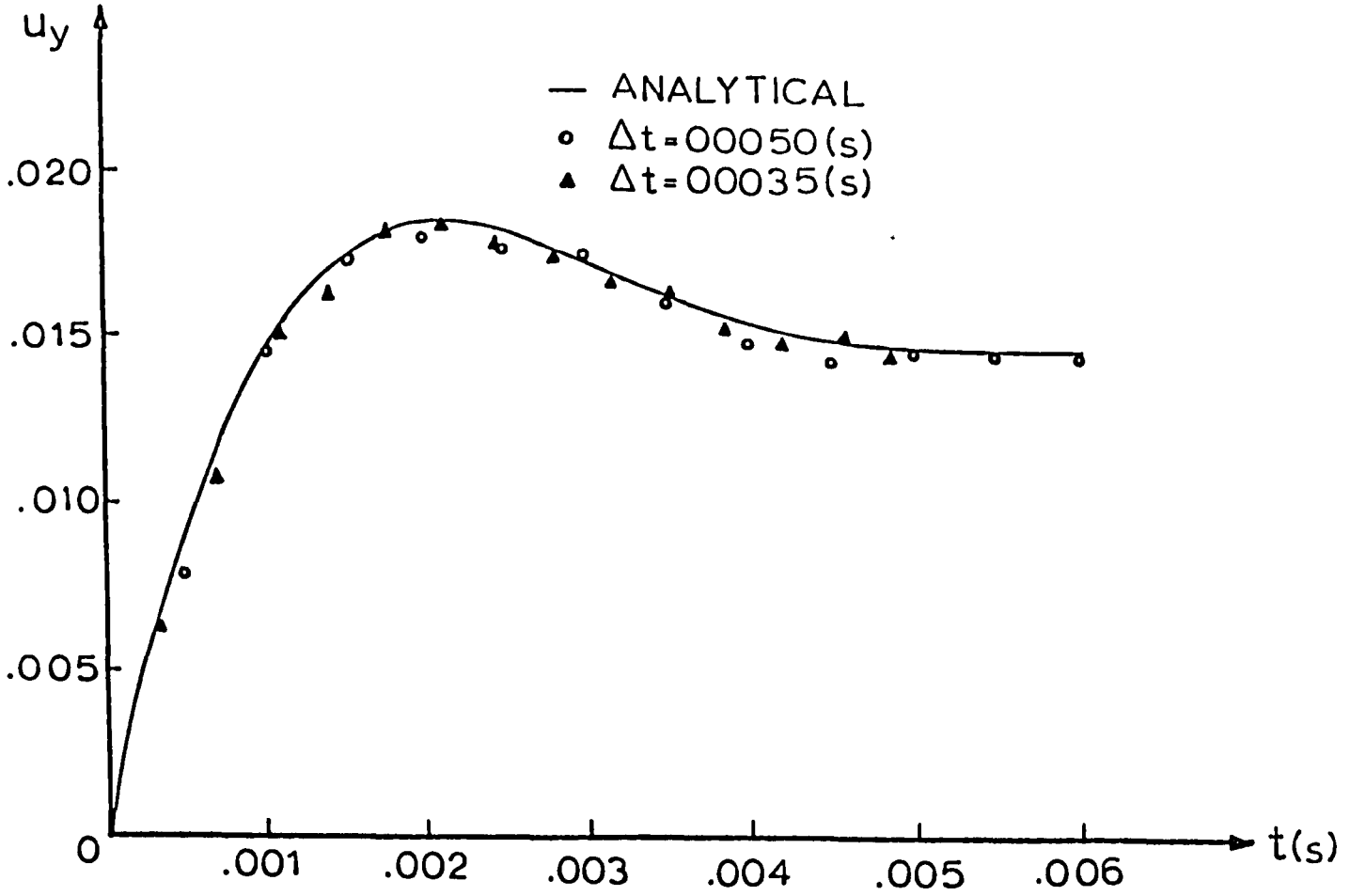

Radial displacements of the cavity surface by transform algorithm

Figure 7.15

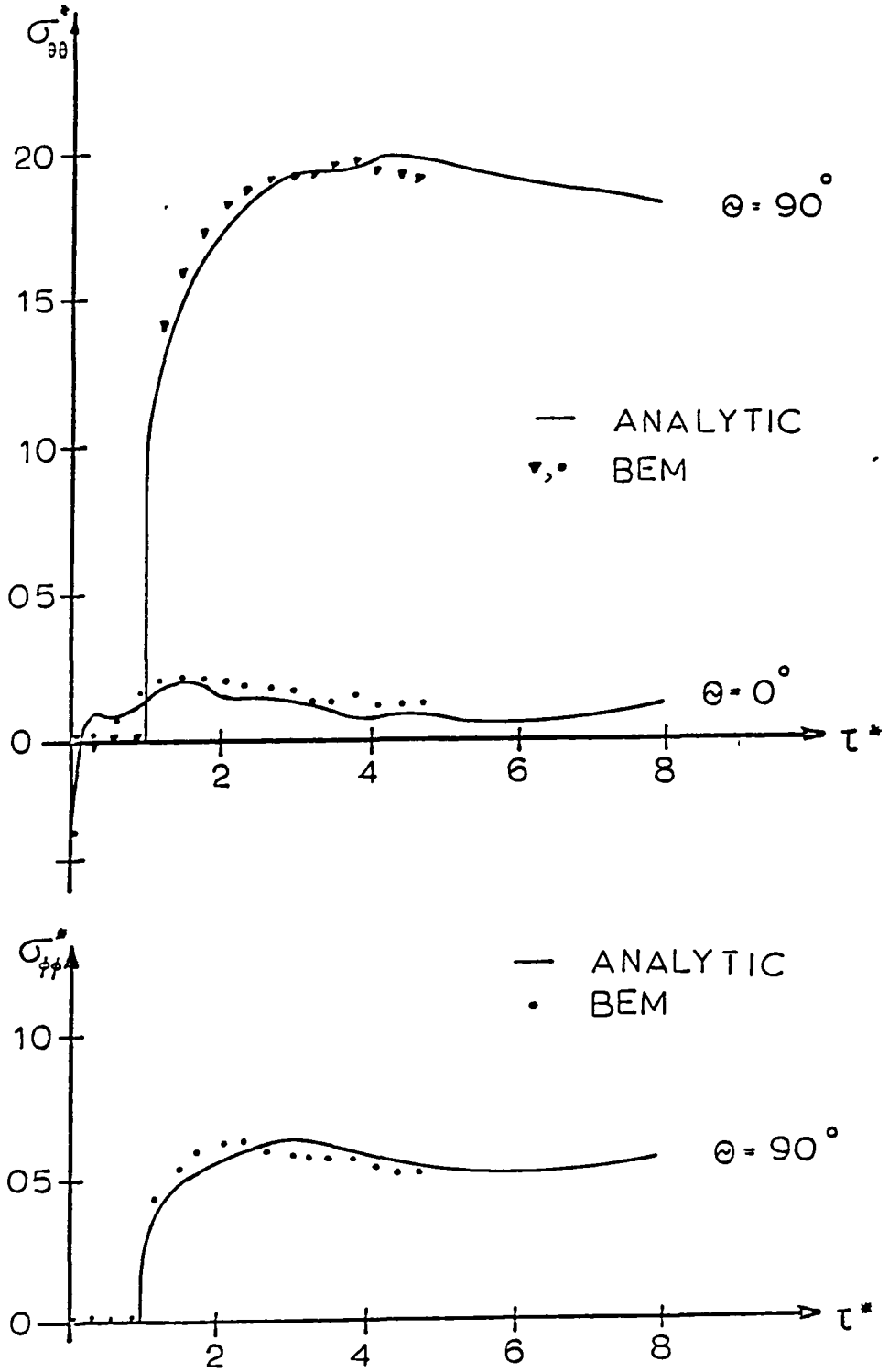

Normalized Hoop stress at the cavity surface by transform algorithm

Figure 7.16

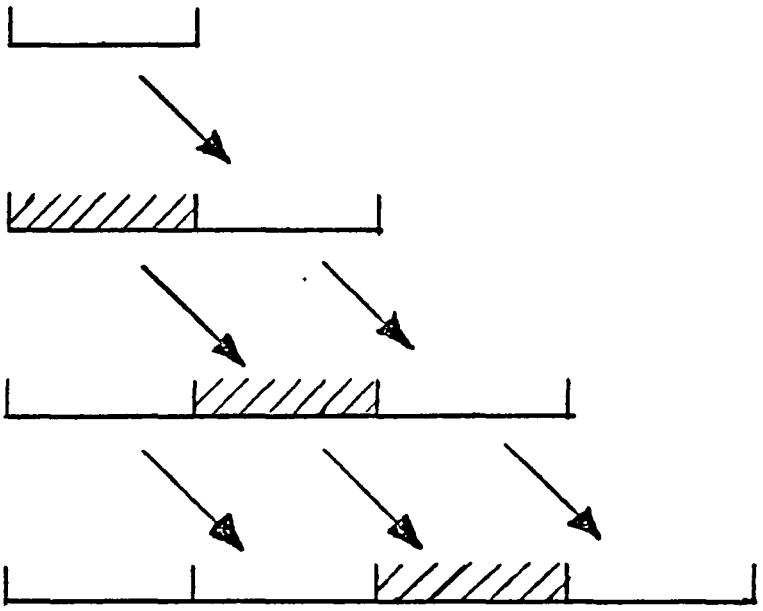

Time-marching process

Figure 8.1

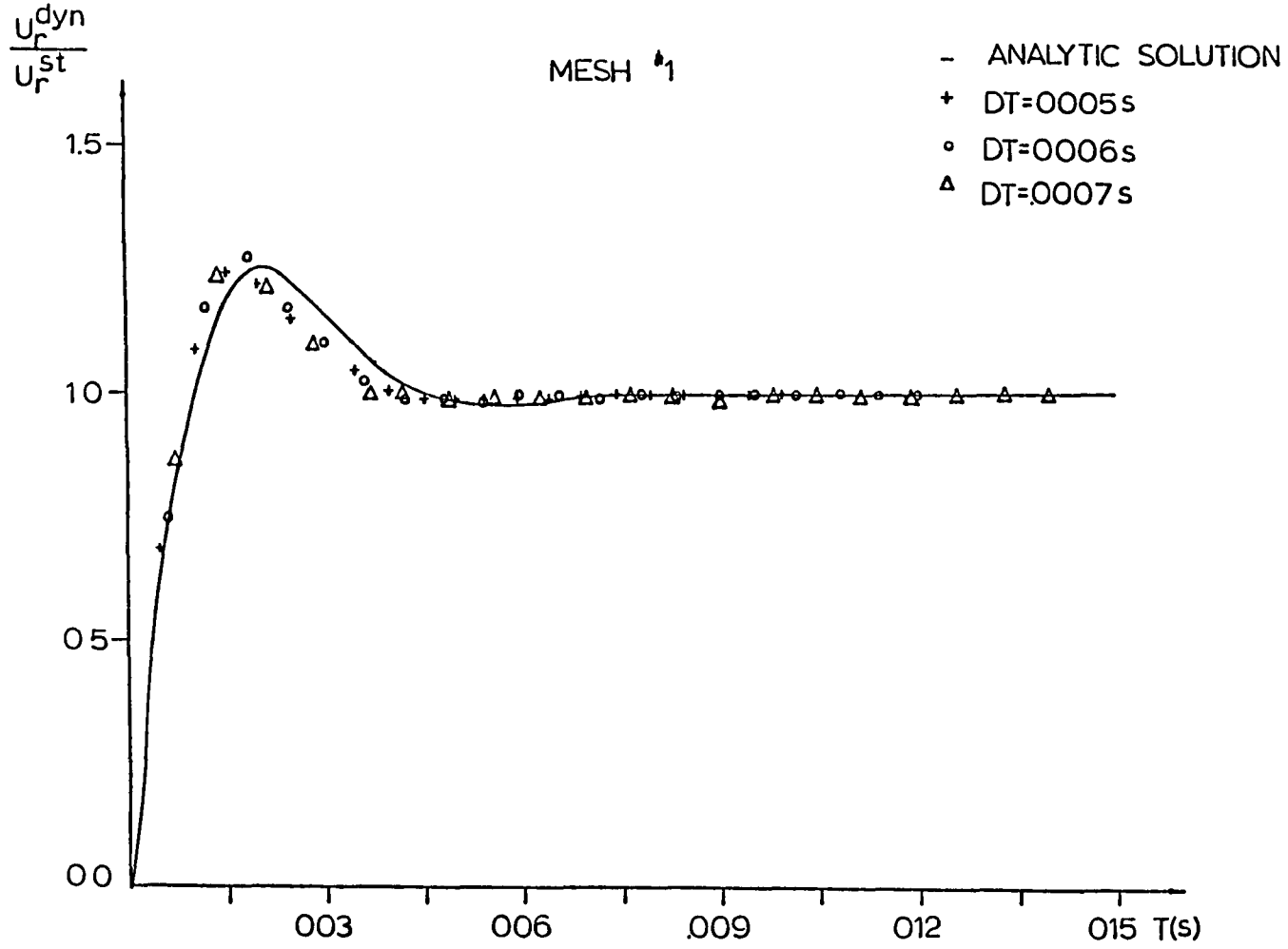

Normalized displacements of the cavity surface

Figure 8.2

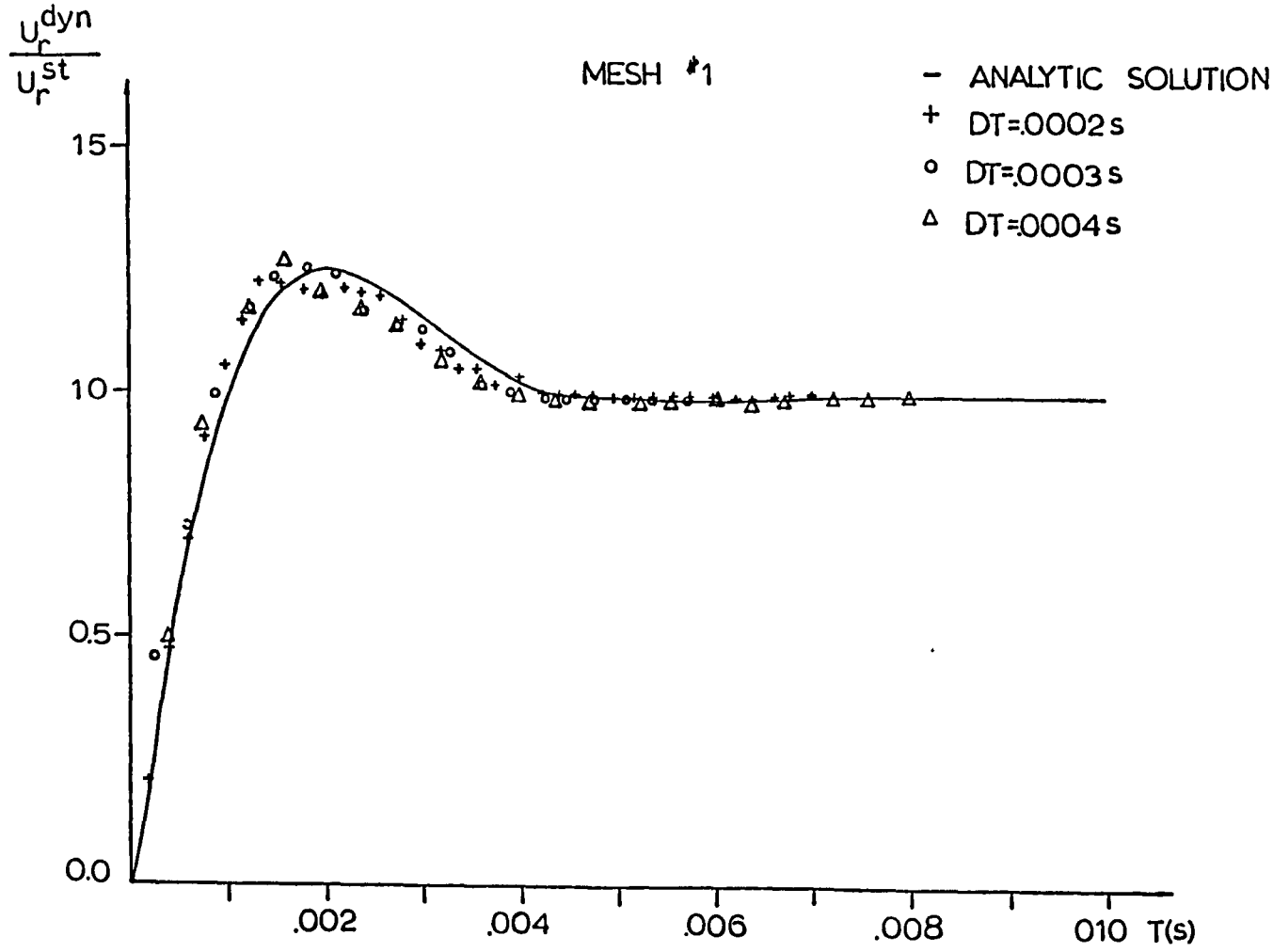

Normalized radial displacements of the cavity surface

Figure 8.3

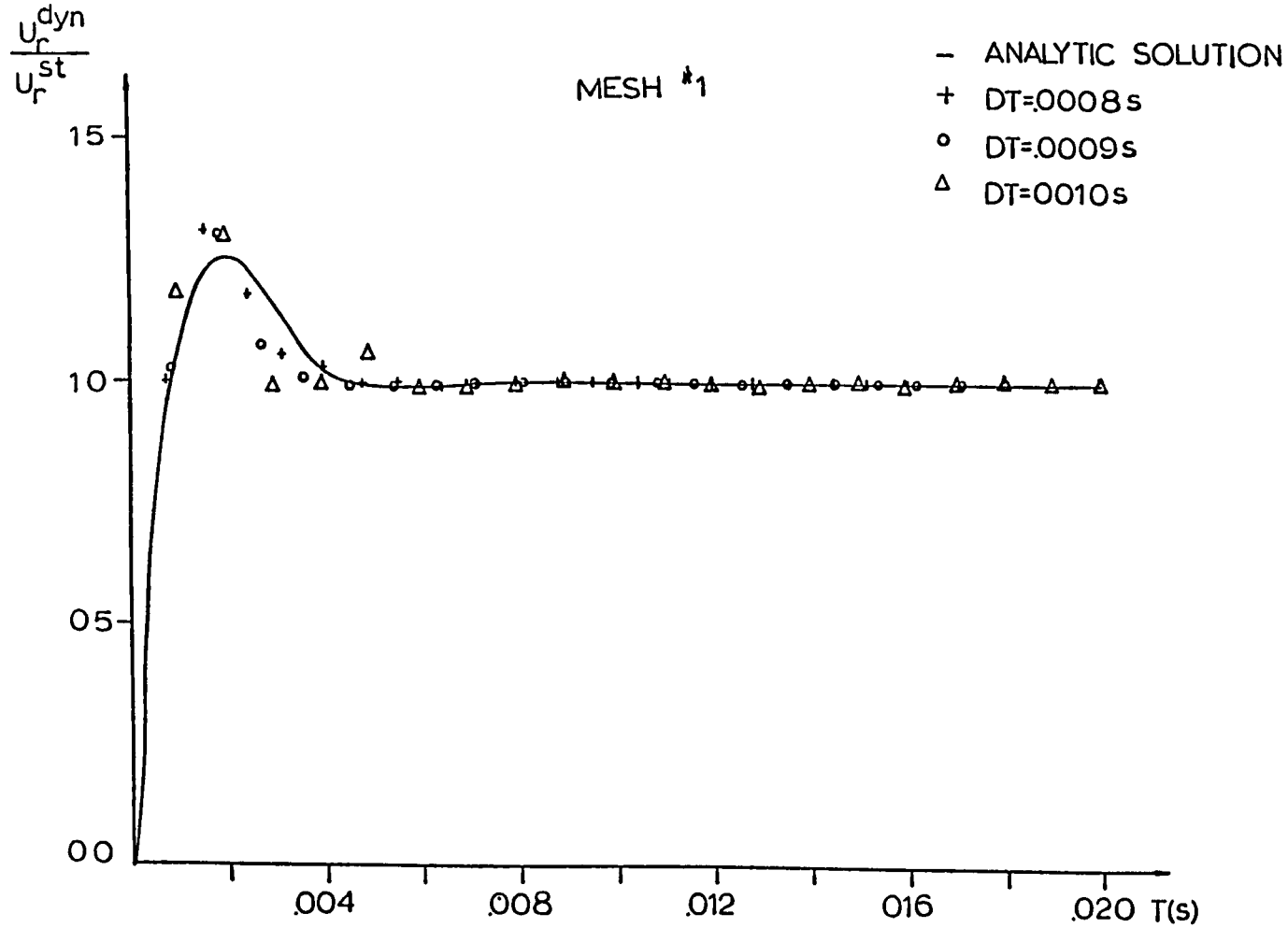

Normalized radial displacements of the cavity surface

Figure 8.4

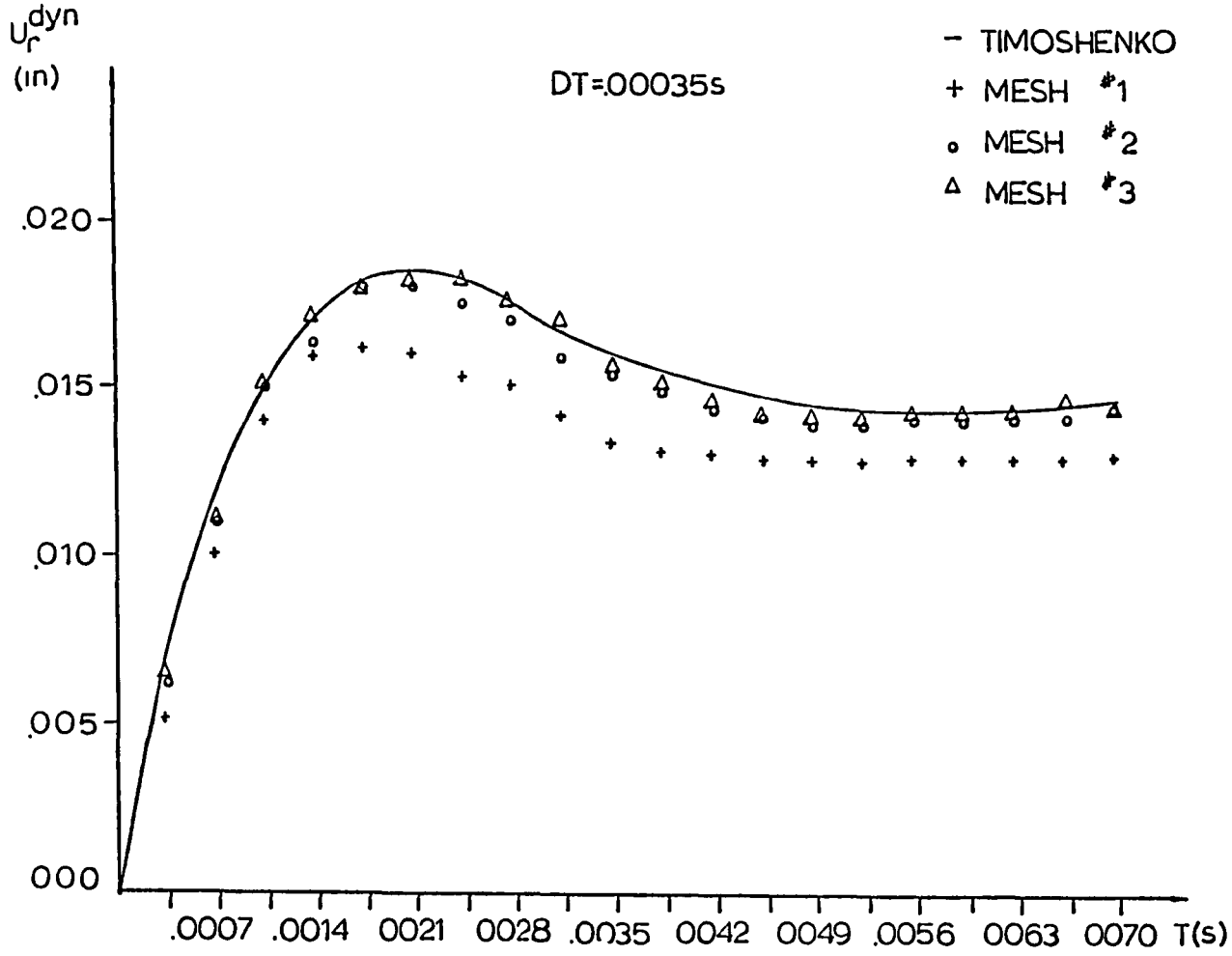

Normalized radial displacements of the cavity surface

Figure 8.5

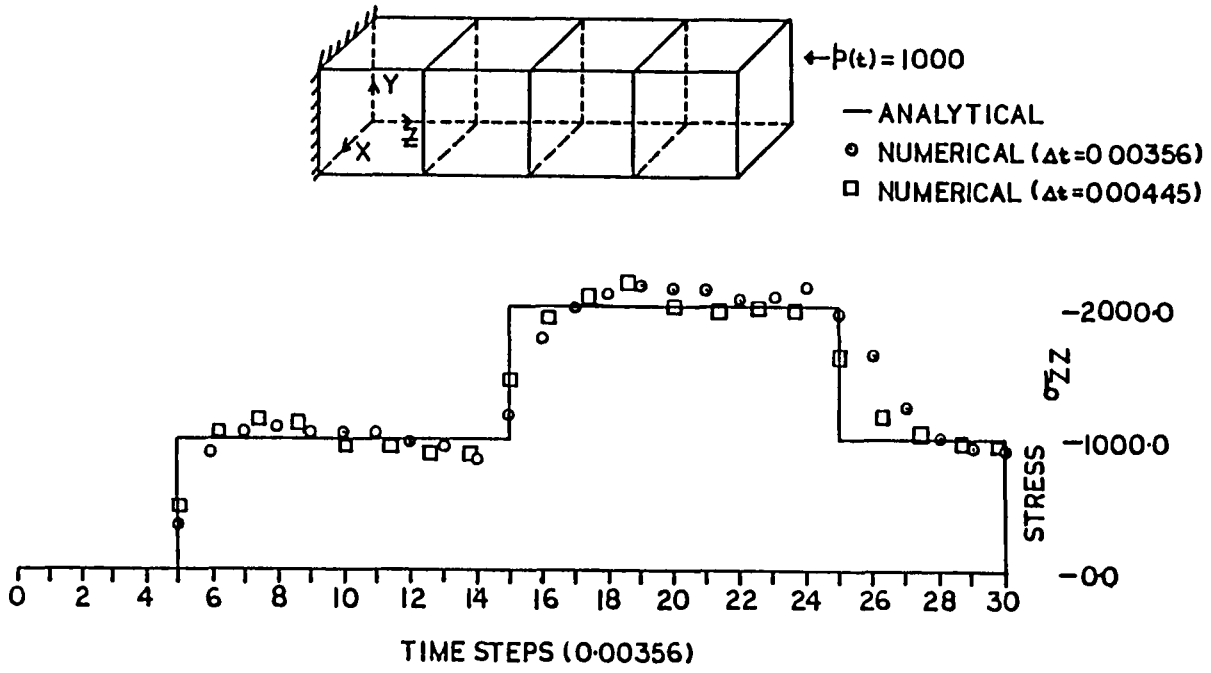

LONGITUDINAL STRESS AT THE MIDSPAN OF A CANTILEVER BEAM SUBJECTED TO AN END LOAD P(t)=1000

Figure 8.6

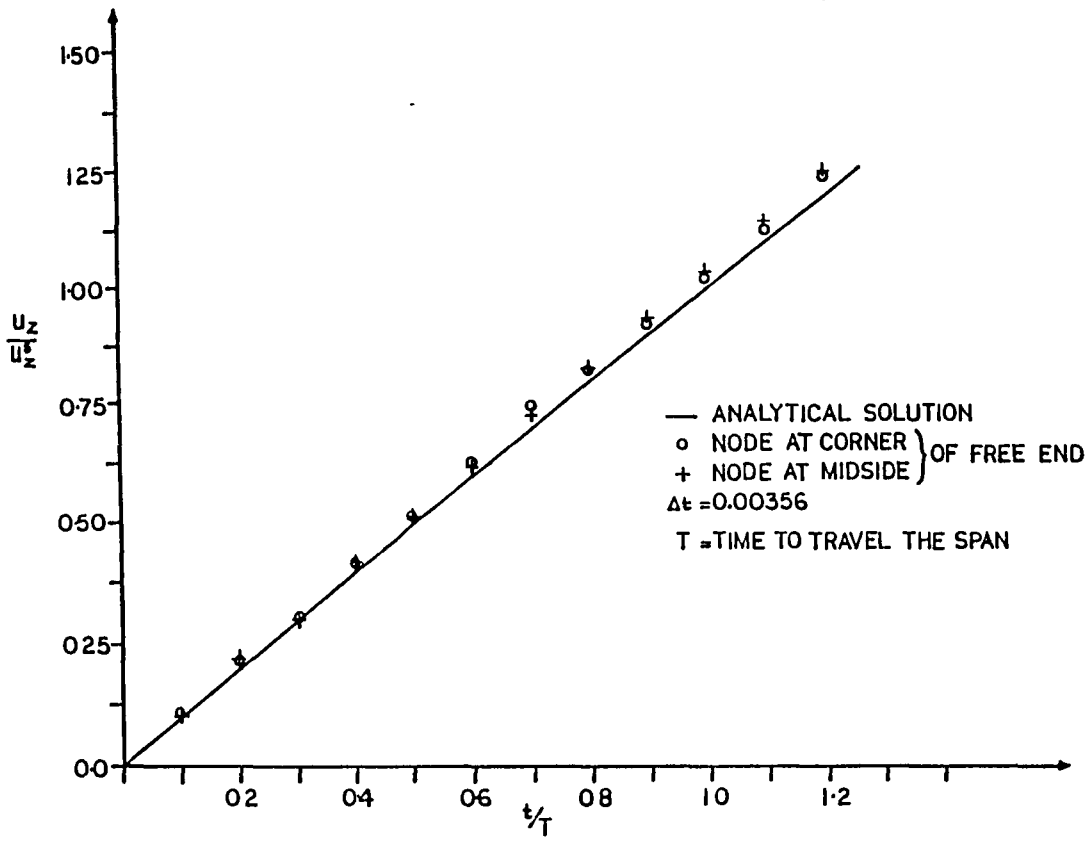

Normalized axial displacements at the free end of the beam

Figure 8.7

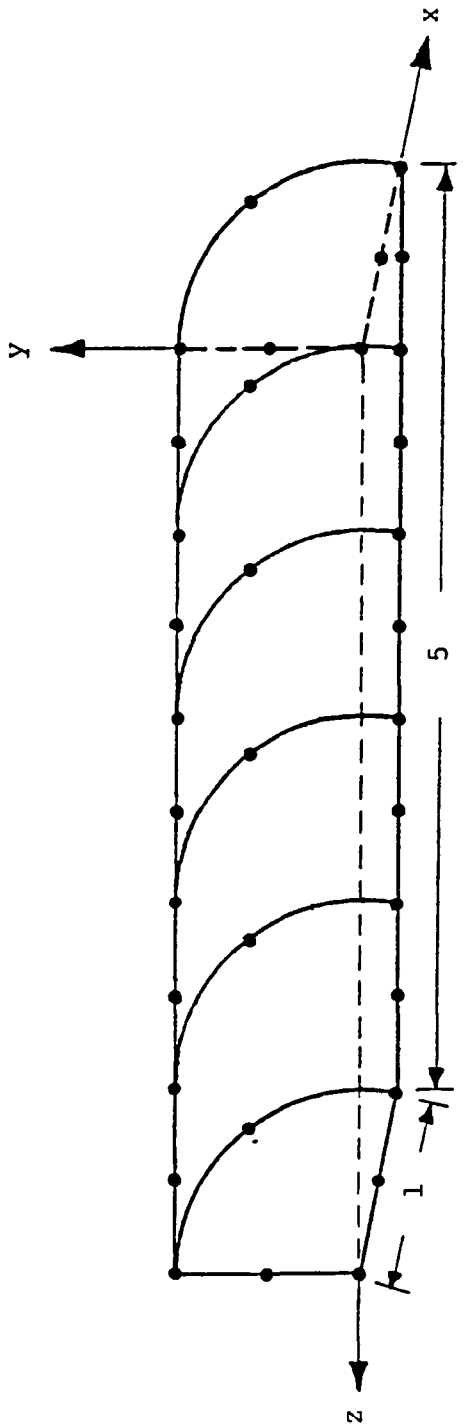

Surface discretization of a circular bar

Figure 8.8

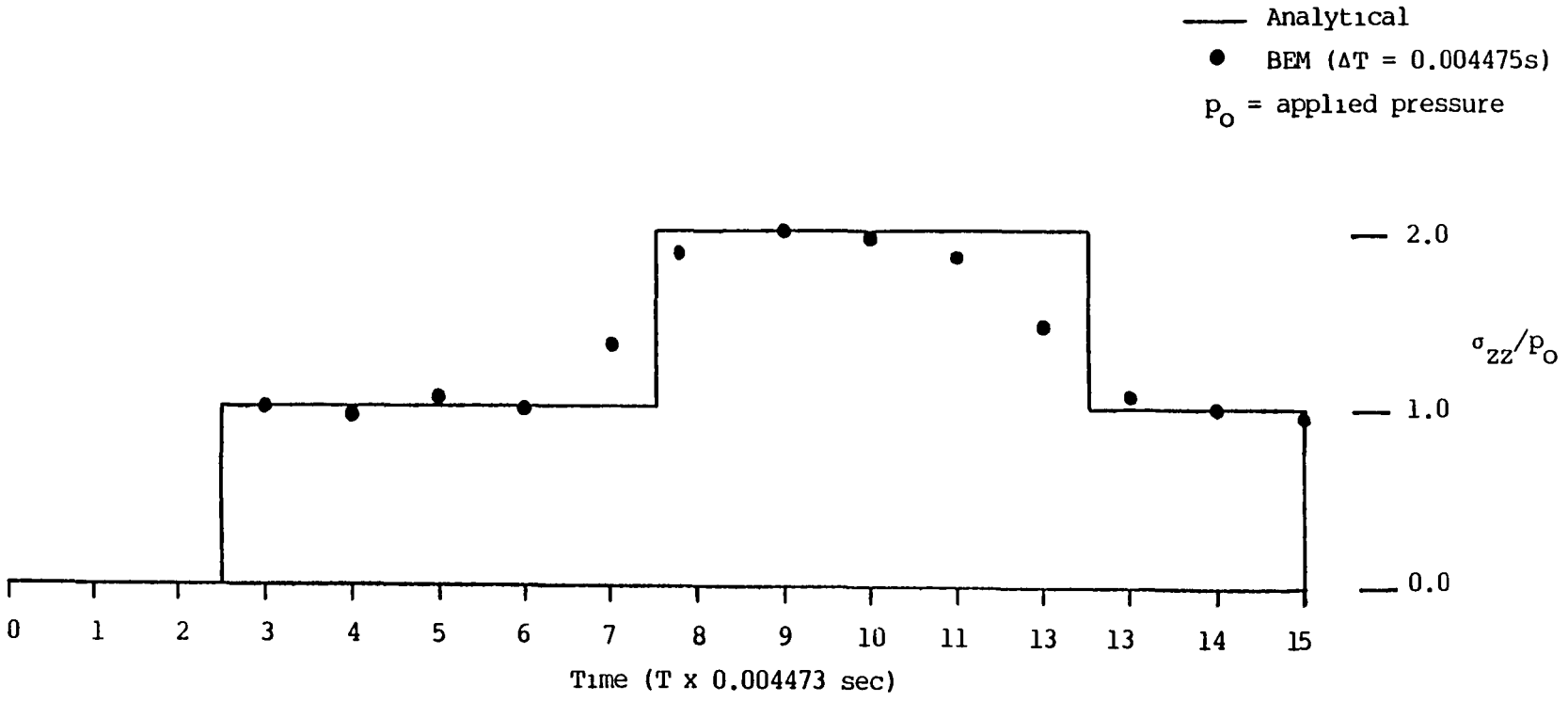

Normalized axial stresses at the midspan of the bar

Figure 8.9

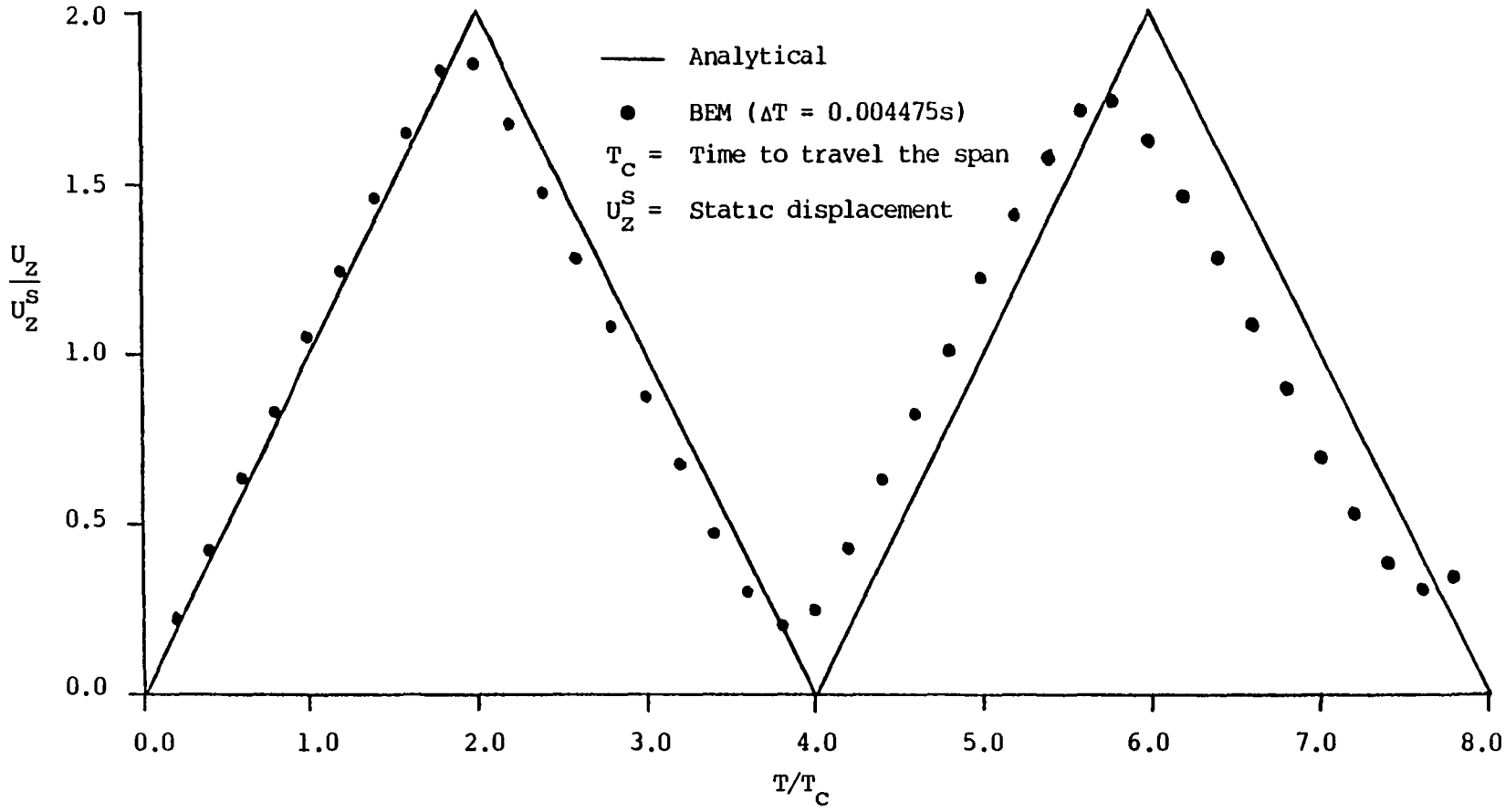

Normalized axial displacements at the free end of the bar

Figure 8.10

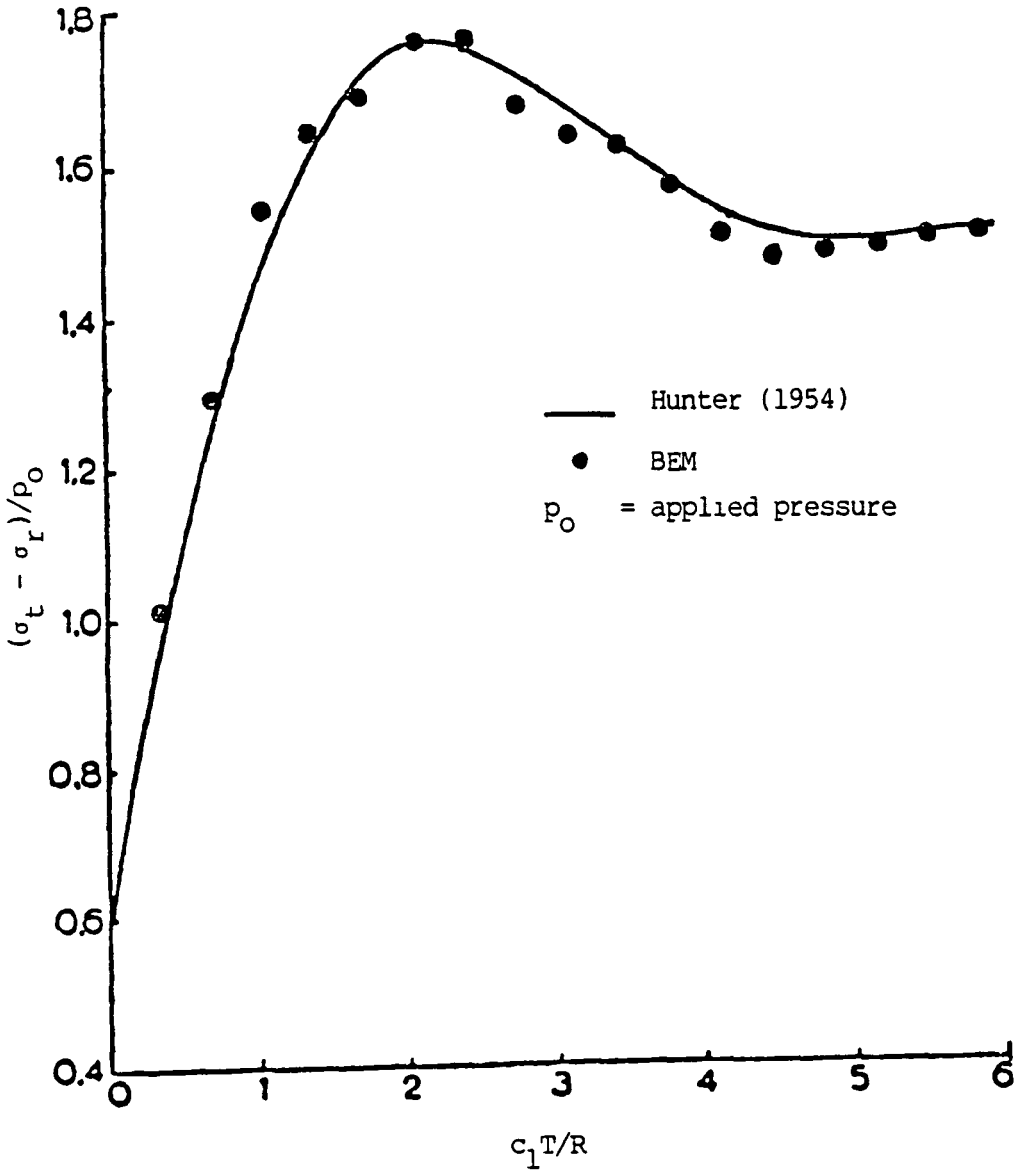

Deviatoric stresses at the cavity surface for suddenly applied and maintained pressure

Figure 8.11

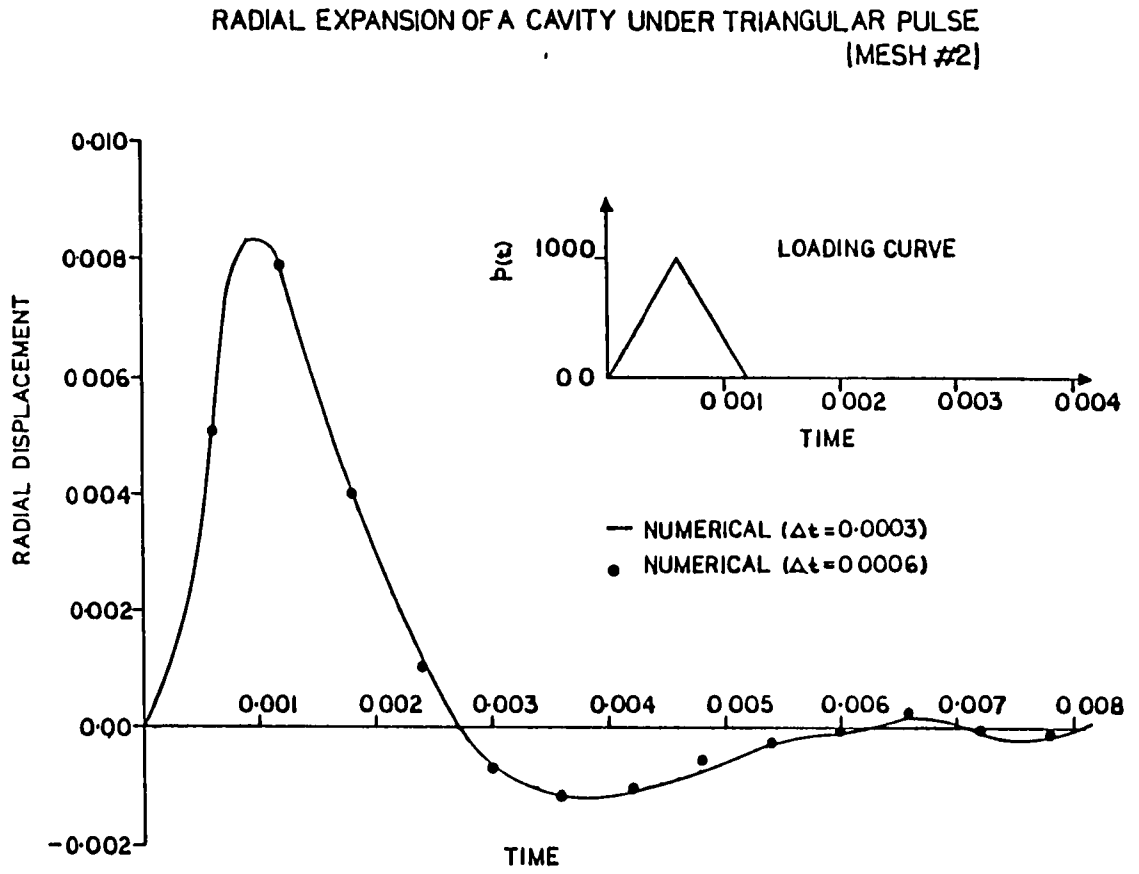
RADIAL EXPANSION OF A CAVITY UNDER TRIANGULAR PULSE
(MESH #2)
RADIAL DISPLACEMENT
0·010
0·008
0·006
0·004
0·002
0·00
-0·002
0·001
0·002
0·003
0·004
0·005
0·006
0·007
0·008
TIME
p(t)
1000
0 0
LOADING CURVE
0 001
0 002
0 003
0 004
TIME
NUMERICAL (Δt=0·0003)
NUMERICAL (Δt=0 0006)

Figure 8.12

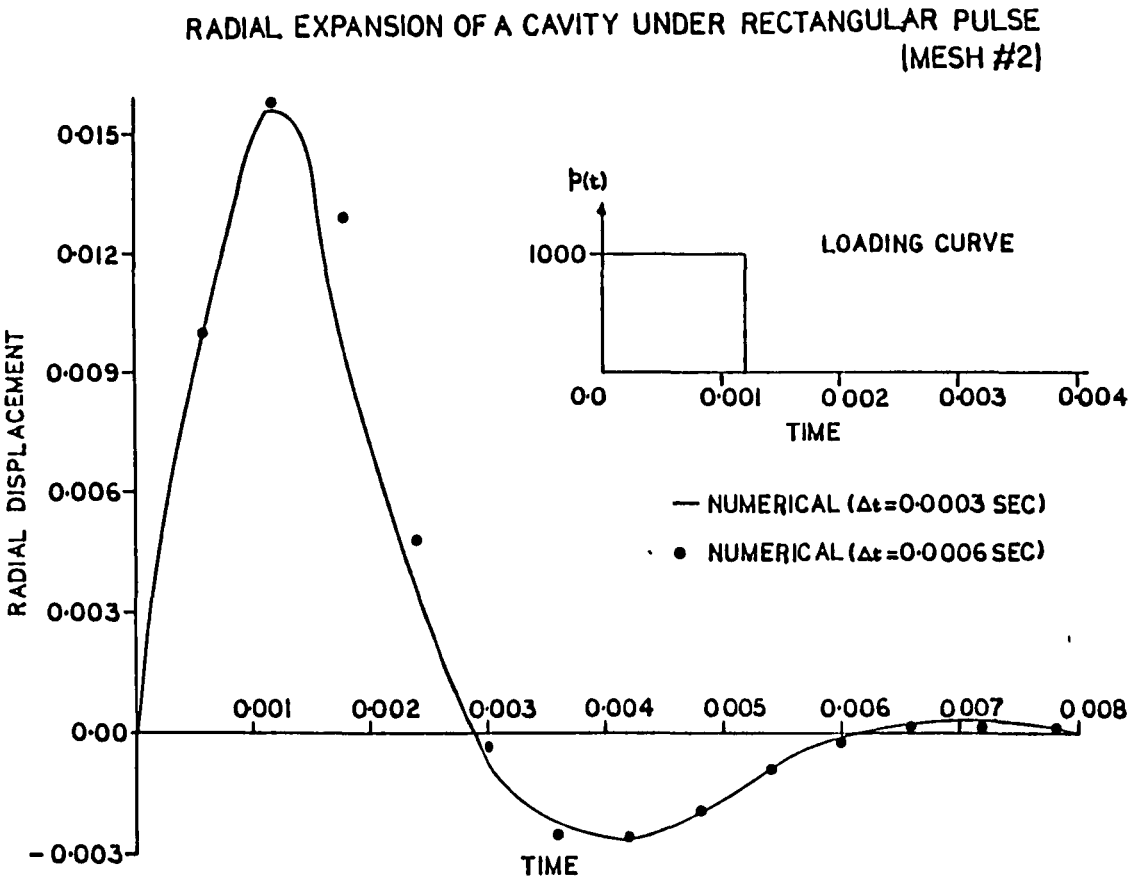
RADIAL EXPANSION OF A CAVITY UNDER RECTANGULAR PULSE
(MESH #2)
RADIAL DISPLACEMENT
0·015
0·012
0·009
0·006
0·003
0·00
-0·003
0·001
0·002
0·003
0·004
0·005
0·006
0·007
0·008
TIME
P(t)
1000
LOADING CURVE
0·0
0·001
0·002
0·003
0·004
TIME
— NUMERICAL (Δt=0·0003 SEC)
• NUMERICAL (Δt=0·0006 SEC)

Figure 8.13

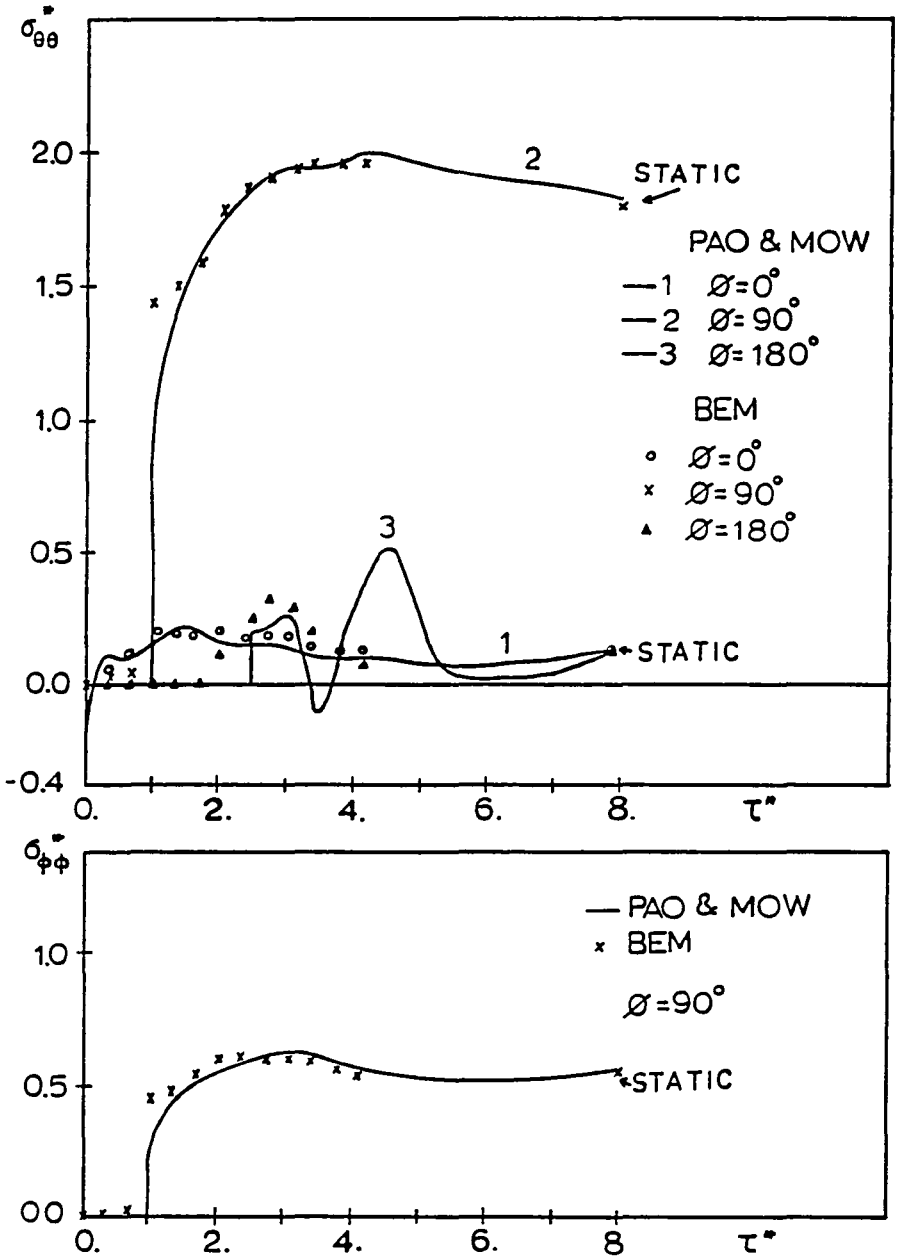

Hoop stresses at the cavity surface for a cavity engulfed by a pressure wave

Figure 8.14

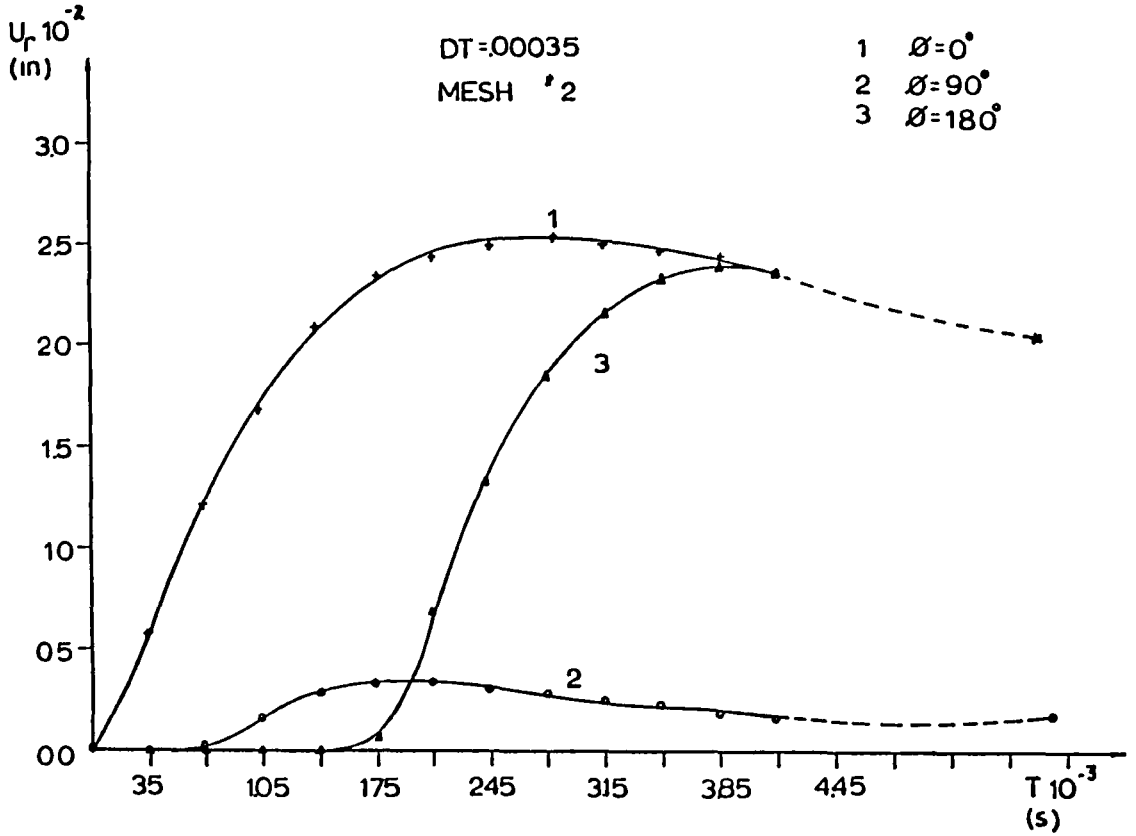

Radial scattered displacements for a cavity engulfed by a pressure wave

Figure 8.15

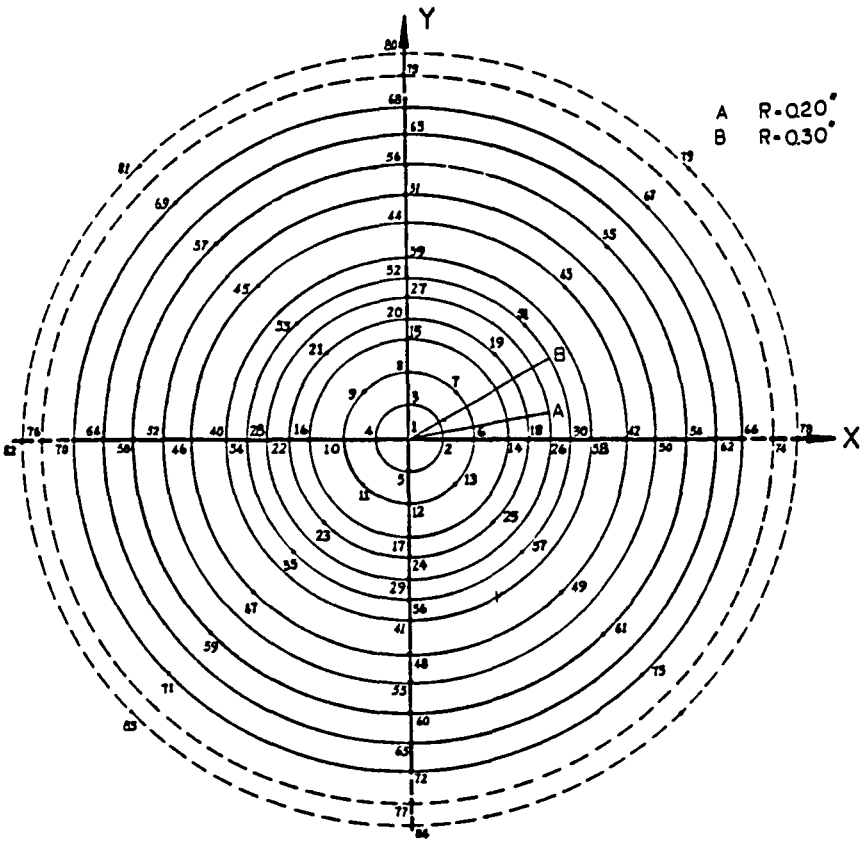

Boundary element discretized for a point load on half-space

Figure 8.16

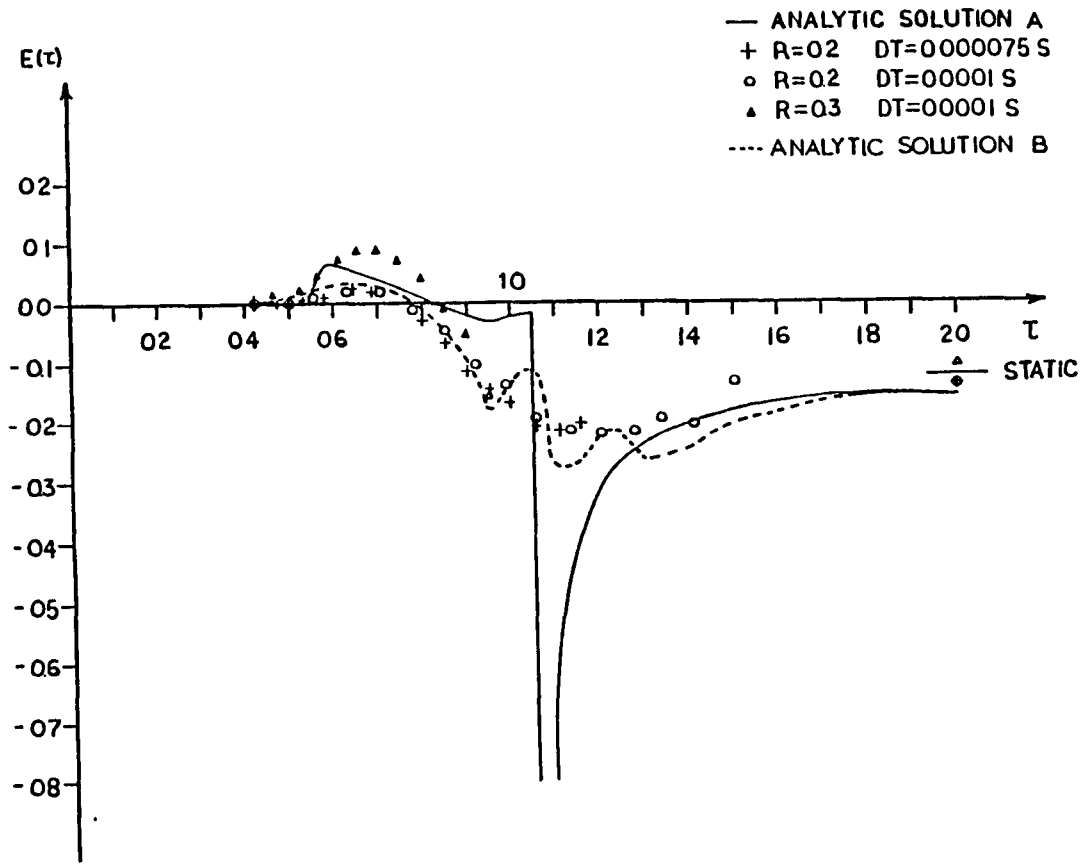

Normalized horizontal displacement history

Figure 8.17

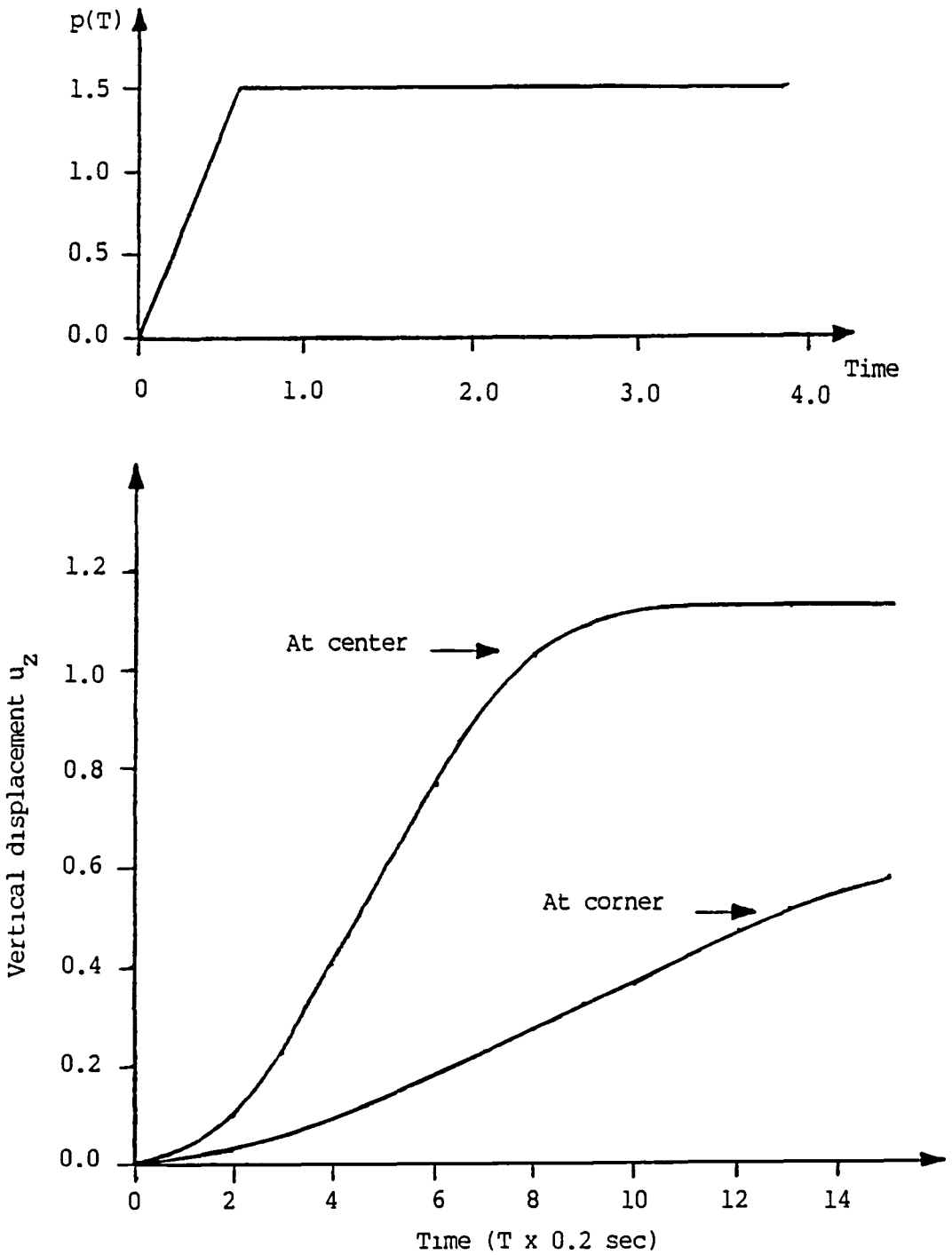

Transient response of a flexible square footing under a prescribed vertical stress distribution

Figure 8.18

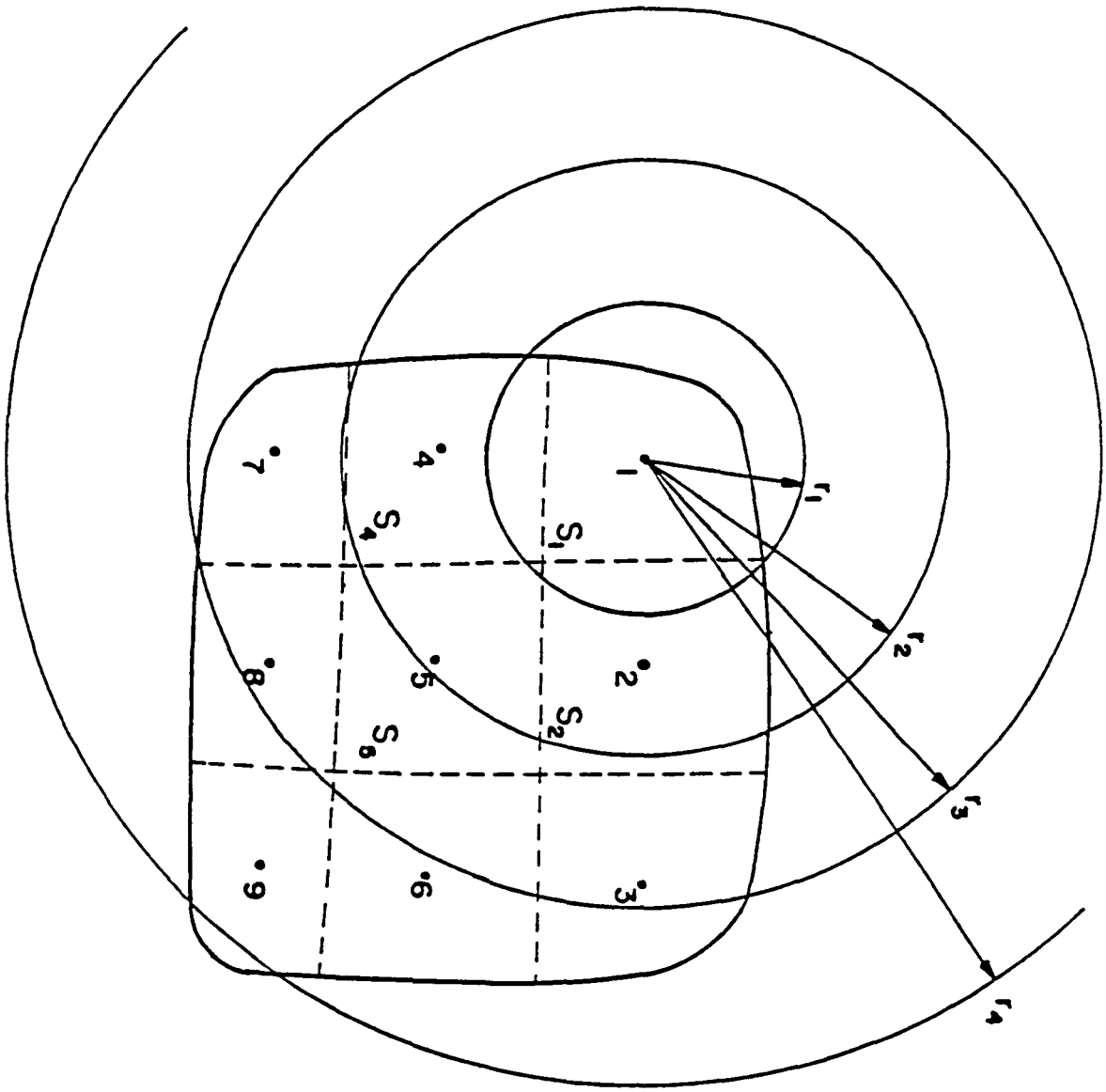

Disturbance propagation from a point as a sequence of co-centric spheres

Figure 8.19

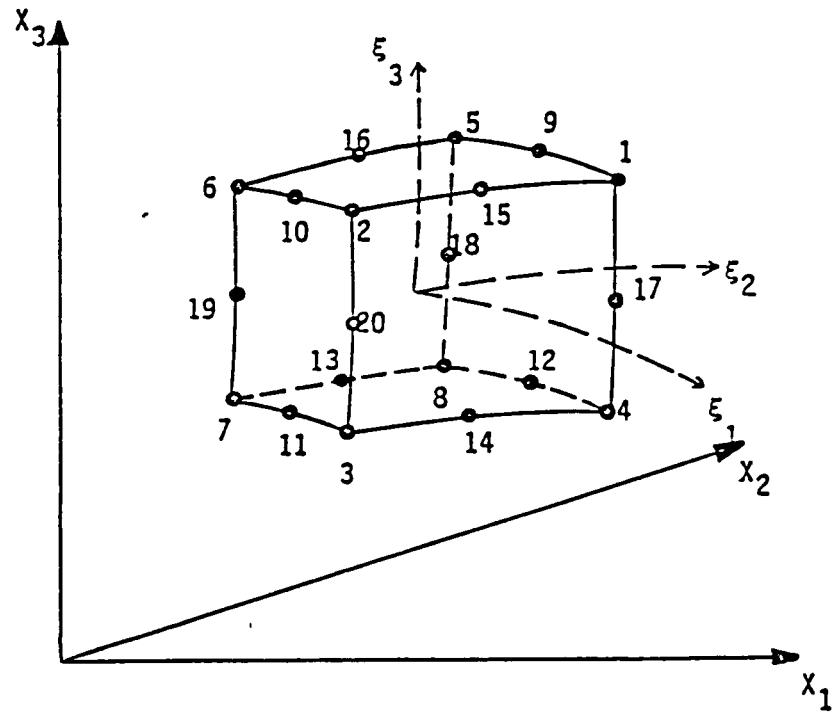

Three-dimensional volume cell

Figure 9.1

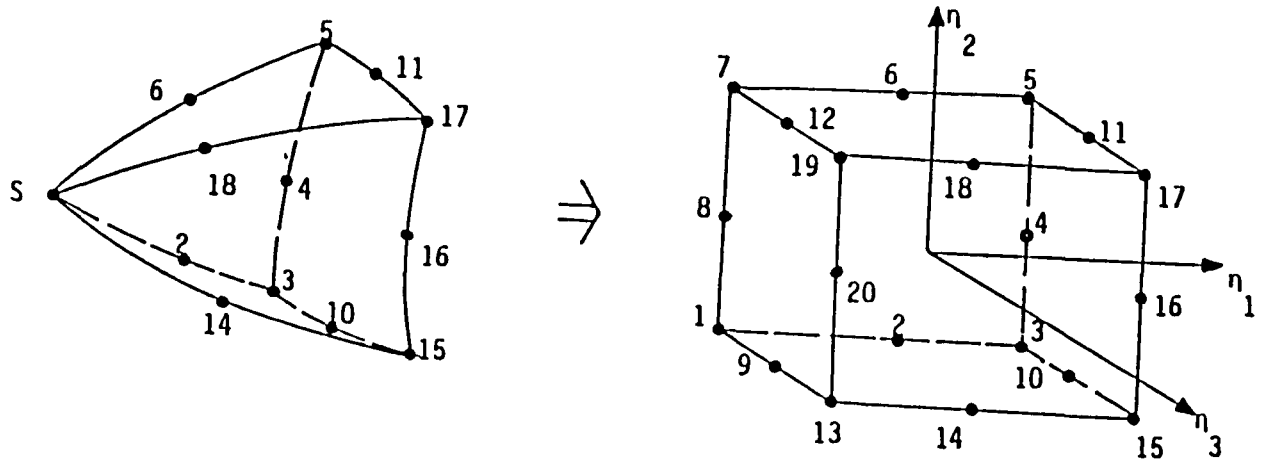

Geometrical mapping of a sub-cell onto a unit cube

Figure 9.2

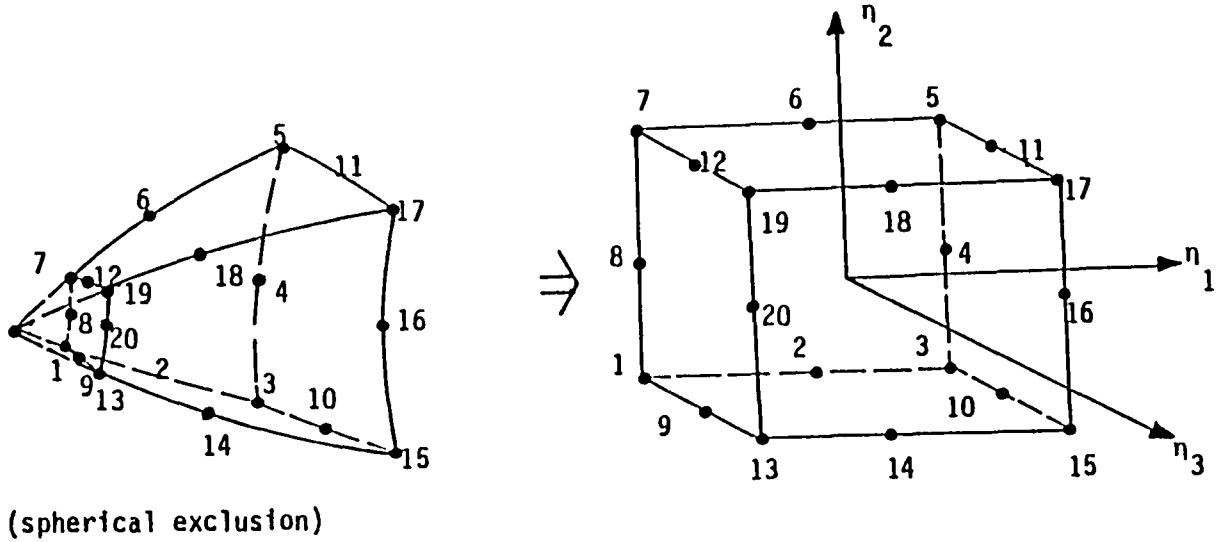

Geometrical mapping of subcell (excluding spherical segment)
onto a unit cube

Figure 9.3

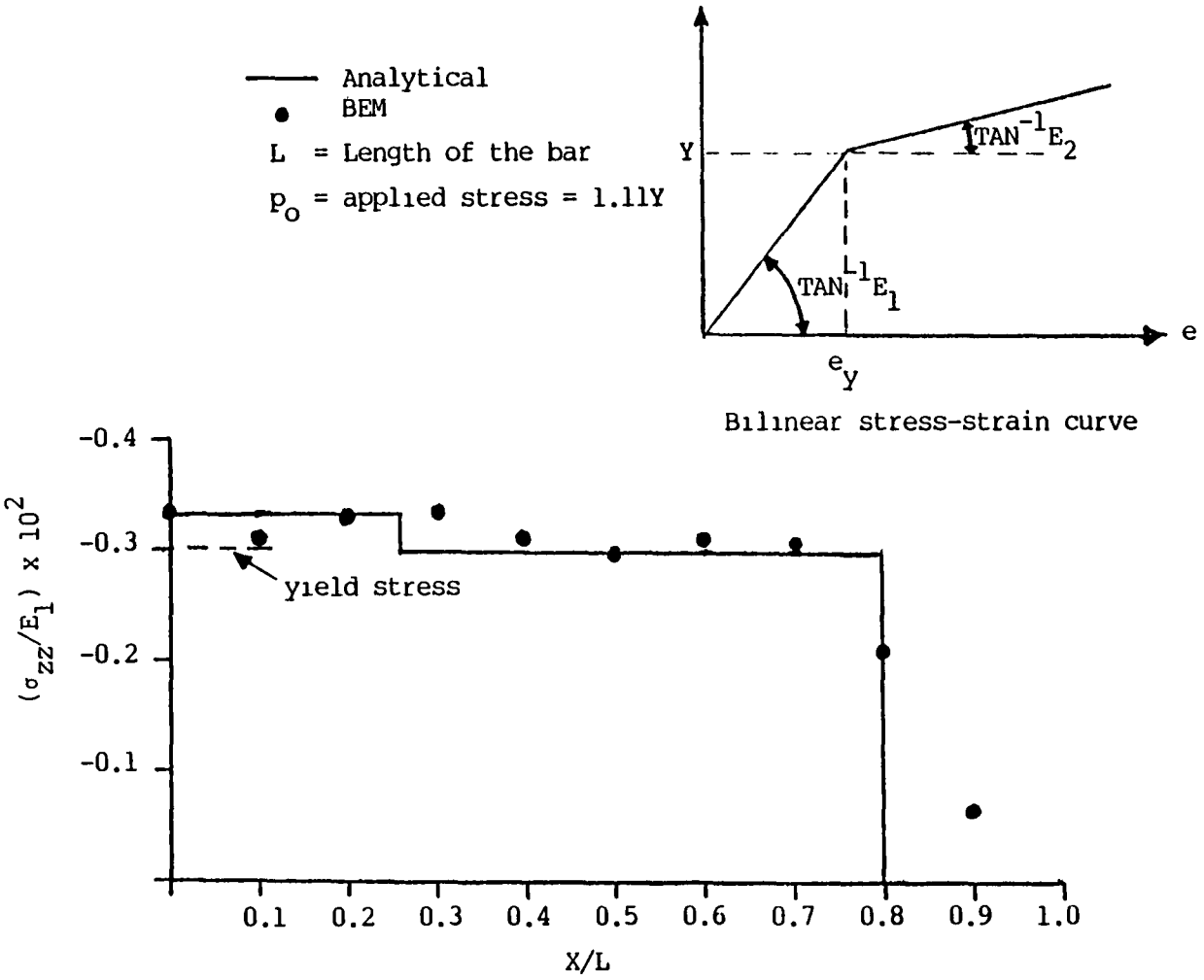

Transient elasto-plastic response of a bar subjected to a suddenly applied and maintained end pressure

Figure 9.4

APPENDICES

APPENDIX A1

BOUNDARY KERNELS FOR TWO-DIMENSIONAL STEADY-STATE DYNAMICS

The tensors $\bar{G}_{ij}$ and $\bar{F}_{ij}$ in the transformed domain are of the form:

$$\bar{G}_{ij}(\underline{x},\underline{\xi},\omega) = \frac{1}{2\pi\mu}\,[A\delta_{ij} - Br_{,i}r_{,j}] \tag{A1.1}$$

$$\bar{F}_{ij}(\underline{x},\underline{\xi},\omega) = \frac{1}{2\pi}\,[P(\delta_{ij}\frac{\partial r}{\partial n} + r_{,j}n_i)$$

$$+ Q(r_{,i}n_j - 2r_{,i}r_{,j}\frac{\partial r}{\partial n} + Rr_{,i}r_{,j}\frac{\partial r}{\partial n} + Sr_{,i}r_{,j}] \tag{A1.2}$$

where

$$A = K_o(z_2) + (1/z_2)[K_1(z_2) - (c_2/c_1)K_1(z_1)]$$

$$B = K_2(z_2) - (c_2/c_1)^2K_2(z_1)$$

$$P = \partial A/\partial r - B/r$$

$$Q = -\,2B/r$$

$$R = -\,2\partial B/\partial r$$

$$S = \{(c_1/c_2)^2 - 2\}(\partial A/\partial r - \partial B/\partial r - B/r)$$

$$n = \text{normal vector} \tag{A1.3}$$

where $z_1 = i\omega r/c_1$ and $z_2 = i\omega r/c_2$; and

K_o, K_1 and K_2 are the Modified Bessel functions of second kind, having the following recursive properties:

$$K_2(z) = K_o(z) + (2/z)K_1(z)$$

$$K_o'(z) = - K_1(z)$$

$$K_1'(z) = - K_o(z) - K_1(z)/z \qquad \text{(A1.4)}$$

where the bar denotes the differentiation w.r.t. z .

Using the recursive formulas (A1.4) the tensors $\bar{G}_{ij}$ and $\bar{F}_{ij}$ can be expressed in terms of Modified Bessel functions of the second kind of orders zero and one. These functions are given below along with their expansions for small and large arguments.

Modified Bessel Function of Second Kind

Zero order:

$$K_o(z) = [\ln(z/2) + \gamma]I_o(z) + \frac{z^2/4}{(1!)^2} + (1 + 1/2)\frac{(z^2/4)^2}{(2!)^2}$$

$$+ (1 + 1/2 + 1/3)\frac{(z^2/4)^3}{(3!)^2} + \ldots \qquad \text{(A1.5)}$$

$$I_o(z) = 1 + \frac{z^2/4}{(1!)^2} + \frac{(z^2/4)^2}{(2!)^2} + \frac{(z^2/4)^3}{(3!)^2} + \frac{(z^2/4)^4}{(4!)^2} + \ldots \qquad \text{(A1.6)}$$

where $\gamma = 0.5772156649$

First order:

$$K_1(z) = (1/z) + \ln(z/2)I_1(z) - z/4 \sum_{m=o}^{\infty} [\psi(m+1) + \psi(m+2)] \frac{(z^2/4)^m}{m!(m+1)!} \qquad \text{(A1.7)}$$

$$I_1(z) = (z/2) \sum_{m=0}^{\infty} \frac{(z^2/)^m}{m!\,\Gamma(m+2)} \qquad \text{(A1.8)}$$

where $\psi(1) = -\gamma$, and

$$\psi(n) = -\gamma + \sum_{m=1}^{n-1} m^{-1} \quad \text{for} \quad n \geq 2 \qquad \text{(A1.9)}$$

Small argument expansion:

If $z \to 0$ (i.e. $\text{abs}(z) < 10^{-8}$)

$$K_0(z) = -\ln(z) \quad \text{and} \quad K_1(z) = 1/z \qquad \text{(A1.10)}$$

Large argument expansion:

If z is large (i.e. $\text{abs}(z) > 3.5$)

$$K_0(z) = \sqrt{\frac{\pi}{2z}}\, e^{-z} \left[1 - \frac{(1)^2}{8z} + \frac{(3)^2}{2!(8z)^2} - \frac{(3)^2(5)^2}{3!(8z)^3} + \frac{(3)^2(5)^2(7)^2}{4!(8z)^4} - \ldots \right] \qquad \text{(A.11)}$$

$$K_1(z) = \sqrt{\frac{\pi}{2z}}\, e^{-z} \left[1 + \frac{3}{8z} - \frac{3x5}{2!(8z)^2} + \frac{3x5x21}{3!(8z)^3} - \ldots \right] \qquad \text{(A1.12)}$$

However, for $\text{abs}(z) > 100$, $K_0(z) = K_1(z)$ 0.0 (A1.13)

APPENDIX A2

BOUNDARY KERNELS FOR THREE-DIMENSIONAL STEADY-STATE DYNAMICS

The tensors $\bar{G}_{ij}$ and $\bar{F}_{ij}$ in the transformed domain are of the form:

$$\bar{G}_{ij}(\underline{x},\underline{\xi},s) = \frac{1}{4\pi\mu}\left[A\delta_{ij} - Br_{,i}r_{,j}\right] \tag{A2.1}$$

and

$$\bar{F}_{ij}(\underline{x},\underline{\xi},s) = \frac{1}{4\pi}\left[P(\delta_{ij}\frac{\partial r}{\partial n} + r_{,j}n_i)\right.$$

$$\left. + Q(n_j r_{,i} - 2r_{,i}r_{,j}\frac{\partial r}{\partial n}) + Rr_{,i}r_{,j}\frac{\partial r}{\partial n} + Sr_{,j}r_{,i}\right] \tag{A2.2}$$

where s is the Laplace transform parameter. In addition,

$$A = \left(\frac{3c_2^2}{s^2r^2} + \frac{3c_2}{sr} + 1\right)\frac{e^{-sr/c_2}}{r} - \frac{c_2^2}{c_1^2}\left(\frac{3c_1^2}{s^2r^2} + \frac{3c_1}{sr} + 1\right)e^{-sr/c_1} \tag{A2.3}$$

and

$$B = \left(\frac{c_2^2}{s^2r^2} + \frac{c_2}{sr} + 1\right)\frac{e^{-sr/c_2}}{r} - \frac{c_2^2}{c_1^2}\left(\frac{c_1^2}{s^2r^2} + \frac{c_1}{sr}\right)\frac{e^{-sr/c_1}}{r} \tag{A2.4}$$

where e is the exponential function. Furthermore,

$$P = \frac{\partial A}{\partial r} - \frac{B}{r}, \quad Q = -\frac{2B}{r}, \quad R = -2\frac{\partial B}{\partial r},$$

and $$S = \left(\frac{c_1^2}{c_2^2} - 2\right)\left(\frac{\partial A}{\partial r} - \frac{\partial B}{\partial r} - \frac{2B}{r}\right) \tag{A2.5}$$

APPENDIX A3

INTERIOR STRESS KERNELS FOR STEADY-STATE DYNAMICS

The interior tensors $\bar{G}_{ijk}$ and $\bar{F}_{ijk}$ for two-dimensional steady-state dynamic analysis are of the form:

$$\bar{G}^{\sigma}_{ijk}(\underline{x},\underline{\xi},\omega) = \lambda\delta_{jk}\frac{\partial G_{mi}}{\partial \xi_k} + \mu\left(\frac{\partial G_{ji}}{\partial \xi_k} + \frac{\partial G_{ki}}{\partial \xi_j}\right) \tag{A3.1}$$

$$\bar{F}^{\sigma}_{ijk}(\underline{x},\underline{\xi},\omega) = \lambda\delta_{jk}\frac{\partial F_{mi}}{\partial \xi_k} + \mu\left(\frac{\partial F_{ji}}{\partial \xi_k} + \frac{\partial F_{ki}}{\partial \xi_j}\right) \tag{A3.2}$$

where

$$\frac{\partial G_{ij}}{\partial \xi_k} = -\frac{1}{2\pi\mu}\left[\delta_{ij}\frac{\partial A}{\partial r}r_{,k} - \frac{\partial B}{\partial r}r_{,k}r_{,i}r_{,j} - B(r_{,i}r_{,jk} + r_{,j}r_{,ik})\right] \tag{A3.3}$$

$$\begin{aligned}\frac{\partial F_{ij}}{\partial \xi_k} = -\frac{1}{2\pi}\Big[&\frac{\partial P}{\partial r}r_{ik}\left(\delta_{ij}\frac{\partial r}{\partial n} + r_{,j}n_i\right) + P(\delta_{ij}r_{,mk}n_m + r_{,jk}n_i)\\ &+ \frac{\partial Q}{\partial r}r_{,k}\left(r_{,i}n_j - 2r_{,i}r_{,j}\frac{\partial r}{\partial n}\right) + Q(r_{,ik}n_j - 2r_{,ik}r_{,j}\frac{\partial r}{\partial n})\\ &- 2r_{,i}r_{,jk}\frac{\partial r}{\partial n} - 2r_{,i}r_{,j}r_{,mk}n_m + \frac{\partial R}{\partial r}r_{,k}r_{,i}r_{,j}\frac{\partial r}{\partial n}\\ &+ R(r_{,ik}r_{,j}\frac{\partial r}{\partial n} + r_{,i}r_{,jk}\frac{\partial r}{\partial n} + r_{,i}r_{,j}r_{,mk}n_m)\\ &+ \frac{\partial S}{\partial r}r_{,k}r_{,i}n_j + S\,r_{,ik}n_j\Big]\end{aligned} \tag{A3.4}$$

where the functions A,B,P,Q,R and S are listed for two and three-dimensional problems in Appendix A1 and A2 , respectively.

APPENDIX A4

BOUNDARY KERNELS FOR TRANSIENT DYNAMICS

The tensors G_{ij} and F_{ij} are of the form:

$$G_{ij}(\underline{x},T;\underline{\xi},\tau) = \frac{1}{4\pi\rho}\left[(3a_{ij}-b_{ij})\int_{1/c_1}^{1/c_2}\lambda\delta(v-\lambda r)d\lambda\right.$$

$$\left. + a_{ij}\{(1/c^2)\delta(v-r/c_1) - (1/c_2^2)\delta(v-r/c_2)\} + (b_{ij}/c_2^2)\delta(v-r/c_2)\right] \tag{A.4.1}$$

where $v = T - \tau$

$$a_{ij} = y_i y_j/r^3 \quad \text{and} \quad b_{ij} = \delta_{ij}/r$$

$$y_i = x_i - \xi_i$$

$$F_{ij}(\underline{x},T;\underline{\xi},\tau) = \frac{1}{4\pi}\left[-6c_2^2(5a_{ij}-b_{ij})\int_{1/c_1}^{1/c_2}\lambda\delta(v-\lambda r)d\lambda + (12a_{ij}-2b_{ij})\right.$$

$$\{\delta(v-r/c_2) - (c_2/c_1)^2\delta(v-r/c_1)\} + 2ra_{ij}/c_2\{\delta'(v-r/c_2)$$

$$- (c_2/c_1)^3\delta'(v-r/c_1)\} - c_{ij}(1-2c_2^2/c_1^2)\{\delta(v-r/c_1) + (r/c_1)\delta'(v-r/c_1)\}$$

$$\left. - d_{ij}\{\delta(v-r/c_2) + (r/c_2)\delta'(v-r/c_2)\}\right] \tag{A4.2}$$

where $v = T - \tau$

$$a_{ij} = y_i y_j y_m n_m/r^5$$

$$c_{ij} = y_j n_i/r^3$$

$$d_{ij} = (y_i n_j + \delta_{ij} y_m n_m)/r^3$$

$$b_{ij} = c_{ij} + d_{ij}$$

APPENDIX A5

INTERIOR STRESS KERNELS FOR TRANSIENT DYNAMICS

The tensors G^{σ}_{ijk} and F^{σ}_{ijk} are of the form:

$$G^{\sigma}_{ijk}(\underline{x},T;\underline{\xi},\tau) = \frac{1}{4\pi}\Big[6c_2^2(5a_{ijk}-b_{ijk})\int_{1/c_1}^{1/c_2}\lambda\delta(v-\lambda r)d\lambda$$

$$- (12a_{ijk}-2b_{ijk})\{\delta(v-r/c_2) - (c_2/c_1)^2\delta(v-r/c_1)\}$$

$$- 2ra_{ijk}/c_2\{\delta'(v-r/c_2) - (c_2/c_1)^3\delta'(v-r/c_1)\}$$

$$+ c_{ijk}(1-2c_2^2/c_1^2)\{\delta(v-r/c_1) + (r/c_1)\delta'(v-r/c_1)\}$$

$$+ d_{ijk}\{\delta(v-r/c_2) + (r/c_2)\delta'(v-r/c_2)\}\Big] \qquad \text{(A5.1)}$$

where $v = T - \tau$

$a_{ijk} = y_i y_j y_k / r^5$

$c_{ijk} = \delta_{jk} y_i / r^3$

$d_{ijk} = (\delta_{ik} y_j + \delta_{ij} y_k)/r^3$

$b_{ijk} = c_{ijk} + d_{ijk}$

$$F^{\sigma}_{ijk}(\underline{x},T;\underline{\xi},\tau) = -\frac{\rho}{4\pi}\Big[12c_2^4(35a_{ijk}-5b_{ijk}+c_{ijk})\int_{1/c_1}^{1/c_2}\lambda\delta(v-\lambda r)d\lambda$$

$$- 4c_2^2(45a_{ijk}-6b_{ijk}+c_{ijk})\{\delta(v-r/c_2) - (c_2/c_1)^2\delta(v-r/c_1)\}$$

$$- 4c_2 r(10a_{ijk}-b_{ijk})\{\delta'(v-r/c_2) - (c_2/c_1)^3\delta'(v-r/c_1)\}$$

$$+ 2c_2^2(1-2c_2^2/c_1^2)(3d_{ijk}-2e_{ijk})\{\delta(v-r/c_1) + (r/c_1)\delta'(v-r/c_1)\}$$

$$+ c_2^2(3f_{ijk} - 2g_{ijk})\{\delta(v-r/c_2) + (r/c_2)\delta'(v-r/c_2)\}$$

$$- 4a_{ijk}r^2\{\delta''(v-r/c_2) - (c_2/c_1)^4\delta''(v-r/c_1)\}$$

$$+ r^2(1-2c_2^2/c_1^2)\{2c_2^2 d_{ijk}/c_1^2 + (1-2c_2^2/c_1^2)e_{ijk}\}\delta''(v-r/c_1)$$

$$+ r^2 f_{ijk}\delta''(v-r/c_2)\Big] \qquad \text{(A5.2)}$$

where $v = T - \tau$

$$a_{ijk} = y_i y_j y_k y_m n_m / r^7$$

$$d_{ijk} = (y_j y_k n_i + y_i y_m n_m \delta_{jk})/r^5$$

$$e_{ijk} = \delta_{jk} n_i / r^3$$

$$f_{ijk} = \{y_i y_j n_k + y_i y_k n_j + y_m n_m(\delta_{ik} y_j + \delta_{ij} y_k)\}/r^5$$

$$g_{ijk} = (\delta_{ij} n_k + \delta_{ik} n_j)/r^3$$

$$b_{ijk} = d_{ijk} + f_{ijk}$$

$$c_{ijk} = e_{ijk} + g_{ijk}$$

APPENDIX A6

VOLUME KERNELS FOR TRANSIENT DYNAMICS

The tensors B_{ilj} , B^{σ}_{iljk} and J^{σ}_{iljk} are as follows:

$$B_{ilj}(\underline{x},T;\underline{\xi},\tau) = \frac{1}{4\pi\rho}\left[-(15a_{ilj}-3b_{ilj})\int_{1/c_1}^{1/c_2}\lambda\delta(v-\lambda r)d\lambda + 1/c_2^2(6a_{ilj}-b_{ilj})\right.$$

$$\{\delta(v-r/c_2) - (c_2/c_1)^2\delta(v-r/c_1)\} + ra_{ilj}/c_2^3\{\delta'(v-r/c_2) - (c_2/c_1)^3\delta'(v-r/c_1)\}$$

$$\left. - c_{ilj}/2c_2^2\{\delta(v-r/c_2) + (r/c_2)\delta'(v-r/c_2)\}\right] \cdot \qquad \text{(A6.1)}$$

where $v = T - \tau$

$$a_{ilj} = y_i y_l y_j / r^5$$

$$c_{ilj} = (\delta_{ij}y_l + \delta_{lj}y_i)/r^3$$

$$b_{ilj} = c_{ilj} + \delta_{il}y_j/r^3$$

$$B^{\sigma}_{iljk}(\underline{x},T;\underline{\xi},\tau) = -\frac{1}{4\pi}\left[6c_2^2(35a_{iljk}-5b_{iljk}+c_{iljk})\int_{1/c_1}^{1/c_2}\lambda\delta(v-\lambda r)d\lambda\right.$$

$$- 2(45a_{iljk}-6b_{iljk}+c_{iljk})\{\delta(v-r/c_2) - (c_2/c_1)^2\delta(v-r/c_1\}$$

$$- 2r/c_2(10a_{iljk}-b_{iljk})\{\delta'(v-r/c_2) - (c_2/c_1)^3\delta'(v-r/c_1)\}$$

$$+ (3f_{iljk}-g_{iljk})(1-2c_2^2/c_1^2)\{\delta(v-r/c_1) + (r/c_1)\delta'(v-r/c_1)\}$$

$$\left. + (1.5d_{iljk} - e_{iljk})\{\delta(v-r/c_2) + (r/c_2)\delta'(v-r/c_2)\right.$$

$$- (2r^2 a_{iljk}/c_2^2)\{\delta''(v-r/c_2) - (c_2/c_1)^4\delta''(v-r/c_1)\}$$

$$+ (r^2 f_{iljk}/c_1^2)(1-2c_2^2/c_1^2)\delta''(v-r/c_1) + (r^2 d_{iljk}/2c_2^2)\delta''(v-r/c_2)\Big]$$

where $v = T - \tau$

$$a_{iljk} = Y_i Y_l Y_j Y_k / r^7$$

$$d_{iljk} = (\delta_{ij}Y_l Y_k + \delta_{lj}Y_i Y_k + \delta_{ik}Y_l Y_j + \delta_{lk}Y_i Y_j)/r^5$$

$$e_{iljk} = (\delta_{ij}\delta_{lk} + \delta_{ik}\delta_{lj})/r^3$$

$$f_{iljk} = \delta_{jk}Y_i Y_l / r^5$$

$$g_{iljk} = \delta_{jk}\delta_{il}/r^3$$

$$b_{iljk} = d_{iljk} + f_{iljk} + \delta_{il}Y_j Y_k / r^5$$

$$c_{iljk} = e_{iljk} + g_{iljk}$$

For 3-D:

$$J^{\sigma}_{iljk} = - \frac{1}{15(1-\nu)}\Big[(7-5\nu)\delta_{ij}\delta_{kl} + (1-5\nu)\delta_{il}\delta_{jk}\Big] \qquad \text{(A6.3)}$$

APPENDIX B

PROPAGATION OF WAVEFRONTS AS SURFACES OF DISCONTINUITY

When a body is disturbed from a quiescent state by excitation at a portion of the boundary or within a restricted domain inside the body, neighboring domains are soon set in motion and put into states of deformation. The moving surface which separates the disturbed from the undisturbed part of the body is called the wavefront. At wavefronts, the field quantities and/or their derivatives may be discontinuous. However, if the material remains coherent and does not fracture, the displacements will certainly be continuous in both space and time. In many situations, involving very sudden loadings, the particle velocities and/or stresses will have sudden variations (discontinuities) at the wavefront over a very small interval of space and time. These variations at the wave fronts can be quite closely approximated by finite jumps based on the basic techniques developed towards the end of last century for the study of propagating surfaces of discontinuity in continuum mechanics.

Love (1904) sets down the following basic kinematical and dynamical conditions that must hold at a propagating surface of discontinuity in an elastic solid.

Kinematic conditions:

Consider a surface of discontinuity S, propagating in an unbounded medium. The situation is shown in figure B.1, for a fixed instant of time. It is assumed that S propagates into region (2), leaving a region (1) behind it, and moves normal to itself with velocity c, i.e., each point $P(\underline{x})$ of S propagates with velocity c, along the outward unit normal vector $\underline{n}$ to S at that point. If one supposes the components of σ_{ij} are discontinuous across S, the jumps will be denoted by the standard bracket notation.

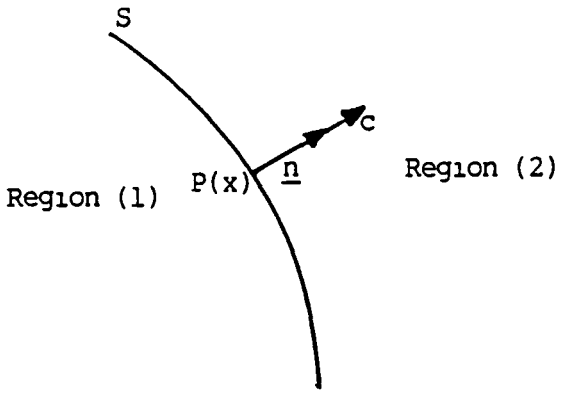

Figure B.1

$$[\sigma_{ij}] = (\sigma_{ij})_2 - (\sigma_{ij})_1 \tag{B.1}$$

where the subscript 1 denotes the value of the field variable on S when S is approached through region (1), and the subscript 2 is employed to denote the value when S is approached through region (2).

As mentioned earlier, since the material should maintain its integrity at the wavefront, the jump in the displacement components at S is zero, i.e.

$$[u_i] = 0 \tag{B.2}$$

Moreover, if the strains and velocities at a wavefront are discontinuous (i.e. shock waves), the finite jumps in them must satisfy the following kinematic relations.

$$\begin{aligned} &[\dot{u}_i] + c[u_{i,j}]n_j = 0 \\ &[\dot{u}_i] + c[\partial u_i/\partial n] = 0 \\ &[\dot{u}_i]n_j + c[u_{i,j}] = 0 \end{aligned} \tag{B.3}$$

However, if the first derivatives of the displacements across S are continuous but the second derivatives are discontinuous (acceleration waves), then the following kinematic relation has to be satisfied at the wavefront.

$$[u_{i,jk}] - q_i n_j n_k = 0$$

$$[\dot{(u_i)}_{,j}] + c q_i n_j = 0$$

$$[u_i] - c^2 q_i = 0 \qquad \text{(B.4)}$$

where q_i is an unknown function.

Dynamical conditions:

The dynamical conditions, which has to be satisfied at the moving surface of discontinuity S , are determined by considering the momentum changes of a thin slice of the medium adjacent to S and the corresponding impulse-momentum equation. It has the form

$$[\sigma_{ij}] n_j + \rho c [\dot{u}_i] = 0 \qquad \text{(B.5)}$$

For acceleration waves, the jumps in the second derivatives of $\underline{u}$ should satisfy the linear momentum equation, i.e.

$$\lambda [u_{m,im}] + \mu [u_{i,jj} + u_{j,ij}] = \rho [u_i] \qquad \text{(B.6)}$$

The fundamental singular solution of transient elastodynamics, for the displacements generated by a suddenly applied concentrated load at a point of the unbounded elastic medium was first developed by Stokes (1899). Love (1903) performed an extensive study of Stokes' solution for initial value problem with arbitrary initial values, and related wavefront discontinuities. He pointed out that Stokes' formula yields correct

results only when the input field quantities are continuous at the wavefront. He also found that the Stokes' formula satisfies the necessary continuity conditions on the displacements (eq. B.2), the kinematical conditions on the velocities and strains (eq. B.3) and the dynamical conditions on the stresses and velocities (eq. B.5), provided the input function is continuous. Thus, if the input excitation is a step loading, it has to be modeled as a ramp loading in the first time step. Also, a very small time step cannot be used for this purpose, because it will result in non-vanishing dilation and rotations at the wavefronts.

APPENDIX C1

ISOPARAMETRIC BOUNDARY ELEMENTS FOR 2-D PROBLEMS

Both the three noded quadratic and two noded linear elements were depicted in figure 4.1. The shape functions for the three noded quadratic elements are:

$$N_1(\eta) = 2(\eta - 1/2)(\eta - 1)$$

$$N_2(\eta) = -4\eta(\eta - 1)$$

$$N_3(\eta) = 2\eta(\eta - 1/2) \qquad \text{(C1.1)}$$

where η is the intrinsic coordinate ($0 \leq \eta \leq 1$).

The shape functions for two noded linear element are:

$$N_1(\eta) = 1 - \eta$$

$$N_2(\eta) = \eta \qquad \text{(C1.2)}$$

The normal unit vectors along the positive x and y axes are defined as:

$$n_1 = (\partial y/\partial \eta)/|J(\eta)|$$

$$n_2 = (-\partial x/\partial \eta)|J(\eta)| \qquad \text{(C.1.3)}$$

where $|J(\eta)|$ is the magnitude of the determinant of the Jacobian matrix (Ref. Sec. IV.4).

APPENDIX C2

ISOPARAMETRIC BOUNDARY ELEMENTS FOR 3-D PROBLEMS

Both the six node triangular and the eight node rectangular surface elements were depicted in figure 6.2. It is worth noticing that these intrinsically planar elements becomes curved in three-dimensional space. The shape functions for the six node triangle are:

$$N_\alpha = \begin{cases} \eta_\alpha(2\eta_\alpha - 1) & \text{if } \alpha = 1,2,3 \\ 4\eta_\beta\eta_\gamma & \text{if } \alpha = 4.5.6 \text{ with } \beta = \alpha - 3 \\ & \quad \text{and } \gamma = \alpha - 2 \end{cases} \qquad \text{(C2.1)}$$

where η_1 and η_2 are two linearly independent coordinates and $\eta_3 = 1-\eta_1-\eta_2$.

The shape functions for the eight node rectangle are:

$$N_\alpha = \begin{cases} 0.25(1+\xi_o)(1+\eta_o)(\xi_o+\eta_o-1) & \text{if } \alpha = 1,3,5,7 \\ 0.50(1-\xi^2)(1-\eta_o) & \text{if } \alpha = 2,6 \\ 0.50(1+\xi_o)(1-\eta^2) & \text{if } \alpha = 4,8 \end{cases} \qquad \text{(C2.2)}$$

where $\xi_o = \xi\ \xi_\alpha$ and $\eta\ \eta_\alpha$, with ξ and η being the two linearly independent coordinates and (ξ_α,η_α) the coordinates of node α.

Two base vectors along the intrinsic coordinates ξ,η (or η_1,η_2) can be defined as

$$\underline{e}_1 = \frac{\partial x}{\partial \xi} d\xi\ \underline{i} + \frac{\partial y}{\partial \xi} d\xi\ \underline{j} + \frac{\partial z}{\partial \xi} d\xi\ \underline{k}$$

$$\underline{e}_2 = \frac{\partial x}{\partial \eta} d\eta\ \underline{i} + \frac{\partial y}{\partial \eta} d\eta\ \underline{j} + \frac{\partial z}{\partial \eta} d\eta\ \underline{k} \qquad \text{(C2.3)}$$

where $\underline{i}$, $\underline{j}$, and $\underline{k}$ are unit vectors along the x, y, and z coordinates,

respectively. Their cross product

$$\underline{e}_3 = \underline{e}_1 \times \underline{e}_2 \qquad \text{(C2.4)}$$

is a vector normal to the surface of the element and its magnitude is equal to the value of the determinant of the Jacobian matrix.

APPENDIX D1

ANALYTICAL TEMPORAL INTEGRATION OF THE TRANSIENT DYNAMIC KERNELS FOR CONSTANT TIME INTERPOLATION

For constant time interpolation the field variables are expressed as

$$f(\underline{x},\tau) = \sum_{n=1}^{N} f_n(\underline{x})\phi_n(\tau) \qquad \text{(D1.1)}$$

where

$\phi_n(\tau) = [H(\tau - (n-1)\Delta T) - H(\tau - n\Delta T)]$;

$f_n(\underline{x})$ represents the spatial variation of the field variable $f(\underline{x},\tau)$ at time $T_n(= n\Delta T)$;

N is total number of time steps; and

H is heaviside function.

Each of the transient dynamic kernels listed in Appendices A4, A5 and A6 has one or more of the following time functions:

(1) $\delta(T - \tau - r/c)$ (D1.2)

(2) $\int_{1/c_1}^{1/c_2} \lambda\delta(T - \tau - r/c)d\lambda$ (D1.3)

(3) $\dot{\delta}(T - \tau - r/c)$ (D1.4)

(4) $\ddot{\delta}(T - \tau - r/c)$ (D1.5)

where c is either pressure wave velocity c_1 or shear wave velocity c_2; and δ is the delta function.

Using equation (D1.1), the time integrals related to the above time functions can be expressed as

$$\int_0^T g(T - \tau - r/c)f(\underline{x},\tau)d\tau$$

$$= \sum_{n=1}^{N} \left[f_n(x) \int_{(n-1)\Delta T}^{n\Delta T} g(T - \tau - r/c)\phi_n(\tau)d\tau \right] \qquad \text{(D1.6)}$$

The time integrals on the right hand side of equation (D1.6) are evaluated analytically as follows.

Time function 1:

$$\int_{(n-1)\Delta T}^{n\Delta T} \delta(T - \tau - r/c)\phi_n(\tau)d\tau = \phi_n(T - r/c) \qquad \text{(D1.7)}$$

Time function 2:

$$\int_{(n-1)\Delta T}^{n\Delta T} \int_{1/c_1}^{1/c_2} \lambda\delta(T - \tau - \lambda r)d\lambda\phi_n(\tau)d\tau$$

$$= \int_{1/c_1}^{1/c_2} \int_{(n-1)\Delta T}^{n\Delta T} \lambda\delta(T - \tau - \lambda r)\phi_n(\tau)d\tau d\lambda$$

$$= \int_{1/c_1}^{1/c_2} \lambda\phi_n(T - \lambda r)d\lambda = \left[(\lambda^2/2)\phi_n(T - \lambda r) \right]_{1/c_1}^{1/c_2} \qquad \text{(D1.8)}$$

An important characteristic of the transient dynamic kernels is the time translation property (Ref. Chapter VIII and Appendix A4). Because of this characteristic, at each time step only the effects of the dynamic history of the first time interval on the current time node needs to be evaluated: i.e. at each time step the analytical time integrations has to be done only for $n = 1$. Thus, equations (D1.7) and (D1.8) reduce to

$$\int_0^{\Delta T} \delta(T - \tau - r/c)\phi_1(\tau)d\tau = \phi_1(T - r/c) = H(T - r/c) - H(T - \Delta T - r/c) \qquad \text{(D1.9)}$$

$$\int_0^{\Delta T} \int_{1/c_1}^{1/c_2} \lambda\delta(T - \tau - r/c)d\lambda\phi_1(\tau)d\tau = \left[(\lambda^2/2)\phi_1(T - \lambda r)\right]_{1/c_1}^{1/c_2}$$

$$= \left[(\lambda^2/2)H(T - \lambda r)\right]_{1/c_1}^{1/c_2} - \left[(\lambda^2/2)H(T - \Delta T - \lambda r)\right]_{1/c_1}^{1/c_2} \qquad \text{(D1.10)}$$

where

$$\left[(\lambda^2/2)H(T - \lambda r)\right]_{1/c_1}^{1/c_2} = 0 \qquad \text{if } T < r/c_1 \ .$$

$$= \frac{T^2}{2r^2} - \frac{1}{2c_1^2} \qquad \text{if } T > r/c_1 \text{ and } T < r/c_2$$

$$= \frac{1}{2c_2^2} - \frac{1}{2c_1^2} \qquad \text{if } T > r/c_2 \qquad \text{(D1.11)}$$

The second term on the right hand side of equation (D1.9) can be obtained in a similar manner by replacing 'T' by 'T-ΔT' in equation (D1.11).

Time function 3:

The time integrals involving time function (3) are approximated by using a backward finite difference scheme, i.e.

$$\int_{(n-1)\Delta T}^{n\Delta T} \dot{\delta}(T - \tau - r/c)f(\underline{x},\tau)d\tau$$

$$= \int_{(n-1)\Delta T}^{n\Delta T} \delta(T - \tau - r/c)\dot{f}(\underline{x},\tau)d\tau$$

$$= \frac{f_n(\underline{x}) - f_{n-1}(\underline{x})}{\Delta T}\,\phi_n(T - r/c) \qquad \text{(D1.12)}$$

APPENDIX D2

ANALYTICAL TEMPORAL INTEGRATION OF THE TRANSIENT DYNAMIC KERNELS FOR LINEAR TIME INTERPOLATION

Assuming the field variables to vary linearly during a time step, a field variable $f(\underline{x},\tau)$ can be expressed as:

$$f(\underline{x},\tau) = \sum_{n=1}^{N} [\bar{M}_1 f_{n-1}(\underline{x}) + \bar{M}_2 f_n(\underline{x})] \qquad \text{(D2.1)}$$

where $\bar{M}_1$ and $\bar{M}_2$ are the temporal shap functions, and are of the form:

$$\bar{M}_1 = \frac{T_n - \tau}{\Delta t} \phi_n(\tau)$$

$$\bar{M}_2 = \frac{\tau - T_{n-1}}{\Delta t} \phi_n(\tau) \qquad \text{(D2.2)}$$

As mentioned in Appendix D1 and Chapter VIII (Section 3), at each time step only the effects of the dynamic history of the first time interval on the current time node needs to be calculated. Therefore, for $n = 1$ (i.e. $T_n = \Delta T$, $T_{n-1} = 0$)

$$f(\underline{x},\tau) = (1 - \frac{\tau}{\Delta T})\phi_1(\tau) f_o(\underline{x}) + (\frac{\tau}{\Delta T})\phi_1(\tau) f_1(\underline{x}) \qquad \text{(D2.3)}$$

The analytical time integrations related to $\phi_1(\tau)$ are same as those described in Appendix D1 and the time integrations related to $\tau\phi_1(\tau)$ are presented as follows.

Time-function 1 (eq. D1.2):

$$\int_0^{\Delta T} \delta(T - \tau - r/c)\tau\phi_1(\tau)d\tau = (T - r/c)\phi_1(T - r/c) \qquad \text{(D2.4)}$$

Time-function 2 (eq. D1.3):

$$\int_0^{\Delta T} \int_{1/c_1}^{1/c_2} \lambda\delta(T - \tau - \lambda r)d\lambda\tau\phi_1(\tau)d\tau$$

$$= \int_{1/c_1}^{1/c_2} \lambda(T - \lambda r)\phi_1(T - \lambda r)d\lambda$$

$$= \int_{1/c_1}^{1/c_2} T\lambda\phi_1(T - \lambda r)d\lambda - \int_{1/c_1}^{1/c_2} r\lambda^2\phi_1(T - \lambda r)d\lambda$$

$$= T\left[(\lambda^2/2)\phi_1(T - \lambda/r)\right]_{1/c_1}^{1/c_2} - r\left[(\lambda^3/3)\phi_1(T - \lambda r)\right]_{1/c_1}^{1/c_2} \qquad \text{(D2.5)}$$

where the term $\left[(\lambda^2/2)\phi_1(T - \lambda/r)\right]_{1/c_1}^{1/c_2}$ is evaluated in the same way as described in Appendix D1, and the second term is evaluated as follows.

$$\left[(\lambda^3/3)\phi_1(T - \lambda/r)\right]_{1/c_1}^{1/c_2}$$

$$= \left[(\lambda^3/3)H(T - \lambda/r)\right]_{1/c_1}^{1/c_2} - \left[(\lambda^3/3)H(T - \Delta T - \lambda r)\right]_{1/c_1}^{1/c_2} \qquad \text{(D2.6)}$$

where

$$\left[(\lambda^3/3)H(T - \lambda r)\right]_{1/c_1}^{1/c_2} = 0 \qquad \text{if } T < r/c_1$$

$$= \frac{T^3}{3r^3} - \frac{1}{3c_1^3} \qquad \text{if } T > r/c_1 \text{ and } T < r/c_2$$

$$= \frac{1}{3c_2^3} - \frac{1}{3c_1^3} \qquad \text{if } T > r/c_2 \qquad \text{(D2.7)}$$

The second term on the right hand side of equation (D2.6) can be obtained in a similar manner.

Time function 3 (eq. D1.4):

$$\int_{(n-1)\Delta T}^{n\Delta T} \dot{\delta}(T - \tau - r/c) f(\underline{x},\tau) d\tau = \frac{f_n(\underline{x}) - f_{n-1}(\underline{x})}{\Delta T} \phi_n(T - r/c) \qquad \text{(D2.8)}$$

Time function 4 (eq. D1.5)

The temporal integrations involving the time function 4 (i.e. $\ddot{\delta}(T - \tau - r/c)$) are approximated by using a backward finite different scheme as follows:

$$\int_{(n-1)\Delta T}^{n\Delta T} \ddot{\delta}(T - \tau - r/c) f(\underline{x},\tau) d\tau$$

$$= \int_{(n-1)\Delta T}^{n\Delta T} \delta(T - \tau - r/c) \ddot{f}(\underline{x},\tau) d\tau$$

$$= \frac{f_n(\underline{x}) - 2f_{n-1}(\underline{x}) + f_{n-2}(\underline{x})}{(\Delta T)^2} \phi_n(T - r/c) \qquad \text{(D2.9)}$$

REPORT DOCUMENTATION PAGE

Form Approved
OMB No 0704-0188

1 AGENCY USE ONLY (*Leave blank*)	2 REPORT DATE	3 REPORT TYPE AND DATES COVERED
	October 1991	Final Contractor Report

4 TITLE AND SUBTITLE

Linear and Nonlinear Dynamic Analysis by Boundary Element Method

5 FUNDING NUMBERS

WU-505-63-5B
C-NAS3-23697

6. AUTHOR(S)

Shahid Ahmad

7. PERFORMING ORGANIZATION NAME(S) AND ADDRESS(ES)

State University of New York at Buffalo
Department of Civil Engineering
Buffalo, New York 14222

8 PERFORMING ORGANIZATION REPORT NUMBER

None

9. SPONSORING/MONITORING AGENCY NAMES(S) AND ADDRESS(ES)

National Aeronautics and Space Administration
Lewis Research Center
Cleveland, Ohio 44135-3191

10. SPONSORING/MONITORING AGENCY REPORT NUMBER

NASA CR-187228

11. SUPPLEMENTARY NOTES

Project Manager, C C. Chamis, Structures Division, NASA Lewis Research Center, (216) 433-3252. Report submitted as a dissertation in partial fulfillment of the requirements for the degree Doctor of Philosophy to the State University of New York at Buffalo, Buffalo, New York in 1986.

12a. DISTRIBUTION/AVAILABILITY STATEMENT

Unclassified - Unlimited
Subject Category 39

12b DISTRIBUTION CODE

13. ABSTRACT ***(Maximum 200 words)***

In this dissertation, an advanced implementation of the direct boundary element method applicable to free-vibration, periodic (steady-state) vibration and linear and nonlinear transient dynamic problems involving two and three-dimensional isotropic solids of arbitrary shape is presented Interior, exterior and half-space problems can all be solved by the present formulation For the free-vibration analysis, a new real variable BEM formulation is presented which solves the free-vibration problem in the form of algebraic equations (formed from the static kernels) and needs only surface discretization. In the area of time-domain transient analysis the BEM is well suited because it gives an implicit formulation. Although the integral formulations are elegant, because of the complexity of the formulation it has never been implemented in exact form In the present work, linear and nonlinear time domain transient analysis for three-dimensional solids has been implemented in a general and complete manner. The formulation and implementation of the nonlinear, transient, dynamic analysis presented here is the first ever in the field of boundary element analysis Almost all the existing formulation of BEM in dynamics use the constant variation of the variables in space and time which is very unrealistic for engineering problems and, in some cases, it leads to unacceptably inaccurate results In the present work, linear and quadratic, isoparametric boundary elements are used for discretization of geometry and functional variations in space In addition higher order variations in time are used These methods of analysis are applicable to piecewise-homogeneous materials, such that not only problems of the layered media and the soil-structure interaction can be analyzed but also a large problem can be solved by the usual sub-structuring technique The analysis have been incorporated in a versatile, general-purpose computer program Some numerical problems are solved and, through comparisons with available analytical and numerical results, the stability and high accuracy of these dynamic analyses techniques are established

14 SUBJECT TERMS	15 NUMBER OF PAGES
Two-dimensional, Three-dimensional; Arbitrary shape, Half space; Vibrations; Transient analysis; Nonlinear; Computer code; Stability	266
	16 PRICE CODE A12

17. SECURITY CLASSIFICATION OF REPORT	18. SECURITY CLASSIFICATION OF THIS PAGE	19 SECURITY CLASSIFICATION OF ABSTRACT	20. LIMITATION OF ABSTRACT
Unclassified	Unclassified	Unclassified	

End of Document